Development of a Class B Evasin-Derived Peptide for Inhibiting Islet Inflammation

Megan Elizabeth Payne

Keble College

University of Oxford

Thesis presented for the degree of

Doctor of Philosophy in Medical Sciences

Trinity Term 2025

Table of Contents

Abstract

Type 1 diabetes (T1D) is a disease characterised by the migration of $CD8^+$ and $CD4^+$ T-cells to pancreatic islets, where they cause inflammation ("insulitis") and destroy insulin-producing beta cells. T-cell targeting drugs have been approved for treating T1D, but are associated with significant immunosuppressive side effects. Targeting T-cell trafficking to islets is an alternative strategy that has the potential to minimise such side effects. Chemokines direct T-cell migration to islets, but the redundancy of the chemokine network has hindered therapeutic development. Tick evasins neutralise the redundant chemokine network, with class A and B evasin proteins inhibiting CC and CXC-chemokines, respectively. Peptides derived from class A evasins are potent inhibitors of chemotaxis. This work hypothesises that potent chemokine-inhibiting peptides can be identified from class B evasins. Phage display library screening of evasin B-derived peptides against biotinylated chemokine targets identified a novel peptide that can bind and inhibit multiple CC and CXC class chemokines, as determined by *in vitro* chemotaxis assays. Combinatorial saturation mutagenesis and phage display selection were used to enhance its affinity for multiple chemokine targets. RNA-sequencing data from cytokine-stimulated human islets were used to model the variety of chemokines in insulitis, providing an approximation of their abundance. The mutated peptide, CM1629, inhibited the migration of $CD8^+$ and $CD4^+$ T-cells to this insulitis chemokine pool. CM1629 did not inhibit monocyte migration, indicating its specificity for T-cells. Mutagenesis resulted in a 19-fold increase in potency for CM1629 compared to the parental peptide, with CM1629 exhibiting nanomolar potency against the insulitis chemokine pool and $CD8^+$ T-cells. AlphaFold3 modelling reveals that tryptophan substitutions enhanced hydrophobic inter-chain interactions, suggesting a mechanism for enhanced potency. CM1629 may be an effective starting point for developing therapeutics that target T-cell trafficking in T1D.

Declaration

I declare that the following work and data presented in this thesis are my own, with the exception of the following bioinformatic analyses:

- Phage display (Figures 2.2, 2.3, 3.2, 3.3, 3.4, 3.8, 3.9, 3.10, 3.11)
- RNA sequencing (Figures 4.1, 5.3)
- Peptide:chemokine inter-chain interactions (Figures 4.20, 4.21)

Publications Relevant to this Thesis

Vales, S., Kryukova, J., Chandra, S. Smagurauskaite, G., **Payne, M**. *et al*. Discovery and pharmacophoric characterization of chemokine network inhibitors using phage-display, saturation mutagenesis and computational modelling. *Nature Communications* **14**, 5763 (2023). https://doi.org/10.1038/s41467-023-41488-z

Kryukova, J., Vales, S., **Payne, M**. *et al*. Development of chemokine network inhibitors using combinatorial saturation mutagenesis. *Communications Biology* **8**, 549 (2025). https://doi.org/10.1038/s42003-025-07778-6

Clark, C., **Payne, M**. *et al*. Robust and redundant chemokine signalling networks drive immune cell trafficking in human immunoinflammatory disease. Manuscript in preparation.

Payne, M., Clark, C., Hafner, K., Davies, G.,Chandra, S. Smagurauskaite, G., Bhattacharya, S. A chemokine inhibiting peptide from a class B evasin that targets T-cell migration. Manuscript in preparation.

Acknowledgements

I would like to express my gratitude and appreciation to my supervisors, Professor Shoumo Bhattacharya, Professor Charles Redwood, Dr Gintare Smagurauskaite, and Mr Graham Davies. The guidance, mentorship, and support you have provided me during my time as a DPhil student has truly meant so much to me. I cannot express my gratitude for all you have taught me.

To all the members of the Bhattacharya group, past and present – I could not have done this without you all. The sense of community, helpfulness, insight, and laughter have supported me throughout these four years. It has been a privilege to learn from all of you. Thank you for your friendship, most of all.

I would also like to thank Ali and all the members of the Hodson group for their help and assistance with setting up islet experiments. Your generosity with your time and in sharing samples is much appreciated.

I would like to thank my family. You have all supported me during the last four years, and I could not be more grateful. You will all be receiving a copy of this thesis for Christmas.

To my partner Ben, thank you for listening to my presentations, checking posters, proofreading, and being my sounding board for all things Chemistry. Doing this alongside you has been a blessing. I look forward to doing the same for you with your thesis, but just since I owe you.

To my parents, Amanda and Stephen, you have filled my life with love, never-ending support, and joy. I am so proud to be your daughter. Anything I achieve, I achieve because of you and for you. I dedicate this thesis to you both. I love you both endlessly.

List of Figures

List of Tables

Peptide Naming Convention

Amino Acid	Single Letter Code	Three-letter code
Alanine	A	Ala
Cysteine	C	Cys
Aspartic acid	D	Asp
Glutamic acid	E	Glu
Phenylalanine	F	Phe
Glycine	G	Gly
Histidine	H	His
Isoleucine	I	Ile
Lysine	K	Lys
Leucine	L	Leu
Methionine	M	Met
Asparagine	N	Asn
Proline	P	Pro
Glutamine	Q	Gln
Arginine	R	Arg
Serine	S	Ser
Threonine	T	Thr
Valine	V	Val
Tryptophan	W	Trp
Tyrosine	Y	Tyr

List of Abbreviations

Abbreviations

ACKR	Atypical chemokine receptor
ANOVA	Analysis of variance
APC	Antigen presenting cell
APC	Allophycocyanin
ATG	Antithymocyte globulin
ATP	Adenosine triphosphate
BB	BioBreeding rat
BLI	Biolayer interferometry
BP	Base pairs
CC	Charlie Clark
CD	Cluster of differentiation
CM	Combinatorial mutant
CFU	Colony forming units
COSMOS	Combinatorial saturation mutagenesis optimisation strategy
CRS	Chemokine recognition site
CSF	Colony stimulating factor
CTLA4	Cytotoxic T-lymphocyte-associated protein 4
CVB	Coxsackie B virus
DAMPS	Damage-associated molecular pattern
DC	Dendritic cell
DMSO	Dimethyl sulfoxide
DNA	Deoxyribonucleic acid
DNTPs	Deoxynucleotide triphosphates
EC	Effective concentration
ECACC	European Collection of Authenticated Cell Cultures
ELISA	Enzyme-linked immunosorbent assay
ELR	Glutamate leucine arginine motif
ER	Endoplasmic reticulum
EW	Emma Wilde
EVAA	Class A evasin
EVAB	Class B evasin
FBS	Foetal bovine serum
FCS	Foetal calf serum
FDA	Food and drug administration
FITC	Fluorescein isothiocyanate
FP	Forward primer
FSC-H	Forward scatter height
FoxP3	Forkhead box protein P3
GADA	Glutamic acid decarboxylase
GAG	Glycosaminoglycan
GCE	Genetic code expansion

GLP-1	Glucagon-like peptide-1
GPCR	G protein-coupled receptor
GVHD	Graft versus host disease
GWAS	Genome-wide association studies
HbA1c	Hemoglobin A1C
HBSS	Hanks' balanced salt solution
HLA	Human leukocyte antigen
HSCT	Hematopoietic stem cell transplant
IAA	Insulin autoantibodies
IAPP	Islet-amyloid polypeptide
IA-2A	Insulinoma-associated protein 2
IC	Inhibitory concentration
ICAM-1	Intercellular adhesion molecule 1
ID	Identification
IHC	Immunohistochemistry
IFN	Inteferon
Ig	Immunoglobulin
IL	Interleukin
IL2RA	Interleukin-2 receptor alpha chain
IPTG	Isopropyl β-D-1-thiogalactopyranoside
IRF-3	Inteferon regulatory factor 3
JAK	Janus kinase
KH	Katrin Hafner
KK	Kalimuthu Karuppanan
KO	Knock out
LB	Lysogeny broth
LCMS	Liquid chromatography-mass spectrometry
LCMV	Lymphocytic choriomeningitis
MDA5	Melanoma differentiation-associated protein 5
MHC	Major histocompatibility complex
MMPs	Matrix metalloproteinases
MP	Megan Payne
mRNA	Messenger ribonucleic acid
MS	Multiple sclerosis
mTOR	Mammalian target of rapamycin
nCAAs	Noncanonical amino acids
NGS	Next generation sequencing
NHS BT	National Health Service Blood and Transplant
NF-κB	Nuclear factor-kappa B
NLR	Nod-like receptors
NMR	Nuclear magnetic resonance
NOD	Non-obese diabetic mice
nM	Nanomolar
nPOD	Network for pancreatic organ donors with diabetes
NS	Not significant
OD	Optical density
NSAIDS	Non-steroidal anti-inflammatory drugs
PAMPS	Pathogen-associated molecular patterns

PBMCs	Peripheral blood mononuclear cells
PBS	Phosphate buffered saline
PBSA	PBS+Albumin
PBST/PT	PBS+Tween
PCR	Polymerase chain recaction
PD-1	Programmed cell death protein 1
PEG	Polyethylene glycol
PI	Propidium iodide
PM	Philomena Mburu
PRR	Pattern recognition receptors
PSI-BLAST	Position-specific iterated basic local alignment search tool
PTM	Post-translational modification
PTPN22	Protein tyrosine phosphatase non-receptor type 22
RA	Rheumatoid arthritis
RIG-I	Retinoic acid-inducible gene I
RNA	Ribonucleic acid
RNA-seq	Ribonucleic acid sequencing
RP	Reverse primer
RPM	Revolutions per minute
ROI	Region of interest
SB	Shoumo Bhattacharya
SC	Soumyanetra Chandra
SSC-H	Side scatter height
SCR	Scrambled
SCBC	Stem-cell derived beta cells
SCID	Severe combined immunodeficiency
SEC	Size exclusion chromatography
SM	Single mutant
STAT1	Signal transducer and activator of transcription 1
STZ	Streptozotocin
T1D	Type 1 diabetes
TCR	T-cell receptor
TGF	Transforming growth factor
TLR	Toll-like receptors
TNF	Tumour necrosis factor
TPM	Transcripts per million
Tregs	Regulatory T-cell
TRNA	Transfer RNA
VEGF	Vascular endothelial growth factor
UC	Ulcerative colitis
UV	Ultraviolet
VCAM-1	Vascular cell adhesion molecule 1
WT	Wild type
ZNT8	Zinc transporter 8
2XYT	2x Yeast extract tryptone
µM	Micromolar

1. Chapter One - Introduction

1.1 Inflammation

Inflammation is a natural response to tissue damage, pathogenic infection, or irritation[1]. Inflammation is a vital component of the innate immune system, triggered by chemical mediators released by damaged tissue or infectious agents, which aims to prevent the spread of infection and promote tissue repair[1]. The Roman physician Celsus first described inflammation and categorised it by four characteristic signs: redness, heat, swelling, and pain. A fifth hallmark of inflammation, loss of function, was subsequently added[2]. There are two primary types of inflammation: acute inflammation, which is short-term, and chronic inflammation, which is longer-term.

1.1.1 Acute Inflammation

Acute inflammation is the body's first response to damage or infection. The acute inflammatory cascade begins within the first 24 hours of the perturbation[3]. Key stages of acute inflammation include the recognition of the insult, the release of inflammatory mediators, the induction of leukocyte recruitment, and the resolution of inflammation[4].

1.1.1.1 Insult Recognition

Tissue-resident immune cells, such as neutrophils, dendritic cells (DCs), and monocytes, are often the first cells to initiate the inflammatory response (**Figure 1.1**). These tissue-resident lymphocytes reside in peripheral tissues and do not circulate[5]. Resident and circulating immune cells detect molecules known as danger-associated molecular patterns (DAMPs), which are produced by cells in response to tissue damage or cellular stress[6]. DAMPs can originate from the intracellular compartment of cells (DNA, RNA, ATP, and histones) or the extracellular space (heparan sulfate and hyaluronan)[6]. Leukocytes can also detect pathogen-associated molecular

patterns (PAMPs) in response to bacterial or viral infections[7]. PAMPs can be a physical component of an infectious agent, such as a viral coat protein or the flagella of a bacterium. PAMPs can also be non-human genetic material, such as bacterial circular DNA or viral RNA[8].

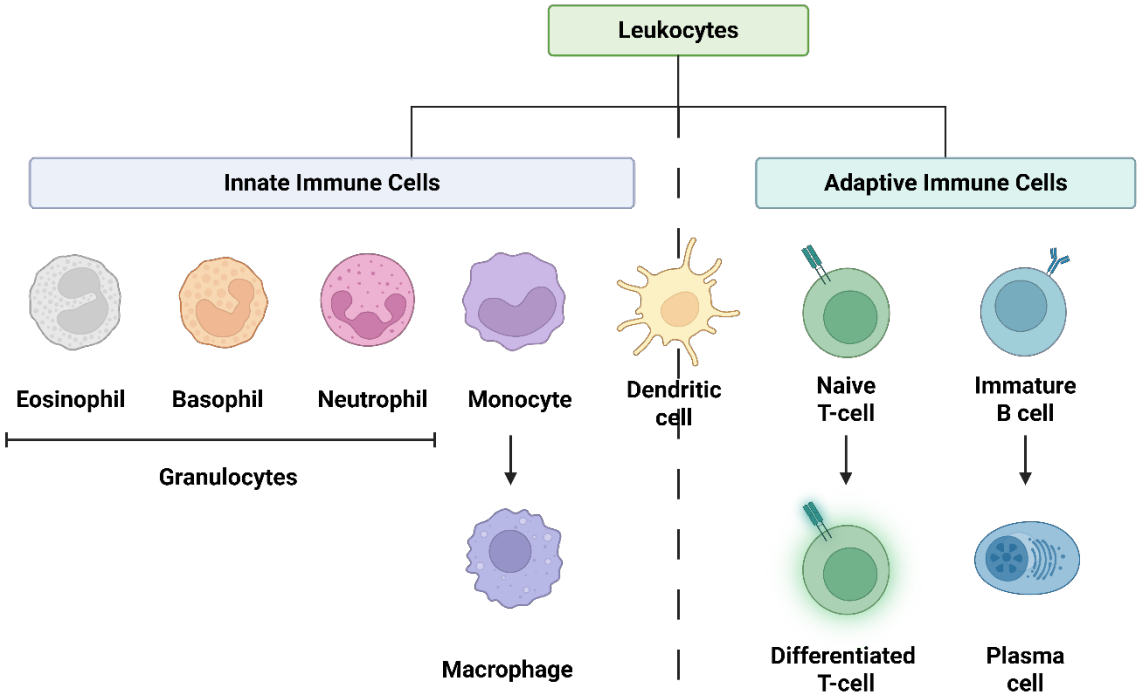

Figure 1.1 – Key leukocytes in the innate and adaptive immune responses. Adapted from Janeway's Immunobiology (9th edition)[9]. Figure made in Biorender.

PAMPs or DAMPs are detected by resident leukocytes via their surface pattern recognition receptors (PRRs)[7]. Activation of a PRR triggers an intracellular signalling cascade within the leukocyte. The specific intracellular cascade triggered depends on the identity of the PRR that has recognised the PAMP or DAMP[10]. The two main subclasses of PRRs are the NOD-like receptors (NLRs) and the Toll-like receptors (TLRs). NLRs respond to bacterial PAMPs and various DAMPs, triggering the NF-κB pathway[11]. TLRs can trigger mitogen-activated protein kinases (MAPKs) or toll/interferon response factors[7]. Pathway activations trigger the recruitment of transcription factors, further propagating the signalling cascade. Following the activation of intracellular pathways, leukocytes release inflammatory mediators[12].

1.1.1.2 Inflammatory Mediators

Inflammatory mediators encompass a range of small molecules, lipids, and proteins released by leukocytes or tissues in response to inflammation. Examples of inflammatory mediators include lipids, enzymes, nitric oxide, reactive oxygen species, histamine, members of the complement cascade, and cytokines[13]. Inflammatory mediators, such as histamine, can dilate blood vessels and increase vascular permeability, allowing leukocyte extravasation to inflamed sites[14].

Cytokines, an important class of inflammatory mediators, can be either pro-inflammatory or anti-inflammatory and facilitate a wide range of functions[15]. Cytokines are a diverse category of small signalling proteins that comprise colony-stimulating factors (CSFs), interleukins (ILs), tumour necrosis factors (TNFs), interferons (IFNs), and chemokines[16]. CSFs regulate the production of leukocytes within the bone marrow during homeostasis and following infection[17]. Interleukins have a variety of roles, but are primarily involved in the differentiation, proliferation, and activation of leukocytes[18]. Tumour necrosis factors are implicated in leukocyte differentiation, cell survival, and apoptosis[19]. Interferons are a key component of antiviral immunity, promoting the differentiation of leukocytes[20]. Chemokines are chemotactic, promoting leukocyte egress to sites of inflammation through the formation of chemokine gradients[21]. Chemokines will be discussed in more depth in Section 1.2.

1.1.1.3 Leukocyte Recruitment

Leukocyte recruitment to sites of inflammation, also known as chemotaxis, is a crucial step in the acute inflammatory process and is mediated by chemokines (**Figure 1.2**)[22]. Leukocyte recruitment begins with the release of pro-inflammatory cytokines, such as TNF-α and IL-1β[23]. In states of homeostasis, the endothelium is smooth and non-adhesive. Pro-inflammatory cytokines increase the expression of molecules such as ICAM-1, VCAM-1, and E-selectin[24]. Circulating leukocytes express complementary adhesion molecules, such as L-selectin[25]. Interactions between the adhesion molecules result in leukocytes slowing down and rolling along

the endothelial surface. This slow roll allows time for stronger interactions to occur, for example, between B2 integrins on the leukocyte surface and ICAM-1 on the endothelium[26]. Leukocytes flatten along the endothelial surface, thereby increasing the area of attachment. Immune cells can then migrate through endothelial junctions in a process known as diapedesis, facilitating migration from the circulation to the tissue along the chemokine gradient[27]. Migrated leukocytes may target the pathogen through phagocytosis or the release of neutrophil extracellular traps[28]. Immune cells may also eliminate tissue debris following injury by releasing further inflammatory mediators. The release of cytokines can further perpetuate the inflammatory cascade or facilitate the resolution of inflammation[29].

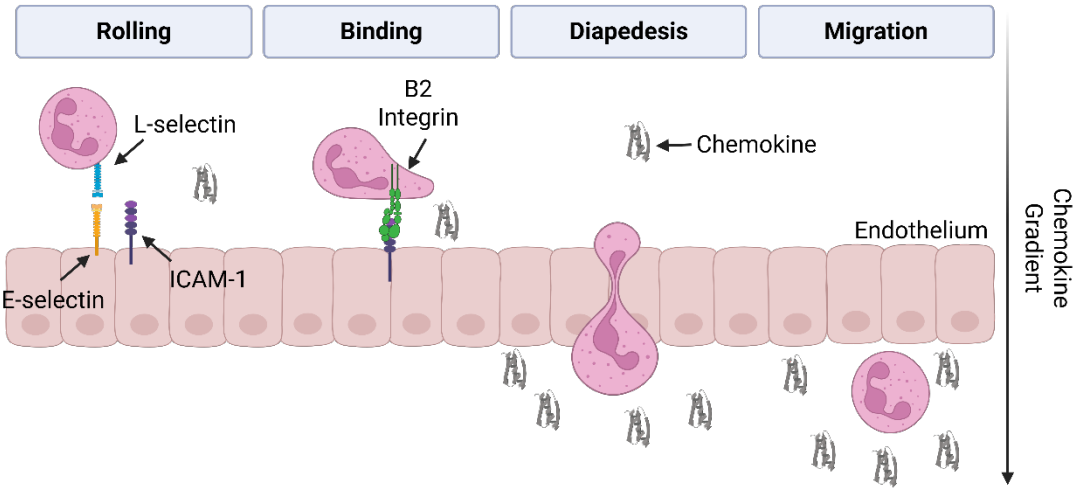

Figure 1.2 – Leukocyte migration. The four stages of leukocyte migration through the endothelium. Migrating along a chemokine gradient, leukocytes encounter an activated endothelium presenting molecules such as E-selectin. Leukocytes roll along the endothelium and interact with corresponding adhesion molecules such as L-selectin. Binding to the endothelium occurs through interactions between B2 integrins and ICAM-1. Cells then migrate through endothelial junctions to the site of inflammation, known as diapedesis. Adapted from Janeway's Immunobiology (9th edition)[9]. Figure made in Biorender.

1.1.1.4 Resolution of Inflammation

The resolution of inflammation is a tightly controlled process which marks the end of inflammation and a return to tissue homeostasis. A key hallmark of resolution is the removal of the cause of inflammation, such as the infectious agent or the damaged tissue, which has been repaired or remodelled[30]. Another feature of resolution is that the production of pro-inflammatory mediators is halted. Key leukocytes involved in resolution are regulatory $CD4^+$ T-

cells (Tregs). Tregs produce anti-inflammatory molecules that suppress the activation of pro-inflammatory leukocytes, thereby preventing the formation of further pro-inflammatory mediators[31]. Many pro-inflammatory mediators have a short half-life and are rapidly subjected to cleavage or degradation after synthesis. Chemokines are cleaved, which inhibits their chemotactic activities. Therefore, once their production has stopped, further leukocyte chemotaxis is halted[32]. Remaining leukocytes can re-enter circulation through lymphatic drainage or are cleared by apoptosis and necrosis. Tissues can re-establish homeostasis following the resolution of inflammation[33]. However, if the resolution of inflammation is not initiated, tissue damage and inflammation can persist unchecked, leading to the development of chronic inflammatory diseases.

1.1.2 Chronic Inflammatory Disease

If inflammation is not resolved, chronic inflammatory diseases develop. Chronic inflammation can develop over years, even in the absence of the original inflammatory signal[34]. Chronic inflammation can be caused by a failure to eliminate an inflammatory signal, repeated exposure to irritants, or a failure to resolve inflammation. If inflammation is not resolved, pro-inflammatory cytokine production is not ceased, and leukocyte egress is not halted[34]. Chronic inflammation and inflammatory diseases can lead to substantial tissue and organ damage. Furthermore, chronic inflammation predisposes individuals to an increased risk of cardiovascular disease, cancer, and further inflammatory diseases[35]. Therefore, chronic inflammatory diseases are responsible for a vast proportion of worldwide deaths and disability.

Examples of chronic inflammatory diseases include atherosclerosis, non-alcoholic fatty liver disease, gout and autoimmune diseases[36]. Incidence of inflammatory diseases is rising globally, particularly within Western populations, with this linked to changes in lifestyle factors. Obesity, chronic stress, an ultra-processed diet, a sedentary lifestyle, and smoking are all linked to an increase in chronic inflammation[37]. Chronic inflammation also increases with age, thereby

increasing the risk of further disease development and the patient's disability burden[38]. Genetic predisposition also increases the likelihood of developing chronic inflammatory diseases, particularly autoimmune diseases[39].

1.1.2.1 Autoimmune disease

Autoimmune diseases are a subclass of chronic inflammatory diseases which develop due to a loss of immunological tolerance. Tolerance is defined as a state where lymphocytes, typically T-cells, are unresponsive to a self-antigen. Central tolerance is controlled through the positive selection of leukocytes that weakly bind to self-major histocompatibility complexes, while cells that strongly bind to self-antigens are negatively selected[40]. In a state of immunological tolerance, leukocytes are exposed to self-antigens throughout their thymic and bone marrow-based development and selection[41]. Self-antigens are presented to leukocytes, and leukocytes that bind to self-antigens are removed through apoptosis[42].

Central tolerance is not wholly effective, and many healthy individuals have circulating self-reactive, also known as autoreactive, leukocytes[43]. Peripheral tolerance acts to either destroy, redirect, or dampen the effects of self-reactive leukocytes. Peripheral tolerance is mediated through the differentiation of naïve $CD4^+$ helper cells into Tregs, and by the actions of IL-2 and TGF-β[44]. Other mechanisms include the exhaustion of T-cells, apoptosis, and processes that render self-reactive leukocytes anergic, making them unresponsive to self-antigen[45].

In autoimmune diseases, tolerance is lost. Leukocytes lose immunological tolerance and begin targeting self-antigen-displaying tissues, perpetuating an unnecessary inflammatory cascade. As the initiating inflammatory factor is 'self', resolution of inflammation through removal of the initiating factor is not possible[46]. Genetically susceptible individuals may have mutations in key components of tolerance, such as the transcription factor FoxP3, which is crucial for the development of Tregs[47]. Pathogenic T-cell subtypes are involved in the pathogenesis of many autoimmune diseases[48]. Negative selection of T-cells is more stringent than that of B-cells, and

peripheral tolerance is focused primarily on T-cells. This focus on T-cells is because T-cells can mediate robust tissue damage[49]. Key examples of common autoimmune diseases include rheumatoid arthritis (RA), ulcerative colitis (UC) and type one diabetes (T1D). T1D will be explored further in Section 1.3.

1.1.2.2 Anti-Inflammatory Drugs

Natural remedies for alleviating pain and inflammation have been used for thousands of years. Ancient Egyptians used myrtle leaves to alleviate menstrual pain[50], and Hippocrates prescribed willow bark for pain management[51]. It is now known that these remedies contain salicylates, a drug class that includes the commonly prescribed anti-inflammatory aspirin[52]. Anti-inflammatory agents are prescribed to manage chronic inflammation and reduce pain. Historically, anti-inflammatory drugs have not been specifically targeted at a disease, but rather at pathways upstream in the inflammatory cascade.

Non-steroidal anti-inflammatory drugs (NSAIDs) are a commonly prescribed class of anti-inflammatories. NSAIDs prevent the synthesis of a type of inflammatory mediator known as prostaglandins by inhibiting cyclooxygenases[53]. Side effects associated with NSAIDs include cardiovascular events, gastrointestinal bleeding, ulcers, blood pressure elevation and acute renal failure[54]. Currently, the molecular mechanism underlying this wide range of side effects remains unidentified.

Colchicine is a neutrophil-targeted therapy used for the treatment of gout, familial Mediterranean fever, and other inflammatory diseases[55]. By reducing the responsiveness of neutrophils to chemokines and other activation signals, colchicine dampens neutrophil-mediated inflammation. Colchicine has been associated with gastrointestinal side effects, muscle pain, muscle degeneration, and long-term kidney damage[55].

Corticosteroids are another widely prescribed class of anti-inflammatory medications[56]. Corticosteroids influence transcription factor production by targeting nuclear glucocorticoid

receptors, resulting in a range of side effects. Long-term use is associated with immunosuppression, worsening inflammation over time, osteoporosis, and hyperglycaemia[57]. With NSAIDS, colchicine and corticosteroids, systemic side effects are a result of the drug's mechanism of action being widespread and not specifically targeted to a disease state.

There is a clear unmet need for patients suffering from chronic inflammation for targeted therapies that resolve inflammation without initiating immunosuppression and creating a further disease burden. As the incidence of chronic inflammatory diseases and autoimmune diseases rises worldwide, new therapies capable of halting inflammation without systemic side effects are sorely needed. The pathophysiology of autoimmune diseases is becoming better understood. New immune-based therapies for autoimmune diseases aim to target, prevent or reduce the specific inflammatory mediator associated with a disease state.

1.2 Chemokines

Chemokines, as described above, are a family of chemotactic proteins. To date, 46 chemokines have been categorised in humans[58]. Chemokines are produced by immune cells and tissues during various stages of the inflammatory process and form gradients that leukocytes use as directional guides to sites of inflammation or injury[59]. If inflammation is not resolved and chemokine production is not halted, chemokines promote further leukocyte egress towards the site of inflammation. Chemokines also play a pivotal role in maintaining homeostatic leukocyte trafficking[60], regulating the migration of immune cells through the lymphatic system, including the spleen, bone marrow, skin, and central nervous system. Therefore, chemokines are vital for the development and maturation of leukocytes[61]. Depending on their spatial location, chemokines can have dual roles, acting as both inflammatory agents and homeostatic chemokines, such as CXCL12[62]. Chemokines have also been implicated in the development of cancer. If cancers exploit the chemokine system, they can prevent anti-tumour immune cell trafficking to tumours while promoting angiogenesis and cellular proliferation[63].

Chemokines are approximately 8 to 12 kDa in size and primarily mediate their effects through G-protein-coupled receptors (GPCRs)[64]. Chemokines have a conserved structure of an α-helix, three β-sheets, an N loop and an unstructured N-terminal domain (**Figure 1.3**). The 30s loop links the β1 and β2 strands, and the 40s loop links the β2 and β3 strands[65]. Chemokines are classified into subfamilies based on their N-terminal cysteine residues, which define their classification. The most abundant classes are the CC and CXC chemokine classes[66]. The CXC chemokine family can also be subdivided based on the presence or absence of a Glu-Leu-Arg sequence in the N-terminal region of the chemokine, known as the ELR motif[67]. The CX3C and C subfamilies are less abundant, comprising of only two XC chemokines and one CX3C chemokine in humans[59].

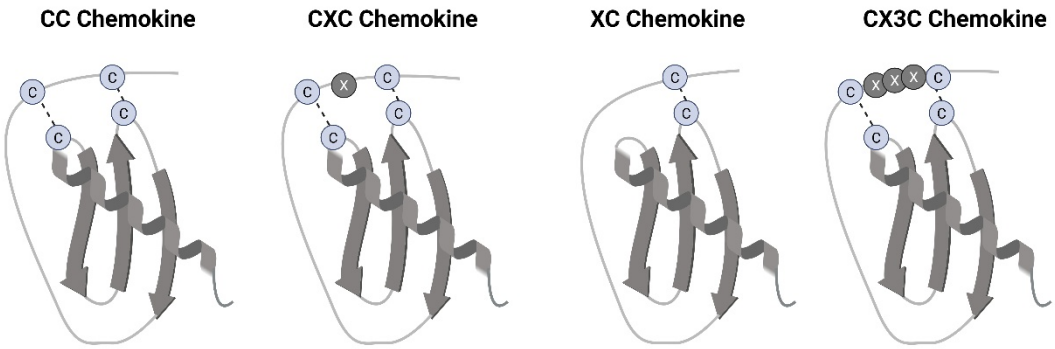

Figure 1.3 – Chemokine class structures. Illustrative structures of chemokine subclasses based on their N-terminal cysteine residues. Figure made in Biorender.

Chemokine receptors are GPCRs, with 18 chemokine receptors expressed on leukocytes in humans. Receptors are named based on the chemokines that bind to them, designated as CCR, CXCR, CX3CR, and XCR[59]. Chemokine receptors have a C-terminal intracellular helix, an unstructured N-terminus, three extracellular loops, three intracellular loops, and seven transmembrane helices[68]. Chemokines interact with chemokine receptors at two locations. The N-terminus of the chemokine binds to the transmembrane helices of the chemokine receptor, known as chemokine recognition site one (CRS1). The second chemokine recognition site (CRS2) is located between the globular core of the chemokine and the N-terminus of the receptor[69].

These interactions induce conformational changes in the structure of the intracellular receptor surface, recruiting G proteins, β-arrestins, and a variety of other components of cellular signalling[70].

Atypical chemokine receptors (ACKRs) also bind to chemokines. ACKRs act as chemokine scavengers, removing chemokines from *in vivo* sites and reducing chemokine abundance in tissues. Reducing circulating chemokine levels aids in the resolution of inflammation and prevents chemokine receptor internalisation on other immune cells[71]. Receptor internalisation is a cellular defence mechanism to prevent cellular overstimulation by chemokines. To reduce cellular responsiveness to chemokines, chemokine receptors can become internalised by the cell[72]. Chemokine internalisation also acts to reduce the levels of circulating chemokines.

Chemokines also interact with glycosaminoglycans (GAGs) expressed on endothelial surfaces. GAGs include heparan sulfate, hyaluronic acid and keratan sulfate[73]. GAGs are negatively charged linear polysaccharide molecules, and chemokine interactions with GAGs facilitate chemokine immobilisation on endothelial membranes[73]. Chemokine immobilisation is critical for establishing chemokine gradients. Recent studies have hypothesised that the sequestering of chemokines by GAGs on endothelial surfaces is a highly dynamic process, allowing chemokines to be reversibly released as a 'cloud'[74]. Released chemokines can then interact with passing or immobilised leukocytes, while reversible GAG binding prevents chemokines from dissociating due to blood flow and shear stress[74]. GAGs function primarily to concentrate chemokines at endothelial sites adjacent to their production. It has been reported that such immobilisation is vital for leukocyte extravasation *in vivo*[75]. Despite this, chemokines can exert their function *in vitro* in the absence of GAGs[76].

1.2.1 Chemokine Signalling Complexity

Chemokine signalling is inherently complex[58, 77]. Complexity in a biological system can be defined by a large number of varied, interconnected components that interact with one another

dynamically[78]. The chemokine network can be considered complex, as it comprises a large number of varied components, including 46 chemokines of four different classes, which interact with 18 receptors[66, 79]. Chemokines are interconnected, as they can activate multiple chemokine receptors on different leukocyte subtypes, as seen with CCL3, which activates the chemokine receptors CCR1 and CCR5[80]. Cryoelectron microscopy has resolved CXCR2 in complex with 15 chemokines[81]. CXCR2 bound to CXCL1/2/3/5/6/7/8, and this activity was validated using assays such as G-protein and arrestin recruitment, indicating promiscuity[81]. High levels of structural similarity between chemokines and their receptors may explain this crossover in chemokine signalling[65]. This high level of interconnectivity results in chemokines recruiting multiple types of immune cells to inflamed tissues[82, 83]. Additional chemokines are produced by recruited leukocytes at the inflamed site, prompting the migration of further leukocytes. Therefore, chemokine production also creates chemokine feedforward loops[84].

Chemokines are rarely secreted independently of one another, and the presence of other chemokines impacts their signalling. Chemokines can form homo- and heterodimers with other chemokines[85]. Homodimers, which are dimers formed by two identical chemokines, form differently depending on the chemokine class. CXC chemokines form homodimers through interactions at the β1 strand. CC chemokines form homodimers by interacting at their N-terminal residues[86]. Chemokines can also heterodimerise with other chemokines. CC chemokine heterodimers tend to be activating but cannot bind to their receptors. CXC heterodimers tend to be inhibitory but can interact with their chemokine receptors[69, 85]. Chemokines, such as CXCL4, can also form tetramers or higher-order oligomers[87]. Homo- and heterodimers provide further evidence for chemokine network complexity, demonstrating the dynamic interconnectivity of the chemokine network.

Chemokine synergism is further complicated by the ability of chemokines to activate chemokine receptors simultaneously or sequentially[88]. When multiple chemokines are present together,

they can synergise, independent of their subclass[89]. The synergy of chemokines results in chemotaxis that exceeds what would be expected from the two chemokines independently[90]. Such activity is difficult to predict from *in vitro* single chemokine studies, which further complicates the analysis of the chemokine network[88].

Post-translational modification (PTM) of chemokines impacts their signalling[91]. Chemokine nitration has been proposed as a natural mechanism to prevent aberrant chemokine signalling[92]. Chemokines can also be citrullinated, which is also known to reduce chemokine signalling[93]. Chemokines can also be cleaved by proteins such as matrix metalloproteinases (MMPs). This cleavage can be deleterious to their function, as exemplified by CCL2 cleavage[94]. Cleavage of the chemokines CCL15 and CCL23 induces a more 'active' version of these chemokines, and results in an increase in signalling[95]. Therefore, the chemokine network can be considered a complex biological system.

1.2.2 Chemokine Network Robustness and Redundancy

The chemokine network is highly complex, as described above, and robust. Biological robustness ensures that systems remain functional despite perturbations[96]. Robustness is a property of highly evolved systems[96]. The chemokine network has existed for over 500 million years, evolving in early vertebrates from a common ancestor, with chemokine and receptor numbers expanding through gene duplication events in bony fish and subsequent mammals[97]. Furthermore, loss-of-function mutations have been observed in humans, that exist without impacting the chemokine network as a whole. CCR5 deletion is associated with HIV-1 resistance[98], and mutations resulting in a defective CX3CR1 receptor are associated with protection from cardiovascular diseases[99]. Such evidence strongly supports the notion that the chemokine network is robust.

Redundancy is a mechanism of robustness. Redundancy in a biological network ensures that several similarly functioning molecules can exist to replicate the function of another if one fails, acting to ensure a system's robustness[96]. Robustness can arise from functional redundancy, in

which molecules do not have to be identical but behave redundantly in a particular context[100]. The chemokine network can be considered redundant[84, 101, 102]. This redundancy implies that one chemokine can act similarly to another in a given inflammatory context, thereby ensuring that chemokine-mediated inflammation is not disrupted if a single chemokine or chemokine receptor is missing[101]. This redundancy is exemplified by lymphocyte subtypes migrating in response to several chemokine ligands[64, 103].

Despite this, it has been argued that the chemokine network is highly specific and not redundant[104]. Evidence supporting this specificity arises primarily from gene deletion experiments in mouse models. The deletion of CCR2 has demonstrated specificity for monocyte migration in inflammation[105], and the chemokine ligands for CXCR3 (CXCL9, CXCL10, and CXCL11) have been described as having non-redundant activity in mouse models of inflammation and viral infections[106]. Limitations of such experiments include that they are performed on inbred mice, which have less diversity in immune cell populations and abundance[107, 108], potentially impacting chemokine network redundancy. Furthermore, mice are housed in pathogen-free environments[109], which are known to limit immune cell activation and result in deficits in immune cell populations, such as $CD8^+$ T-cells[110, 111]. The environment and genetic condition of these mice are vastly different from those of humans, who are constantly exposed to pathogens[112] and are genetically heterogeneous[113]. These limitations should be taken into account when examining chemokine redundancy in mouse models.

The primary argument that the chemokine network is redundant arises from nature. Many organisms have developed pan-chemokine inhibitors to target and neutralise the immune system. Natural selection has enabled organisms to develop mechanisms that evade the immune system by targeting chemokines. It is hypothesised that the evolution of ways to evade the immune system of hosts would particularly benefit parasitic organisms, allowing them to breed and survive[84]. A type of parasitic worm, *Schistosoma mansoni*, possesses proteins that

can bind to multiple classes of chemokines. Such proteins are capable of inhibiting chemokines both *in vitro* and *in vivo*[114]. Viruses, such as herpes, also possess chemokine-binding proteins. The M3 herpesvirus protein can bind to all chemokine classes and block *in vitro* chemokine activity[115]. Another key example is tick salivary proteins, known as evasins[116]. Evasins will be discussed in more detail in Section 1.6.

If parasitic organisms described above could neutralise the chemokine network by targeting a small number of chemokines or chemokine receptors, it would follow that natural selection would have done this. As nature has developed chemokine inhibitors that can target a vast portion of the chemokine network, it is logical that the chemokine network is indeed redundant. Another key argument for chemokine network redundancy is the failure of chemokine-targeting therapies, which will be discussed in Section 1.5.

1.3 T1D

T1D is an autoimmune disease, characterised by progressive beta cell loss within pancreatic islets. As beta cells are the cell type responsible for insulin production, beta cell loss leads to hyperglycaemia (**Figure 1.4**)[117]. Patients are therefore unable to respond to raised glucose when they eat. Symptoms include rapid weight loss, polydipsia and polyuria, among others[118]. Diabetes was historically diagnosed through the tasting of urine and was described as 'honey urine' due to the excess glucose making the urine taste sweet. The first reported cases date back to the second century AD, when Greeks noted that a rare condition was causing weight loss, excessive urination, and rapid death[119].

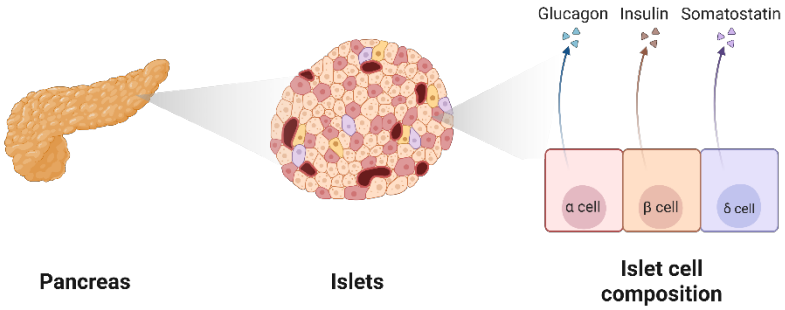

Figure 1.4 – Islet human anatomy. Within the pancreas, there are groups of hormone-producing endocrine tissue called the islets of Langerhans. Islets are composed of alpha cells, which produce glucagon; beta cells, which produce insulin; and delta cells, which produce somatostatin. Figure made in Biorender.

As untreated T1D results in hyperglycaemia, this disease can result in mortality if not diagnosed rapidly[120]. Conversely, insulin therapy is associated with hypoglycaemia, with prolonged periods of low blood glucose resulting in a diabetic coma and death[121]. Approximately 4% to 10% of T1D deaths are associated with hypoglycaemic events[122-124]. These deaths occur primarily in young patients aged 15-30[125]. Patients are also at risk of developing ketoacidosis, which accounts for 13-19% of T1D patient deaths[123, 124, 126]. Due to macrovascular complications, T1D patients also experience high levels of cardiovascular complications, such as coronary artery disease. Approximately 50% of female and 70% of male T1D patients have detectable calcification of their coronary artery by the time they are in their mid-40s[127]. Diabetic nephropathy, retinopathy and neuropathy all impact patients due to microvascular abnormalities[128]. T1D patients have an average loss of 12 years of life expectancy[129, 130]. If diagnosed as a child, life expectancy is reduced by a further two and a half years[130].

Worldwide, less than 1% of the general population has T1D. Incidence rates are rising in European and sub-Saharan African populations[131], as well as in the Middle East, North America, and Central America[132]. The global incidence rate is rising at an approximate annual rate of between 2% to 5%[133] or doubling every 25 years[134, 135]. Due to misdiagnosis and high mortality levels in countries classified as 'low-income countries', it has also been argued that the accurate levels of T1D are underestimated[136]. With underestimated figures, an increased incidence rate, high

mortality risks, and the impact on patients' quality of life, T1D is a disease which requires global attention.

1.3.1 T1D Models

To study T1D and disease pathogenesis, analysing human tissue from pre-diabetic and newly diagnosed individuals would be ideal. Pancreatic biopsies are rarely performed, and as many newly diagnosed patients are young children or adolescents, it is often not possible to procure pancreatic tissue. In 2014, the first-ever study sampling pancreas tissue from adults newly diagnosed with T1D was published[137]. One patient experienced significant post-operative bleeding, and two had leakage of pancreatic juice, accounting for 50% of the patients who underwent surgical resection. A patient also complained that they were not provided with adequate information regarding the surgical risks. The study was discontinued due to ethical concerns[137]. Therefore, other models have been developed to study T1D.

Mouse models are commonly used to study a range of inflammatory conditions, including T1D. The non-obese diabetic (NOD) mouse model spontaneously develops T1D[138]. The NOD mouse shares key features of human T1D pathogenesis, including autoantibody development and insulitis (inflammation surrounding pancreatic islets)[139]. The NOD mouse shares genetic polymorphisms with human disease[140]. Pathogenesis in the NOD mouse begins with autoimmunity, followed by a progressive loss of beta cells, resulting in hyperglycaemia at approximately 12 to 16 weeks of age[141]. Similarly, to humans, autoreactive T-cells have been identified as a driver of pathogenesis[142, 143]. Crucially, successful T1D therapies were first identified in NOD models, despite being significantly less effective in humans compared to the mouse[144, 145].

Limitations of the NOD model include discrepancies between the contributions of T-cell populations driving T1D in humans and those in NOD mice[139]. T1D development in NOD mice is almost entirely linked to females, whereas there is an almost equal gender split in humans[146].

NOD mice and all rodent models are interbred. Interbred species lack the genetic diversity of humans, making it difficult to extrapolate information from mice to a general human population[147]. There are inherent differences between the immunology and immune systems of humans and mice[148], which have complicated the translation of therapeutic approaches from the NOD mouse to human trials. Humanised NOD models are also available, which may accelerate the transition from mouse data to human trials[139]. Other rodent models include the spontaneous BioBreeding (BB) rat[149] and inducible models, such as the streptozotocin-induced (STZ) diabetic model[150].

Due to the discrepancies between the development of T1D in mice and humans, as well as the general limitations of mouse models, the investigation of T1D development using human tissue has been expanded. Databases have been established with pancreatic autopsy and biopsy samples from T1D patients. The Network for Pancreatic Organ Donors with Diabetes (nPOD) is one such tissue biobank[151]. Human islet transplants for the treatment of T1D require specialised islet isolation facilities to extract the scattered islets from pancreatic tissue[152]. If rejected for transplant, it is possible to gain access to human islets for scientific study[153]. Culturing islets with IL-1β, TNF-α, and IFN-γ is a common strategy to mimic beta cell inflammation[154]. Stimulation of beta cells with such cytokine cocktails produces transcriptional signatures similar to those observed in beta cells from T1D donors[155].

Table 1.1 – T1D models, their strengths and limitations

Type 1 Diabetes Model	Strengths	Limitations
NOD mouse	Shared genetics with human T1D, spontaneous disease development, treatment translated from NOD to human	Expensive, inbred strains lacking genetic diversity, sex differences
STZ rodents	Inducible model, less expensive	Potential off-target toxicity, does not fully recapitulate autoimmunity
T1D cadaveric samples	Human tissue, understanding of disease heterogeneity, tissue biobank	Limited access to tissues, fixed static samples, variation between time course of diabetes
Cytokine-stimulated human islets	Human tissue, cytokine-stimulating mimics transcriptional T1D signatures	Complicated islet isolation, hypoxia reperfusion injury of islets when isolated, variation between donors

1.3.2 Pathogenesis of T1D

T1D is characterised by autoreactive T-cell destruction of insulin-producing beta cells within pancreatic islets[156]. T1D can be categorised into three stages (**Figure 1.5**). However, the exact aetiology of T1D is unknown and complex. Newborn studies in genetically susceptible families suggest that the autoimmune process may begin in children as early as 12 to 18 months of age[157, 158]. Beta cell dysfunction may precede T1D diagnosis by more than five years[159]. Upon diagnosis, patients can have lost 90% of their functional beta mass, depending on their age at diagnosis[160, 161]. If diagnosed as teenagers or older, patients can retain ~50% of their beta cell mass[162]. This insulin-producing beta mass may allow patients to experience a brief remission period when insulin treatment is initiated[163]. T1D disease progression is also heterogeneous, as the age of diagnosis influences the rate of beta cell loss. Rapid beta cell decline is often observed in children and adolescents, whereas diagnosis in adulthood is typically associated with a more gradual decline in beta cell mass[164].

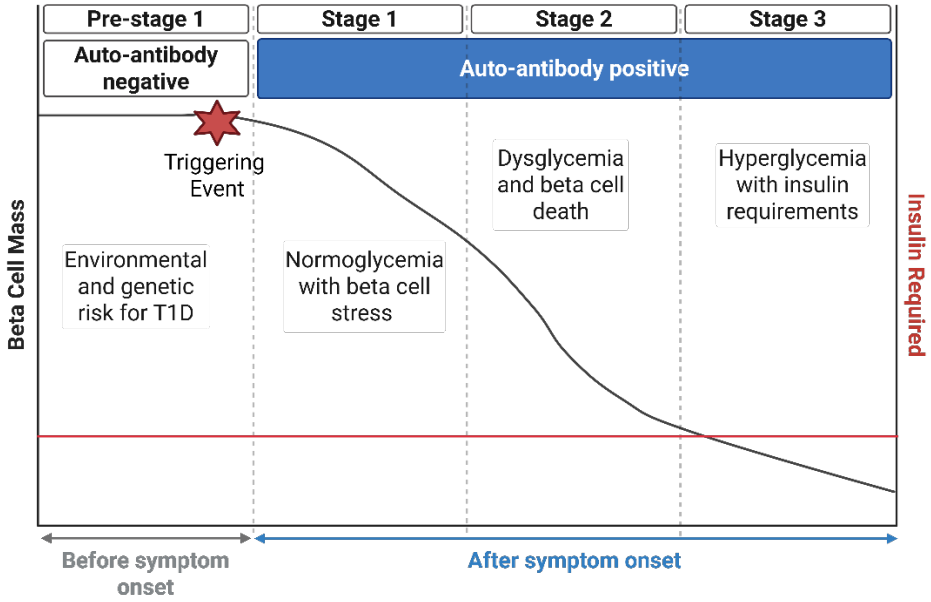

Figure 1.5 – The stages of T1D. Type 1 diabetes (T1D) is characterised by three stages, where beta cell mass gradually declines until insulin therapy is required. Before symptom onset, patients are at risk for T1D due to environmental and genetic factors, and T1D can be triggered by an event such as a viral infection. Stage one of T1D is characterised by auto-antibody positivity and normoglycemia. Stage two of T1D is characterised by dysglycemia and progressive beta-cell decline. Stage three of T1D is characterised by hyperglycaemia requiring insulin. Adapted from the TrialNet ribbon [165]. Figure made in Biorender.

Several factors contribute to the pathogenesis of T1D. T1D is highly heritable, primarily due to genetic polymorphisms in human leukocyte antigen (HLA) genes[166]. Alongside this, an environmental perturbation is required for T1D development, such as a viral infection[167]. Growing evidence also suggests that beta cells are specifically vulnerable to stress, which may predispose beta cell components to become the target of autoantibodies[168]. Inflammation within the islets, also known as insulitis, is a hallmark of T1D, and beta cell stress contributes to the development of insulitis[154]. Autoreactive T-cells that have escaped thymic selection can then target beta cells. Not all pathways described below will explain T1D development in all patients; a combination of factors likely explains the pathogenesis[169].

1.3.2.1 Genetic Factors in T1D

While GWAS evidence has identified over 60 genetic loci associated with T1D in Caucasian populations, genes located in HLA regions have the most significant effect on genetic susceptibility[170]. HLA genes are part of the major histocompatibility complex (MHC), which

enables immune cells to distinguish between self and non-self. HLA proteins are found on the surface of almost all tissues within the body, displaying peptide epitopes[171]. Displayed epitopes are typically produced through phagocytosis and processing of 'non-self' foreign bodies. Antigen-presenting cells (APCs) present peptide epitopes to other leukocytes, providing activation signals and facilitating the differentiation of leukocytes. APC subtypes include resident or circulating macrophages, DCs, and B cells[172]. The gene regions responsible for encoding the HLA system are highly polymorphic. This polymorphism allows for immune responses to be mounted against a variety of rapidly evolving microbial pathogens[173].

Approximately 40% of the genetic risk for T1D is associated with the HLA class II locus, which is responsible for providing activation signals to $CD4^+$ T-cells[174]. Class I HLA proteins present peptides to the MHC class I complex on $CD8^+$ T-cells, whilst class II HLA proteins present peptides to the MHC Class II complex on $CD4^+$ T-cells[175]. In T1D and other autoimmune diseases, HLA genes are linked to disease development due to the presentation of 'self' epitope peptides, which activate immune cell populations and trigger an autoimmune cascade[176]. Molecular mimicry may also play a role here, with viral epitope presentation potentially triggering islet autoimmunity through antigen cross-reactivity[177]. However, molecular mimicry has not been established as a causative factor in T1D, with research on this topic being highly controversial[178]. HLA polymorphisms within the HLA class I locus have also been associated with an increased risk of T1D, highlighting the role of cytotoxic $CD8^+$ cells in the development of T1D[179].

Other genetic variants not associated with HLA impact on the risk of T1D. Many of these genes are associated with beta cell function or T-cell function. The insulin gene has been linked to the genetic risk of T1D. If proinsulin or insulin is not expressed well in the thymus, insulin-autoreactive T-cells are more likely to escape selection[180, 181]. Other linked genes include CTLA4, IL2RA, and PTPN22, all of which are associated with T-cells[182]. Taken together, genetic evidence highlights the crucial role of the adaptive immune response in the development of T1D.

Due to the well-characterised genetics of T1D, genetic risk scores can now be calculated with high levels of accuracy. Based on 67 single-nucleotide polymorphisms, T1D could be identified in the UK Biobank with an area under the curve of 0.92[183]. Risk scores can contribute towards disease prediction, which is vital for surveillance and early treatment intervention.

T1D-associated haplotypes are present in approximately 95% of T1D patients[184]. Only 5% to 15% of those with T1D-associated haplotypes will go on to develop T1D themselves in the general population[133, 185]. Therefore, environmental factors, in addition to genetic risk factors, are required for the manifestation of T1D.

1.3.2.2 Environmental Factors

Whilst strongly predictive, genetics and even the presence of autoantibodies (Section 1.3.2.3) do not definitively predispose the development of T1D. A key observation indicating the importance of environmental factors is that individuals migrating from a low-incidence T1D country to a high-incidence country have an increased risk of developing T1D[186-188].

Suggested environmental risk factors have been identified primarily through epidemiological data. Factors proposed include the gut microbiome, which is also being investigated for a whole range of autoimmune diseases. Low levels of vitamin D and other dietary factors are being investigated[189]. Not all environmental factors are negatively associated with T1D. Examples of protective environmental factors include omega-3 fatty acid intake, extended breastfeeding periods, and intestinal microbiome diversity[190, 191]. These environmental factors have not yet been extensively studied. The difficulty in defining causative factors in T1D may be explained in part by the heterogeneity of T1D[164].

The most studied T1D-linked environmental factor is viral infections, particularly enteroviruses, which are associated with T1D development. Epidemiological data from coxsackieviruses (CVB) and the onset of T1D suggest a linkage, with many children with T1D having serological evidence of an enteroviral infection[167, 192, 193]. Evidence of an increased risk of T1D was observed following

CVB1 infections[194]. T1D diagnoses peak during the winter months, which coincides with the peak incidence of viral infections[195]. However, definitive causal relationships between viral infections and beta cell autoimmunity have yet to be established due to conflicting evidence. Analysis of pancreatic autopsy samples reveals limited evidence of viral infections[196].

The mechanism of viral infections leading to beta cell autoimmunity has also yet to be established. Viral infections may also exacerbate beta cell endoplasmic reticulum (ER) stress. Viral infections may increase the demand for insulin, adding metabolic stress to the beta cells and initiating the development of T1D[197]. While mouse models have been used to attempt to prove these hypotheses, a molecular mechanism based on human data remains undefined[198]. The evidence for viral involvement in T1D remains controversial.

1.3.2.3 Autoantibody Development

Autoantibody development is a hallmark of T1D and is highly predictive of T1D development. The best-characterised autoantibodies in T1D recognise the insulin B-chain peptide (IAA), glutamic acid decarboxylase 65 (GADA), insulinoma-associated protein 2 (IA-2A), and zinc transporter 8 (ZnT8A)[199]. Autoantibodies can be measured rapidly in patients' serum, allowing for the testing of genetically susceptible families[200]. The time from seroconversion (the presence of autoantibodies) to the onset of T1D is highly heterogeneous and depends on the number of autoantibodies present. A person with a single autoantibody is at a low risk of developing T1D. If two or more autoantibodies are present, particularly over multiple tests, there is an almost 100% chance of developing T1D[201].

Autoantibodies are not a major driver of beta cell death on their own. Islet-specific autoantibodies can be transferred from a mother with T1D to their foetus[202], and these children have a similar risk of developing T1D if they have a father with T1D, without transfer of autoantibodies. This data provides evidence that autoantibodies passed from mother to foetus

do not damage the foetal beta cells[203]. However, as antibodies are predominantly beta cell-specific, the presence of multiple autoantibodies can represent beta cell damage and insulitis.

1.3.2.4 Insulitis

Insulitis is defined as an inflammatory infiltrate surrounding pancreatic islets containing 15+ immune cells (defined by the CD45 cell marker) present in at least three islets[204]. Upon diagnosis, T1D patients have insulitis in 10% to 30% of their insulin-positive islets[205]. Meta-analysis indicates that insulitis is present in 73% of newly diagnosed patients aged 0-14 years, compared to 29% in those aged 15-39 years[206, 207]. As insulin-positive islets can be present in patients up to 50 years post-diagnosis of T1D, insulitis-mediated destruction of beta cells is heterogeneous[208, 209]. In both newly diagnosed and long-term T1D patients, islets without beta cells are present (pseudo-atrophic islets) and may constitute a significant proportion of the islet mass. Insulitis is rare in these insulin-negative islets, with the majority of insulitis occurring in islets containing beta cells[210, 211]. This pathology data indicates that insulitis occurs steadily over a long period in T1D, affecting beta cells asynchronously.

Insulitis is problematic to study from human samples. Islets represent only two percent of the pancreas[212], and islet biopsies are infrequently collected due to the side effects of the surgery. As insulitis is transient, biopsies may miss instances of insulitis[137]. Therefore, the NOD mouse has been used extensively to model insulitis. Insulitis is more extensive in the NOD model than in humans[151, 213], with insulitis in BB rats more closely resembling human insulitis[214]. Inferences regarding insulitis from rodent models should be interpreted with caution.

Insulitis induction occurs through the activation of PRRs on beta cells. Human islets exposed to IL-1β and IFN-γ, or infected with CVBs, can upregulate TLR3, RIG-I, and MDA-5[196, 215]. PRR ligands, such as dsRNA from damaged beta cells, can also interact with TLR3, activating transcription factors like IRF-3 and NF-κB. These transcription factors stimulate beta cells to produce type I interferons, chemokines, or trigger apoptosis through ER stress[216-218]. The production of IFN-α

and IFN-β results in the activation of the STAT-1 transcription factor, which further stimulates the production of interferon and chemokines, as well as the overexpression of MHC molecules[217, 219]. Apoptosis of beta cells amplifies insulitis by providing further danger signals to surrounding beta cells.

Beta cells are uniquely susceptible to stress due to their high metabolic burden and the quantity of insulin they secrete. In T1D, the genetic markers of ER stress are CHOP and BiP[220]. Response to inflammatory cytokines or viral infections can trigger ER stress and apoptosis in human beta cells[221, 222]. The overload hypothesis theorises that environmental pressures may cause excessive strain on the beta cells, which sensitises them to autoimmunity[197]. ER stress can trigger beta cell dysfunction, rendering cells unable to convert proinsulin into its active form, insulin. Misfolded insulin may also accumulate in the ER during periods of stress[223]. Misfolded insulin may be more antigenic than native insulin, further predisposing stressed beta cells to immune targeting[168].

Beta cell antigens, such as proinsulin, are recognised by APCs. Once processed, the antigen can then be presented via class II MHC molecules to T-cells[224]. Beta cells and activated lymphocytes produce additional chemokines and cytokines[225]. Chemokine production recruits leukocytes from pancreatic lymph nodes, which in turn produce additional inflammatory mediators, thereby perpetuating further beta cell destruction[226]. Therefore, chemokines act as vital mediators in the feedforward loop of insulitis.

A key step in the development of T1D is the loss of central and peripheral self-tolerance, resulting in the formation of autoreactive T-cells that recognise beta cell antigens. Autoreactive T-cells are considered the main effectors of beta cell destruction[227], and will be discussed in Section 1.3.2.5. Insulitis can also be characterised by defects in peripheral tolerance, including impaired Treg function, which genetic polymorphisms can influence in genes such as IL2RA, CTLA4, and IL-10[228].

During insulitis, insulin-positive beta cells exhibit abnormal patterns of insulin release. Data from NOD mouse models demonstrate that beta cell dysfunction occurs during insulitis. Islets from NOD mice can regain their regular pattern of insulin secretion when isolated and cultured *in vitro* for seven days, free from the inflammatory milieu of insulitis[229]. Crucially, this has been replicated using human samples. Beta cells taken from T1D organ donors had preserved insulin release when stimulated with glucose. However, their first-phase insulin release was defective[230]. Islets isolated by biopsy from newly diagnosed T1D patients recovered their function when cultured[231]. Due to the islets' ability to regain their first-phase insulin release at this stage, this may represent a key targetable stage in the development of T1D, if patients can be identified who retain a significant proportion of their beta cell mass.

1.3.2.5 Beta Cell Death and T-cells

The most common infiltrating cell type in insulitis is the $CD8^+$ T-cell[232]. Alongside T-cells being the focus of thymic selection to prevent autoreactive T-cells, they also require three activation signals to differentiate into effector cells. Naïve autoreactive $CD8^+$ cells can home to sites of insulitis from pancreatic lymph nodes, where they first encounter antigens displayed on APCs[233, 234]. $CD8^+$ T-cells can then receive co-stimulation and cytokine exposure from resident APCs[235, 236]. $CD8^+$ cells can then home to sites of insulitis by following chemokine gradients created by beta cells and recruited leukocytes[237, 238]. Stressed beta cells upregulate the display of beta cell antigens via their MHC class I molecule, providing the antigen stimulus[239]. Activated autoreactive $CD8^+$ cells can then mediate direct beta cell killing through the release of TNF-α, IFN-γ, FASL, and perforin[240-242]. Other beta cells then display the released beta cell antigens, making themselves targets for the now-activated autoreactive $CD8^+$ cells[243]. The positive feedback loop can now propagate, with more insulitis yielding more beta cell death (**Figure 1.6**).

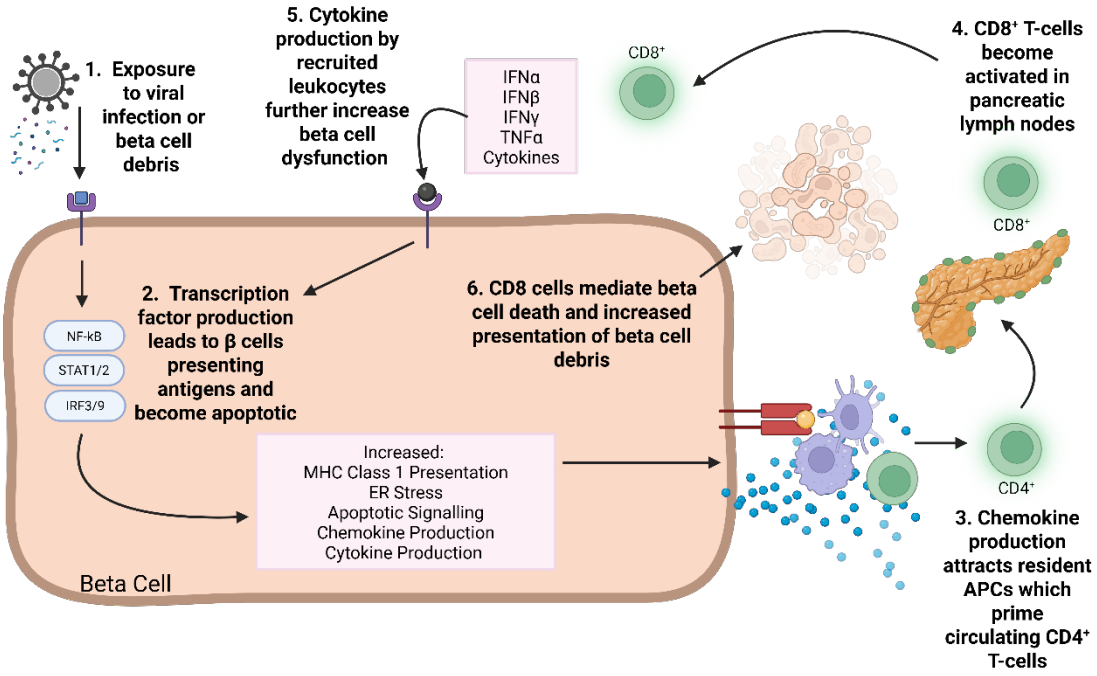

Figure 1.6 – Beta cell death in T1D. Exposure to a viral infection or beta cell debris triggers an intracellular signalling cascade in beta cells. Transcription factor production leads to the upregulation of MHC class I molecules, the production of chemokines and cytokines, and ER stress. Beta cell antigens are presented to APCs, providing activation signals to $CD4^+$ and $CD8^+$ T-cells. Autoreactive $CD8^+$ T-cells can migrate from the pancreatic lymph nodes to the site of insulitis, producing more cytokines and leading to beta cell apoptosis. Adapted from Eizirik et al[154]. Figure made in Biorender.

Autoreactive $CD4^+$ T-cells also play a role in the development of T1D[244]. Autoreactive $CD4^+$ cells can be exposed to beta cell antigens, via APCs, in the pancreatic lymph nodes during circulation[245]. This exposure can differentiate naïve $CD4^+$ cells into distinct $CD4^+$ lineages. $CD4^+$ Th1 cells are pro-inflammatory and enhance antigen presentation in the pancreatic lymph nodes. Th1 cells then migrate to the pancreas, secreting pro-inflammatory cytokines that induce beta cell death[246]. $CD4^+$ T-cells play a pivotal role in presenting antigens. Both autoreactive $CD4^+$ and $CD8^+$ cells have been identified in T1D patients. $CD8^+$ autoreactive cells that recognise insulin, IA-2A, and GAD65 have been identified in T1D biopsy samples[247]. $CD4^+$ cells cultured from pancreatic islets were shown to recognise proinsulin peptides[248]. GAD65 autoreactive $CD4^+$ cells and IGRP autoreactive $CD8^+$ cells have been detected in the circulation of T1D patients who received pancreas transplants. The presence of these autoantibodies was associated with T1D recurrence in these patients[249].

Adoptive transfer experiments using the NOD model have significantly contributed to the understanding of the pathogenic roles of T-cell populations in T1D. Transferring immune cell populations from NOD mice to NOD mice with severe combined immunodeficiency (SCID), which have no functioning immune cells, has aided understanding of which immune populations are required for T1D development (**Figure 1.7**). The majority of evidence indicates that both $CD4^+$ and $CD8^+$ cells are required for T1D development[250]. However, studies have shown that $CD8^+$ cells can induce diabetes in NOD-SCID mice, even in the absence of $CD4^+$ cells[251]. The requirement for $CD8^+$ cells in T1D was also confirmed in adoptive transfer experiments using the BB rat model[252]. MHC class I-deficient NOD mice were resistant to T1D, again implicating the role of $CD8^+$ T-cells in T1D pathogenesis[253, 254]. In the absence of $CD4^+$ cells expressing the MHC class II molecules, T1D progression was slowed, and $CD8^+$ cells did not achieve 'optimal' effector functions'[244]. Information gathered from mouse models and human data has rapidly advanced the understanding of insulitis and beta-cell death, guiding the development of new treatments for T1D.

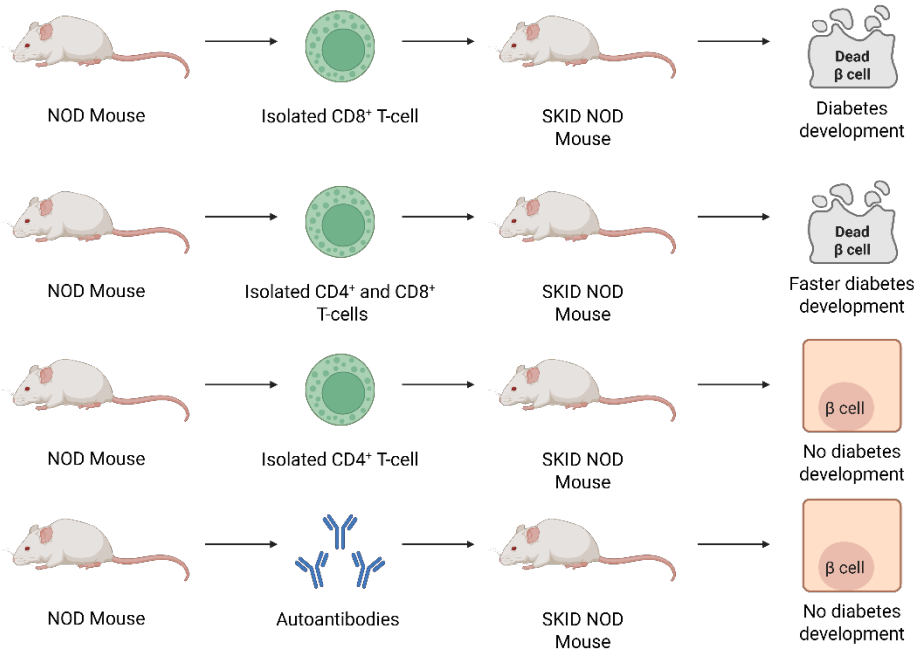

Figure 1.7 – Adoptive transfer experimental overview. Adoptive transfer experiments are commonly used to determine which immune populations can transfer type 1 diabetes (T1D) to a mouse model without a functioning immune system. Immune cells are isolated from non-obese diabetic (NOD) mice and transferred into an NOD mouse with severe combined immunodeficiency (SCID). The transfer of $CD8^+$ T-cells results in the development of T1D. The transfer of both $CD8^+$ and $CD4^+$ T cells also contributes to the development of T1D. The transfer of $CD4^+$ T-cells or autoantibodies alone fails to result in T1D development in NOD SKID mice. Figure made in Biorender.

1.3.3 T1D Treatments

Historically, glycaemic control has been the primary aim in the management of T1D, to minimise further complications in patients[255]. In the era of immune targeting therapies, the aim of T1D treatments is now focused on prevention or delay. While the prevention of T1D has not yet been possible, the discovery of new treatments has demonstrated that it is now possible to delay the development of stage three T1D (**Figure 1.5**)[256].

In studying T1D clinical trials, the endpoints typically include C-peptide levels. C-peptide is cleaved from proinsulin during the production of insulin by the beta cell. Therefore, C-peptide is used as a proxy for insulin production or beta cell function[257]. Standard endpoints to measure key aspects of blood glucose control also include a patient's insulin dosage to achieve glycaemic

stability, their glycated haemoglobin levels (HbA1c), and the number of hypoglycaemic events[258, 259].

1.3.3.1 Insulin Therapy

Treatments for patients with T1D have primarily focused on insulin therapy. Historically, this was the only treatment that extended a patient's life. Injectable insulin revolutionised T1D treatment, preventing death by ketoacidosis and reducing the risk of macro- and microvascular complications[260]. Subcutaneous insulin is injected several times per day, but patients may still experience hypoglycaemic episodes and may necessitate further treatment[261]. New technologies, such as insulin pumps, can automatically inject insulin and have been associated with improved glycaemic control and a greater sense of well-being in patients[262]. Continuous glucose monitoring devices, available on smartphones, have also revolutionised glucose management and eliminated the need for capillary sampling[263]. It is worth noting that such devices require frequent changing, are not without discomfort for patients, and induce a mental health burden on patients due to the level of self-management required[264]. The development of insulin analogues has enabled longer-acting insulin therapies, resulting in fewer insulin infusions[265].

1.3.3.2 Islet Transplantation

Islet transplantation is indicated as a treatment option for T1D patients who have recurrent episodes of severe hypoglycaemia and are nonresponsive to other medical interventions[266]. Islet transplantation is considered safe, minimally invasive, and can result in long-term glycaemic control with minimal hypoglycaemic events post-transplant[267, 268]. Patients' quality of life has been vastly improved post-transplant due to improvements in T1D symptoms and reduced insulin requirements[269].

However, there is a limited supply of donor pancreases that fit the requirements for transplant. Islet isolation is a technically complex process that requires specialist centres[270]. Only a small

number of islets survive transplantation, meaning that an excess of islets is required when transplanted. Inflammation and hypoxia are primarily responsible for the rapid and progressive loss of beta cells post-transplant[271]. Islet isolation places a large amount of stress upon the beta cells due to mitochondrial dysfunction, ER stress, ischemia, and slow revascularisation[272]. Isolated islets from at least two pancreases are required to transplant enough islets to a patient[273]. Currently, there is not enough human tissue to treat all patients who could benefit from islet transplantation. Approximately five years post-transplant, only 50% of patients maintain insulin independence[274]. Immunosuppressive medications are required with transplantation, and side effects bring harm to the patient's quality of life[275]. Currently, islet transplants are not curative for T1D.

To expand the number of available islets, stem-cell-derived beta cells (SCBCs) have been suggested as a transplant option[276]. New protocols have enabled the differentiation of mature beta cells, demonstrating mature cell markers[276]. Transplanted SCBCs have effectively controlled blood glucose in animal models. A clinical trial evaluating the efficacy of a single infusion of SCBCs in T1D demonstrated improved glycaemic control and eliminated the need for insulin[277]. A further trial demonstrates interim one year outcomes in a phase one trial of transplanted SCBCs, showing improved glucose control in patients[278].

SCBCs could even be created from a patient's cells and transplanted in an autologous transplant[279]. Such procedures would remove the need for immunosuppressive medication. With autologous SCBCs, there is a risk that the patient's immune system could once again mount a response and target the transplanted 'self' beta cells[280]. This risk can be mitigated by transplanting the cells in a protective capsule[281]. All described therapeutic avenues are being intensely studied.

1.3.3.3 T-cell targeted therapies

The first immune-targeting therapy for T1D was cyclosporine. Cyclosporine is an inhibitor of a protein phosphatase, called calcineurin, which is required for T-cell activation[282]. Newly diagnosed patients briefly went into remission but relapsed post-treatment. Due to the side effects of cyclosporine, such as cancer and nephrotoxicity, long-term usage was prohibited[283]. Autologous hematopoietic stem cell transplant (HSCT) has also been investigated as a potential treatment to reverse T1D. The immunosuppressive regimen post-transplant included anti-thymocyte globulin (ATG), which targets T-cells[284]. Initial evidence was promising, with 20 out of 23 patients being insulin-free four years post-transplant. Only 3/23 patients remained insulin-free six years post-transplant[285]. Whilst disappointing, such therapies provide robust evidence behind the pathogenic role of T-cells in the development of T1D.

To prevent beta cell death after islet transplantation, various immunosuppressive regimens have been trialled. Insulin independence at one year post-operation has improved from 10%[286] to 58% using the Edmonton protocol[287]. This protocol included daclizumab, an anti-CD25 antibody that targets activated T-cells, an mTOR inhibitor that blocks IL-2 signalling, and a calcineurin inhibitor (described above). The targets of these three drugs are components required for the activation of cytotoxic T-cells. Despite this, chronic immunosuppression remains an issue for patients following transplantation[288].

Teplizumab is the first FDA-approved treatment for prolonging the time patients spend in stage two of T1D, before progressing to clinical stage three, where insulin therapy is required[289]. Particularly in young patients, the time before stage three development is associated with a considerable improvement in quality of life and a prolonged lifespan[290]. Patients who received teplizumab, on average, took 48.8 months to develop stage three T1D, which is twice the time compared to the placebo group[289].

Teplizumab is an anti-CD3 monoclonal antibody administered as a two-week infusion[145]. Teplizumab binds to the CD3/TCR complex present on T-cells, resulting in apoptosis or the development of tolerance. The exact mechanism of action is unknown, but teplizumab is believed to prevent the expansion of autoreactive $CD8^+$ cells and promote an exhausted, anergic phenotype of $CD8^+$ cells, while retaining Treg activity[291]. It has been reported that an immunological response persisted in a subset of patients at seven years post-treatment, characterised by an increased frequency of anergic $CD8^+$ cells expressing the inhibitory receptor PD-1[292].

A variety of studies in phase two and phase three clinical trials have demonstrated that teplizumab can prevent a decline in beta cell mass, preserve C-peptide levels, and result in reduced insulin needs in newly diagnosed T1D patients[292, 293]. Teplizumab is well tolerated when administered as one or two 14-day infusions. The most common side effects include a rash, nausea, and lymphopenia, which are typical signs of low-grade immunosuppression[145, 293-296]. If teplizumab were to be administered more frequently, there is a risk of patients developing more significant immunosuppression. Therefore, further infusions are unlikely to be trialled.

Further T-cell targeting therapies include a low dose of ATG, which is purified rabbit serum that contains cytotoxic IgG antibodies against T-cells. ATG was seen to slow the rate of beta cell decline but may be inferior to teplizumab, as repeated exposure may cause serum sickness[297]. Alefacept is a protein that binds to the costimulatory CD2 molecule on effector T-cells. Despite beneficial effects, including reduced insulin requirements, at 12 months post-treatment, there was no effect on C-peptide levels compared to placebo[298]. Abatacept is a CTLA-Ig fusion protein that prevents stimulation of the T-cell CD28 molecule. Again, despite beneficial early data[299], abatacept failed to delay the progression of T1D in humans[300].

1.3.3.4 Other Immune Targeting Therapies

Other immune targets have been investigated for T1D. Rituximab, an anti-CD20 monoclonal antibody targeting B-cells, was trialled in recent-onset T1D patients. After two years, there was no difference in C-peptide levels between the treatment and placebo groups[301]. Infusions of isolated and expanded patient Tregs have demonstrated good safety and tolerability profiles[302]. Treg therapies aim to re-establish tolerance by using the Tregs to suppress autoreactive T-cells. Only 50% of patients retained their insulin production two years post-treatment in a phase one trial[303]. Treg therapies were then trialled combined with low-dose IL-2, a cytokine required by both cytotoxic $CD8^+$ cells and Tregs for their development. The addition of IL-2 resulted in off-target expansion of $CD8^+$ cells[304]. Rituximab was also investigated alongside Treg therapies, which demonstrated superiority in maintaining T1D remission compared to either monotherapies and is being investigated further[305].

Targeting inflammation has had modest success. Targeting TNF-α has been investigated using anti-TNFα monoclonal antibodies such as golimumab and etanercept[306]. Golimumab has demonstrated preserved C-peptide levels compared to placebo at a two year follow-up and is now being further investigated[307]. Baricitinib, a JAK1 and JAK2 cytokine inhibitor, demonstrated significantly higher C-peptide levels than the placebo at 48-week follow-up, but it did not affect HbA1c[308]. Imatinib, a small tyrosine kinase inhibitor, also showed preserved C-peptide levels compared to the placebo at a one year follow-up, but no effect was observed at a at two year follow-up[309].

The treatments described above have been curative or shown significant effects in rodent models of T1D. Rituximab reversed T1D in the NOD mouse[310]. Treg therapies reversed T1D in the NOD mouse[311], and a CD3-antibody reversed T1D in the NOD mouse[144]. Despite the promise of treatments in NOD models, current T1D treatments do not yet prevent the development of

diabetes in humans. Teplizumab and low-dose ATG remain the most effective current treatments, according to a recent meta-analysis, but the risk of immunosuppression was noted[298].

Trialling a combination of therapies is now a significant source of investigation, but this is limited by the need to have individual clinical trials for each treatment to meet safety requirements. Due to pharmaceutical companies' reluctance to test their drugs against competitors, gathering information on the effectiveness of one treatment compared to another remains challenging. Pharmaceutical companies may not be enticed to enrol their drug in a combination trial if their competitor's monotherapy appears more effective, despite the potential success of the combination therapy. It also remains a concern that most clinical trials compare a treatment to a placebo, rather than to another treatment. Therefore, T1D patients are limited in their current treatment options. Immune-targeting therapies should be explored to avoid immunosuppression.

1.4 The Role of Chemokines in T1D

Pathogenic autoreactive T-cells have been identified as the primary perpetrators of beta cell destruction[227]. Targeting T-cells using teplizumab has yielded modest success in T1D treatments, delaying the progression of stage two T1D to stage three for an average of 48 months[292]. Due to the risk of immunosuppression associated with further infusions of teplizumab, investigating mechanisms to target T-cells within the islet microenvironment may be beneficial for T1D patients. Disrupting the T-cell chemokine axis is a proposed pathway[312].

Chemokines have been implicated in the pathogenesis of T1D (**Table 1.2**)[312]. However, deducing the role of specific chemokines in T1D is a complex process. In T1D, chemokines are produced by beta cells, alpha cells and delta cells within the islets in response to the insulitis microenvironment. Recruited immune cells also produce chemokines[154]. Chemokines can be profiled using techniques such as ELISA using peripheral blood samples. An increase in

chemokines associated with $CD4^+$ Th1 T-cells, such as CCL3 and CXCL10, can be detected in the serum of recently diagnosed T1D patients[313-315]. CCL3 levels found in serum were correlated with a decline in C-peptide in T1D patients, but there was considerable overlap in chemokine expression between T1D patients and control subjects[316]. The pathogenic process of T1D occurs in the islet microenvironment and the draining lymph nodes within the pancreas[236]. Approximately two percent of the pancreas tissue is composed of islets, meaning chemokines produced by islets are unlikely to be reflected in circulation[154]. Data obtained from peripheral blood will therefore be unlikely to reflect the chemokines in the islet microenvironment.

Table 1.2 – Chemokine expression in T1D

Species	Tissue Location	Implicated chemokine
NOD mice	Islet RNA	CCL2, CCL4, CCL5, CCL19, CCL22, CXCL9, CXCL10, CXCL11, CXCL13, XCL1[317]
LCMV mice	Islet RNA	CXCL9, CXCL10, CXCL11, CCL5[318]
LCMV mice	Islet RNA	CXCL9, CXCL10, CXCL11, CCL5[319]
T1D patients	Serum	CXCL10[314, 315, 320]
Individuals at high risk for T1D	Serum	CCL3, CCL4[313]
Newly diagnosed T1D patients	Beta cell IHC	CXCL10[321, 322]
T1D patients	Islet IHC	CCL5, CCL8, CXCL9, CXCL10, CX3CL1[323]
Cytokine-stimulated human islets	Islet RNA	CCL5, CCL8, CCL22, CXCL9, CXCL10, CX3CL1[324]
Newly diagnosed T1D patients	Islet RNA	CXCL10[323]

Another option is to use cadaveric islets from T1D patients. Islets can be isolated or tissue sections procured from an autopsy. Immunohistochemistry (IHC) can be used to identify chemokines in tissue sections, or tissue can be sent for RNA sequencing (RNA-seq)[323, 325]. Due to the lack of available tissue from biopsies and cadaveric islets, deceased healthy donor islets can be stimulated with cytokines to mimic the early stages of insulitis[323]. Human tissue is

challenging to procure, even from healthy donors. Commonly used models are therefore rodent models of T1D, including the NOD mouse[139]. The strengths and weaknesses of models used to deduce the chemokines in T1D will be discussed below.

1.4.1 Rodent Chemokine Data

The benefit of using rodent models rather than studying human tissue is that genes can be knocked out or deleted, often referred to as KO models. Knocking out chemokines or chemokine receptors provides investigators with specific information about the role of a chemokine or receptor in T1D rodent models. Inducible T1D models are often used to study T1D in this way, as researchers can observe the time point at which T1D development is induced, which is challenging to study in spontaneous NOD models.

In NOD mice, IL-1β and IFN-γ levels increased steadily as insulitis developed, starting from six to eight weeks of age[317]. This data highlights the rationale behind cytokine-stimulating islets with such chemokines to mimic insulitis. CCL2, CCL4, CCL5, CCL19, CCL22, CXCL9, CXCL10, CXCL11, CXCL13, and XCL1 were detected via transcriptome analysis of NOD islets[317]. Upregulation of the chemokine receptors CCR2, CXCR4, and CXCR6 was observed on leukocytes present in the islets during insulitis between eight and 16 weeks of age. Several chemokine transcripts were not present at four and six weeks of age, demonstrating that chemokine and chemokine receptor expression increased as insulitis developed[317]. CCL2 mRNA expression was also observed to increase over time as insulitis develops, peaking at eight weeks[326]. NOD mice also demonstrated upregulated mRNA CXCL10, CCL2,CCL7, CCL12 and CCL5 upon transfer of inflammatory $CD4^+$ Th1 cells[327]. Such evidence highlights the role of multiple chemokines in the spontaneous development of T1D, with chemokine levels increasing as insulitis progresses.

Another T1D model is a transgenic mouse expressing a viral glycoprotein on their beta cells. When exposed to a lymphocytic choriomeningitis virus (LCMV), mice develop T1D rapidly, T-cells infiltrate their islets, and beta cells are destroyed[328]. Post-infection, the expression of RNA for

CXCL9, CXCL10, CXCL11, and CCL5 significantly increased[318]. To study the role of chemokines in disease induction, CXCL10 was blocked with an anti-CXCL10 antibody at the time of viral delivery. With CXCL10 blockade, 70% of mice did not develop T1D, insulin production was preserved, and cellular infiltration was abrogated. If CCL5 or CXCL9 were blocked separately, T1D still developed[318].

In the same LCMV transgenic model, mRNA expression of CXCL9, CXCL10, CCL2, and CCL5 was significantly upregulated, alongside expression of IL-1β, TNF-α, and IFN-γ. A CXCR3 KO significantly delayed T1D onset and reduced T-cell infiltration, but was not preventative[319]. Targeting of CXCL10 has also been trialled in LCMV models of islet transplantation. LCMV mice were infected and then received islet engraftments from CXCL10 KO LCMV mice or control LCMV mice. Islets from control mice were all destroyed by day 30 post-transplant, whereas 58% of mice retained functional islet mass from the CXCL10 KO islets and showed reduced islet infiltration[238]. An anti-CXCL10 antibody was then trialled alongside islet engraftment, and 25% of mice demonstrated islet retention and insulin production[238]. This data was neatly repeated in a streptozotocin (STZ) inducible model[328]. CXCL10 KO mouse islets reversed T1D in STZ-induced diabetic mice, and an anti-CXCL10 antibody significantly improved the rate of normoglycemia restoration compared to a control antibody[329].

Further evidence for targeting the chemokine network in T1D comes from the M3 protein, which was identified in the murine herpesvirus 68. The M3 protein has previously been characterised as a broad-spectrum chemokine inhibitor[75]. NOD mice demonstrated age-dependent increases in chemokine expression, which correlated with the infiltration of cells into the islets within NOD mice[330]. NOD mice were then created that expressed the M3 protein exclusively on their beta cells. As expected, 80% of the WT NOD mice developed T1D. Expression of M3 prevented the development of T1D in all 66 mice (**Figure 1.8**). Mice had no infiltration within their islets but had infiltration in other organs, demonstrating site specificity[331]. Using an inducible STZ model, no

mice developed T1D when they expressed the M3 protein selectively on their beta cells[330]. Unfortunately, the M3 protein is unsuitable for clinical translation. As a viral protein, there is a considerable risk of immunogenicity if it were to be administered to a patient. However, this work clearly emphasises the role of chemokines in the pathogenesis of T1D.

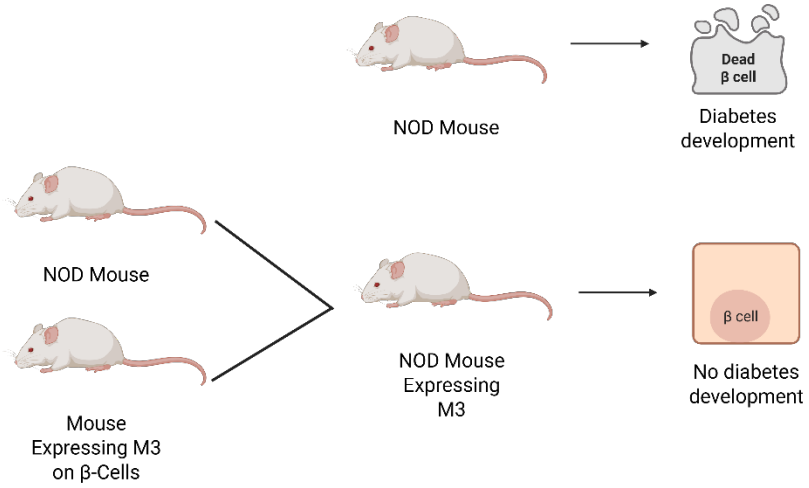

Figure 1.8 – Selective expression of viral M3 protein on beta cells prevents T1D in the NOD mouse. Non-obese diabetic (NOD) mice spontaneously develop type one diabetes (T1D). The M3 protein is a pan-chemokine-inhibiting viral protein derived from the herpes virus. NOD mice were engineered to express the M3 viral protein selectively on their beta cells. The selective expression of M3 on beta cells within NOD mice prevented the development of T1D. Figure made in Biorender.

The role of chemokines in the pathogenesis of T1D in NOD models is further exemplified with the use of the decoy CC chemokine receptor, D6[332]. NOD mice were generated that express the D6 receptor exclusively on their beta cells, which reduced the severity of insulitis and lymphocyte infiltration[333]. Compared to the total prevention of T1D development by the pan-chemokine M3 protein, D6 beta cell expression prevented the development of T1D in 60% of NOD mice by day 84[333]. This difference suggests that targeting both CC and CXC chemokines prevents T1D to a greater degree than by blocking CC chemokines alone.

Rodent models have also been used to investigate combination therapies. Many trialled combinations have shown benefits over using teplizumab alone, including an IL-1 receptor antagonist[334], an anti-CD20 antibody[335], and an anti-CXCL10 antibody. In both NOD and LCMV models, anti-CD3 followed by anti-CXCL10 administration led to persistent remission of T1D. In

LCMV models, both monotherapies achieved remission in 38% and 36% of animals, respectively[336]. When both therapies were administered, 70% of mice achieved persistent remission, likely due to a significant reduction in lymphocyte infiltration into the islets. In NOD mice, 55% of the mice were classified as being in remission when both therapies were administered[336]. These studies imply that chemokines may be targetable for T1D therapies.

A caveat of the above research is the heavy reliance on mouse models of T1D, which utilise mouse chemokines. It is widely accepted that the mouse immune system is vastly different to the human immune system. There are several examples of chemokines for which there is no homologue in mice and vice versa. CXCL8 does not exist in mice, and CXCL15 does not exist in humans, for example[59]. In stroke models using human, mouse, and rat cells, marked differences are observed in chemokine expression levels, even at baseline, and in homologous chemokines[337]. Information regarding the effects of chemokine targeting in preventing T1D in mouse models should therefore be treated with caution. Particularly in models using M3, the pan chemokine inhibitor was present on the islets prior to the development of T1D. In T1D, it would be unlikely to find patients who had no insulitis at all, making it challenging to target them prior to disease induction. Emphasis should be placed on successful interventions following the development of T1D, rather than prior to it.

1.4.2 Data from Human Tissue and Clinical Trials

Gene expression in human islets from T1D patients exhibits a profound upregulation in chemokine pathways[338]. Stimulation of human islets with cytokines such as TNF-α and IFN-γ led to the production of chemokines, including CCL5, CCL8, CCL22, CXCL9, CXCL10, and CX3CL1[323]. Despite this, the process of isolating human islets may stimulate chemokine production due to periods of ischemia and reperfusion[339]. A solution to this would be to use control islets that come from healthy individuals or have not been cytokine-stimulated.

Stained pancreas sections of three newly diagnosed patients demonstrated CXCL10 expression on beta cells[321]. The corresponding chemokine receptor, CXCR3, was highly expressed by infiltrating T-cells[321]. These findings were confirmed in five additional newly diagnosed patients, who also identified beta cells as the primary source of CXCL10[322]. RNA from a further four T1D patients confirmed CXCL10 as the most abundant chemokine[323]. This evidence taken together implicates chemokines, particularly CXCL10, in the pathogenesis of T1D.

Following evidence that blocking CXCR1/2 in NOD and STZ models prevented and reversed T1D[340], a CXCR1/2 inhibitor was trialled in newly diagnosed T1D patients[341]. Ladarixin did not significantly affect C-peptide levels between the treatment and the placebo groups. A CXCR1/2 inhibitor has also been trialled to prevent islet cell death following transplantation. Based on promising mouse data, where CXCR1/2 blockade resulted in improved islet survival and reduced lymphocyte infiltration[342, 343], a CXCR1/2 inhibitor was tested in a phase two human clinical trial[342]. Patients who had undergone an islet transplant were given reparixin, a CXCR1/2 inhibitor, and compared to patients who only received the standard ATG immunosuppression. Grafts were lost in all three control participants. Of the four patients who received reparixin, all had significantly better post-transplant outcomes[342]. Unfortunately, when reparixin progressed to a stage three clinical trial, there was no significant difference in C-peptide levels between patients who received the treatment and those who received a placebo alongside regular immunosuppression[344]. Despite this, the above clinical trials highlight the pathogenic and targetable role of chemokines within T1D and islet transplantation.

The migration of autoreactive T-cells from the pancreatic lymph nodes to the sites of insulitis is mediated by chemokine gradients[154]. Targeting such chemokine gradients, potentially in combination with a T-cell inhibiting drug such as teplizumab, would mask the beta cells from their autoreactive killers. Despite the promise of such an idea, targeting chemokines therapeutically

has thus far failed to yield successful drugs that target inflammation through chemokine inhibition[103].

1.5 The Failure of Chemokine Targeting

Chemokines have been identified as therapeutic targets for inflammatory diseases[84, 345]. Despite their promise, only three chemokine or chemokine receptor-targeting drugs have progressed to the clinic. Maraviroc targets CCR5 and has been approved for the treatment of HIV[346, 347]. Plerixafor inhibits CXCR4 and treats hypogammaglobulinemia[348]. Mogamulizumab inhibits CCR4 for the treatment of T-cell lymphomas[349]. However, these drugs do not target inflammation or inflammatory diseases, and multiple chemokine-targeting drugs have failed to show benefits to patients in clinical trials[103, 350].

As described previously, one proposed reason behind the failure of chemokine targeting is chemokine network redundancy[101, 102]. Due to the complexity of the chemokine network, with multiple chemokine receptors present on various leukocyte subtypes and chemokines activating multiple chemokine receptors, targeting a single chemokine or chemokine receptor may not be sufficient to prevent aberrant inflammation. This functional redundancy is a theory behind the failure of chemokine-targeting drugs[350].

Chemokine-targeting clinical trials commonly target one chemokine or chemokine receptor[103]. By targeting a small portion of the chemokine network and failing, these trials reinforce the key argument behind chemokine network redundancy and may explain the failure of chemokine-targeting therapies. Chemokine production increases exponentially following the induction of inflammation or autoimmunity[351, 352]. By targeting a single chemokine or chemokine receptor, clinical trials have not been successful, as the redundancy of the chemokine network necessitates targeting multiple chemokines and receptors to thwart disease progression and chemokine feedforward amplification in inflammation[103, 353].

Another proposed argument is that pharmacological issues may have prevented success in chemokine targeting trials. The protein interface between a chemokine and its receptor is highly dynamic and therefore challenging to target[354]. It has been proposed that high levels of chemokine receptor occupancy are required to affect chemokine receptor signalling[69]. Insufficient doses of antagonists have also been extensively reviewed as a failure of chemokine receptor targeting. Due to the feedforward nature of chemokine and chemokine receptors, upwards of 90% of receptor occupancy may be required to establish a therapeutic effect[353].

When considering the CXCR1/CXCR2 receptor antagonists, which were trialled in newly diagnosed T1D patients and following islet transplantation, chemokine redundancy may explain the failure of reparixin and ladarixin. This failure may be explained by chemokine network redundancy, as well as the differences between mouse and human chemokine networks[148]. Between species, chemokines and receptors vary in their sequence and function. These differences are exemplified by small molecules having different affinities for CCR1 between human, rat, and mouse receptors of the same chemokine[355-357]. Coupled with chemokine redundancy, this may explain why 'curative'[144, 335, 358, 359] therapies in the NOD rodent T1D model either failed or were significantly less effective in human clinical trials[296, 360-362].

To target the chemokine network in inflammatory diseases and T1D, targeting multiple chemokines or chemokine receptors may be necessary due to chemokine redundancy. Newer developments in targeting inflammatory diseases focus on multiple targets, rather than a single chemokine or receptor. An exemplar is the monoclonal antibody LY3041658, which can inhibit seven CXC chemokines[363]. Inflammatory diseases can be characterised by the expression of 20+ chemokines[364, 365]. Therefore, knowing which chemokines and how many chemokines to target is difficult to estimate. Furthermore, targeting multiple chemokines or receptors poses a risk of immunosuppression, particularly when targeting chemokines involved in leukocyte homeostatic

trafficking, such as CCR7[366]. Despite this, targeting chemokines to modulate inflammation remains an attractive prospect that warrants further investigation.

1.6 Evasins

The evolution of promiscuous chemokine-targeting molecules by parasites and viruses underpins the validity of chemokine network redundancy[114, 115, 367]. Harnessing nature's endeavours to target the chemokines may allow us to successfully target the chemokine network in inflammatory diseases, such as T1D[331].

Ticks are parasitic blood sucking arachnids. They secrete a variety of proteins upon biting their host to evade immune detection. Anticoagulants[368, 369], analgesics[370], complement inhibitors[371], and proteins that neutralise components of the immune system[372], prevent the host from mounting an immune response to the bite. Natural selection has allowed ticks to develop these proteins, enabling them to feed for longer and obtain a larger blood meal[373]. Ticks also secrete classes of proteins called evasins. Over 50 evasins have been identified in ticks, which bind to chemokines and prevent them from interacting with chemokine receptors on host leukocytes[116, 374]. By preventing chemokines from interacting with their receptors, evasins prevent leukocyte migration to the bite site[375].

Ticks secrete two structurally unrelated subclasses of evasins. There are 21 known class A evasins (EVAA), which bind to and inhibit CC chemokines exclusively. EVAA are typically between 89 and 126 amino acid residues in length. Key examples of EVAA are evasin 1 (EVA1) and evasin 4 (EVA4)[376]. EVAA commonly have eight cysteine residues, forming four disulfide bridges. Crystal structures of evasins in complex with chemokines reveal their mechanism of action; the N-terminus of EVA4 binds between the N-loop and the third beta strand of chemokines[377]. The N-terminus of EVA1 interacts with the same chemokine region, and the C-terminus of EVA1 binds to the N-terminus of chemokines[378]. As these are key locations for chemokine and chemokine

receptor interactions, evasins thus prevent chemokines from binding to chemokine receptors. Through phylogenetic analysis, EVAAs have been subdivided into three classes, designated as A1, A2, and A3[374].

There are 29 known class B evasins (EVAB), which bind to and inhibit CXC chemokines exclusively. EVABs are between 60 and 100 amino acids in length, and the most commonly referred to EVAB is evasin 3 (EVA3)[375]. EVABs have six conserved cysteine residues and form three disulfide bridges, commonly referred to as a knottin structure[379]. EVA3 interacts with and prevents CXCL8 from forming dimers, thereby preventing interactions with CXCR1/2. EVA3 also disrupted CXCL8 from interacting with GAGs[380]. Class B evasins are subdivided based on which CXC chemokines they bind to. One subclass binds to CXC ELR+ chemokines, and one subclass binds to CXC ELR- chemokines[379].

Evasin proteins can bind to and neutralise multiple chemokines, while retaining chemokine class specificity[116, 381]. The promiscuous nature of evasins may be due to conformational plasticity[382], or differential segments of evasins may bind to different chemokines[383, 384]. As ticks require several days to feed on their host, they inject multiple evasins at the bite site to neutralise inflammation and prevent chemokine feedforward loops[84]. The three genera of ticks, *Rhipicephalus, Amblyomma,* and *Ixodes*, produce both classes of evasin proteins[116, 374]. The production of both CC and CXC chemokine inhibitors by all tick classes implies that the inhibition of both chemokine classes is required to overcome chemokine redundancy[116].

1.6.1 Evasin Identification and Development

Evidence for the first CXCL8-neutralising protein was found in the saliva of Ixodid ticks[385]. Chemokine binding proteins that could inhibit CXCL8, CCL2, CCL3, CCL5 and CCL11 were then identified[386]. The evasins EVA1, EVA3 and EVA4 were discovered[387]. EVA4 could neutralise 18 CC chemokines, demonstrating differences in the breadth of action between evasins. EVA3 bound exclusively to CXC chemokines, demonstrating evasin chemokine class specificity[375]. A crystal

structure of CCL3 bound to EVA1 was the first of its kind, revealing the binding location of evasin to CC chemokines and the mechanism of action[388].

The Bhattacharya group utilised the position-specific iterative-basic local alignment search tool (PSI-BLAST) to search for homologous sequences to the evasins EVA1, EVA3 and EVA4[389]. By screening 350 sequences against CC chemokines using yeast surface display, 26 CC-binding evasins were identified[389]. The Stone group validated an additional 250 sequences through homology searching, yielding eight further evasins[390]. Crucially, two evasins identified by both groups overlapped. Further work by the Bhattacharya group characterised 27 CXC-binding evasins[379]. First identified using yeast surface display, the class B evasins were denoted by their tick genus: Ixori (*Ixodes*), Rhisa (*Rhipicephalus*), and Ambca (*Amblyomma*). The newly identified class B evasins were expressed and screened for chemokine binding using biolayer interferometry (BLI)[379]. Out of the 27 evasins, 26 bound to CXC chemokines and showed specificity for either ELR+ or ELR- chemokines[379]. Sequence alignment indicated that the EVABs shared between 26% and 50% sequence identity, and X-ray crystal structures of the evasins EVA3 and P1142 were obtained, identifying the knottin disulphide structure of EVAB[379]. Specificity for ELR+ or ELR- chemokines was transferred between EVA3 and P1142 by generating hybrid evasins with swapped knottin loops, implying that the knottin structure of loops determines CXC-chemokine binding promiscuity[379].

The Bhattacharya group engineered evasins to increase their chemokine binding breadth[391]. The terminal 29 residues of EVA1 were replaced with 44 amino acid residues of the EVAA P672. By doing so, EVA1 gained the ability to bind to CCL8[391]. N-terminal domain swapping to increase chemokine binding ability was neatly repeated[392]. The Bhattacharya group then went on to design dual chemokine class binding evasins, termed ‘double-warhead’ and ‘triple-warhead’ evasins[393]. Combining EVAB P1156 and EVAA P1243 through a GGGGS linker demonstrated dual class binding but could not bind to all chemokines that their respective evasins could[393].

Combining EVA3 (Class B, CXC ELR+ binding evasin), P1142 (Class B, CXC ELR- binding evasin) and P991 (Class A, CC binding evasin) created an evasin called P1834 capable of binding to 14 CC and CXC chemokines (produced by the Bhattacharya laboratory, unpublished).

1.6.2 Evasins in Inflammatory Models and Limitations

EVA1, EVA3 and EVA4 have robustly demonstrated in vivo efficacy in inflammatory models. In mouse models, EVA1 demonstrated effectiveness in models of GVHD[394], pulmonary fibrosis[395] and psoriasis[375]. EVA3 has demonstrated effectiveness in rodent models of ischemia-reperfusion injury[396], pancreatitis[397], and arthritis[375]. EVA4 is effective in rodent models of myocardial inflammation[398] and colitis[399].

Pharmaceutical companies have not pursued evasins, despite their successful publication record. As a non-human protein, if administered to a patient, evasins could lead to an immunogenic reaction. Immunogenicity was reported with EVA1 in a mouse model, resulting in an immunoglobulin G response[375]. Evasins are heavily glycosylated, as indicated by their high molecular weight in gel electrophoresis[379]. Glycosylation complicates large-scale production and increases manufacturing costs. Evasins may require parental delivery in chronic inflammatory diseases, which would make repeated administration less desirable for patients[84]. Due to chemokine class specificity, at least two evasins (or a dual warhead evasin) would likely have to be administered to target the redundant chemokine network. Therefore, full-length evasins are currently undesirable as therapeutics.

1.6.3 Evasin-derived Peptides

Due to the limitations of using evasins directly, groups have aimed to translate the promise of evasins into a more attractive therapeutic modality. Translating the evasin protein into a therapeutic peptide is an option which has been trialled. Success has been achieved in developing peptides from proteins found in snake venom[400] and the saliva of lizards[401]. This

success demonstrates that translation from protein to peptide can retain the native protein's effects without immunogenicity. It has been reported that peptides below five kDa do not elicit immunogenic reactions[402].

A series of 16 amino acid peptides were isolated from the evasin P672, called BK1.1-1.3. The peptide BK1.1 retained the evasins' ability to inhibit CCL2, CCL3, CCL7 and CCL8-induced *in vitro* cell migration (**Figure 1.9**). BK1.3 demonstrated *in vivo* activity in a rodent model of inflammation. However, the parental evasin P672 remained more potent than any of the BK peptide series in *in vitro* cell migration models[403]. X-ray crystal and NMR investigations into EVA4 in complex with CCL5 guided the identification of a 17-amino acid peptide, capable of inhibiting CCL5 *in vitro* cell migration[377]. The peptide covers the sequence of EVA4 from Glu-14 to Asn-31. This peptide fully inhibited the cell migration of a monocyte cancer cell line at a concentration of 10 μM, whereas EVA4 inhibited cell migration at 100 nM, but no definitive IC50 values are reported[377]. Such evidence demonstrates that peptides derived from evasins can be identified that retain evasin-like chemokine inhibition, albeit at a reduced potency.

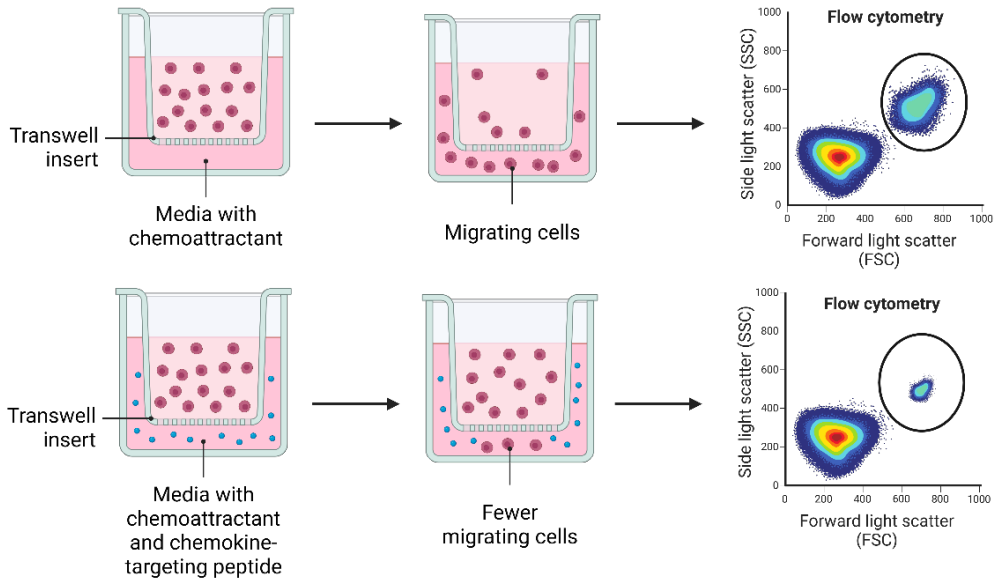

Figure 1.9 – Overview of *in vitro* cell migration assays. Cells are placed into the top chamber of a transwell chemotaxis plate. The bottom chamber of the plate contains chemokines, creating a chemokine gradient between the top and bottom chambers. The base of the top chamber has a porous membrane which allows cells to migrate into the bottom chamber of the plate along the chemokine gradient. Cells that have migrated into the bottom chamber can be counted using flow cytometry. If the bottom transwell chamber contains a chemokine-targeting molecule, such as an evasin-derived peptide, the chemokine gradient will be abrogated. Fewer cells will migrate into the bottom chamber and can then be visualised by flow cytometry. Flow cytometry analysis utilises side light scatter (SSC) to determine a cell's granularity and internal complexity. Forward light scatter (FSC) is used to determine a cell's size. Coupling SSC and FSC allows for a cell population to be determined, gated, and counted. Cellular debris is commonly visualised in flow cytometry as a population with low SSC and FSC, as shown in the bottom left corner of flow cytometry plots. Figure made in Biorender.

Building on the work established by the BK peptide series, the Bhattacharya group developed an evasin-derived peptide discovery pipeline. Phage display, a method for high-throughput screening of peptides[404], was used to identify which 16-amino acid regions of class A evasins bound to chemokines. A peptide, designated as HD2, was identified from EVA4[76]. Phage display revealed that HD2 could bind to both CC and CXC chemokines, a finding confirmed by BLI. This surprising dual chemokine class action was confirmed with *in vitro* cell migration assays[76]. This finding was novel, as all evasins or their derivative peptides had shown chemokine class specificity. AlphaFold modelling was used to propose steric hindrance as the mechanism of action. It was hypothesised that by binding to key regions on chemokines, HD2 prevented the chemokines from interacting with their respective chemokine receptors[76].

Despite this promising data, HD2 was limited by its micromolar potency[76]. High-throughput approaches to improve peptide characteristics, such as binding affinity, include affinity maturation[405], deep mutational scanning[406], and yeast display[407]. These methods are designed to improve binding to a single target. HD2 development aimed to enhance binding and chemokine inhibition against multiple chemokine targets, making typical mutagenesis protocols described above less suitable. Proceeding with a structural investigation was also not suitable, as it would be cost-prohibitive to obtain crystal structures of 46 chemokines in complex with 18 chemokine receptors. Therefore, the Bhattacharya group employed their newly developed method for peptide improvement, termed the Combinatorial Saturation Mutagenesis Optimisation Strategy (CoSMOS)[408]. The 16-amino acid peptide sequence was mutated, where each amino acid was substituted for all possible amino acids using a degenerate NNK codon[409]. Several single-amino acid peptide mutants from HD2 were identified, characterised in cell migration assays, and the beneficial mutations were combined and rescreened in phage display[408]. Two combinatorial peptides of interest (CM304 and CM307) were identified. Both peptides demonstrated markedly enhanced potency in single chemokine assays compared to HD2[408].

To model inflammatory diseases, a more complex *in vitro* model was required. Single-chemokine cell migration assays are limited in their ability to reflect the complex inflammatory milieu of inflammatory diseases. Thus, the Bhattacharya group used bulk RNA sequencing to determine the chemokines present in RA, atherosclerosis, and insulitis[408]. Both CM304 and CM307 inhibited the migration of primary human immune cells to these three chemokine mixtures, with significantly enhanced potency compared to the HD2 peptide[408].

Identifying peptides from evasins may circumvent issues with the risk of evasin immunogenicity and manufacturing problems. Despite this, translating peptides from evasin proteins was associated with a loss of potency. The newly validated CoSMOS pipeline is a method of identifying chemokine-binding peptides from evasins and translating them into highly potent

peptides targeting the chemokines present in inflammatory diseases. Given that the HD2 peptide series originated from a class A evasin and demonstrated success across multiple disease models, the question arose whether similar successful peptides could be identified from a class B evasin.

1.7 Aims and Hypotheses of this Work

The body of work presented above demonstrates that targeting the chemokine network for the treatment of inflammatory disorders is a viable option to abrogate inflammation. Targeting the chemokine network in T1D could be a novel therapeutic strategy and may be effective in combination therapy to delay the progression of patients to stage three T1D.

The hypothesis underlying this work is that a dual-class chemokine-binding peptide can be identified from class B evasin sequences and improved using mutagenesis to target chemokines present in insulitis.

This work aims to :

- To identify a dual chemokine class binding peptide from class B evasin sequences using phage display. Objectives: To screen the class B evasin library using both CC and CXC chemokines; and to use next-generation sequencing to identify dual class chemokine binding peptides.
- To functionally characterise peptides of interest using *in vitro* cell migration assays. Objectives: To test dual class chemokine binding peptides in chemotaxis assays using $CD8^+$ T-cells and THP-1 cells; to compare peptide activity compared to a scrambled peptide negative control; and to determine peptide potency by completing IC50 curves.
- To improve peptide properties using combinatorial saturation mutagenesis. Objectives: To create a NNK phage library; to screen the NNK phage library in phage display; to functionally characterise single mutants of interest in functional chemotaxis assays

using $CD8^+$ T-cells and THP-1 cells; to create a combinatorial phage library; and to screen the combinatorial phage library in phage display.

- To validate the lead peptide candidate in a model of insulitis. Objectives: To functionally characterise combinatorial peptides using an 'insulitis' chemokine pool using $CD8^+$ T-cells, THP-1 cells, and primary monocytes and to develop a $CD4^+$ T-cell line for further peptide characterisation.

2. Chapter Two - Identification and Characterisation of EB429

2.1 Introduction

2.1.1 Chemokine Network Complexity in Inflammation

Chemokines, also known as chemotactic cytokines, are responsible for recruiting leukocytes to sites of inflammation and injury[59]. They drive this recruitment through binding GPCR chemokine receptors on immune cells[410]. Chemokines have thus been identified as a potential therapeutic target for inflammatory diseases[411]. Chemokines are particularly relevant in the context of autoimmune diseases, where aberrant chemokine-driven leukocyte recruitment causes tissue damage[350, 365].

Historically, chemokine targeting in inflammatory diseases has been unsuccessful[350, 353]. Whilst no specific cause for this failure has been accepted, one proposed reason is that targeting a single chemokine or receptor fails to overcome the redundancy of the chemokine network[103]. A single chemokine can bind to multiple chemokine receptors, and receptors often have multiple chemokine ligands[79]. Following leukocyte recruitment to inflammatory sites, leukocytes themselves release additional chemokines, creating a chemokine feed-forward loop. Chemokines are also capable of synergising with one another, exacerbating leukocyte migration further[88]. Many of the trialled chemokine-targeting therapies were antibodies, targeting a single chemokine or a single chemokine receptor[412]. Targeting a single chemokine or receptor may have been the reason these therapies failed to show a beneficial effect in clinical trials[103].

2.1.2 Evasins

Evasins may provide a solution to targeting the complex chemokine network. Through millions of years of evolution, ticks have evolved a class of salivary proteins, termed evasins. Evasins are secreted in the saliva of ticks and are injected when they bite their host[381]. Evasins bind to chemokines present at the bite site in their host, thereby suppressing leukocyte recruitment and local inflammation[84]. By preventing local inflammation at the bite site, ticks can remain undetected by their host and feed for longer. One key feature of evasins is their ability to bind to multiple chemokines, but this binding is limited to a specific chemokine class. Class A evasins bind exclusively to CC chemokines, whilst class B evasins bind to CXC chemokines exclusively[116].

Evasins can effectively reduce inflammation in multiple animal models of diseases, as demonstrated in models of pulmonary fibrosis[413], liver disease[414], and atherosclerosis[415]. However, pharmaceutical companies have failed to pursue evasins as treatments for inflammatory diseases. The risk of protein immunogenicity and the expense required to manufacture large, heavily glycosylated proteins may explain this[416].

2.1.3 Evasin-derived Peptides

There are multiple benefits to creating novel peptide therapeutics derived from evasins, rather than using evasin proteins directly. Peptides are cheaper to produce than proteins, which confers a cost advantage over proteins, making them a more attractive treatment modality to develop[417]. Peptide-based drugs often exhibit favourable safety profiles in clinical trials and are widely regarded as having lower immunogenicity concerns than larger proteins[416]. Peptides serve as an attractive scaffold for functionalisation to enhance their pharmacological properties. Peptide side chains can be modified, and functional groups can be added, improving bioavailability, increasing half-life, and reducing the likelihood of peptide degradation[418]. A key example of this is the addition of a polyethylene glycol (PEG) group, termed PEGylation. The addition of a PEG

group increases a peptide's half-life by preventing renal clearance, inhibiting proteolytic cleavage, and enhancing peptide solubility[419]. These examples support the feasibility of evasin-derived peptide therapeutics.

Peptide sequences derived from evasins have been identified and characterised. The Bhattacharya research group was the first to identify a series of peptides from evasin 672 using hydrogen-deuterium exchange mass spectrometry. These peptides could bind to multiple CC chemokines and were effective in an *in vivo* model of inflammation[403]. The work described by Denisov *et al*[377] also identified peptides derived from evasins that could bind to CCL5, although the efficacy of this peptide was not explored *in vivo*. This work demonstrates that short peptides derived from evasin proteins can be utilised to bind and inhibit multiple chemokines, overcoming the potential issues associated with using full-length evasins. Using structural insights of chemokine and evasin complexes to guide rational peptide design is costly and time-consuming, thus limiting this approach for therapeutic development.

2.1.4 Phage Display Evasin Peptide Identification

The Bhattacharya laboratory aimed to develop methods for identifying peptides from evasins without requiring structural insights. A method of phage display combined with next-generation sequencing was developed. Phage display is a commonly used technology in drug discovery for screening large candidate libraries and identifying hits that bind to a target of choice[420]. Phage display has led to the identification of several prominent peptide-approved drugs[421]. Romiplostim has been approved for the treatment of immune thrombocytopenia[422], and ecallantide has been approved for the treatment of angioedema[423]. Phage display libraries encoding 16-amino acid peptides were constructed. These peptides covered the entire amino acid sequences of evasin proteins, staggered by one amino acid at a time. The evasin-derived peptides were presented on the phage and screened against immobilised chemokines in three

enrichment rounds. Next-generation sequencing (NGS) was used to identify promiscuously binding peptide sequences.

The screening of a class A evasin library yielded unexpected results. A peptide, termed HD2, was identified. Despite originating from a class A evasin, HD2 was seen to bind to and functionally neutralise the migration of both CC and CXC chemokines[76]. This result was novel, since cross-class chemokine specificity had not previously been described in evasins or in evasin-derived peptides. In tandem with the creation of the class A evasin library, a class B evasin library was created and screened against CXC chemokines only (Payne at al, manuscript in preparation).

2.1.5 Aims and Hypotheses

Through the development of HD2 and other peptides from the class A evasin library, the Bhattacharya lab has demonstrated that promiscuous chemokine-binding peptides can be identified from evasin sequences. This work hypothesises that peptides capable of binding to multiple chemokine classes can also be identified by screening the class B evasin library with CC chemokines. Therefore, the work described in this chapter aimed to screen the class B evasin library against CC class chemokines and to characterise the top-binding peptide using functional cell migration assays.

This chapter aims to:

- Screen the class B evasin library with CC class chemokines to identify chemokine-binding peptides with dual-class binding.
- Characterise peptides of interest identified by phage display in functional cell migration assays.

2.2 Results

2.2.1 Phage Display Screening of the EVAB Library Identifies Chemokine Binding Peptides

The class B evasin library was screened against 15 biotinylated chemokines in parallel (**Figure 2.1).** Peptides that bound to their target chemokine were identified by NGS, following three rounds of amplification and phage display selection. The enrichment (E) of each peptide to a chemokine was compared to the input library and denoted as log2E, which is correlated with binding affinity[424]. MP performed the CC chemokine screening, while KH and KK conducted the CXC screening.

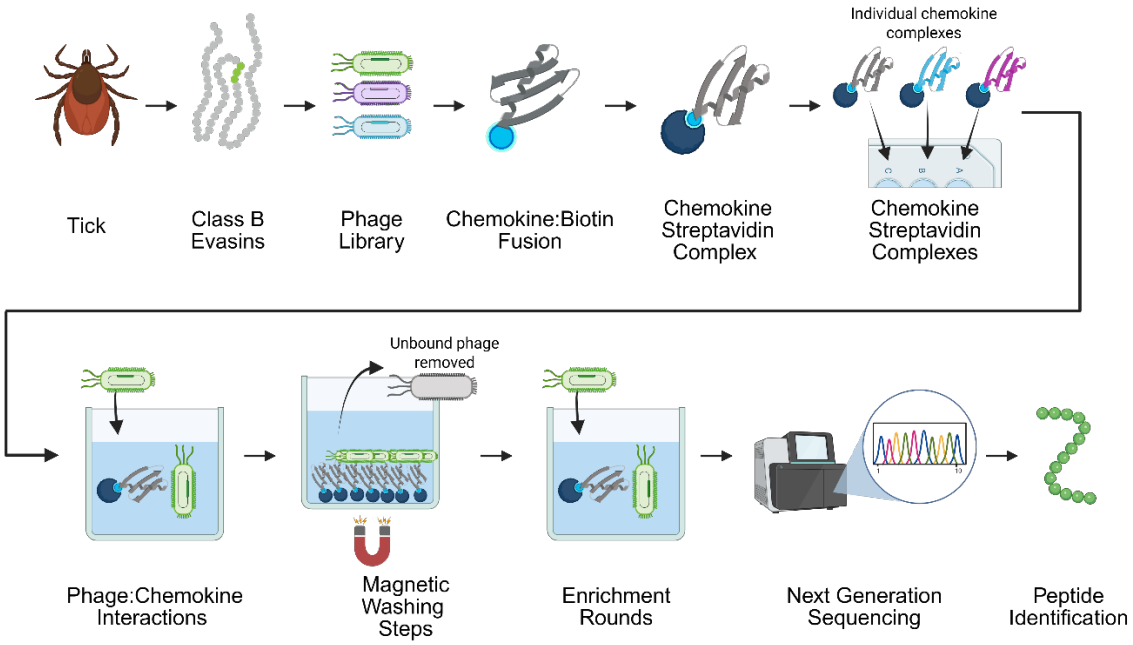

Figure 2.1 – Phage display pipeline. The sequences of salivary chemokine-neutralising proteins, called evasins, were extracted from ticks. A phage library was constructed, displaying 16 amino acid evasin sequence-derived peptides. Biotinylated chemokines were incubated with streptavidin nanobeads in a 96-well plate, with each chemokine complex in a separate well. The phage library was added to each chemokine in parallel, and washing steps were used to remove unbound phage. Phage binding was enriched over three rounds of selection. Enriched peptides were identified using next-generation sequencing. Figure made in Biorender.

Each 16-amino-acid peptide was mapped to its parental evasin sequence, and enrichment for the individual target chemokines was represented as log2E values **(Figure 2.2)**. Individual peptide log2E values are represented as stacked bars, with log2E values shown on the left-hand axis, and colours denoting the chemokine bait. To identify which 16-amino-acid sections of the evasin bound to multiple chemokines, residue log2E was calculated (rlog2E). Rlog2E is the total sum of the log2E values that overlap by an amino-acid residue. Rlog2E is shown as a curve, with the rlog2E values on the right-hand axis. The highest rlog2E can be seen for the evasins E1096, E1132 and E1168.

Evasin regions of interest (ROIs) are shown as grey bars underneath the evasin and peptide plots. ROIs were defined by the rlog2E, where the upper boundary exceeded the 95% confidence interval of the median rlog2E, which is represented in the figure by a brown line intersecting the evasin and peptide plots horizontally. In an ROI for the evasin E1096, binding was identified to CXC chemokines and several CC chemokines (CCL15, CCL17, CCL18, CCL20 and CCL22).

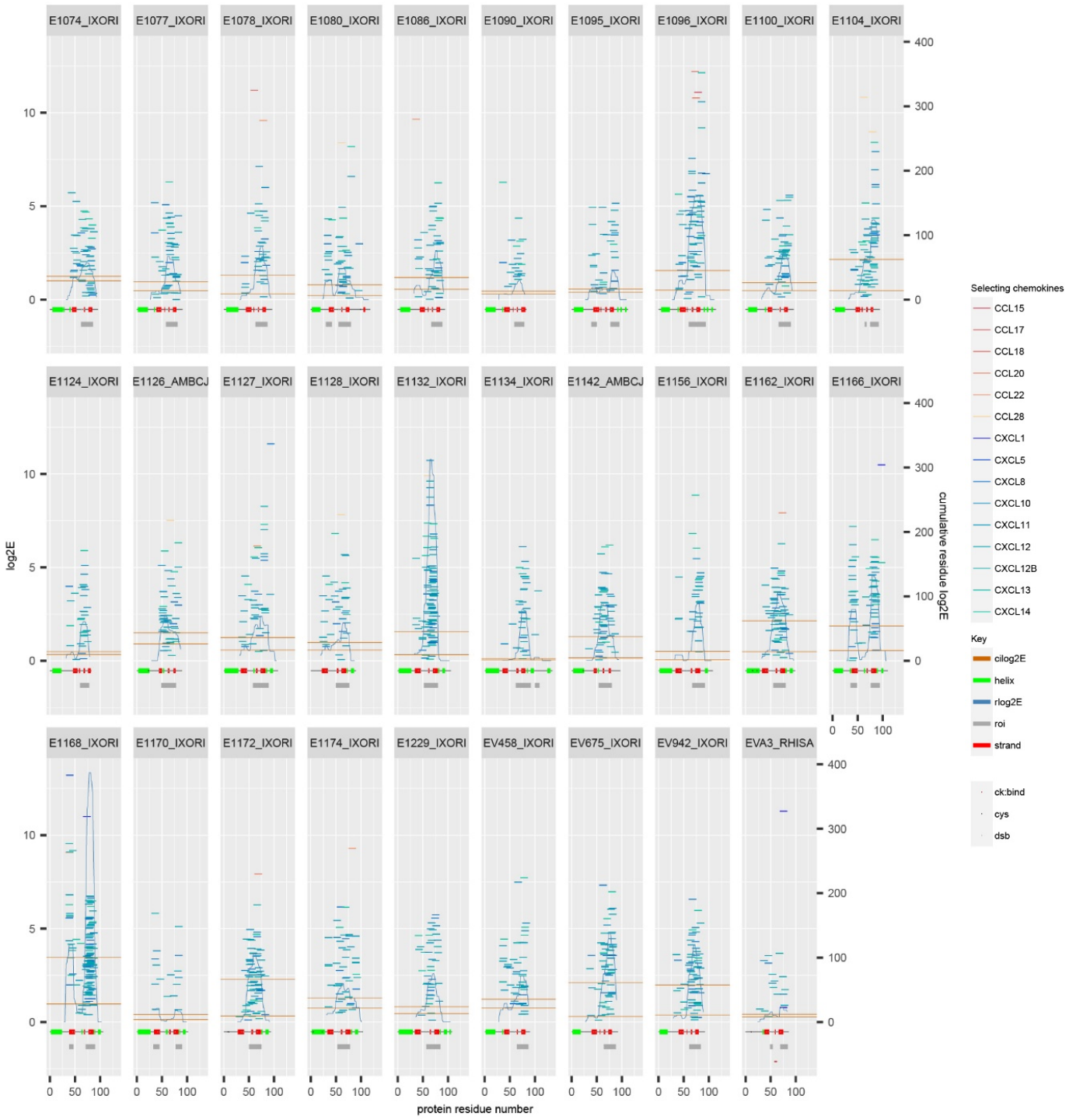

Figure 2.2 – Mapping of enriched peptides to parental evasin proteins. Alignment of enriched peptides to parental proteins. Faceted plots show indicated class B evasins in each subpanel, identified by UniProt entry names. X-axis in each plot indicates the evasin residue position. The left Y-axis scale indicates peptide log2E, and the right Y-axis scale the residue log2E. Peptides are represented as horizontal tiles, coloured by the selecting chemokine. Peptide log2E was calculated as described above. Residue log2E (rlog2E) is the sum of log2Es of peptides overlapping a residue and shown as a smoothed curve of rolling median over a window of seven residues. Regions of interest (roi) were defined as rlog2E exceeding the 95% upper confidence interval of median rlog2E. Structural features (helix, strand) were obtained from the UniProt entry. Abbreviations: cilog2E – 95% confidence interval of median rlog2E for the entire protein, roi – region of interest, ck:bind – chemokine binding sites, cys – cysteine, dsb – disulfide-bonded cysteine. Data analysed by SB.

2.2.2 Identification of a Promiscuous Binding Peptide EB429

Peptides of interest were selected from phage display analysis if they bound to at least three chemokines with a log2E greater than five. This threshold was set to identify promiscuous chemokine-binding peptides. 13 peptides met this threshold **(Figure 2.3)**. The tile plot of individual log2E values shows that two peptides, EB1927 and EB429, are enriched against both CXC and CC chemokines. EB1927 only bound to one CC chemokine, CCL22. EB429 demonstrates enrichment to all five tested CC chemokines, albeit with a low log2E. EB429 also shows high enrichment values for the CXC chemokines tested, particularly for CXCL11 and CXCL13. EB429 was selected for further testing and characterisation due to its high level of binding enrichment to CXC chemokines and binding to several CC chemokines.

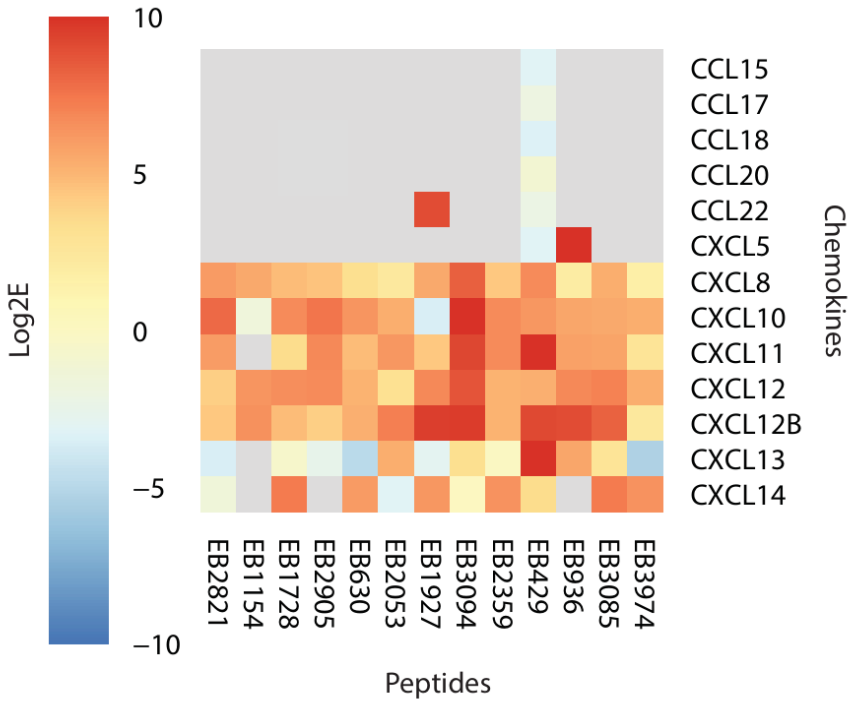

Figure 2.3 – Tile plot of 13 peptides that bind at least three chemokines with log2E > 5. Peptides were identified from phage display screening of the class B evasin library. Rows show the selecting chemokine and columns denote the peptide. The scale bar shows log2E values**.** Grey tiles indicate where a peptide was not identified in the phage display experiment. Data analysed by SB.

2.2.3 Chemotaxis Assays Demonstrate Dual Class EB429 Chemokine Inhibition

The EB429 peptide was selected for characterisation as it showed the broadest chemokine binding profile in phage display. The functional ability of EB429 was tested using *in vitro* cell migration assays with both CC and CXC chemokines.

Dose-response curves were performed for individual chemokines to determine the EC80 values, which represent the chemokine concentration at which 80% of the cells migrate. The EC80 chemokine concentration was used in chemokine inhibition assays (**Figure 2.4**).

EB429 was tested in single chemokine inhibition assays with activated $CD8^+$ T-cells to the chemokines CXCL9, CXCL10, CXCL11, CXCL12α, CCL19, and CCL21 **(Figure 2.5, Figure 2.6)**. Chemotaxis was compared to a scrambled control peptide (EB429 SCR), which contains the same amino acids as EB429 in a random order. EB429 significantly inhibited T-cell migration to

five chemokines compared to EB429 SCR. The most potent inhibition of chemotaxis was seen for the chemokines CXCL9 and CXCL11. No significant inhibition was observed with CCL21 or other tested THP-1 chemokines **(Figure 2.7)**. This result confirms the ability of EB429 to bind to both CXC and CC chemokines, demonstrating that it can functionally inhibit T-cell migration to CXCL9, CXCL10, CXCL11, CXCL12α, and CCL19.

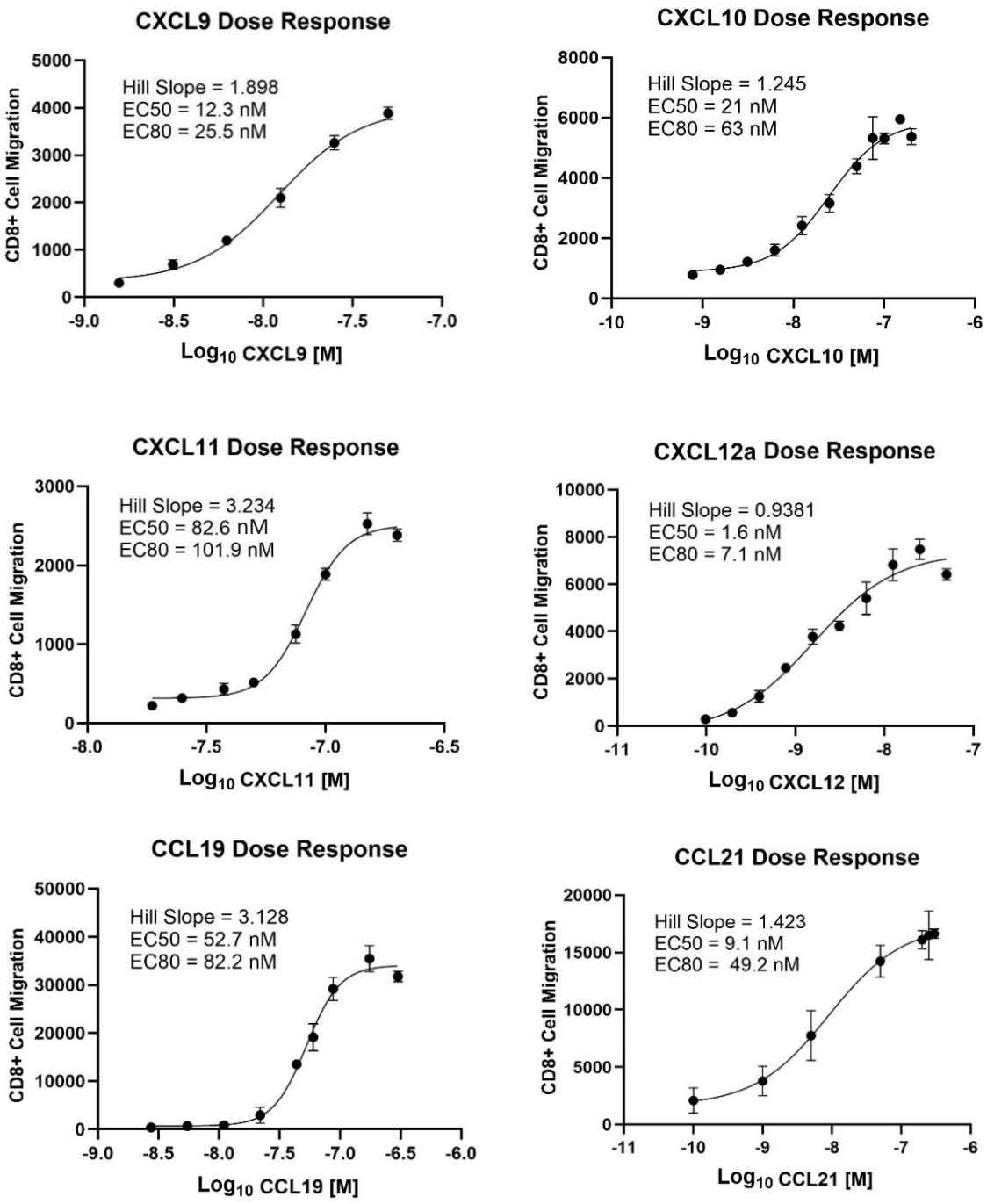

Figure 2.4 – Cell migration in response to indicated chemokines. Representative dose-response curves of indicated chemokines with activated $CD8^+$ T-cells. Migrated cell count values are displayed on the Y-axis. The X-axis shows the concentration of chemokine as a Log10 of molar concentration. Each data point shows the mean value of the technical replicates at each concentration of chemokine tested, with their standard deviation error bars shown. EC80 and EC50 values were calculated by plotting a 3-parameter dose-response log-logistic plot using GraphPad Prism.

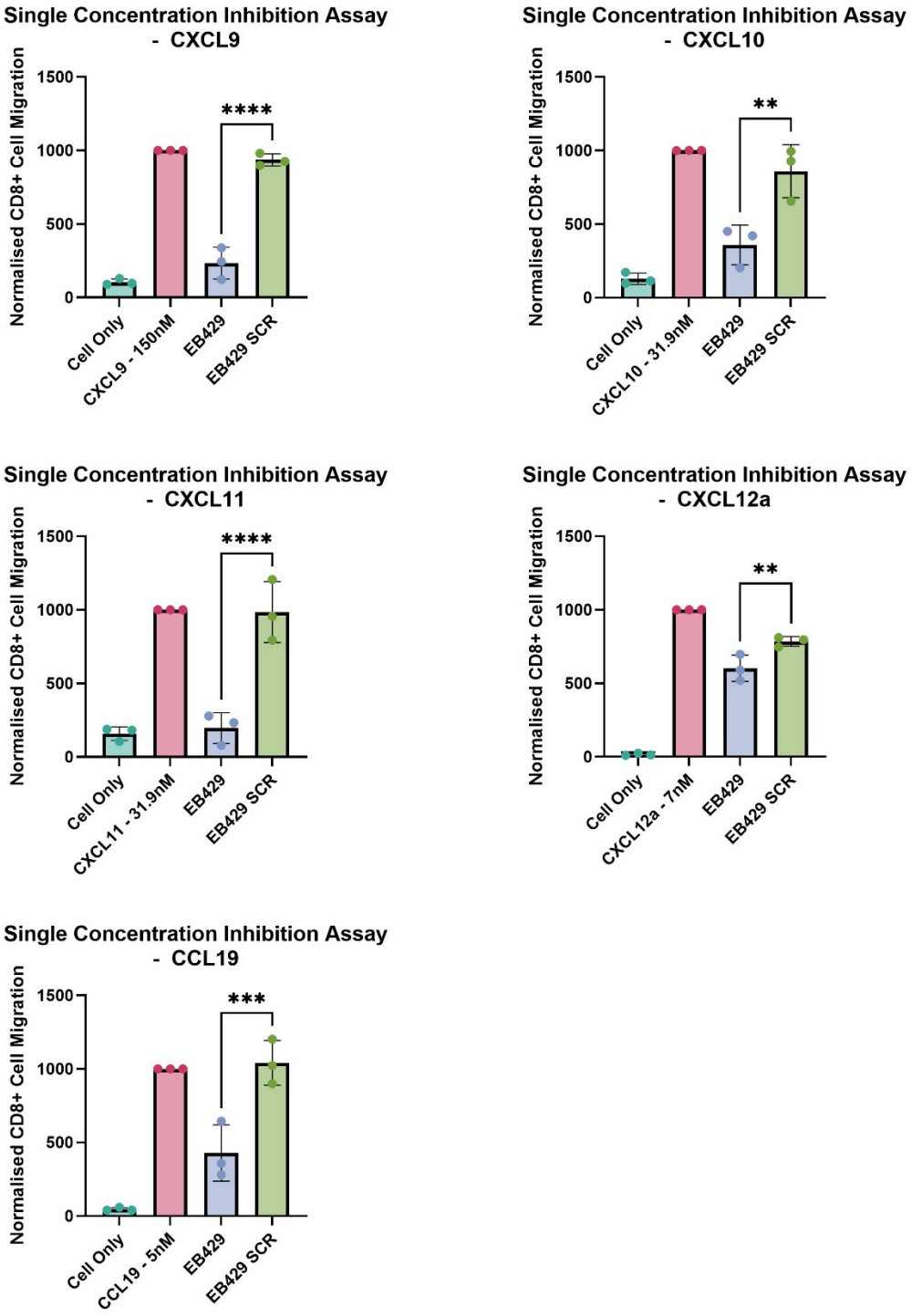

Figure 2.5 – Effect of EB429 on CD8⁺ T-cell migration to CXC and CC chemokines. Bar charts with standard deviation error bars depicting the effect of EB429 on activated CD8⁺ T-cell migration to CXC and CC chemokines. All experiments were performed as three technical replicates and three biological replicates. Individual data points indicate mean values of technical replicates per experiment. Cell migration values were normalised to the mean value of migrated cell counts to the EC80 chemokine concentration and set to 1000 cells, as displayed on the Y-axis. The X-axis shows experimental constituents. Peptides were tested at a final concentration of 10 µM. Chemokines were tested at their EC80 doses, as indicated. EB429 SCR was used as a negative control, containing the scrambled amino acid residues of EB429. The statistical significance of EB429 was calculated compared to EB429 SCR using a one-way ANOVA and a Dunnett's test for multiple comparisons. Asterisks indicate the following: ****$p \leq 0.0001$, ***$p \leq 0.001$, **$p \leq 0.01$, *$p \leq 0.05$.

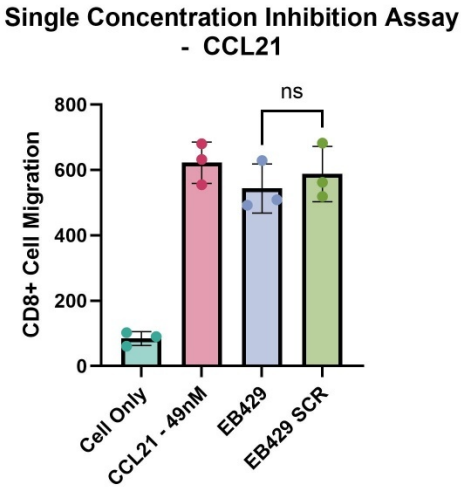

Figure 2.6 – Effect of EB429 on CD8⁺ T-cell migration to CCL21. Bar charts with standard deviation error bars depicting the effect of EB429 on CD8⁺ T-cell migration to CCL21. The experiment was performed as three technical replicates indicated by individual data points. The Y-axis shows CD8⁺ T-cell migration values. The X-axis shows experimental constituents. Peptides were tested at a final concentration of 10 µM. CCL21 was tested at its EC80 dose, as indicated. EB429 SCR was used as a negative control, containing the scrambled amino acid residues of EB429. The statistical significance of EB429 was calculated compared to EB429 SCR using a one-way ANOVA and a Dunnett's test for multiple comparisons.

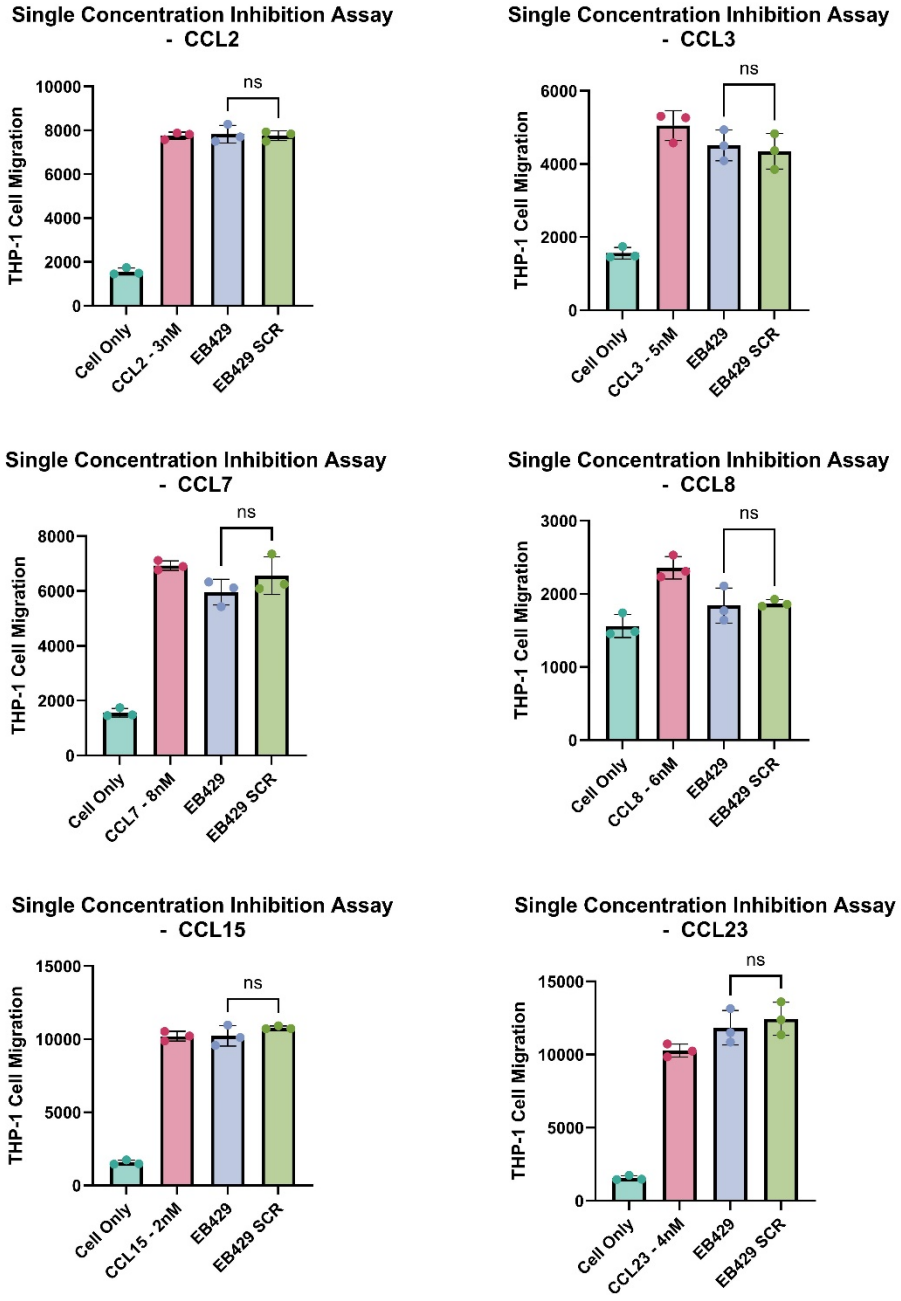

Figure 2.7 – Effect of EB429 on THP-1 migration to CXC and CC chemokines. Bar charts with standard deviation error bars depicting the effect of EB429 on THP-1 migration to CC chemokines. All experiments were performed as three technical replicates indicated by individual data points. The Y-axis shows THP-1 cell migration values. The X-axis shows experimental constituents. Peptides were tested at a final concentration of 10 μM. Chemokines were tested at their EC80 doses, as indicated. EB429 SCR was used as a negative control, containing the scrambled amino acid residues of EB429. The statistical significance of EB429 was calculated compared to EB429 SCR using a one-way ANOVA and a Dunnett's test for multiple comparisons.

2.2.4 Inhibitory Dose-response Curves Identify Micromolar EB429 Potency

To evaluate the potency of EB429, inhibitory dose-response curves were performed against the exemplar chemokine CXCL10 **(Figure 2.8)**. Potency was determined by measuring the IC50 value, which is the peptide concentration at which 50% of cells migrate. The mean IC50 value was 4.885 µM. Due to EB429's potency being in the micromolar range, potency against other chemokines was not investigated at this stage.

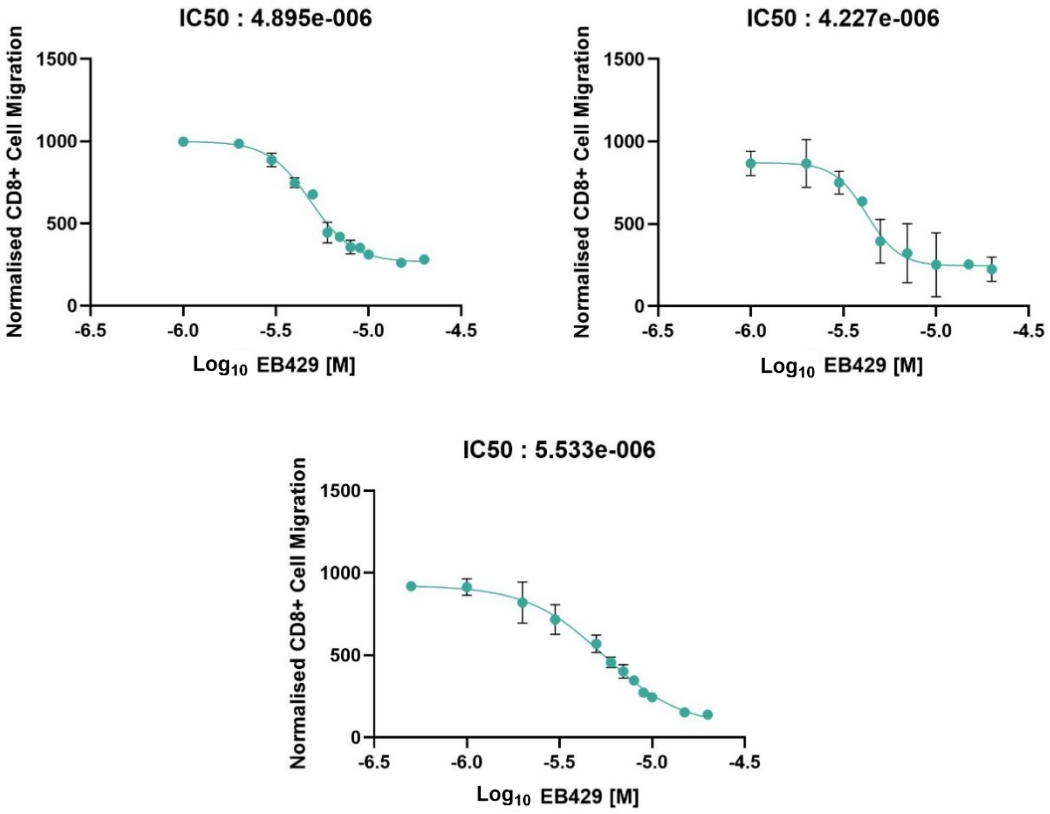

Figure 2.8 – Inhibitory dose-response curves of EB429 against the chemokine CXCL10. Triplicate dose-response curves depicting the potency of EB429 against the chemokine CXCL10, using activated $CD8^+$ T-cells. Cell migration values were normalised to the mean values of migrated cell counts without EB429 and set to 1000 cells, as indicated on the Y-axis. The X-axis shows the concentration of EB429 as a Log^{10} of molar concentration. Each data point represents the mean value of the technical replicates for each concentration of EB429 tested, with standard deviation error bars shown. IC50 values were calculated by plotting a 3-parameter inhibitor dose-response log-logistic plot using GraphPad Prism.

2.2.5 AlphaFold Modelling Predicts EB429 Occupies Chemokine Receptor Binding Sites

To elucidate the potential mechanism of action of EB429, AlphaFold3 modelling was performed to investigate how EB429 interacts with CC and CXC chemokines. EB429 was modelled with CXCL10 and CCL19, and CXCL10 was modelled with CXCR3 and CCL19 with CCR7. The modelling indicates that EB429 is in proximity to the first β-sheet and the α-helix of CXCL10 (**Figure 2.9**). Modelling also shows that EB429 is in proximity to the N-loop, N-terminus and third β-sheet of CCL19 (**Figure 2.10**). These regions correspond to the predicted receptor-binding sites for CXCL10 and CCL19 to the chemokine receptors CXCR3 and CCR7, respectively. As these regions are required for chemokine binding to its receptor, this suggests that EB429 sterically hinders chemokine binding to the respective chemokine receptor.

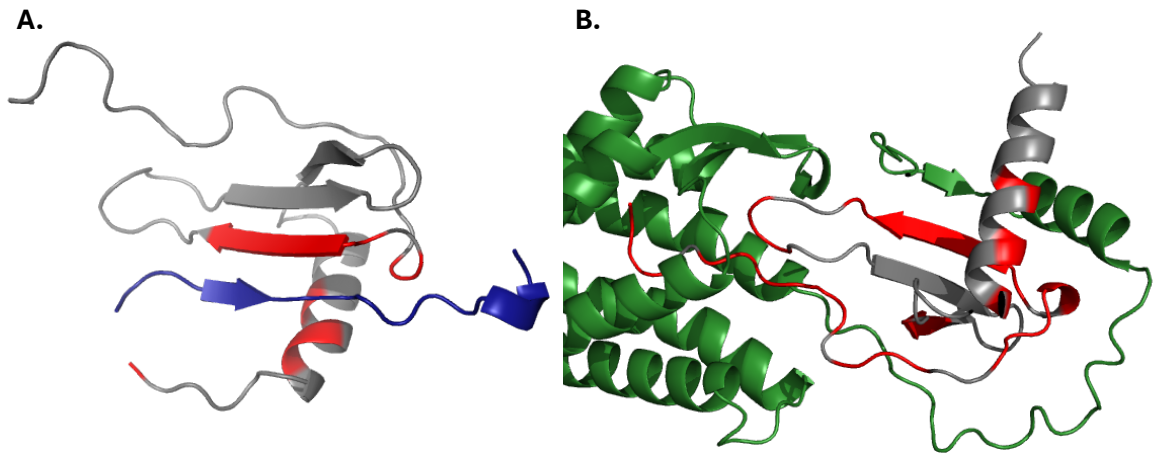

Figure 2.9 – AlphaFold modelling of EB429 and CXCL10.A. AlphaFold3 predicted binding models of CXCL10 to EB429. CXCL10 is shown in grey, and EB429 is shown in blue. The binding interface of CXCL10:EB429 within 5 angstroms is highlighted in red on CXCL10. **B.** AlphaFold3 predicted binding models of CXCL10 to CXCR3. CXCL10 is shown in grey, and CXCR3 is shown in green. The binding interface of CXCL10:CXCR3 within 5 angstroms is highlighted in red on CXCL10. Figure made in PyMOL

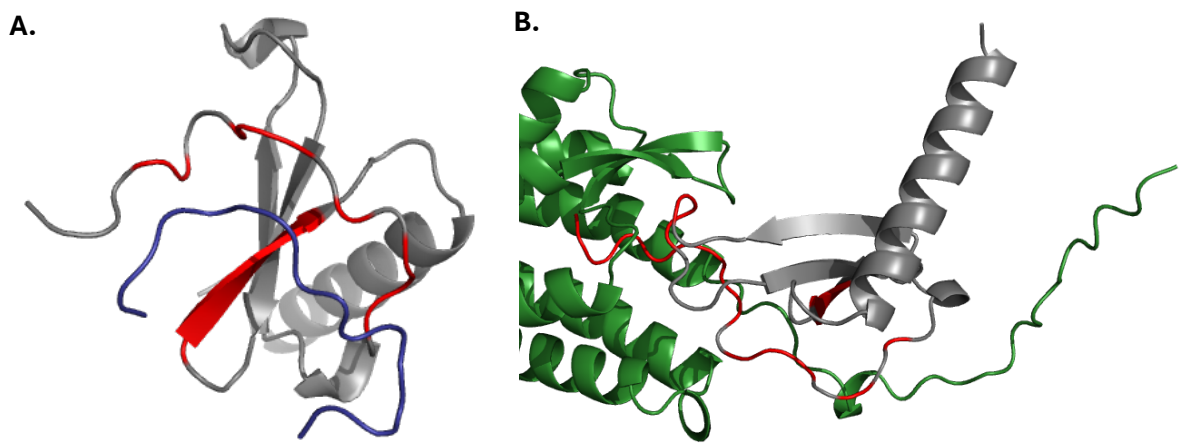

Figure 2.10 – AlphaFold modelling of EB429 and CCL19. A. AlphaFold3 predicted binding models of CCL19 to EB429. CCL19 is shown in grey, and EB429 is shown in blue. The binding interface of CCL19:EB429 within 5 angstroms is highlighted in red on CCL19. **B**. AlphaFold3 predicted binding models of CCL19 to CCR7. CCL19 is shown in grey, and CCR7 is shown in green. The binding interface of CCL19:CCR7 within 5 angstroms is highlighted in red on CCL19. Figure made in PyMOL.

2.3 Discussion

Inflammation, as described in part by the migration of immune cell subtypes to sites of tissue injury, is mediated by chemokines[425]. Despite the chemokine network being an attractive target for therapeutic intervention in inflammatory diseases, there has been little progress in translating this into clinically beneficial treatments[353]. Evasin proteins have been thoroughly characterised *in vivo* as capable of neutralising the chemokine network in inflammatory diseases[381]. However, evasins are undesirable as therapeutics due to risks of immunogenicity and high manufacturing costs. Phage display screening offers an opportunity to identify chemokine-binding peptide sequences from evasins[76] without the need for expensive structural insights.

This chapter has confirmed the hypothesis that promiscuous chemokine-binding peptides can be identified from the class B evasin library. Furthermore, a peptide identified from phage display screening, EB429, can functionally neutralise both CC and CXC chemokines *in vitro*. Using AlphaFold3 modelling, a potential mechanism of action of EB429 has been identified, predicting binding to chemokine receptor binding sites. The main therapeutic limitation of EB429 is its low potency, with IC50 values being within the micromolar range.

2.3.1 Phage Display Identifies CC and CXC Binding Peptides

The work in this chapter identifies a peptide sequence from a class B evasin capable of binding to CC and CXC chemokine classes, which, to our knowledge, has not been previously reported. The identification of EB429 is a novel result, as class A and class B evasins are structurally distinct protein sub-classes. One further peptide capable of binding to CC and CXC chemokines was also identified by phage display in this chapter. However, it was not investigated as it showed binding to only one CC chemokine. This chapter aimed to identify a promiscuous binding peptide, as chemokine-inhibiting treatments targeting a single chemokine have shown limited therapeutic benefit in clinical trials[103].

Screening of the class B evasin library yielded fewer promiscuous peptide binders compared to the screening of the class A evasin library[76]. Using the same selection criteria for both libraries, 30 peptides of interest were identified from the class A evasin screen, compared to 13 from the class B evasin screen. The class A library contained 4,741 peptides, compared to 4,439 in the class B library, making the library sizes roughly comparable. It is possible that sequences derived from class A evasins are more promiscuous binders than those from class B. Generally, far fewer class B evasins have been explored than class A. The most extensively explored class B evasin is EVA3, known to inhibit ELR^+ chemokines and prevent neutrophil recruitment to a murine peritoneal cavity and knee joint[375]. Class B evasins bind exclusively to ELR^+ or ELR^- CXC chemokines, forming two distinct classes[379]. As there are fewer numbers of CXC chemokines in the ELR^+ or ELR^- groups than CC chemokines to which class A evasins bind, class B evasins may be capable of binding to fewer chemokines promiscuously than class A evasins.

To prevent a non-specific peptide from being identified in phage display, experiments described in this chapter use the negative control complement protein C5a. C5a was selected as a negative control because it is a chemotactic protein of a similar size to a chemokine, but not a chemokine itself[426]. Any peptide sequences that bound to C5a were excluded from subsequent analysis.

Multiple wash steps were included post-incubation to prevent the non-specific binding of phage-displaying peptides to the plate. Three selection rounds are used to select peptides that bind to their chemokine target with high affinity. Peptide sequences in the input phage library are identified using next-generation sequencing. Libraries with fewer than 95% of the desired peptide sequences are remade and sequenced again to ensure high library coverage. Enrichment of peptides following phage display is calculated compared to their presence in the input phage library, shown as log2E, ensuring that enrichment is not overestimated if a peptide is present in large numbers in the input library.

A key consideration is that, although phage display has identified peptides capable of binding to chemokines, this binding does not necessarily mean that these peptides will inhibit chemokine function. Peptides may bind to the chemokine in areas not needed for cell signalling and chemokine receptor binding. Peptides may also increase chemokine signalling and not necessarily inhibit migration. Consequently, the workflow used ensured that peptide hits were validated using *in vitro* cell migration experiments.

2.3.2 Novel Properties of Evasin-derived Peptides

The proposed hypothesis for why identified peptides (previously described[76]) can bind to multiple chemokine classes, while their parental evasins cannot, has yet to be confirmed. It is possible that previously identified peptides derived from evasin sequences were capable of binding to multiple chemokine classes, but this has not been studied. As it was widely believed that these peptides would have the chemokine class specificity of their parent evasin, they may never have been tested against different chemokine classes. For instance, testing of the Eva4 mutant peptide Glu14–Asn31 using CXC chemokines was not reported[377].

Due to their shorter length and greater conformational flexibility, peptides may access chemokine-binding sites that are inaccessible to full-length evasins[427], potentially facilitating binding to multiple chemokine classes. Evasin proteins will be affected by steric hindrance to a

larger degree than their peptide derivatives. Due to the evasin proteins having a locked conformation, they will also lack the flexibility of a peptide[428]. Furthermore, the sequence of amino acids that bind to CC chemokines may have been obscured in the evasin and exposed in a peptide sequence. This combination of factors may allow the linear peptide sequence to bind to a larger range of chemokines than evasins.

Another potential explanation is that EB429 has an unpaired cysteine residue, which would likely be oxidised to form a disulphide bond within the parental evasin. A previously identified peptide within the laboratory, HD2, also had an unpaired cysteine residue and could bind to multiple chemokine classes, unlike its parental evasin[76]. Cysteine residues have various functions; they can form disulphide bonds and also increase a peptide's non-covalent interactions[429]. Previous work has indicated the importance of cysteine residues. When mutated to alanine or serine, peptides appear to lose their binding ability, as demonstrated by phage display[76]. Further evidence for the importance of cysteine is demonstrated by the peptide BK1.5, which loses its ability to block chemotaxis when its cysteine residue is removed[403].

2.3.3 Cell Migration Assays Confirm EB429 Inhibition of CC and CXC Chemokines

EB429 was shown to bind to multiple CC and CXC chemokines in phage display screening and was selected for further testing. In transwell *in vitro* cell migration experiments using activated $CD8^+$ T-cells, EB429 functionally inhibited the chemokines CXCL9, CXCL10, CXCL11, CXCL12α, and CCL19. The negative control used here was a randomly scrambled peptide sequence of EB429, termed EB429 SCR. Using a scrambled peptide sequence as a control ensures that the peptide's function is sequence-specific and that the amino acid residues themselves do not confer chemokine binding ability. Using such a control demonstrates that the amino acid residues in their specific sequence provide the function of the peptide, not the residues themselves in any position.

Inhibition of CXCL9, CXCL10, CXCL11 and CCL19 by EB429 was statistically significant, and inhibition of CXCL12a was modest but significant. No inhibition was seen for the chemokine CCL21 using $CD8^+$ T-cells, or across multiple CC chemokines tested in the THP-1 cell line. EB429's ability to neutralise chemokines, therefore, appears to be specific to T-cell chemokines. T-cell specificity may be due to EB429's ability to neutralise those specific chemokines that recruit $CD8^+$ T-cells, or it may be specific to $CD8^+$ T-cells.

Information about whether the parental evasin of EB429 (E1096) binds to CC or CXC chemokines would help to unpick the specificity of EB429. Previously published results using BLI showed that E1096 does not bind to CXCL9, CXCL10, CXCL11 or CXCL12a. CCL19 was not tested in this experiment as it focused on CXC chemokines and class B evasins. E1096 only showed modest binding to the chemokine CXCL8[379]. At the time of testing EB429, a cell line that could migrate to CXCL8 was unavailable. Further analysis of E1096 would help us deduce more about the ability of EB429, but this testing was beyond the scope of the work in this thesis.

2.3.4 AlphaFold Predicts EB429 Binds to Chemokine Receptor Binding Sites

In this chapter, AlphaFold3 has been used to model peptide binding to respective chemokines and chemokines to their respective receptors. While multiple approaches are available[430, 431], modelling with AlphaFold was selected due to its highly accurate predictions of α-helices and β-sheets[432]. AlphaFold3 was selected as the most up-to-date version of the software, known to have improved structural prediction accuracy[433]. EB429 was predicted to interact with CXCL10 at the first β-sheet and the α-helix, and with CCL19 at the N-terminus and third β-sheet. These regions correspond to the predicted binding sites of these chemokines to their cognate chemokine receptors. Therefore, the proposed mechanism of action for EB429 is that it occludes the receptor binding sites on chemokines.

Previous modelling was performed using AlphaFold2-Multimer on the peptide HD2 to elucidate the proposed mechanism of action of the peptide chemokine inhibition. HD2 was predicted to bind to different sites, depending on whether the chemokine was of the CC or CXC class, similar to EB429. With CC chemokines, the peptide was predicted to bind to the N-terminus, β3-strand, and N-loop[76]. This proposed modelling is in concordance with the NMR-based model of CCL5 and the sequence of Evasin 4 known as Ev4Glu14-Asn31. The 17-amino acid sequence differs from HD2 by only three residues and can be assumed to have a similar binding pattern[377]. HD2 binds to CXC chemokines at the β1-strand and α-helix. These two identified regions for HD2 binding to CC or CXC chemokines overlap with the predicted binding pattern of chemokines binding to their chemokine receptors, as seen for EB429. This modelling increases confidence in the proposed mechanism of action, occluding the chemokine receptor binding site on chemokines. This binding would prevent chemokines from exerting their effects on leukocytes by blocking the chemokine receptor interactions that facilitate cell migration[76].

2.3.5 IC50 Dose-response Curves Identify Low Potency of EB429

For a potential therapeutic to be a candidate for development in a drug discovery pipeline, potency is vital. Potent drugs are beneficial as they are associated with a more favourable safety profile, as a smaller amount of the therapeutic agent needs to be administered[434]. Increasing potency is also of interest to pharmaceutical companies, as it is associated with lower production costs[435]. Potency can be determined by completing dose-response curves of the peptide to deduce the IC50 value. The IC50 value is the half-maximal inhibitory concentration needed to inhibit a process (chemotaxis in this thesis) by 50%. For the peptide EB429, the mean IC50 value against CXCL10 was 4.88 micromolar. Due to the micromolar CXCL10 IC50 value, no further IC50 curves were established.

The low potency of the EB429 peptide is a limiting factor in determining its therapeutic effectiveness. Micromolar potency means a higher peptide concentration must be administered

to neutralise chemotaxis effectively. For EB429, from the transition from protein to peptide, the ability to bind to multiple chemokine classes may have been exchanged for a loss of potency. This mirrors the reduced potency observed with the CCL5-neutralising EVA4-derived peptide[377]. Reduced potency may result from peptides being more energetically unfavourable than proteins, due to their lack of conformation and ability to rotate[436]. Coupled with the complexity of the chemokine network, it is unclear whether targeting only five chemokines would be sufficient to overcome the chemokine network in a disease state. Before this can be investigated, EB429 requires improvement of its drug-like properties.

2.3.6 Limitations

2.3.6.1 Phage Display

Regions of EVA3 shown to bind to and functionally inhibit chemokines previously[379] did not appear as a region of interest in this phage display screening. The phage display screening identified one peptide from the EVA3 sequence, which bound to CXCL8 with a log2E of 3.15. This peptide sequence did not align with the previously described binding regions of EVA3[380]. There are multiple reasons why this known binding region of EVA3 was not identified in this phage display experiment. Peptides are displayed on the phage via fusion of their C-terminus with the p8 coat protein of the phage. Fusion at the C-terminus may interfere with chemokine binding. Peptides may be missed if they do not display well on the phage, creating expression bias. Furthermore, chemokines are biotinylated and immobilised on streptavidin nanobeads. It is possible that this alters the presentation of the chemokines and allows for the selection of non-optimal binding peptides.

2.3.6.2 Cell Migration Assays

The results obtained for individual chemokines using transwell chemotaxis assays cannot recapitulate the complexities of cell migration *in vivo*. Chemokines and chemokine receptors are known to synergise[88]. Furthermore, chemokines have low-affinity interactions with GAGs,

present on endothelial cells. These interactions are thought to promote the formation of chemokine gradients necessary for cell migration[73]. The lack of GAGs, selectins, and integrins in the transwell system limits the biological deductions that can be made about a peptide's functional ability from this assay alone.

When testing the function of EB429, if there was no evidence of inhibition, EB429 was tested once, due to the time and cost associated with such assays. Further limitations of cell migration assays are discussed in chapter three.

2.3.6.3 AlphaFold3 Modelling

Modelling of EB429 with AlphaFold3 should be inferred with caution. The mechanism of action of EB429 is gathered from modelling only. X-ray crystallography or NMR[437] would resolve the structure of a given peptide and chemokine. Such experiments would be costly and time-consuming for multiple peptides against multiple chemokines, as well as for chemokines interacting with their cognate chemokine receptors. While modelling provides a time-effective solution, inferences from this modelling need to be confirmed with structural studies to make definitive statements on the mechanism of action.

2.4 Conclusions and Future Directions

In summary, phage display, NGS, and cell migration assays have identified a peptide derived from a class B evasin that is capable of inhibiting multiple chemokine classes. This work reaffirms the results of the group's previous work and establishes that the phage display evasin library screening pipeline can identify novel promiscuously binding peptides. This result is significant because class A and B evasins are structurally distinct subclasses. The major limitation of this work remains the low potency of EB429, as shown by IC50 curves with CXCL10. In the following chapter, peptide improvement strategies will be discussed. Subsequent efforts will aim to

enhance the potency and broaden the chemokine binding range of EB429 to enhance its therapeutic potential.

3. Chapter Three - Molecular Evolution of EB429

3.1 Introduction

EB429 was identified by phage display screening of the class B evasin library. Phage display demonstrated that EB429 bound to CC and CXC chemokines and was selected for characterisation in functional chemotaxis assays. EB429 significantly inhibited the migration of multiple CXC chemokines and CCL19, confirming the cross-chemokine binding seen in phage display. This dual-class inhibition was a novel result, as no cross-class chemokine binding or inhibition had been reported for a class B evasin or derivative peptide. Despite this positive result, the potency of EB429 was in the micromolar range when tested against CXCL10. Therefore, the drug-like properties of the peptide EB429 require improvement before it can be considered a viable chemokine targeting therapy.

3.1.1. Peptide Therapeutics

Over the last two decades, technological advances have rapidly expanded the potential of peptide therapeutics. As of December 2023, 80 peptide drugs were in the clinic, 200 were being tested in clinical trials, and over 600 were in the advanced stages of pre-clinical work[(438)]. Advances in peptide pharmacokinetic properties and bioavailability have contributed to this[(439)]. However, peptide drugs often suffer from short half-lives, due to rapid renal clearance and susceptibility to proteolytic lysis[(440)].

Many approaches now exist to improve peptide properties. C-terminal amidation prevents peptide degradation by enzymes such as exopeptidases[(441)]. Similarly, the N-terminus of the peptide can be acetylated, which is also protective against enzymatic degradation[(442)]. Cyclic peptides demonstrate enhanced resistance to enzymatic cleavage compared to their linear

counterparts, while also conferring benefits such as increased target affinity[443]. PEGylation of peptides involves attaching a peptide to a polyethylene glycol chain (PEG) to improve solubility and increase the peptide's size to prevent rapid excretion by the kidneys[419]. Replacing conventional L-amino acids with D-enantiomers can further extend half-life[444]. A short half-life or peptide renal clearance can be beneficial, as exemplified by oxytocin, where rational drug design aimed to produce a drug with rapid renal clearance to prevent drug accumulation with repeated administration[445]. Different modifications can be selected to enhance specific functional properties of a peptide, depending on the drug-like property that needs to be addressed.

3.1.2 Peptide Improvement Strategies

Another peptide property that research may aim to improve is the binding affinity of a peptide for its biological target. Deep mutational scanning[406], affinity selection mass spectrometry[405], and yeast display[407] have all been utilised as high-throughput methods to enhance protein and peptide binding affinity. This work aims to employ a peptide improvement strategy to enhance the potency of EB429, which is currently in the micromolar range. One facet of potency is the binding affinity to a target[446]. EB429's potency may be enhanced by improving its binding affinity. The techniques described above are typically used to enhance the binding affinity of a molecule to one target. The work described in this chapter aims to enhance the potency of EB429 against multiple chemokine targets, for which the techniques described above were less suitable.

Saturation mutagenesis is a widely used tool in protein engineering. Saturation mutagenesis can improve both antibody binding affinities and pharmacokinetic properties in tandem[447]. In this mutagenesis strategy, a codon in a protein or peptide sequence is substituted with all possible natural amino acids. Codon substitution can be done at one position or all amino acid positions using a degenerate codon, such as the NNK codon[448]. Saturation mutagenesis, coupled with phage display, allows for the screening of multiple peptide mutants against multiple chemokines.

3.1.3 The CoSMOS Pipeline

The coupling of combinatorial saturation mutagenesis, phage display, and next-generation sequencing was previously established within the group and was termed the Combinatorial Saturation Mutagenesis Optimisation Strategy (CoSMOS)[408]. This pipeline successfully enhanced the drug-like properties of the peptide HD2, thereby improving the peptide's potency and the number of chemokines to which HD2 could bind and inhibit. CoSMOS was conducted in two stages. The first step was to identify single mutant peptides with one amino acid change that showed improved binding compared to HD2, with inhibition validated in cell migration assays. Secondly, the 16 top-hit beneficial single mutations were combined to identify combinatorial mutants that showed additive benefits compared to the single mutants. To test peptide efficacy in a disease-relevant *in vitro* model, RNA sequencing data was analysed to create pools of chemokines expressed in diseased tissues. Combinatorial mutants successfully inhibited the migration of primary human immune cells to these complex chemokine pools, demonstrating their effectiveness in *in vitro* disease-relevant complex mixtures of chemokines. The combinatorial mutants also showed significantly enhanced potency over HD2, illustrating the benefits of the CoSMOS pipeline.

3.1.4 Aims and Hypotheses

The EB429 peptide exhibits therapeutic potential through its dual chemokine class binding and inhibition of primary T-cell chemotaxis, but it requires improvement of its drug-like properties. This chapter hypothesises that the CoSMOS pipeline will enable the identification of EB429 mutant peptides with enhanced potency and inhibition breadth. Therefore, this chapter aims to apply the CoSMOS strategy to the EB429 peptide sequence, improve the potency and binding range, and evaluate the effectiveness of the CoSMOS protocol.

This chapter aims to:

- Generate an NNK mutant EB429X library.
- Screen the EB429X library using phage display and next-generation sequencing.
- Characterise single mutant peptides in cell migration validation assays to identify mutants with enhanced potency and inhibition breadth.
- Generate a combinatorial EB429XC library.
- Screen the EB429XC library using phage display and next-generation sequencing.

3.2 Results

3.2.1 EB429XP Phage Library Generation

To test whether changing single amino acid residues in the EB429 sequence would lead to improved chemokine binding in phage display compared to EB429, a mutant phage library was designed and constructed. Using the degenerate NNK codon, saturation mutagenesis generated a phage library including the EB429 sequence and 304 single-residue mutant peptides (**Figure 3.1)**. Quality control steps to ensure library quality included titering the library and performing a phage spot test. The spot test demonstrates that the phage can infect bacteria, thereby ensuring the phage's functionality.

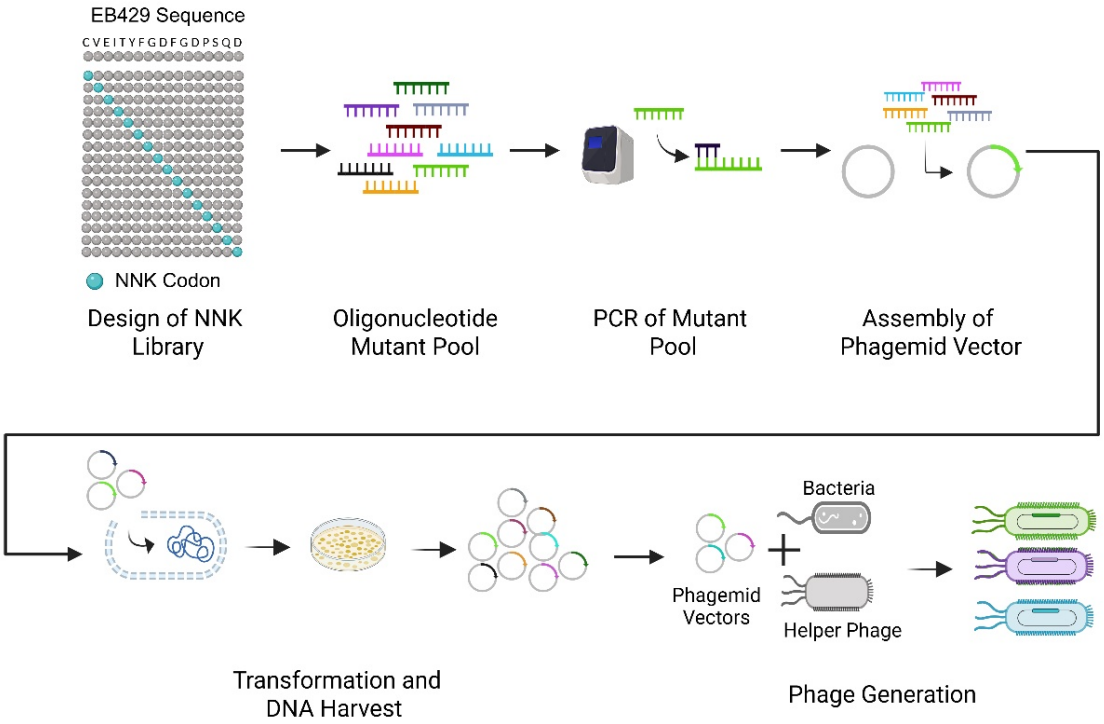

Figure 3.1 – Saturation mutagenesis library design and generation workflow. Experimental design of the NNK saturation mutagenesis library. An NNK codon replaces every residue of the EB429 sequence, creating a library of 304 mutants. The mutant library is synthesised as an oligonucleotide pool and assembled into a phagemid vector. The phagemid vectors are then transformed into bacteria. Phage is generated in transformed bacteria with helper phage.

The EB429 NNK phage display library was created, and a sample was sent for NGS to determine peptide coverage. Given the library's small size, full (100%) library coverage was desired. The first three attempts to generate the library did not yield all the required peptide mutants. As the second and third libraries contained all mutants when combined, a sample of EB429XP2 and EB429XP3 was pooled and sent again for NGS. This pooled sample, termed EB429XP4, contained the EB429 sequence and all 304 single-residue mutant peptides (**Figure 3.2**).

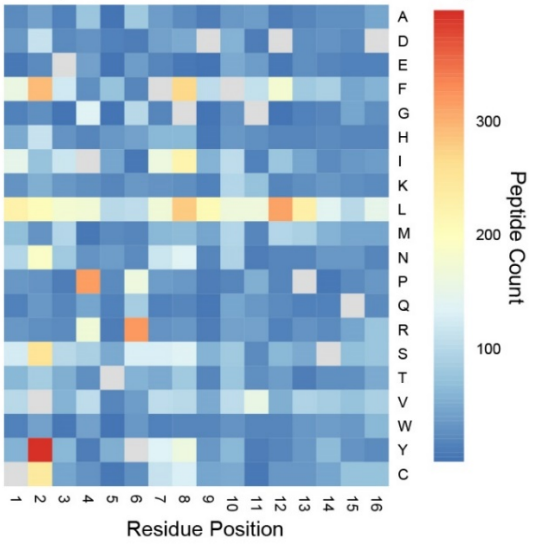

Figure 3.2 – EB429XP4 phage library peptide composition tile plot. Tile plot of peptide counts in the EB429XP4 phage library. The residue position is shown on the X-axis, and the heatmap of peptide counts is shown on the Y-axis. The scale is colour-coded, with low peptide counts shown in blue and high peptide counts shown in red. Data analysed by SB.

The (wild type) WT EB429 sequence was overrepresented in the library, and the frequency of peptides varied due to the differing frequency of codons within the NNK system. The presence of EB429 within the library is an artefact of the NNK phage library design, as the WT EB429 sequence was produced 16 times by replacing every amino acid with an NNK codon. The EB429 overrepresentation resulted in all mutant peptides competing with the WT EB429 sequence when screened in phage display. This overexpression of WT EB429 ensures that mutants identified by phage display would have outcompeted the WT EB429 sequence for chemokine binding.

3.2.2. EB429XP Phage Library Screening and Mutant Analysis

The EB429XP4 library was screened against 23 biotinylated chemokines in parallel. As described previously, NGS identified peptides that had bound to the chemokine targets following three selection rounds. Peptide enrichment was calculated by comparing the peptide output after phage display with the input library, designated as a log2E value. For each EB429 mutant peptide, the log2E values for a peptide chemokine pair were then compared to the log2E values of the WT EB429 for that chemokine. This comparison gave each mutant EB429 peptide a delta log2E value (Δlog2E). The Δlog2E was calculated to identify peptides with higher chemokine enrichment

compared to the WT EB429 sequence. Any peptides that demonstrated enrichment to the negative control chemoattractant C5a were excluded from the analysis.

As this work aimed to increase potency and binding breadth, mutant peptides of interest were identified by looking at two variables. Mean Δlog2E was used to identify mutant peptides that showed an increase in overall enrichment across all selecting chemokines, to identify peptides with broader chemokine-binding profiles. Peak Δlog2E was used to identify mutant peptides with significantly higher enrichment for specific chemokines, thereby selecting peptides with enhanced potency. To account for both breadth and potency, peptides were ranked by their mean and peak Δlog2E, and 16 selected 'improving' mutants were identified with mutations across 13 residue positions (**Figure 3.3**).

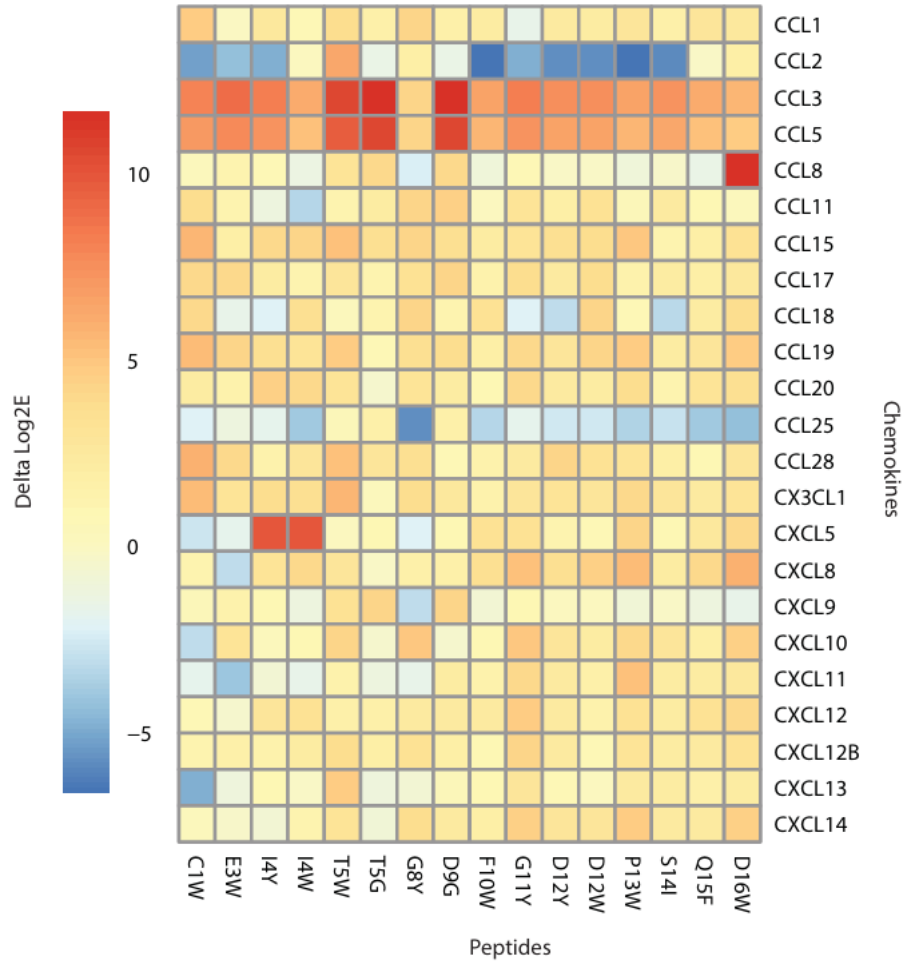

Figure 3.3 – Top 16 EB429 single mutant peptide tile plot. Tile plot of delta log2E (Δlog2E) of single EB429 mutant peptides. Δlog2E refers to mutant peptide enrichment in phage display compared to the parental WT EB429 enrichment. Positive Δlog2E indicates higher binding than EB429 of a peptide to a given chemokine, whilst negative Δlog2E indicates lower binding to a chemokine than EB429. The mutant residue position is shown on the X-axis, and selecting chemokine is on the Y-axis. The scale is colour-coded, with negative Δlog2E values in blue and positive Δlog2E values in red. Data analysed by SB. The log2E of the WT EB429 peptide in phage display was ~0. This lack of enrichment is likely due to EB429 mutants outcompeting WT EB429 for chemokine binding. Despite EB429 originating from a class B evasin capable of binding solely to CXC chemokines, the EB429 mutants showed enrichment against all 23 chemokines tested. However, only five peptides showed enrichment against CCL2, and only three peptides showed enrichment against CCL25.

The peptides T5W and D16W had a significant log2E compared to EB429 when selecting mutants with the highest mean log2E and from amongst the top 16 selected 'improving' mutants. G11Y had a significant log2E compared to EB429 when examining mutations that maximised peak XC

binding and mean XC binding. P13Y had a significant log2E when examining mutations that maximised mean XC binding (**Figure 3.4**). As the peptides T5W, G11Y, P13W, and D16W showed the highest enrichment in the binding parameters described above, they were selected for validation in chemotaxis assays.

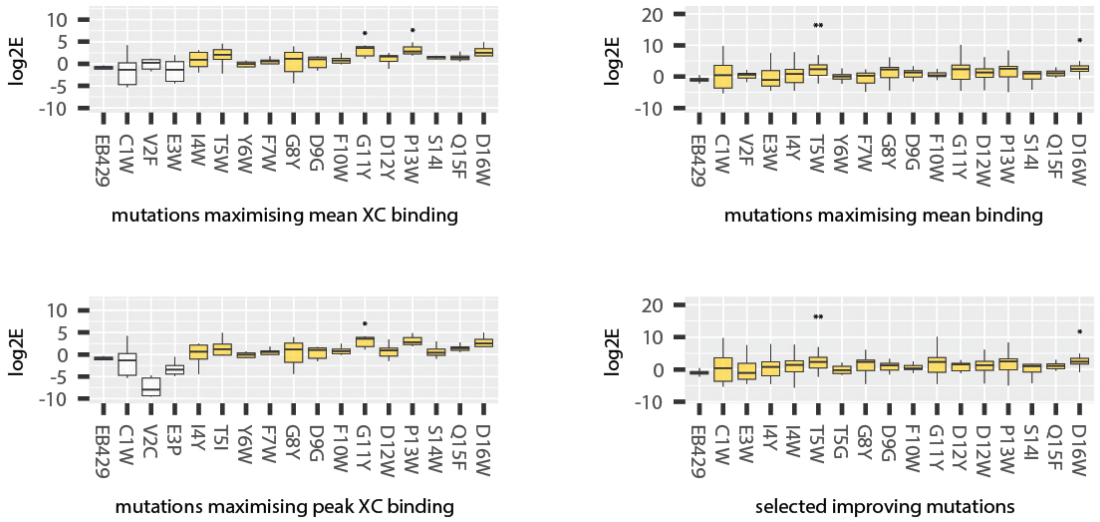

Figure 3.4 – Effect of EB429 mutations on log2E. Box-whisker plots demonstrating the impact of single EB429 mutants on log2E as identified by phage display. The log2E refers to mutant peptide enrichment in phage display compared to the parental WT EB429 enrichment. Individual plots indicate their selection criteria with titles. The top left-hand plot identifies the 16 mutants with the highest log2E compared to EB429 when looking at mutations that maximise mean binding to XC chemokines. The bottom left-hand plot identifies the 16 mutants with the highest log2E compared to EB429 when looking at mutations that maximise peak binding to XC chemokines. The top right-hand plot identifies the 16 mutants with the highest log2E compared to EB429 when looking at mutations that maximise mean binding to all chemokines. The bottom right-hand plot identifies the 16 mutants with the highest log2E compared to EB429 when ranking all mutations that maximise mean and peak log2E to all chemokines. EB429 or mutant peptides are identified on the x-axis, and log2E is shown on the y-axis. EB429 is coloured in blue as the negative control, and mutations demonstrating an improvement in log2E compared to EB429 are shown in yellow, as identified using a two-sided Dunnett's test for multiple comparisons with a threshold value of >0.55. Asterisks indicate the following: **p ≤ 0.01, *p ≤ 0.05. Data analysed by SB.

3.2.3 EB429 Single Mutants are Potent Inhibitors of CXC Chemokines

The chemokine inhibition of the EB429 mutants T5W, G11Y, P13W, and D16W was compared to the WT EB429 peptide in cell migration assays using $CD8^+$ T-cells. The positive controls were HD2 single mutant peptides[408] or the triple warhead evasin P1834, as appropriate for each assay. EB429 SCR peptide contained WT EB429 amino acids in a randomly shuffled sequence and was used as a negative control peptide.

The EB429 mutant peptides all inhibited $CD8^+$ T-cell chemotaxis to CXCL9, CXCL10, CXCL11, CXCL12α and CCL19 (**Figure 3.5**). The inhibition by these mutant peptides was statistically significant for all chemokines tested, except for CXCL9. The T5W mutant peptide was most potent as it inhibited chemotaxis to baseline levels ('cell only' column). T5W also outperformed the positive control in assays with CXCL11 and CCL19. All peptides showed improvement in inhibition compared to EB429 across at least one chemokine.

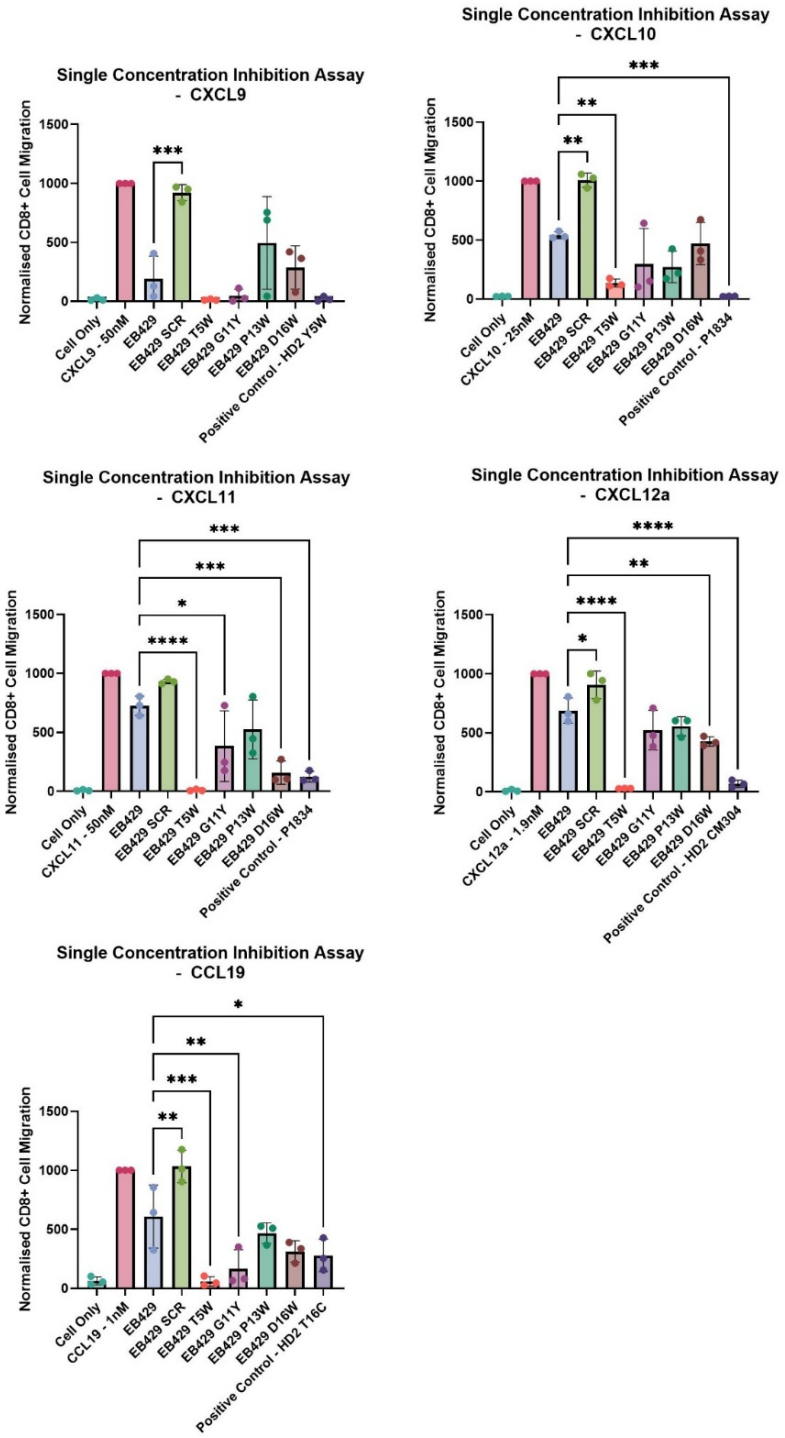

Figure 3.5 – Effect of EB429 single mutants on CD8⁺ T-cell migration to CXC and CC chemokines. Bar charts with standard deviation error bars depicting the effect of EB429 mutants on activated CD8⁺ T-cell migration to CXC and CC chemokines. All experiments were performed as three technical replicates and three biological replicates. Individual data points indicate mean values of technical replicates per experiment. Cell migration values were normalised to the mean value of migrated cell counts to the EC80 chemokine concentration and set to 1000 cells, as displayed on the Y-axis. The X-axis shows experimental constituents. Peptides were tested at a final concentration of 10 µM. Chemokines were tested at their EC80 doses, as indicated. EB429 SCR was used as a negative control, containing the scrambled amino acid residues of EB429. The statistical significance of EB429 was calculated compared to EB429 SCR using a one-way ANOVA and a Dunnett's test for multiple comparisons. Asterisks indicate the following: ****p ≤ 0.0001, ***p ≤ 0.001, **p ≤ 0.01, *p ≤ 0.05.

3.2.4 EB429 Single Mutants Demonstrate Inhibition of CCL21

To test whether an increase in chemokine binding breadth had also been achieved, the single mutant peptides were tested against a range of CC chemokines, against which EB429 showed no effect. This testing was conducted using the THP-1 cell line and $CD8^+$ T-cells. The EB429 mutants demonstrated no effect against selected THP-1 CC chemokines (**Figure 3.6**).

Despite this, the EB429 single mutant peptides demonstrate inhibition of the $CD8^+$ migrating chemokine CCL21 (**Figure 3.7**). Previous data indicated that EB429 could not inhibit CCL21 (**Figure 2.6**). The T5W peptide was able to inhibit chemotaxis to baseline levels. G11Y and D16W also demonstrated inhibition comparable to T5W. The binding to CCL21, coupled with improved potency (demonstrated by testing at a single concentration), supports the functional improvement of EB429 single mutants.

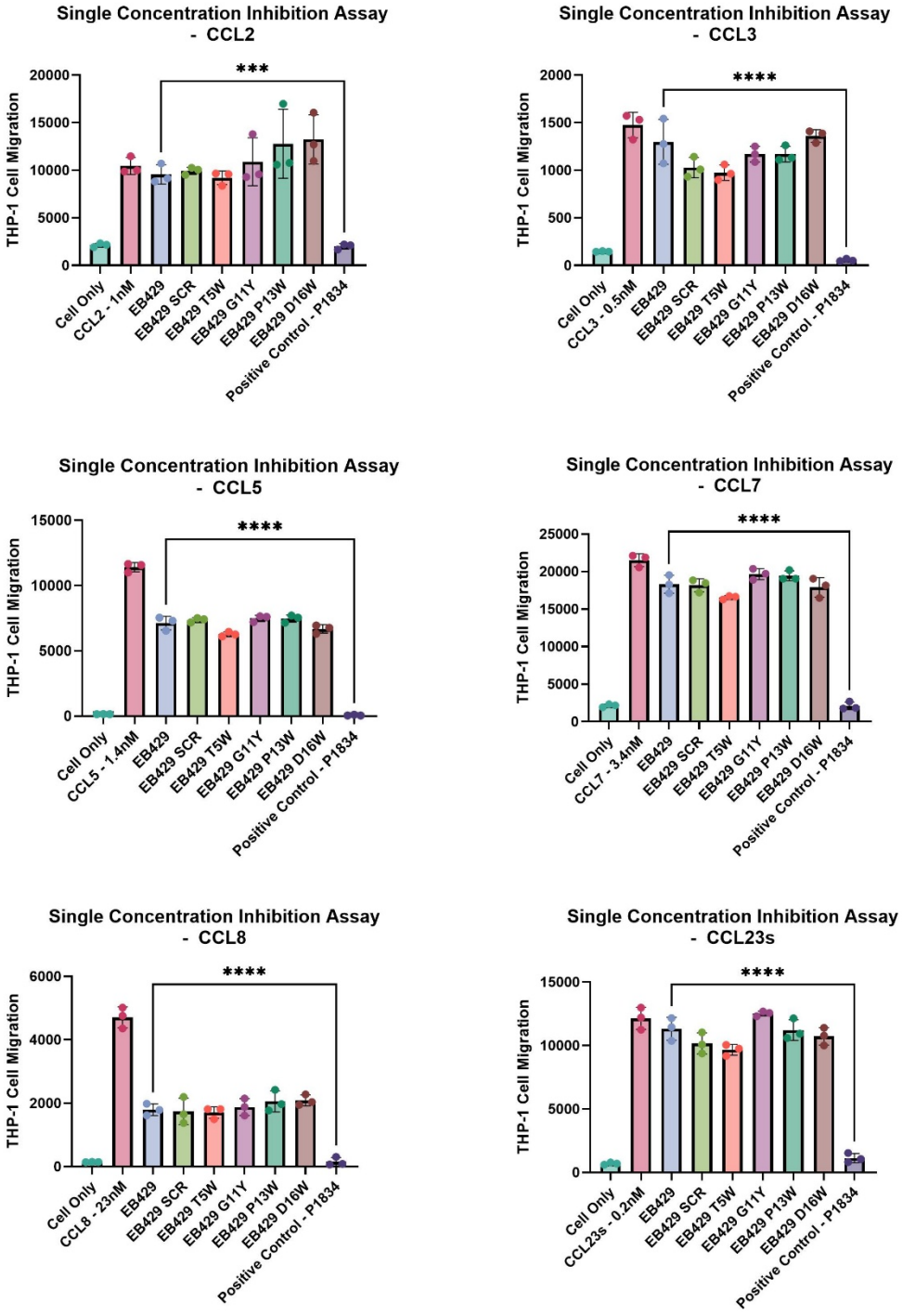

Figure 3.6 – Effect of EB429 single mutants on THP-1 migration to CC chemokines. Bar charts with standard deviation error bars depicting the effect of EB429 on THP-1 migration to CC chemokines. All experiments were performed as three technical replicates indicated by individual data points. The Y-axis shows THP-1 cell migration values. The X-axis shows experimental constituents. Peptides were tested at a final concentration of 10 μM. Chemokines were tested at their EC80 doses, as indicated. EB429 SCR was used as a negative control, containing the scrambled amino acid residues of EB429. The statistical significance of EB429 was calculated compared to EB429 SCR using a one-way ANOVA and a Dunnett's test for multiple comparisons. Asterisks indicate the following: ****p ≤ 0.0001, ***p ≤ 0.001, **p ≤ 0.01, *p ≤ 0.05.

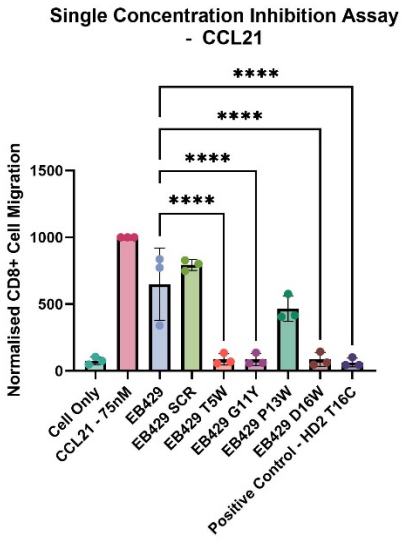

Figure 3.7 – Chemotaxis assays demonstrating the ability of EB429 mutants to inhibit CD8⁺ T-cell migration to CCL21. Bar charts with standard deviation error bars depicting the effect of EB429 mutants on activated CD8⁺ T-cell migration to CCL21. The experiment was performed as three technical replicates and three biological replicates. Individual data points indicate mean values of technical replicates per experiment. Cell migration values were normalised to the mean value of migrated cell counts to the EC80 chemokine concentration and set to 1000 cells, as displayed on the Y-axis. The X-axis shows experimental constituents. Peptides were tested at a final concentration of 10 μM. Chemokines were tested at their EC80 doses, as indicated. EB429 SCR was used as a negative control, containing the scrambled amino acid residues of EB429. The statistical significance of EB429 was calculated compared to EB429 SCR using a one-way ANOVA and a Dunnett's test for multiple comparisons. Asterisks indicate the following: ****p ≤ 0.0001, ***p ≤ 0.001, **p ≤ 0.01, *p ≤ 0.05.

3.2.6 EB429XC Library Generation

The top 16 selected EB429 single mutations were then tested to determine whether combinations of these mutations would be more effective than the single mutants themselves. Identifying beneficial combinations of mutations was necessary, as all four mutant peptides demonstrated an improvement over EB429 (to varying levels of significance) for all tested chemokines. Therefore, an EB429 combinatorial library, termed EB429XC, was created. The library consisted of EB429, EB429 SCR, 16 single EB429 mutants and all possible combinations of these 16 mutations. The library compromised 3,777 mutant peptides (**Figure 3.8**). The EB429XC library was created as previously described. NGS analysis of the EB429XC library indicated that 3651 of the 3777 peptide mutants were present, indicating 97% cloning efficiency.

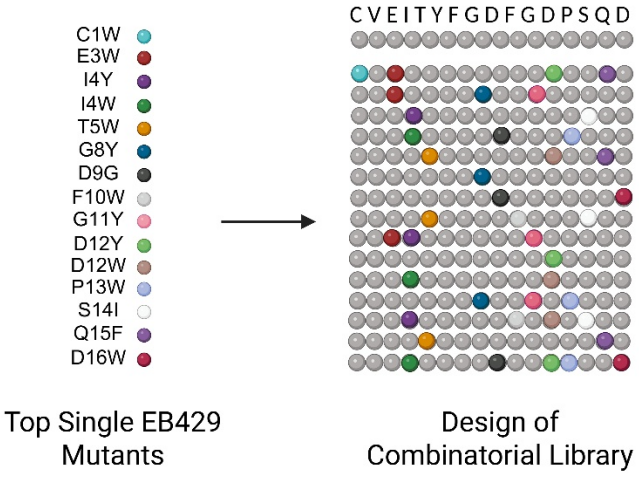

Figure 3.8 – Combinatorial mutagenesis library design. Experimental design of the combinatorial mutagenesis library. The top single mutant EB429 peptides identified from the saturation mutagenesis were combined to create a 3777-peptide mutant library. Figure made in Biorender.

3.2.7 EB429XC Phage Library Screening and Mutant Analysis

The EB429XC phage library was screened against 28 biotinylated chemokines in parallel (an increased number of chemokine targets due to increased supplier availability). C5a was used as the negative control, and any peptides binding to C5a were excluded from the analysis. The log2E was calculated as described previously. The Δlog2E for each single and combinatorial EB429 peptide was calculated as described previously, compared to WT EB429. This analysis method ensured that there was no bias in the analysis of single mutants compared to combinatorial mutants. The median Δlog2E was calculated for each combinatorial mutant across all screened chemokines, which ranked the Δlog2E values. The 20 'best' (CM-max) and 'worst' (CM-min) mutants were identified. Mutants were compared with the Δlog2E of the single mutants and the CM-max and CM-min mutants (**Figure 3.9**).

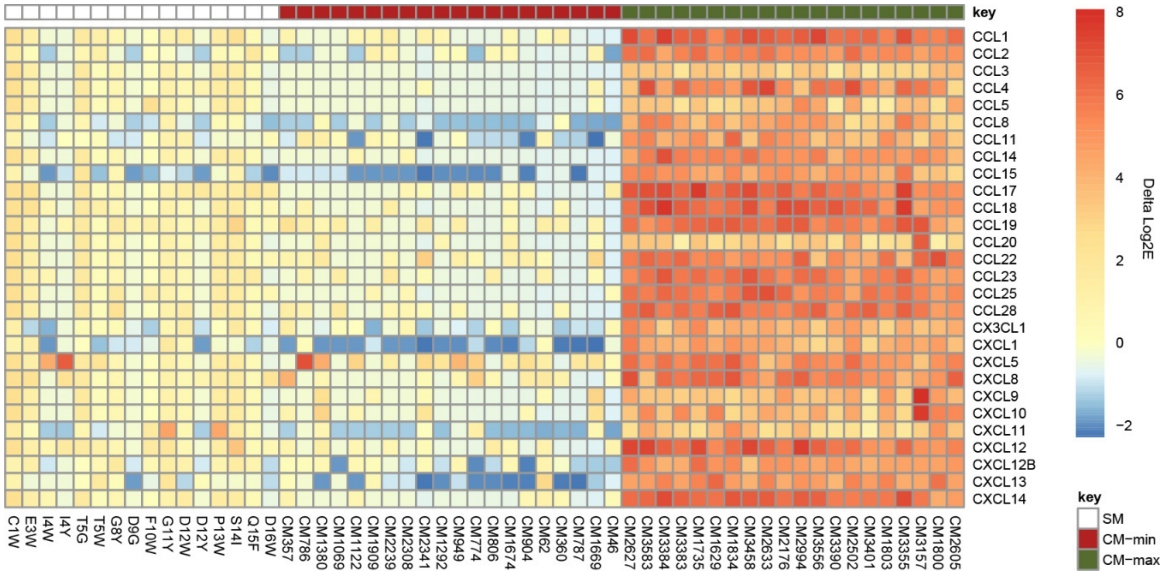

Figure 3.9 – EB429XC phage display tile plot. Tile plot of delta log2E (Δlog2E) of single mutant (SM) and combinatorial (CM) EB429 peptides. Δlog2E refers to mutant peptide enrichment in phage display compared to the parental WT EB429 enrichment. Positive Δlog2E indicates higher binding than EB429 of a peptide to a given chemokine, whilst negative Δlog2E indicates lower binding to a chemokine than EB429. Median Δlog2E ranked the CM peptides across all chemokines. The top 20 ranked CM peptides (CM-max) and the worst 20 are shown (CM-min). The mutant residue position is shown on the x-axis, and selecting chemokine is on the y-axis. The scale is colour-coded, with negative Δlog2E values in blue and positive Δlog2E values in red. Data analysed by SB.

All the CM-min mutants showed a decline in Δlog2E compared to WT EB429. The single mutant peptides also show Δlog2E values of ~0 (except for I4W and I4Y binding to CXCL5). The CM-max mutants exhibit high Δlog2E values compared to WT EB429.

The sequences of the CM-min and CM-max peptides were aligned using 'ClustalW' to identify whether there were discrepancies between mutations that maximised chemokine binding and those that reduced chemokine binding (**Figure 3.10**). There is no overt similarity between the CM-min and CM-max mutant sequence alignments, except for the residues C1, V2, E3, Y6 and F7. The lack of substitutions at the first three residues was due to mutations at these sites increasing non-specific binding to C5a, thus being excluded from the analysis. The Y6 and F7 substitutions are identical in CM-min and CM-max, as no top single mutants had mutations in these positions. Therefore, the combinatorial library did not include any mutations at these positions. The mutation profiles across the 10th to 12th positions are comparable for the CM-min and CM-max peptides.

Studying the CM-max peptides, 19 out of 20 of the best-binding peptides contained the T5W mutation. The substitution of Y at residue eight and W at residue 13 was a common feature of CM-max peptides, compared to CM-min peptides. The max binding group demonstrated significantly more aromatic residue substitutions, with peptides including five tyrosine or five tryptophan substitutions. The inclusion of T5W, G11Y, P13W, and D16W across the majority of the CM-max peptides supported the rationale behind further peptide validation in *in vitro* assays.

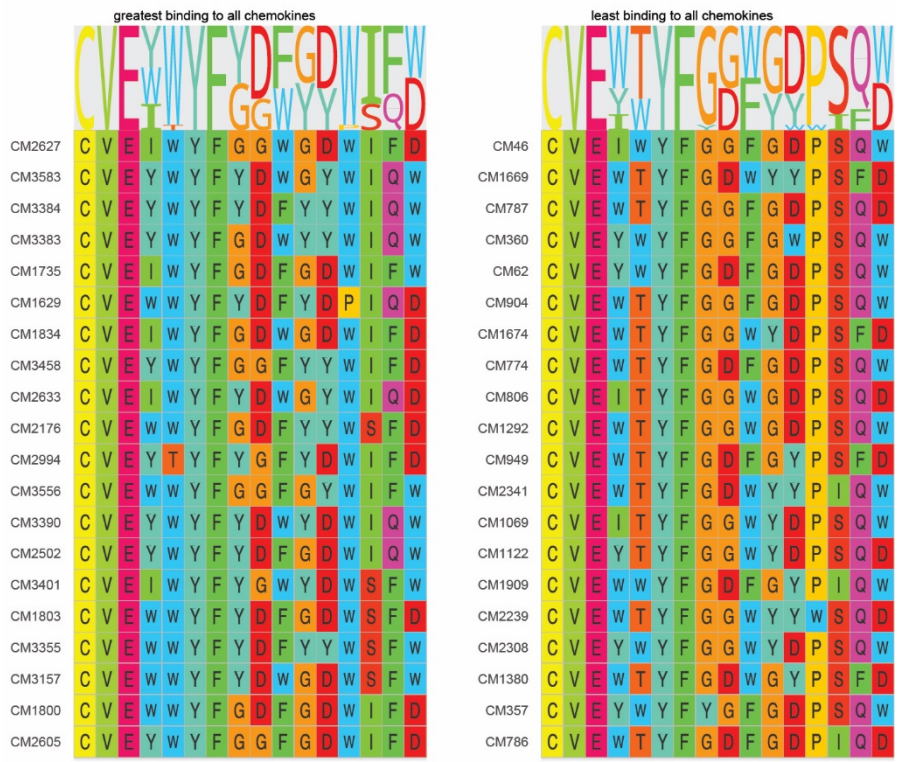

Figure 3.10 – Sequence alignment of the 20 best and 20 worst combinatorial peptides. Sequence alignment for indicated combinatorial EB429 peptides and indicated conserved residues. Sequences were aligned using ClustalW. Median Δlog2E ranked the combinatorial peptides across all chemokines. The top 20-ranked combinatorial peptides and the worst 20 are shown, as indicated. The first three residues are identical between the best and worst peptides, as mutations at these sites increased non-specific binding to C5a as identified by phage display, and were excluded from analysis. Residues are coloured using the Taylor scale. Data analysed by SB.

When deciding which mutant peptides to select and test in cell migration validation assays, the mutant peptide with the highest median Δlog2E was chosen, CM2627 (**Table 3.1**). To characterise mutant peptides with a variety of mutations, the best and worst 20 combinatorial mutants were analysed by creating an unrooted tree (**Figure 3.11**). The unrooted tree utilised the previously performed

sequence alignments of CM-min and CM-max peptides. The unrooted tree investigated the similarity between peptide sequences by calculating the pairwise evolutionary distance for each peptide compared to CM2627 using an identity matrix. This analysis grouped the CM-min and CM-max peptides separately. As CM2627 had the highest ∆log2E, the selection of four other CM-max peptides was made for validation based on their distance from CM2627. Using this tree, the peptides CM1629, CM3355, CM3384, and CM3583 were selected. In this way, peptide testing could encompass a range of mutations at various positions, providing more information about the different combinations of mutations.

Table 3.1 – Selected combinatorial peptides, sequences and Δlog2E as identified by phage display

Peptide Name	Sequence	Δlog2E
CM2627	CVEIWYFGGWGDWIFD	5.65
CM3384	CVEYWYFYDFYYWIQW	5.54
CM1629	CVEWWYFYDFYDPIQD	5.39
CM3583	CVEYWYFYDWGYWIQW	5.56
CM3355	CVEWWYFYDFYYWSFW	4.81

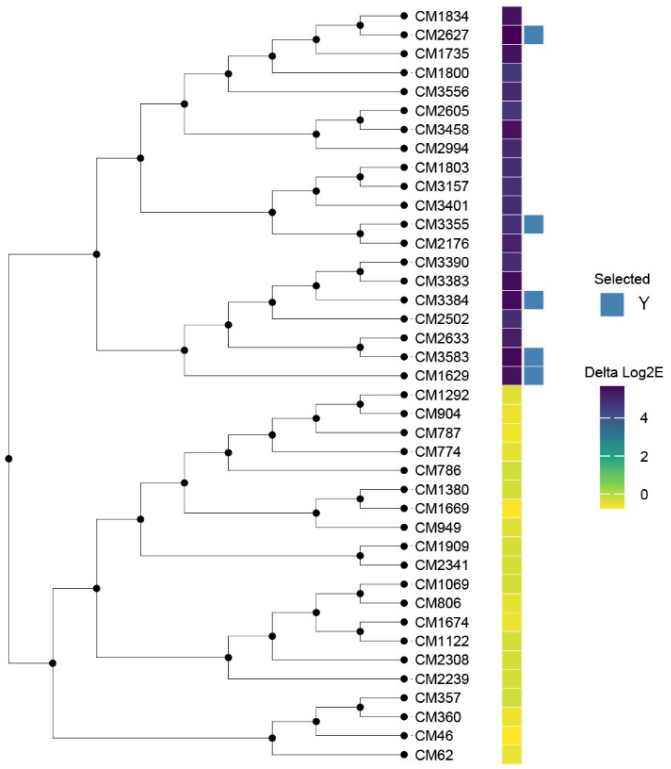

Figure 3.11 – Unrooted tree of EB429 best and worst combinatorial mutants. Unrooted tree of the top 20 (CM-max) and worst 20 (CM-min) combinatorial EB429 peptides, as identified by phage display, ranked by median Δlog2E. Peptides are indicated by the rightmost nodes, with subsequent nodes indicating sequence similarity, where more nodes indicate greater distance between the sequences and therefore less sequence similarity. The peptide with the highest median Δlog2E was identified as CM2627. ClustalW was used to align peptide sequences, and pairwise evolutionary distances were calculated for peptides from CM2627 using an identity matrix. Peptides were ranked based on their sequence distance from CM2627, and the peptides with the highest distance from the CM-max group are highlighted with blue squares. The scale is colour-coded, with negative Δlog2E values in yellow and positive Δlog2E values in blue. Data analysed by SB.

3.3 Discussion

Peptide and protein improvement strategies have undergone rapid development over the past few decades, facilitated by high-throughput techniques such as yeast surface display and phage display[404, 407]. The Bhattacharya laboratory developed the CoSMOS pipeline to improve the physical properties of chemokine-binding peptides, such as HD2. This pipeline combines saturation mutagenesis, phage display, and next-generation sequencing to identify single-mutant peptides with enhanced chemokine binding. Single mutations are combined and re-screened using phage display to identify beneficial mutation combinations. Cell migration validation

demonstrated that CoSMOS can successfully identify peptides with enhanced potency and increase the number of chemokines that the peptides can inhibit[408].

In this chapter, the CoSMOS pipeline was applied to the peptide EB429. EB429 was first identified in chapter two, but bound to a limited number of chemokines and displayed only micromolar potency against CXCL10. Using the CoSMOS pipeline, single mutants of EB429 have been identified that exhibit significantly enhanced inhibition of $CD8^+$ cells, as demonstrated by chemotaxis assays. Mutants were more potent at inhibiting $CD8^+$ migration to several CXC chemokines when tested at equimolar concentrations, and inhibition was also observed to a new chemokine, CCL21. Combinatorial mutagenesis identified beneficial combinations of these mutations, demonstrating high delta log2E values (Δlog2E). This data supports testing of the combinatorial mutants in cell migration assays.

3.3.1 Saturation Mutagenesis Produced Single Mutants with Improved Potency and Binding Range

The work in this chapter has identified single-residue mutant EB429 peptides with significant improvements over the WT EB429 peptide. The NNK saturation mutagenesis strategy was selected because it generates fewer stop codons than alternative degenerate codon strategies. To prevent further stop codons, an NDT codon strategy may also be used, but the NDT codon restricts the number of amino acids that can be used to 12[449]. However, the NNK codon encodes for A, T, G, or C in the first two codon positions and codes for T or G in the final codon position[450]. This substitution creates all 20 possible standard amino acid residues at each amino acid position in the 16-amino acid peptide sequence whilst introducing only one stop codon.

As described in Vales *et al.*, a clear correlation was observed between the phage display data of HD2 single alanine mutants and their migratory abilities in cell migration assays[76]. If a peptide had a high Δlog2E, as identified by phage display, it would perform better as an inhibitor of

chemotaxis, with a Spearman correlation coefficient (R) of 0.76[76]. This evidence, coupled with the identification of potent EB429 single-mutant peptides via phage display, provides confidence that the phage display output correlates with the identification of potent chemokine inhibitors.

Phage display enabled the identification of four mutant peptides, which were subsequently validated in chemotaxis assays. Statistically significant inhibition was seen for the chemokines CXCL10, CXCL11, CXCL12α and CCL19 compared to EB429. There was no significant improvement in the inhibition of CXCL9 by EB429. This lack of significance is a consequence of EB429 being a potent inhibitor of CXCL9. Inhibition was also achieved for the chemokine CCL21 with the peptides T5W, G11Y, and P13W.

The mutant peptides were characterised primarily in assays using primary human $CD8^+$ T-cells, isolated from leukocyte cones. Due to donor heterogeneity, dose-response curves and EC80 values had to be established for each donor and often differed significantly between donors. This phenomenon is less pronounced when using a standardised cell line, such as THP-1 cells. The variation between donors may explain the differing EC80 chemokine values between Figures 2.5 and 3.5, as well as the differing effect of EB429 on the inhibition of CXCL11. The difference in the potency of CXCL11 may also be due to the use of different peptide batches, which may vary slightly in concentration due to manual pipetting inconsistencies when peptides are resuspended. The use of primary cells, where donor heterogeneity is observed in response to chemokines, provides confidence that peptides may be effective in reducing $CD8^+$ T-cell migration in patients; however, this approach may also introduce further sources of variation. No other discrepancies in inhibition were observed with EB429.

3.3.2 The CoSMOS Pipeline has Identified Combinatorial EB429 Mutants with High Delta Log2E Values

The CoSMOS pipeline was first applied to the HD2 sequence, yielding results that indicated peptides could be mutated to enhance their binding range and potency to their chemokine targets[408]. This chapter demonstrates that combining single "improving" EB429 mutations can allow the identification of peptides with a higher Δlog2E compared to single mutants. The high Δlog2E of the CM-max mutants likely explains the lack of enrichment seen for the single mutants, as they may have been outcompeted due to the higher binding affinity of the CM-max peptides. Furthermore, employing the same technology confirmed the previously published findings regarding the potential application of CoSMOS, validating CoSMOS as an effective high-throughput platform for peptide optimisation.

The negative values for the CM-min mutants in this chapter demonstrate that all 'beneficial' single mutations cannot be randomly combined, as they may have deleterious effects on chemokine binding when combined. Thus, combinatorial mutagenesis demonstrates that not all beneficial mutations can be combined at random, and that phage display is a pivotal step in identifying beneficial combinations of mutations.

Through NNK mutagenesis and subsequent phage display screening, it was discovered that peptides containing aromatic residues had a higher Δlog2E than those containing other amino acid residues. As a higher Δlog2E would imply a higher binding affinity to the chemokine targets, engineering peptides with multiple aromatic residues may increase the non-specific binding of the peptide to other off-target proteins. Aromatic residues are known to contribute to various interactions, such as Pi-Pi stacking and dispersion forces[451]. C5a was used as a control in the phage display experiments to prevent non-specific peptide interactions, with any peptides binding to C5a being excluded from subsequent analysis. Despite this, the combinatorial

mutants were not characterised in cell migration assays in this chapter. This work will be explored in chapter four.

Identifying a peptide chemokine inhibitor from a class B evasin is a positive result, building on the success of potent peptide inhibitors identified by CoSMOS through the evolution of the HD2 peptide[408]. A new peptide sequence, identified from a structurally distinct evasin subtype, is a novel finding. The significance of this result is exemplified by the significant inhibition observed with the mutant T5W. This chapter has validated the CoSMOS pipeline and identified novel peptides capable of inhibiting CXC and CC class chemokines.

3.3.3 Limitations

3.3.3.1 NNK Mutagenesis

The tile plot of the top-hit single mutants, as identified by phage display, appears different from the analysis of the combinatorial mutants, particularly for the chemokines CCL3 and CCL5. The reason behind this discrepancy is that the methods used for analysing the phage display from the NNK library and the combinatorial library differed. Briefly, this arises from the different approaches used for dealing with peptides that have zero proportion of counts in the input phage library but are present in the output. This results in enrichment values of infinity, and to avoid this, zero proportions were replaced with the lowest input proportion in the experiment[408]. Where the proportion of count in output was not available, it was replaced with the lowest output proportion in the experiment rather than zero, which would result in a -Infinity log2E[408]. This analysis led to an artefactual elevation in Δlog2E to the chemokines CCL3 and CCL5. An improved method to avoid issues with infinity was subsequently applied to the bioinformatic analysis of combinatorial mutants. Adjusted counts for input and output libraries were generated from raw counts by adding 1 to all counts to avoid division by zero, and frequency determined[408]. Potential inhibitory peptides may have been missed due to the skewed analysis of the single mutant library. Despite

this, the identification of T5W and subsequent enhancement of combinatorial peptides have led to the discovery of promiscuous and potent binding peptides by employing the CoSMOS pipeline.

3.3.3.2 Cell Migration Assays

All chemotaxis experiments described thus far have used single chemokines. It is widely known that upwards of 30 chemokines can play a role in specific inflammatory diseases[84]. Further testing is required in a model that can reflect the biological role of chemokines, which cannot be recapitulated using single chemokine assays. Therefore, testing of combinatorial peptides using single chemokines was not completed. The lack of testing limits insights that can be made about their effects on cell migration assays at this stage.

The chemokines used in these experiments are made in bacteria. Proteins produced in bacterial cells can have different crystal structures from their native or mammalian-produced counterparts, despite having nearly identical sequences[452]. Such structural changes may affect the results seen in cell migration assays. Whilst using chemokines made using bacteria was necessary for consistency, these chemokines may behave differently from their native counterparts. This discrepancy stresses the need for a biologically relevant model which does not rely on recombinant chemokines, such as an *in vivo* air-pouch model.

3.4 Conclusions and Future Directions

In conclusion, CoSMOS has successfully mutated the EB429 sequence, enabling the discovery of EB-derived peptides with increased potency and breadth of inhibition. The characterisation of single mutants made it clear that testing peptides against all possible chemokines in cell migration assays was not appropriate due to the time and significant costs associated with these assays. Furthermore, testing in cell migration assays against individual chemokines lacks biological relevance. Many chemokines have active roles in diseased tissues and do not work in isolation. In previous work, this limitation has been overcome by generating pools of synthetic

chemokine pools that mimic disease states and using them to characterise the therapeutic potential of anti-chemokine peptides[408]. This approach was applied to the study of the selected combinatorial EB429 mutants and is described in the following chapter.

4. Chapter Four - Biological Activity of EB429 Combinatorial Peptides in Models of Insulitis

4.1 Introduction

As described in chapter three, saturation mutagenesis of the EB429 sequence yielded single-residue mutant peptides with significantly enhanced chemokine inhibition. The T5W mutant exhibited potent inhibition and binding to a new CC chemokine, CCL21. The EB429 sequence was further mutated using the CoSMOS methodology developed by the group[408]. Single mutations were combined, and the combinatorial mutants were screened in phage display. Selected combinatorial mutants demonstrated significantly enhanced chemokine binding compared to the single mutant peptides. Whilst encouraging, the combinatorial peptides require characterisation in cell migration assays. A key limitation of performing single-chemokine cell migration assays is that chemokines do not function in isolation[90]. In previous work this limitation has been overcome by using pools of synthetic chemokines that mimic the disease state[408]. This approach was applied to study the selected combinatorial EB429 mutants in cell migration assays with a focus on chemokines expressed in T1D islets.

4.1.1 Chemokines in T1D

T1D is characterised by the immune-mediated destruction of insulin-producing beta cells within islets. Progressive destruction of beta cells results in patients becoming nonresponsive to blood glucose, requiring exogenous insulin as their disease progresses and as they lose functional beta cell mass[453]. Insulitis, is a hallmark of T1D[226]. Insulitis is associated with immune infiltration and robust chemokine production. T-cells which recognise islets, termed autoreactive, follow chemokine gradients and migrate to the sites of insulitis. Beta cell destruction is mainly

facilitated through autoreactive $CD8^+$ T-cells[454]. Autoreactive $CD4^+$ T-cells provide the required activation signals to the $CD8^+$ cells[156]. Both $CD8^+$ and $CD4^+$ T-cells are therefore crucial for the development of T1D[250]. Recent advances in T1D treatments focus on teplizumab, a CD3-targeting treatment that results in T-cell depletion and exhaustion[292]. Two infusions over two weeks prevented T1D progression from stage two to stage three for approximately 18 months[298]. Despite this, treatments such as teplizumab have risks of opportunistic infections. Therefore, there is a clinical unmet need for the treatment of T1D.

Several lines of evidence suggest that chemokines play a role in the pathogenesis of T1D. Pancreas sections from newly diagnosed T1D patients revealed CXCL10 expression by beta cells, accompanied by corresponding CXCR3 expression on infiltrating T-cells[321]. Targeting CXCR1/2 has been explored as a means to prevent beta cell destruction following islet transplantation[342]. This chemokine therapy did not improve C-peptide levels post-transplant in a stage three clinical trial[344]. From mouse data, targeting chemokines has been shown to prevent the development of T1D. Using a CC chemokine decoy receptor D6, the development of T1D was prevented in 60% of NOD mice[333]. Using the herpesvirus-derived M3 protein, a pan-chemokine inhibitor, the selective expression of M3 on beta cells prevented 100% of NOD mice from developing T1D[331].

Targeting chemokines, which recruit T-cells, in the islets may be a novel strategy for T1D. By targeting chemokines in the islets, $CD8^+$ T-cells may be prevented from migrating and thus destroying the insulin-producing beta cells. The EB429 peptides appear to be T-cell-specific and potent inhibitors of chemokines that recruit $CD8^+$ T-cells. To validate whether the EB-peptides could be a novel treatment for T1D, they must be tested in assays which reflect the biologically relevant chemokines in T1D, using $CD8^+$ and $CD4^+$ T-cells.

4.1.2 Models of T1D

Several well-characterised models recapitulate insulitis (**Table 1.1**). As described in chapter one, the ideal model for T1D would be the NOD mouse model. The NOD mouse model spontaneously

develops autoimmunity and insulitis. Insulitis can be observed from weeks six to eight, with immune cell subtypes similar to those in human T1D[455]. NOD models are expensive, and more evidence of peptide effectiveness is required before progressing to the mouse. Therefore, an intermediate step is needed between *in vitro* chemotaxis assays and murine models.

Chemokines can be profiled from patients' serum. Serum-based methods detect chemokine quantities in circulation, which are unlikely to represent chemokines in or around islets accurately[456]. Pancreas tissue from recently diagnosed T1D patients would be the ideal tissue to deduce chemokine expression. Over the last decade, the network for pancreatic organ donors with diabetes has been established and allows investigation using T1D tissue from recently deceased T1D patients[151]. While scRNA sequencing has been performed on such tissues[457], the chemokine network based on scRNA sequencing has not been systematically examined as yet. Another approach that is commonly used is to stimulate donor human islets with cytokines[458-460]. Cytokine stimulation mimics insulitis and has been used to determine chemokine expression[323]. Due to the scarcity of human tissue, induced pluripotent stem cell-derived beta cells (SCBCs) are an attractive alternative[461]. However, inducing beta cell differentiation from SCBCs is highly challenging and costly, and the standards of cell maturation vary across protocols.

4.1.3 Deducing Chemokine Levels in T1D

Bulk RNA sequencing can be used to estimate chemokine expression levels in a tissue of interest by determining the transcript abundance of chemokines. Single-cell RNA-seq data could also be used if chemokine quantities from individual cell types were required, but may miss low-abundance transcripts[462]. A limitation of RNA-based quantifications is that transcript abundance may not accurately reflect actual chemokine quantities due to variations in translation and post-translational processes[463, 464]. Proteomic-based investigations could be used to quantify specific chemokine quantities in tissue[465].

For this project, islet tissue from newly diagnosed individuals with T1D would be ideal, but this was not possible to obtain. An attractive alternative is cytokine-stimulated human islets. The RNA-sequencing method was selected to create a chemokine pool from a publicly available dataset[466]. Access to healthy donor islets enabled a complementary proteomic approach, so the approach of cytokine-stimulating human islets was also pursued.

4.1.4 Aims and Hypotheses

Targeting $CD8^+$ recruiting chemokines is a novel approach to prevent $CD8^+$ T-cell-mediated destruction of beta cells within the pancreas. This targeting may prevent the progressive destruction of beta cells upon diagnosis of T1D or could be supplemented with treatments such as teplizumab. The method of peptide testing previously described used single chemokine cell migration assays. Chemokine networks in disease states are complex and synergistic, involving upwards of 20+ chemokines. Biologically relevant models of T1D and the chemokines implicated are required to evaluate the EB-peptide series. The hypothesis is that an EB429-derived peptide will effectively prevent T-cell migration to a pool of insulitis mimicking human chemokines.

The primary aim of this chapter is to characterise the EB429 peptide series using a chemokine pool based on RNA-sequencing data from cytokine-stimulated human islets. Using this model, IC50 curves will be generated, allowing for the determination of peptide potency.

This chapter aims to:

- Characterise the EB429 mutant peptide series in an RNA-sequencing-based pool of human insulitis-like chemokines.
- Determine the potency of lead EB429 mutant peptides using $CD8^+$ T-cells.
- Develop a human $CD4^+$ T-cell line and test the top mutant peptides using this cell line.

4.2 Results

4.2.1 RNA-sequencing Data Demonstrate Chemokine Gene Abundance of the Cytokine-stimulated Human Islets

The dataset GSE226888 was selected because it provided bulk RNA-sequencing data from human islets subjected to cytokine stimulation, which mimics early insulitis in T1D. The dataset included RNA-seq data from five cadaveric islets stimulated with IL-1β and IFN-γ for 24 hours[466]. Chemokine expression levels in this dataset were analysed by SB (**Figure 4.1**)[408]. Based on chemokine expression, a synthetic chemokine pool was created such that individual chemokine molar concentrations were at ratios determined by the mean relative expression of chemokines in the dataset (**Table 4.1**). This chemokine pool was named "insulitis". The chemokine XCL2 was not available for purchase and was excluded from the chemokine pool.

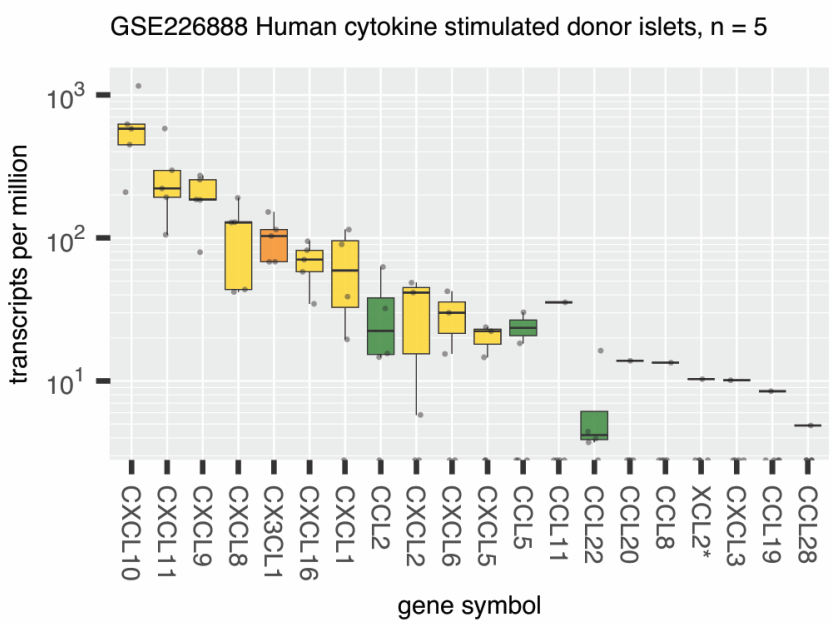

Figure 4.1 – Bulk RNA-seq of chemokine expression in cytokine-stimulated human islets. Box-whisker plot of chemokine expressed in five cytokine-stimulated human islets. Information was retrieved from the GEO database, dataset GSE226888. Chemokine genes are shown on the x-axis, and the chemokine transcripts per million are shown on the y-axis. Chemokines are colour-coded by chemokine class. Yellow-shaded chemokines are CXC chemokines, green-shaded chemokines are CC chemokines, and the orange-shaded chemokine is CX3CL1. An asterisk (*) indicates a chemokine that is not available for purchase. Data analysed by SB.

Table 4.1 – Chemokines and their respective concentrations and volumes in the insulitis pool

Chemokine	Concentration (μM)	Volume in 1mL (μL)
CXCL10	3.98789	398.8
CXCL11	1.84811	184.8
CXCL9	1.2918	129.2
CXCL8	0.70482	70.5
CX3CL1	0.66769	66.8
CXCL16	0.44904	44.9
CXCL1	0.34731	34.7
CCL2	0.16514	16.5
CXCL2	0.12674	12.7
CXCL6	0.11593	11.6
CXCL5	0.08012	8.0
CCL5	0.06409	6.4
CCL11	0.04682	4.7
CCL22	0.03749	3.7
CCL20	0.01826	1.8
CCL8	0.01775	1.8
CXCL3	0.01336	1.3
CCL19	0.01121	1.1
CCL28	0.00646	0.6

4.2.2 Insulitis Pool Testing Demonstrates Combinatorial Peptide Efficacy

To characterise the EB CM-derived peptides, they were first tested against the insulitis chemokine pool using $CD8^+$ T-cells. Dose-response curves were performed to determine the chemokine dose to be used (**Figure 4.2**). The chemokine concentration selected for testing was the EC50 value, as it provided a large dynamic assay range without being cost-prohibitive. EB429, EB429 SCR, and all single and combinatorial mutants were tested using the insulitis pool in a single-concentration inhibition assay **(Figure 4.3)**. Any peptide inhibition of this complex chemokine pool was significant compared to inhibition in single chemokine assays previously performed. Therefore, the EB429 SCR negative control peptide was used as the point for comparison and statistical analysis. The positive control for these experiments was HD2 CM304, the group's best inhibiting peptide at the time of testing. All peptides were tested at equimolar concentrations.

Modest inhibition of $CD8^+$ migration to the chemokine pool was observed for EB429. Significant inhibition was observed for the best single mutant, T5W. Significant inhibition was also observed for the combinatorial mutants CM1629, CM2627, CM3355 and CM3384, but only slight inhibition was observed for CM3583.

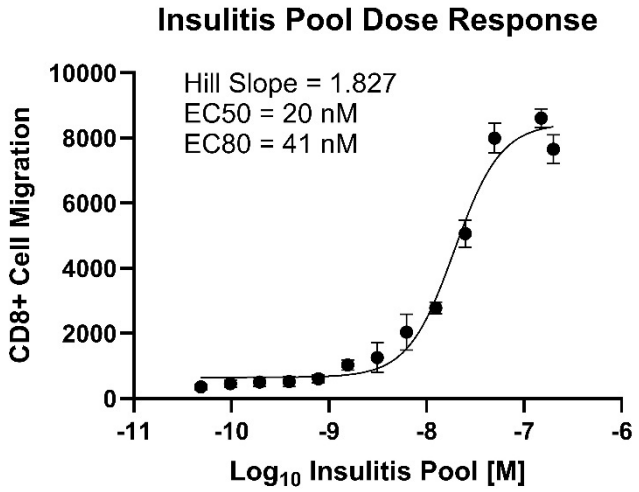

Figure 4.2 – Representative dose-response curve of the insulitis pool using activated $CD8^+$ T-cells. Migrated cell count values are displayed on the Y-axis. The X-axis shows the concentration of the chemokine pool as a Log10 of molar concentration. Each data point shows the mean value of the technical replicates at each concentration of the chemokine pool tested, with their standard deviation error bars shown. EC80 and EC50 values were calculated by plotting a 3-parameter dose-response log-logistic plot using GraphPad Prism.

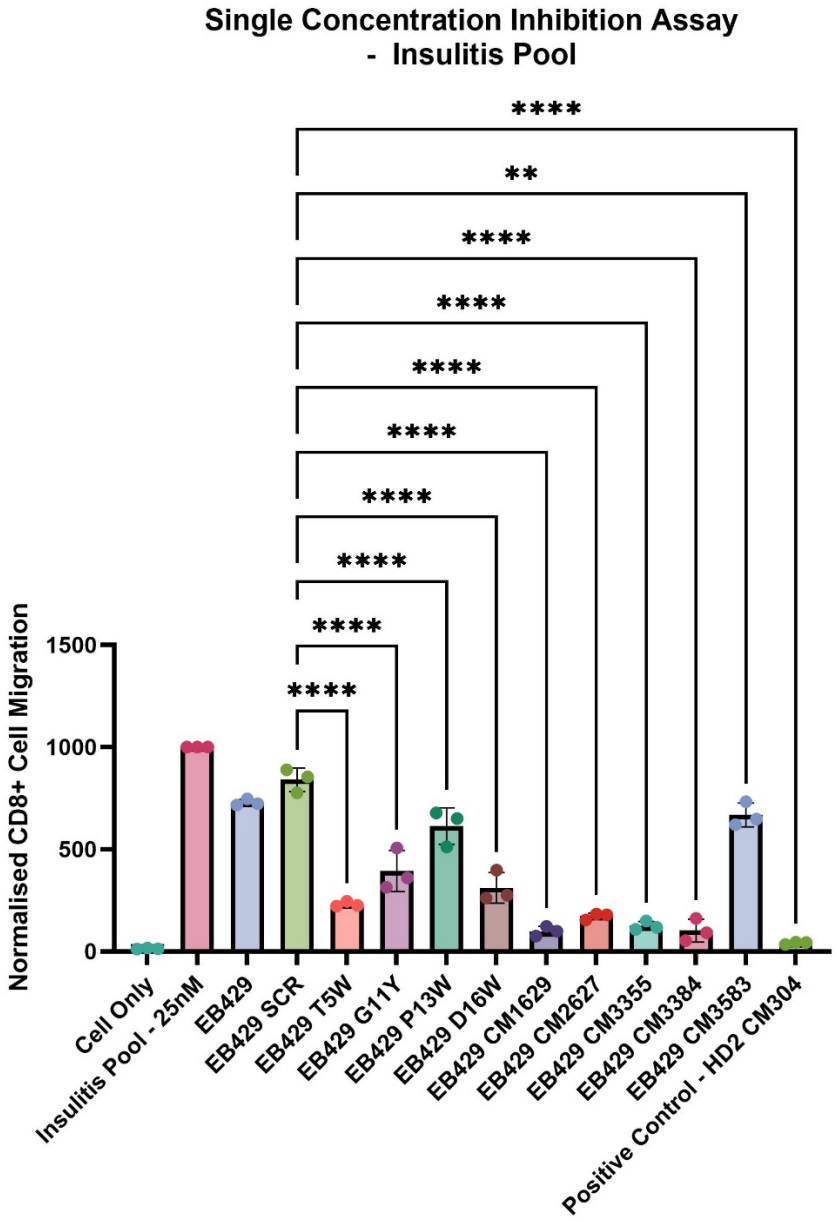

Figure 4.3 – Effect of EB429 combinatorial mutants on CD8⁺ T-cell migration to the insulitis chemokine pool. Bar charts with standard deviation error bars depicting the effect of EB429 mutants on activated CD8⁺ T-cell migration to the insulitis chemokine pool. The experiment was performed as three technical replicates and three biological replicates. Individual data points indicate mean values of technical replicates per experiment. Cell migration values were normalised to the mean value of migrated cell counts to the EC50 chemokine concentration and set to 1000 cells, as displayed on the Y-axis. The X-axis shows experimental constituents. Peptides were tested at a final concentration of 10 µM. EB429 SCR was used as a negative control, containing the scrambled amino acid residues of EB429. The statistical significance of EB429 mutants was calculated compared to EB429 SCR using a one-way ANOVA and a Dunnett's test for multiple comparisons. Asterisks indicate the following: ****p ≤ 0.0001, ***p ≤ 0.001, **p ≤ 0.01, *p ≤ 0.05.

4.2.3 Characterisation of EB-CM Mutants Demonstrates Cell Death for Three Mutants and CM1629 T-cell Specificity

To further characterise the combinatorial mutants, they were tested using the THP-1 cell line. Again, dose-response curves were performed to determine the chemokine dose to be used (**Figure 4.4**). To maintain consistency with testing using $CD8^+$ cells, the EC50 chemokine dose was used. EB429, EB429 SCR, and all single and combinatorial mutants were tested using the insulitis pool in single-concentration inhibition assays **(Figure 4.5)**. The analysis and controls used were identical to the previous single-concentration inhibition assays with $CD8^+$ cells. No inhibition was observed for any single mutant. The combinatorial mutants CM2627, CM3355 and CM3384 significantly inhibited THP-1-driven migration to the insulitis pool, compared to EB429 SCR.

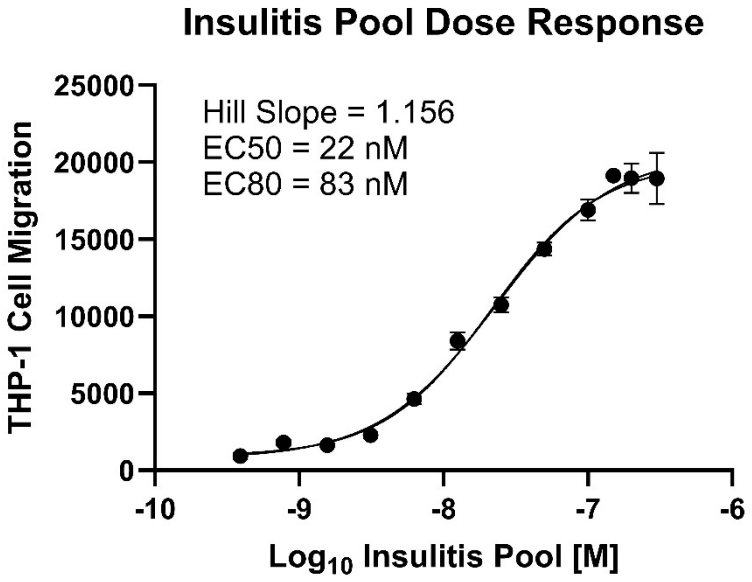

Figure 4.4 – Representative dose-response curve of insulitis pool using THP-1 cells. Migrated cell count values are indicated on the Y-axis. The X-axis shows the concentration of the chemokine pool as a Log10 of molar concentration. Each data point shows the mean value of the technical replicates at each concentration of the chemokine pool tested, with their standard deviation error bars shown. EC80 and EC50 values were calculated by plotting a 3-parameter dose-response log-logistic plot using GraphPad Prism.

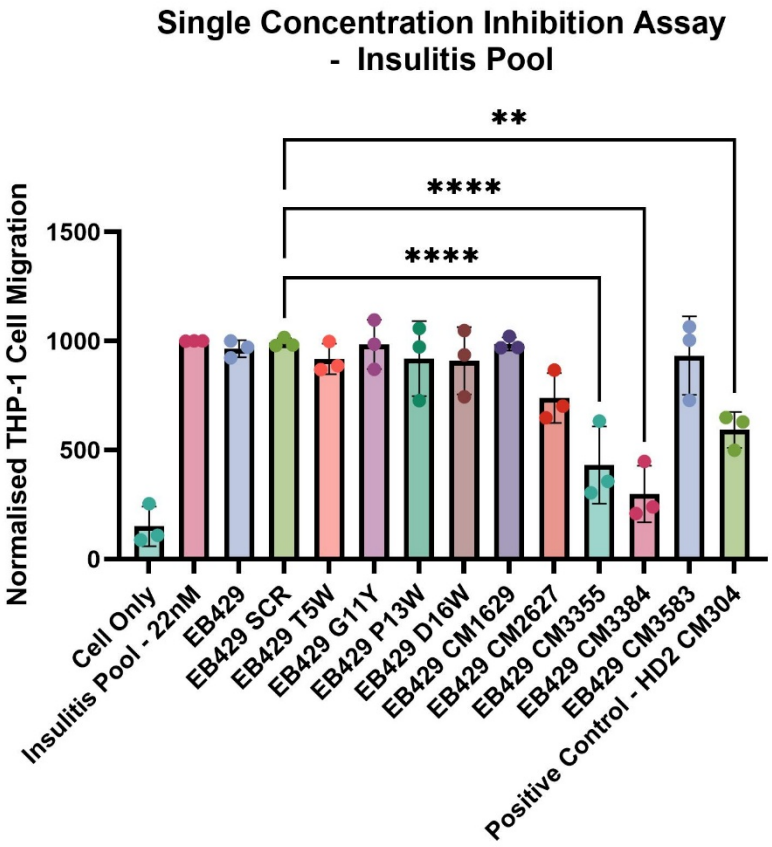

Figure 4.5 – Effect of EB429 combinatorial mutants on THP-1 cell migration to the insulitis chemokine pool. Bar charts with standard deviation error bars depicting the effect of EB429 mutants on THP-1 cell migration to the insulitis chemokine pool. The experiment was performed as three technical replicates and three biological replicates. Individual data points indicate mean values of technical replicates per experiment. Cell migration values were normalised to the mean value of migrated cell counts to the EC50 chemokine concentration and set to 1000 cells, as displayed on the Y-axis. The X-axis shows experimental constituents. Peptides were tested at a final concentration of 10 μM. EB429 SCR was used as a negative control, containing the scrambled amino acid residues of EB429. The statistical significance of EB429 mutants was calculated compared to EB429 SCR using a one-way ANOVA and a Dunnett's test for multiple comparisons. Asterisks indicate the following: ****p ≤ 0.0001, ***p ≤ 0.001, **p ≤ 0.01, *p ≤ 0.05.

To characterise whether the combinatorial mutants were non-specific, testing was performed using primary monocytes and the chemotactic agent C5a. Dose-response curves were completed to determine the dose of C5a to be used **(Figure 4.6)**. The peptides were tested at an EC80 concentration of C5a as the cost was not limiting in this assay **(Figure 4.7)**. A positive control C5a neutralising antibody was used. Statistical significance was compared to the peptide EB429 SCR. The peptides CM2627, CM3355 and CM3384 inhibited monocyte-induced C5a migration. Inhibition was not observed for CM1629 or CM3583.

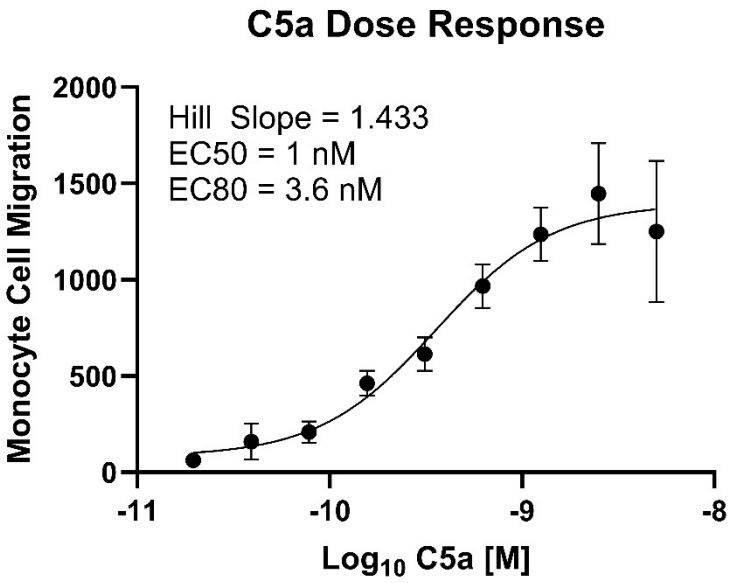

Figure 4.6 – Representative dose-response curve of C5a using monocytes. Migrated cell count values are indicated on the Y-axis. The X-axis shows the concentration of C5a as a Log10 of molar concentration. Each data point shows the mean value of the technical replicates at each concentration of the C5a tested, with their standard deviation error bars shown. EC80 and EC50 values were calculated by plotting a 3-parameter dose-response log-logistic plot using GraphPad Prism.

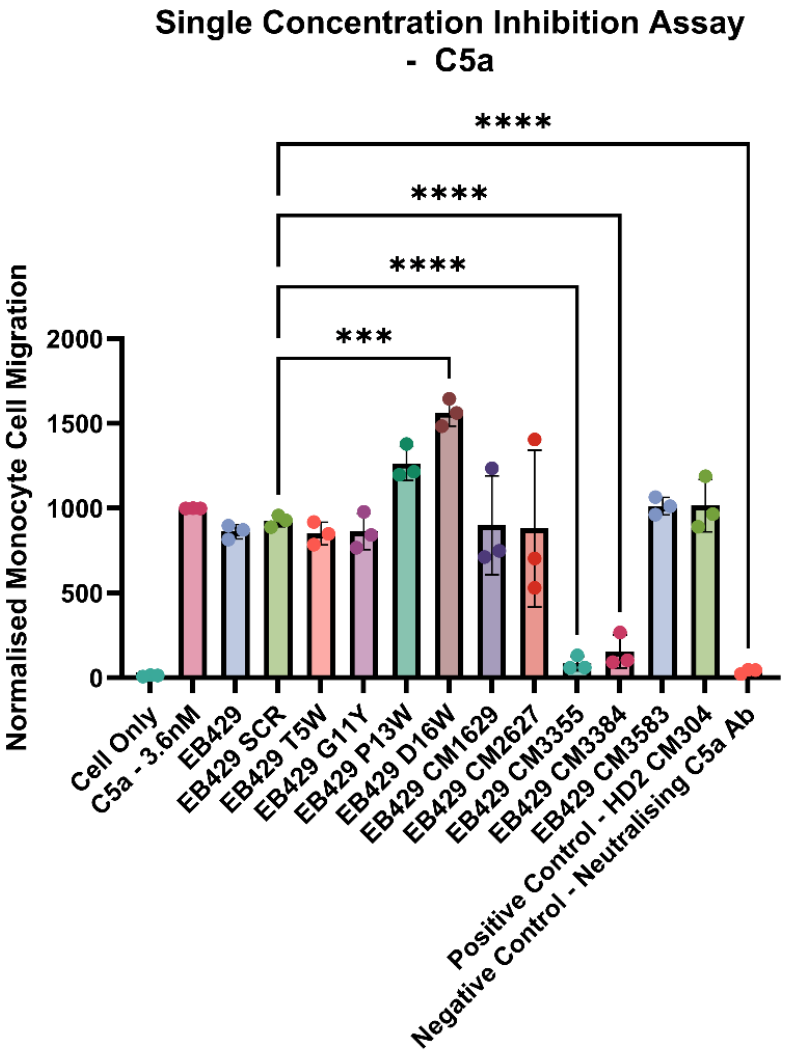

Figure 4.7 – Effect of EB429 combinatorial mutants on monocyte migration to the chemoattractant C5a. Bar charts with standard deviation error bars depicting the effect of EB429 mutants on monocyte cell migration to the chemoattractant C5a. The experiment was performed as three technical replicates and three biological replicates. Individual data points indicate mean values of technical replicates per experiment. Cell migration values were normalised to the mean value of migrated cell counts to the EC50 chemokine concentration and set to 1000 cells, as displayed on the Y-axis. The X-axis shows experimental constituents. Peptides were tested at a final concentration of 10 μM. EB429 SCR was used as a negative control, containing the scrambled amino acid residues of EB429. The statistical significance of EB429 mutants was calculated compared to EB429 SCR using a one-way ANOVA and a Dunnett's test for multiple comparisons. Asterisks indicate the following: ****p ≤ 0.0001, ***p ≤ 0.001, **p ≤ 0.01, *p ≤ 0.05.

Given the apparent non-specific effects observed with several combinatorial mutants, the peptides were tested for their ability to induce cell death through propidium iodide labelling. Peptides were incubated with cells for two hours, replicating the time the peptide would be exposed to the cells in cell migration assays. Cell viability was assessed by adding propidium iodide (PI). The gating strategy was established using cells boiled at 100 °C for 10 minutes to set

the PI-positive gate. Testing was performed using $CD8^+$ cells **(Figure 4.8, Figure 4.9, Figure 4.10)**. The peptides CM2627, CM3355 and CM3384 induced $CD8^+$ cell death. No cell death was observed for the peptide CM1629 or CM3583. No peptides affected cell migration when tested in the absence of chemokine **(Figure 4.11)**. Due to these results, CM2627, CM3355 and CM3384 were not investigated further.

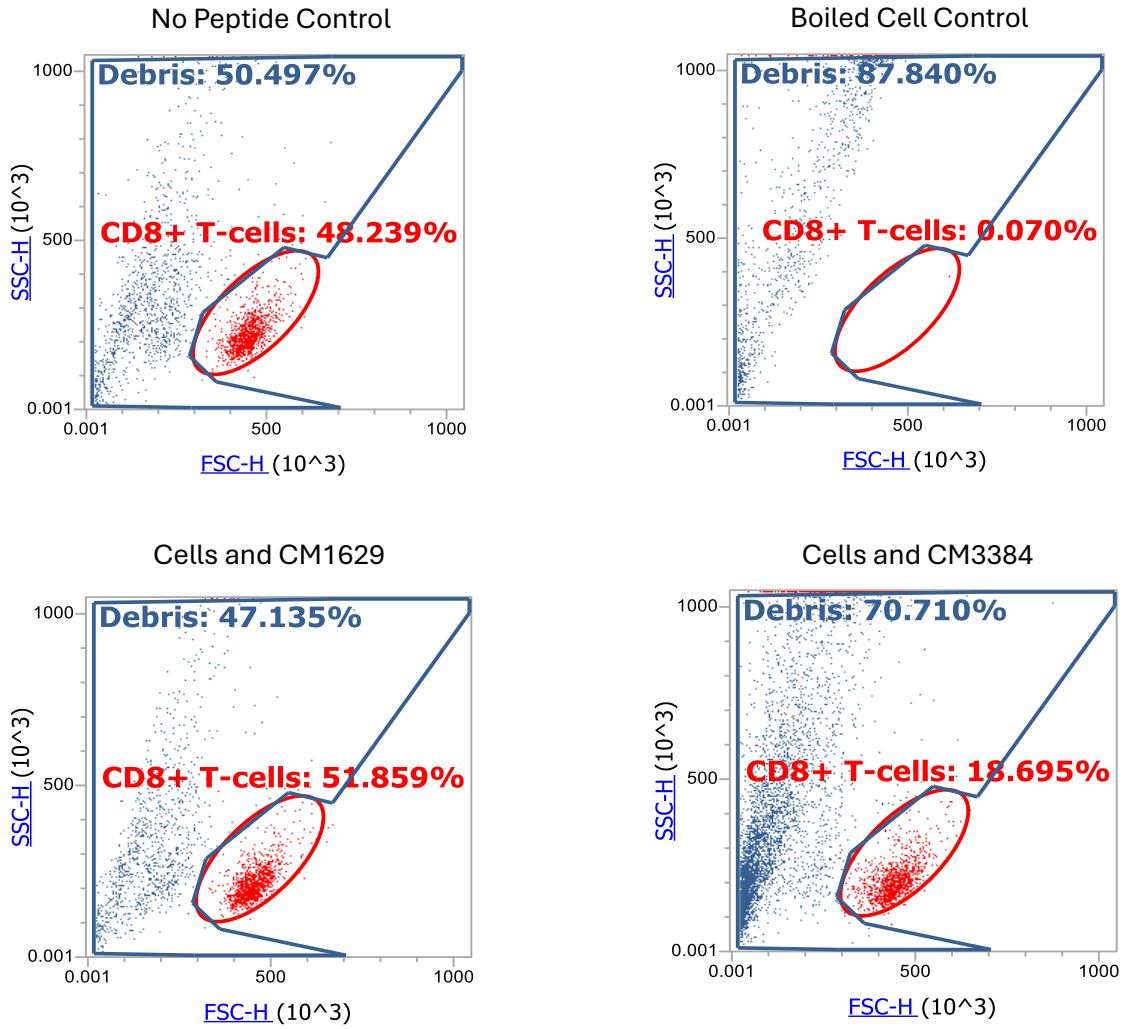

Figure 4.8 – Representative flow cytometry dot plots of $CD8^+$ T-cells incubated with peptides. Representative $CD8^+$ T-cells dot plots, either incubated with or without peptides. Cells were gated into two regions (Debris and $CD8^+$ T-cells), drawn around the distinct cell population and the cellular debris. The X-axis shows forward scatter height (FSC-H), and the Y-axis shows side-scatter height (SSC-H). All experiments were performed as three biological replicates.

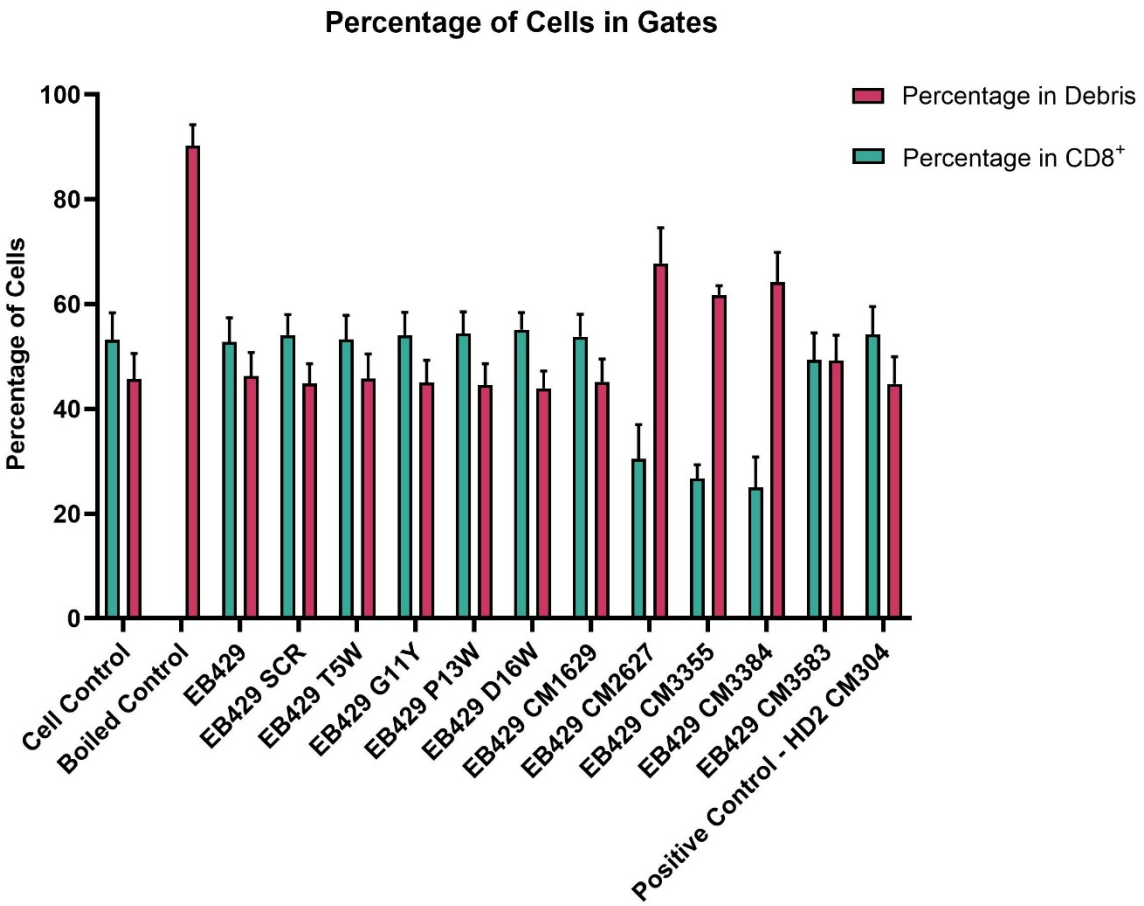

Figure 4.9 – Percentage of cells in debris and CD8⁺ gates following incubation with peptides. Bar chart with standard deviation error bars showing the relative abundance of the two gating regions of CD8⁺ T-cells. CD8⁺ T-cells were either incubated with or without peptides. Cells were gated into two regions (Debris and CD8⁺ T-cells), drawn around the distinct cell population and the cellular debris. The X-axis shows the condition of the CD8⁺ T-cells or which peptide they were incubated with, and the Y-axis shows the percentage of CD8⁺ T-cells falling in each gate. All experiments were performed as three biological replicates.

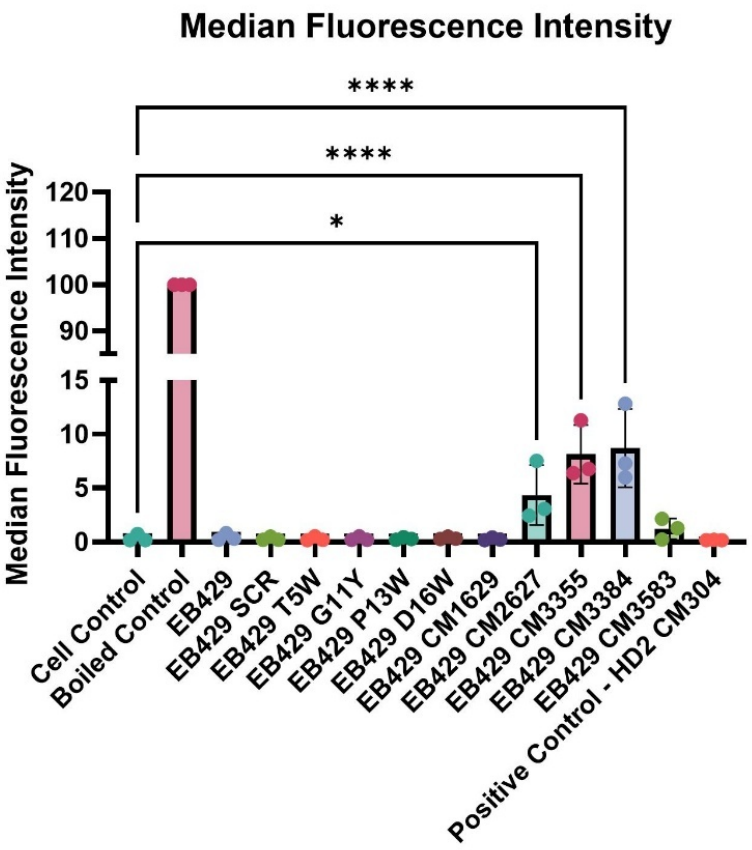

Figure 4.10 – Propidium iodide median fluorescence intensity of CD8⁺ cells following incubation with peptides. Bar charts showing the median fluorescence intensity measured in all cells by propidium iodide fluorescence dye. CD8⁺ T-cells were either incubated with or without peptides. The X-axis indicates the condition of the CD8⁺ T-cells or the peptide with which they were incubated. Median fluorescence intensity values were normalised to the mean fluorescence intensity of the boiled control, set to 100, as indicated on the Y-axis. The experiment was performed as three biological replicates and individual data points (the mean of technical replicates is shown). The statistical significance of EB429 mutants was calculated compared to the cell-only control using a one-way ANOVA and a Dunnett's test for multiple comparisons. Asterisks indicate the following: ****p ≤ 0.0001, ***p ≤ 0.001, **p ≤ 0.01, *p ≤ 0.05.

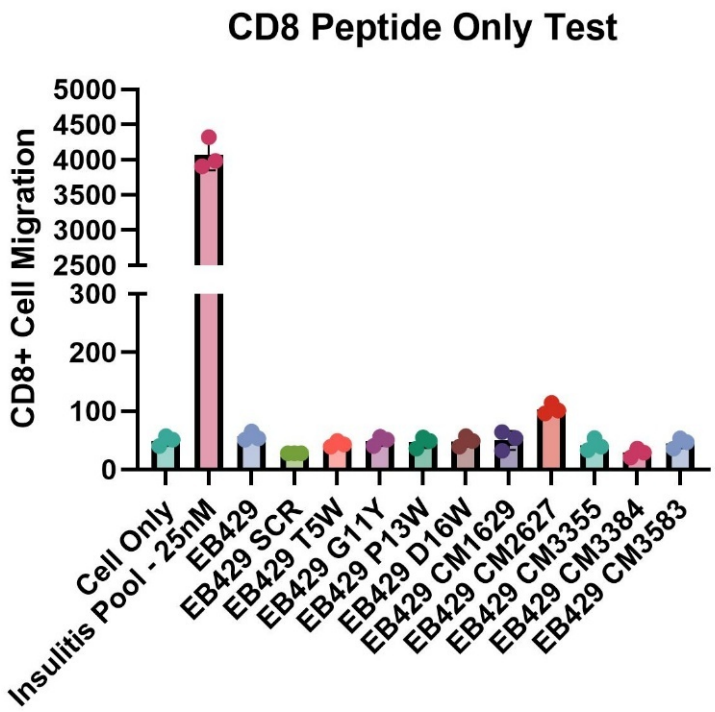

Figure 4.11 – Effect of EB429 combinatorial mutants on CD8⁺ T-cell migration in the absence of chemokine. Bar charts with standard deviation error bars depicting the effect of EB429 on CD8⁺ T-cells in the absence of chemokine. The experiment was performed with technical replicates indicated by individual data points. The Y-axis shows CD8⁺ cell migration. The X-axis shows experimental constituents. Peptides were tested at a final concentration of 10 µM. Cell-only migration was used as a negative control. The statistical significance of EB429 mutants was calculated compared to cell-only migration using a one-way ANOVA and a Dunnett's test for multiple comparisons.

4.2.4 Characterisation of a Negative Control CM1629 peptide, CM1629 SCR

The peptide CM1629 was selected as the best combinatorial mutant because it inhibited CD8⁺ T-cell migration to the insulitis pool without exhibiting nonspecific activity or cell death. A negative control peptide, CM1629 SCR, was created using the same strategy as EB429 SCR. The CM1629 SCR peptide demonstrated comparable inhibition to EB429 using the insulitis pool **(Figure 4.12)**. CM1629 significantly inhibited CD8⁺ migration to the insulitis pool, compared to CM1629 SCR. Therefore, the CM1629 SCR was adopted as the negative control peptide for CM1629.

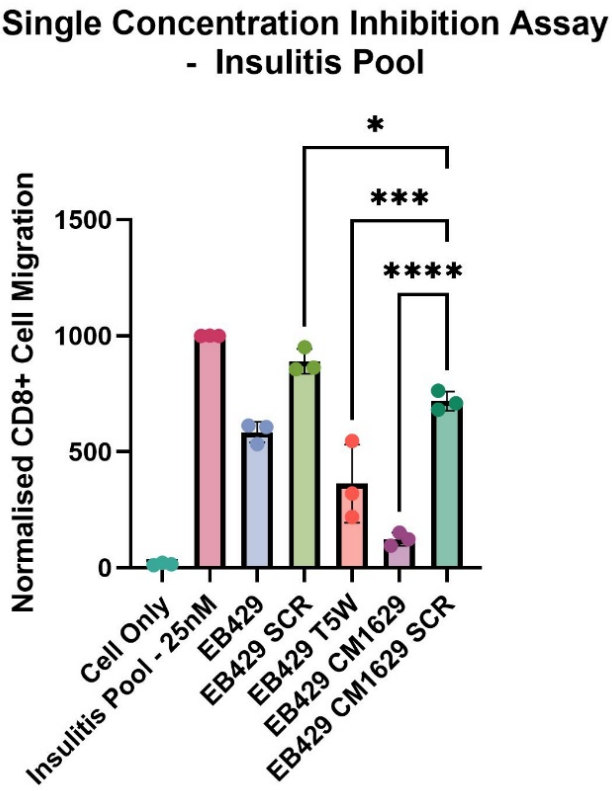

Figure 4.12 – Effect of selected EB429 combinatorial mutants on CD8⁺ T-cell migration to the insulitis chemokine pool. Bar charts with standard deviation error bars depicting the effect of EB429 mutants on activated CD8⁺ T-cell migration to the insulitis chemokine pool. The experiment was performed as three technical replicates and three biological replicates. Individual data points indicate mean values of technical replicates per experiment. Cell migration values were normalised to the mean value of migrated cell counts to the EC50 chemokine concentration and set to 1000 cells, as displayed on the Y-axis. The X-axis shows experimental constituents. Peptides were tested at a final concentration of 10 µM. CM1629 SCR was used as a negative control, containing the scrambled amino acid residues of CM1629. The statistical significance of EB429 mutants was calculated compared to CM1629 SCR using a one-way ANOVA and a Dunnett's test for multiple comparisons. Asterisks indicate the following: ****p ≤ 0.0001, ***p ≤ 0.001, **p ≤ 0.01, *p ≤ 0.05.

4.2.5 CM1629 is Effective Against CD4⁺ T-cells and the Insulitis Pool

As both CD4⁺ and CD8⁺ T-cells have pathogenic roles in T1D[156], a CD4⁺ T-cell line was developed. Briefly, cells were isolated using a CD4⁺ isolation kit from a leukocyte cone. CD4⁺ T-cells are known to have varied chemokine receptor expression depending on their subclassification. Th1 CD4⁺ T-cells typically express CCR2, CCR5, and CXCR3, Th2 CD4⁺ T-cells express CCR1, CCR3, CCR4, and CCR8, CCR7 is commonly expressed by naïve CD4⁺ T-cells, and Treg CD4⁺ T-cells express CCR3, CCR4, CCR5, and CXCR3[467]. CD4⁺ T-cells were characterised by labelling using available antibodies to cell surface receptors (**Figure 4.13**). Cells indicate 99% receptor labelling

for CD4. No receptor labelling for CD8 was observed. Cells also indicate 75% receptor expression for the chemokine receptor CCR4, 27% for CCR7 and 66% for CXCR3. Other chemokine receptor expression was negligible. This flow cytometry experiment confirms that these cells constitute a homogenous $CD4^+$ T-cell population with no $CD8^+$ T-cell contamination. The chemokine expression pattern suggests that these cells comprise a mixed $CD4^+$ T-cell population, with CCR4 indicating the presence of Th2, Th17, Th22, and Tregs, CXCR3 expression suggesting Th1, Th9, and Tregs, and CCR7 indicating naïve and Treg populations[467]. These indicated cell types are consistent with the $CD4^+$ T-cell subtypes that traffic in peripheral blood[467], and indicate that this cell population would respond in chemotaxis assays.

Dose-response curves were performed using $CD4^+$ T-cells and the insulitis pool **(Figure 4.14)**. The peptides EB429, EB429 SCR, T5W, CM1629 and CM1629 SCR were tested in single-concentration inhibition experiments **(Figure 4.15)**. The negative control peptide used was CM1629 SCR. EB429 showed no significant inhibition compared to CM1629 SCR, and T5W showed slight inhibition. CM1629 demonstrated significant inhibition of $CD4^+$ T-cell migration to the insulitis pool. Testing indicates that CM1629 can significantly inhibit both $CD4^+$ and $CD8^+$ T-cells.

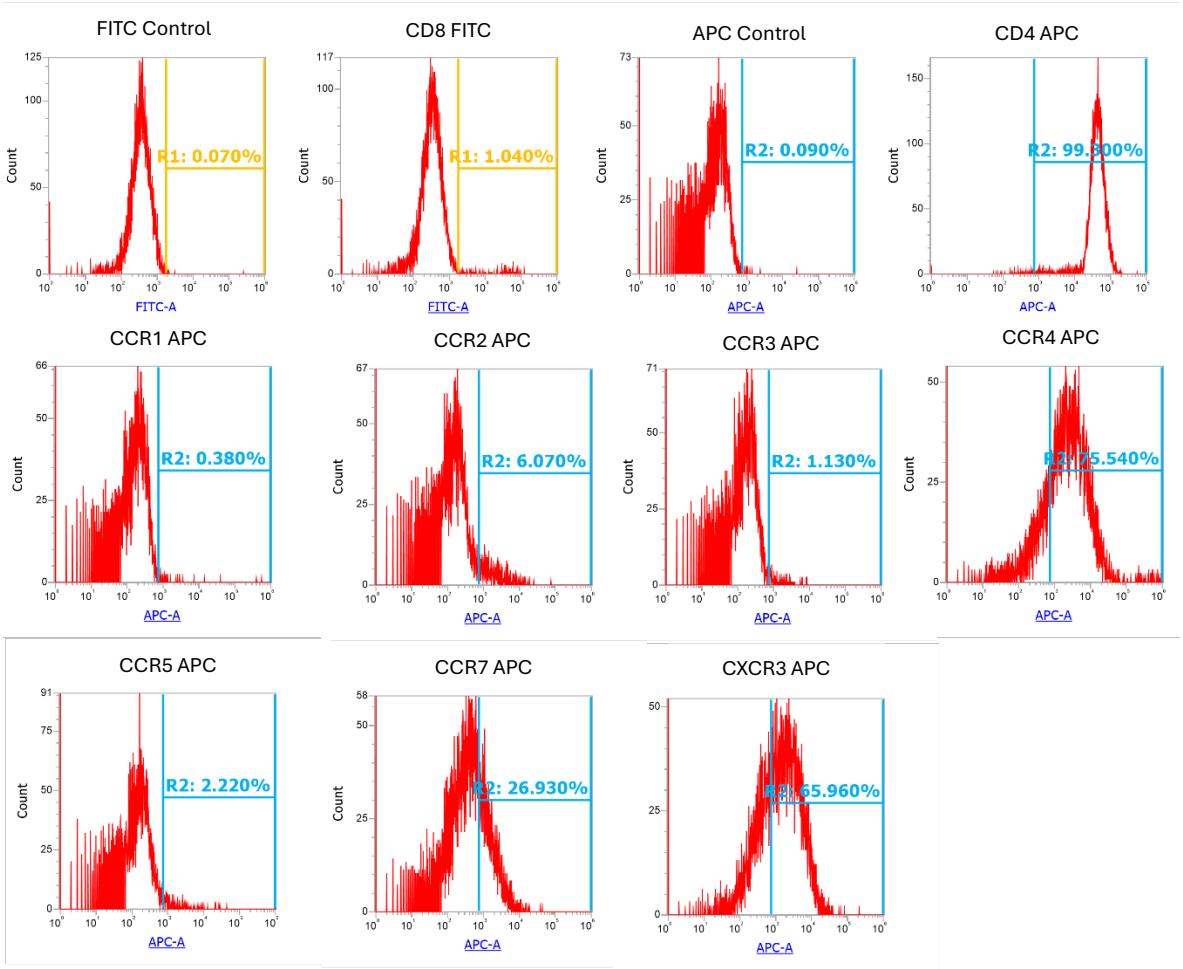

Figure 4.13 – Cell receptor labelling of CD4⁺ T-cells. Histogram plots of activated CD4⁺ T-cell labelling using antibodies to cell surface receptors. The antibody used for labelling is indicated above the histogram plot. Gating was based on FITC control (yellow, indicated by R1) or APC control (blue, indicated by R2) conjugated antibodies. The X-axis shows cell count, and the Y-axis shows fluorescence intensity.

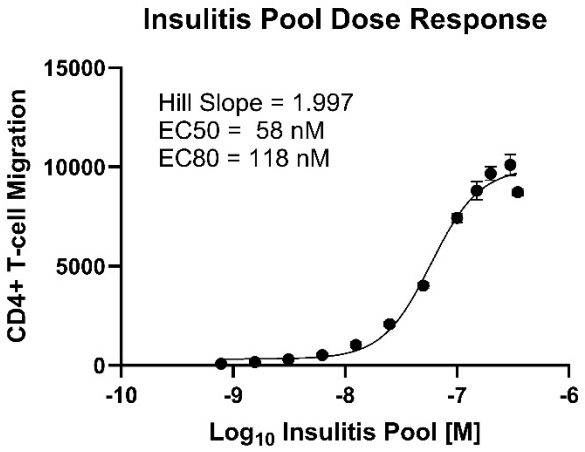

Figure 4.14 – Representative dose-response curve of insulitis pool using activated CD4⁺ T-cells. Migrated cell count values are indicated on the Y-axis. The X-axis shows the concentration of the chemokine pool as a Log10 of molar concentration. Each data point shows the mean value of the technical replicates at each concentration of the chemokine pool tested, with their standard deviation error bars shown. EC80 and EC50 values were calculated by plotting a 3-parameter dose-response log-logistic plot using GraphPad Prism.

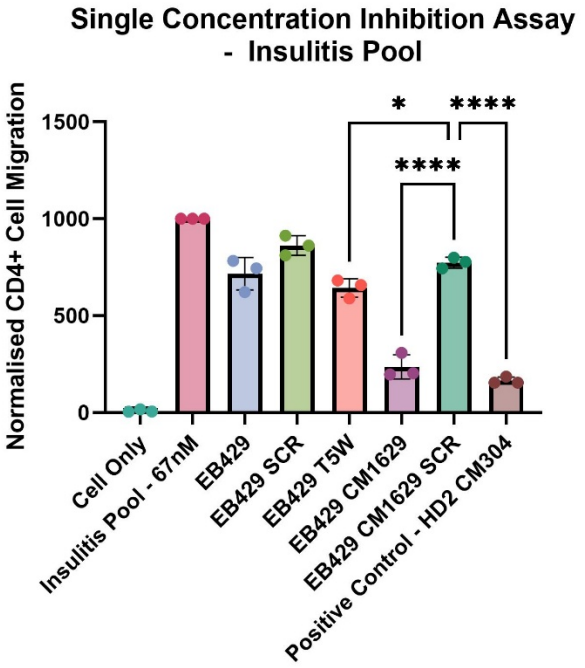

Figure 4.15 – Effect of selected EB429 combinatorial mutants on CD4⁺ T-cell migration to the insulitis chemokine pool. Bar charts with standard deviation error bars depicting the effect of EB429 mutants on activated CD4⁺ T-cell migration to the insulitis chemokine pool. The experiment was performed as three technical replicates and three biological replicates. Individual data points indicate mean values of technical replicates per experiment. Cell migration values were normalised to the mean value of migrated cell counts to the EC50 chemokine concentration and set to 1000 cells, as indicated on the Y-axis. The X-axis shows experimental constituents. Peptides were tested at a final concentration of 10 µM. CM1629 SCR was used as a negative control, containing the scrambled amino acid residues of CM1629. The statistical significance of EB429 mutants was calculated compared to CM1629 SCR using a one-way ANOVA and a Dunnett's test for multiple comparisons. Asterisks indicate the following: ****p ≤ 0.0001, ***p ≤ 0.001, **p ≤ 0.01, *p ≤ 0.05.

4.2.6 Combinatorial Mutagenesis Confirms Potency Improvements

To confirm potency improvements from EB429 to T5W and finally to CM1629, IC50 curves were performed using $CD8^+$ T-cells and the insulitis pool **(Figure 4.16)**. The mean IC50 for EB429 was 11.36 µM. The mean IC50 for T5W was 1.78 µM. The mean IC50 for CM1629 was 602 nM. IC50 values were converted to pIC50 (negative $\log_{10}$ of IC50 expressed as moles/litre [M]) to allow for statistical differences to be analysed between IC50 values for EB429, T5W and CM1629 (**Figure 4.17**). This result confirms that potency has significantly improved from EB429 to T5W and from T5W to CM1629.

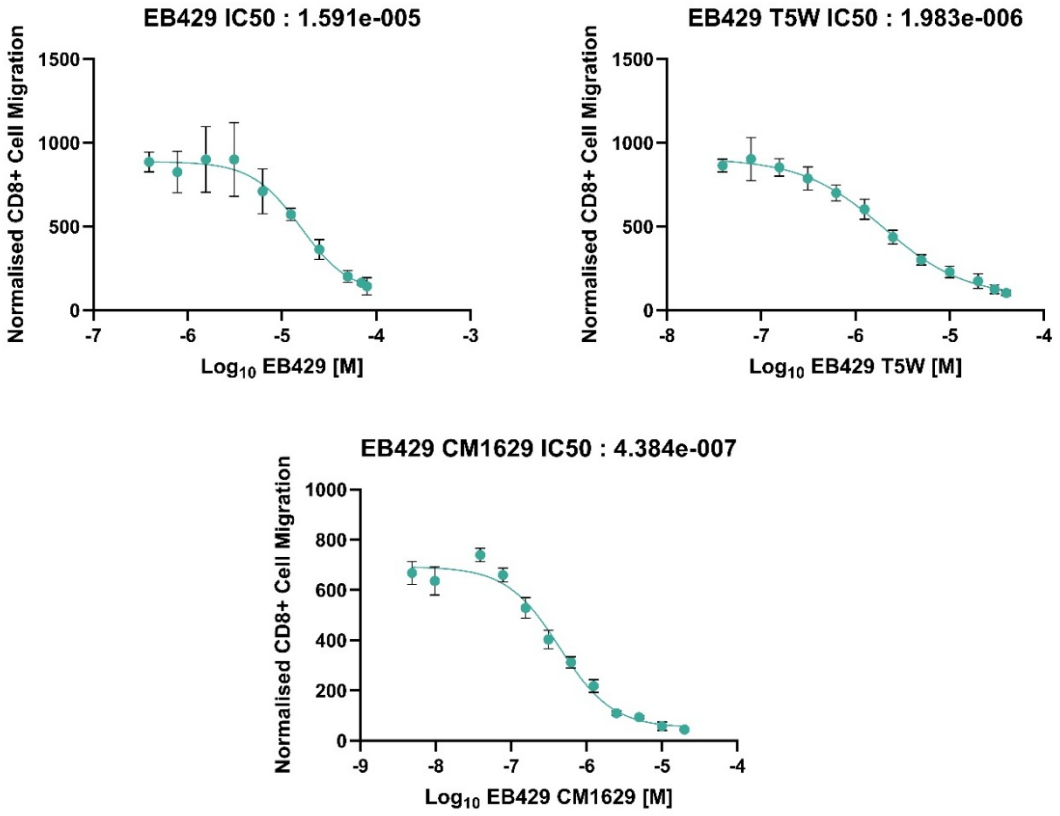

Figure 4.16 – Inhibitory dose-response curves of EB429, T5W, and CM1629. Representative dose-response curves depicting the potency of EB429, T5W and CM1629 against the chemokine insulitis pool, using activated $CD8^+$ T-cells. Cell migration values were normalised to the mean values of migrated cell counts without peptide and set to 1000 cells, as indicated on the Y-axis. The X-axis shows the concentration of peptide as a Log10 of molar concentration. Each data point represents the mean value of the technical replicates for each peptide concentration tested, with standard deviation error bars shown. IC50 values were calculated by plotting a 3-parameter inhibitor dose-response log-logistic plot using GraphPad Prism.

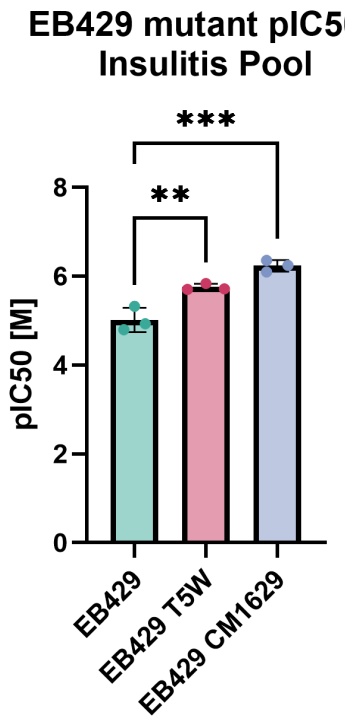

Figure 4.17 – Effect of EB429, T5W, and CM1629 on pIC50. Bar charts with standard deviation error bars depicting the effect of EB429 mutants on pIC50 (negative $\log_{10}$ of IC50 expressed as moles/litre [M]) against the chemokine insulitis pool. The experiment was performed as three technical replicates and three biological replicates. Individual data points indicate biological replicates. The Y-axis shows pIC50 and the X-axis shows experimental constituents. The statistical significance of EB429 mutants was calculated compared to EB429 using a one-way ANOVA and a Dunnett's test for multiple comparisons. Asterisks indicate the following: ****p ≤ 0.0001, ***p ≤ 0.001, **p ≤ 0.01, *p ≤ 0.05.

4.2.7 AlphaFold3 Modelling Predicts CM1629 Increases Hydrophobic Interactions with Chemokines

To deduce a potential mechanism of action for CM1629, AlphaFold3 modelling was performed. EB429, T5W and CM1629 were modelled with CXCL10 **(Figure 4.18)**. EB429, T5W and CM1629 were modelled with CCL19 **(Figure 4.19)**. Modelling indicated that all 3 peptides occupy the same receptor binding site on the chemokine.

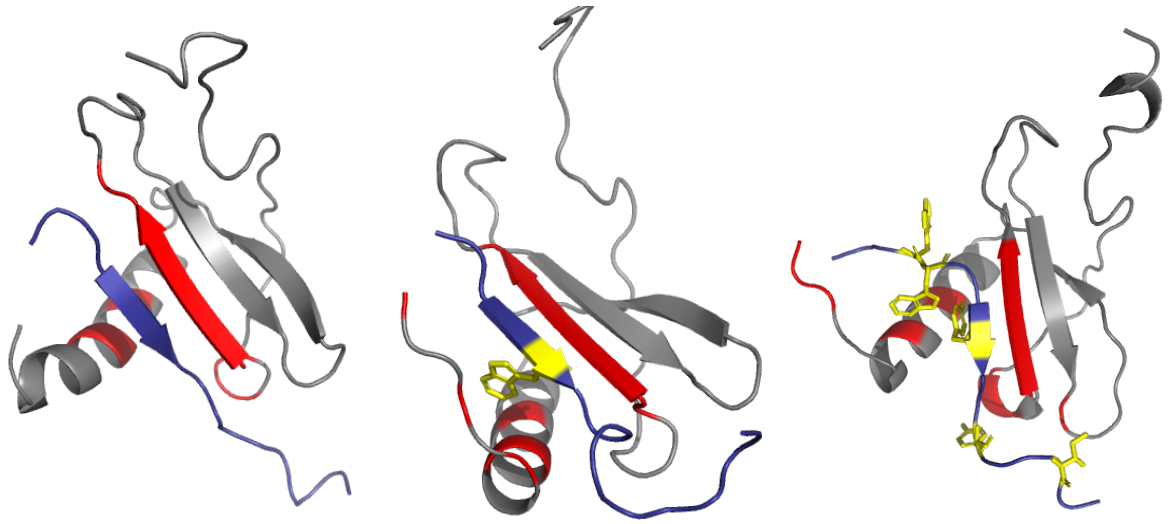

Figure 4.18 – AlphaFold3 modelling of EB429, T5W and CM1629 to CXCL10. Left to right, EB429:CXCL10, T5W: CXCL10 and CM1629: CXCL10. AlphaFold3 predicted binding models of CXCL10 to EB429/T5W/CM1629. CXCL10 is shown in grey, and the peptide is shown in blue. Mutated residues are highlighted in a yellow stick format. The CXCL10:peptide binding interface within 5 angstroms is highlighted in red on CXCL10. Figures made in PyMOL.

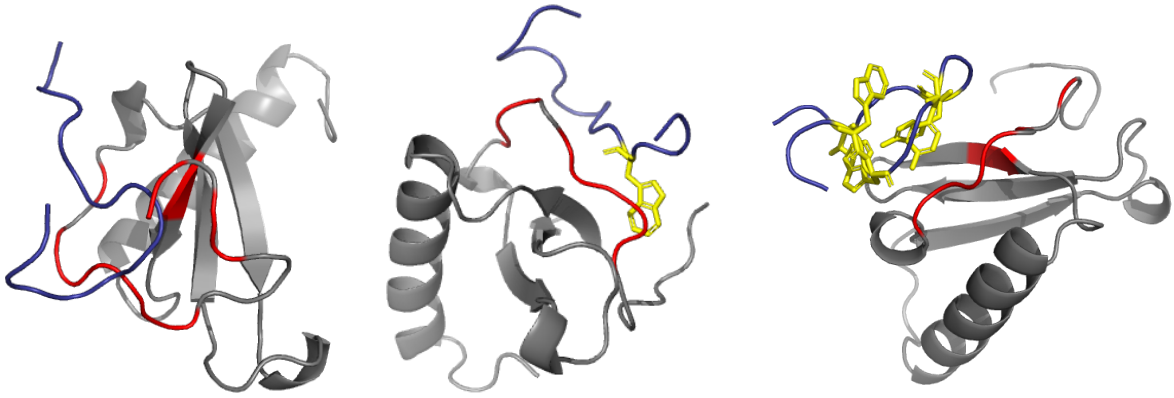

Figure 4.19 – AlphaFold3 modelling of EB429, T5W and CM1629 to CCL19. Left to right, EB429:CCL19, T5W:CCL19 and CM1629:CCL19. AlphaFold3 predicted binding models of CCL19 to EB429/T5W/CM1629. CCL19 is shown in grey, and the peptide is shown in blue. Mutated residues are highlighted in a yellow stick format. The CCL19:peptide binding interface within 5 angstroms is highlighted in red on CCL19. Figures made in PyMOL.

Analysis of peptide:chemokine modelling with Arpeggio was used to identify inter-chain bonds and interactions. No significant increase in hydrophobic interactions was observed in T5W and CM1629 when compared to EB429 (**Figure 4.20**). However, a significantly increased number of hydrophobic interactions were observed at the mutated 5th residue of T5W, and the 4th and 5th mutated residues in the CM1629 peptide (**Figure 4.21**). No other significant bonds or interactions

were observed between all three peptides. These results suggest that the increase in potency observed from EB429 to T5W and from T5W to CM1629 could be explained through an increase in hydrophobic interactions with the chemokine targets.

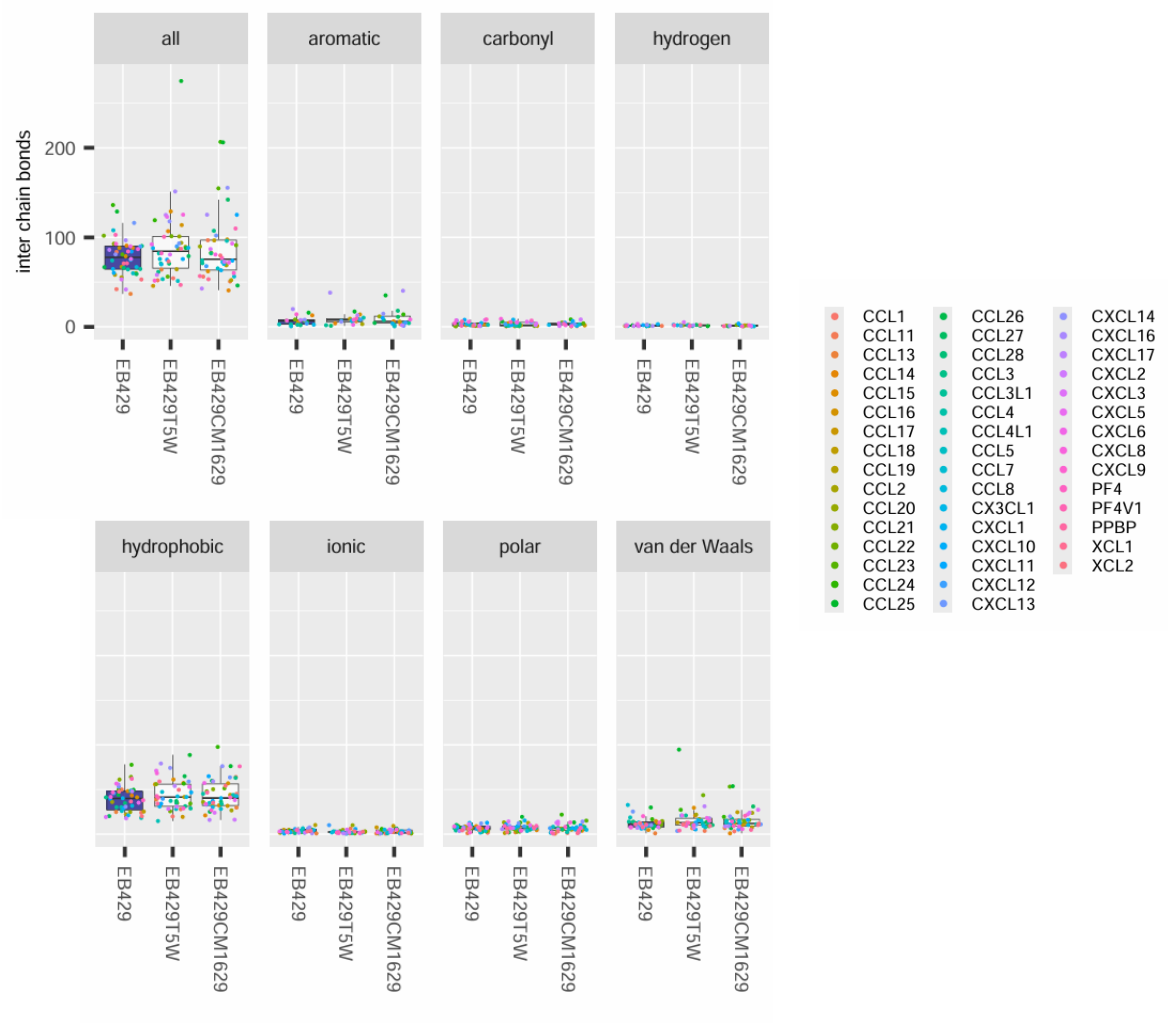

Figure 4.20 – Effect of EB429 T5W and EB429 CM1629 mutations on peptide:chemokine interactions via AlphaFold3 modelling. Box-whisker plots of the number of inter-chain interactions between peptides and modelled chemokines. 138 AlphaFold3 models were generated for the peptides EB429, EB429 T5W and EB429 CM1629 to the indicated chemokines. The Y-axis shows the number of predicted inter-chain bonds between peptides and chemokines. The X-axis shows the peptide, with individual data points illustrated by the chemokine against which the peptide has been modelled. The statistical significance of peptides was calculated compared to EB429 using a two-way ANOVA and a Dunnett's test for multiple comparisons. Asterisks indicate the following: ****p ≤ 0.0001, ***p ≤ 0.001, **p ≤ 0.01 and *p ≤ 0.05. Data analysed by SB.

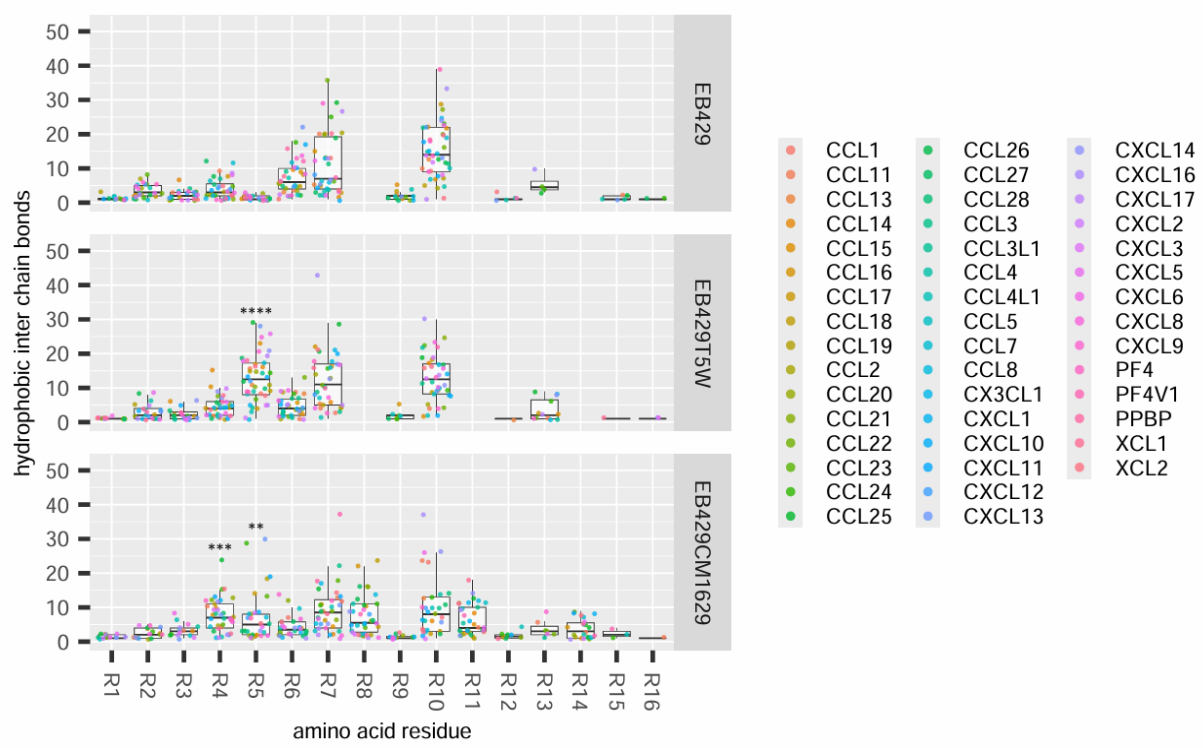

Figure 4.21 – Effect of EB429 T5W and EB429 CM1629 mutations on hydrophobic inter-chain interactions via AlphaFold3 modelling. Box-whisker plots of the number of hydrophobic inter-chain interactions between peptides and modelled chemokines by peptide residue. 138 AlphaFold3 models were generated for the peptides EB429, EB429 T5W and EB429 CM1629 to the indicated chemokines. The Y-axis shows the number of predicted hydrophobic inter-chain interactions between peptides and chemokines. The X-axis shows the peptide residue, with individual data points illustrated by the chemokine against which the peptide has been modelled. The statistical significance of peptides was calculated compared to EB429 using a two-way ANOVA and a Dunnett's test for multiple comparisons. Asterisks indicate the following: ****$p \leq 0.0001$, ***$p \leq 0.001$, **$p \leq 0.01$ and *$p \leq 0.05$. Data analysed by SB.

4.3 Discussion

T1D is characterised by the progressive loss of insulin-producing beta cells within the islets of the pancreas, rendering patients unable to respond to meal-induced increases in blood glucose. Autoreactive $CD8^+$ T-cells are primarily responsible for destroying beta cells[454]. Autoreactive $CD8^+$ T-cells receive activation signals from autoreactive $CD4^+$ T-cells[227]. A revolutionary new T1D therapy, teplizumab, depletes and exhausts T-cells[291]. Teplizumab delays clinical T1D onset by 18 months, but increasing doses may be associated with immunosuppression[145]. Targeting chemokines that recruit $CD8^+$ and $CD4^+$ T-cells to the islets represents a novel strategy to prevent autoreactive T-cells infiltration into islets without causing immunosuppression.

In this chapter, the combinatorial peptide CM1629 has been characterised in a chemokine pool designed to mimic chemokines in insulitis. EB429-derived combinatorial peptides were identified in chapter three but were not assessed in cell migration assays. This chapter aimed to create a model that provided insight into the chemokine milieu associated with T1D. A chemokine pool was constructed based on RNA-seq data of cytokine-stimulated deceased-donor human islets[408]. CM1629 significantly inhibited the migration of $CD8^+$ and $CD4^+$ T-cells to the insulitis chemokine pool. This chapter suggests that CM1629 may have promise as a novel therapy for T1D.

4.3.1 Bulk RNA-seq Data Provides an Insight into Chemokine Abundance in Insulitis

To improve upon single-chemokine cell migration assays used in the previous chapters, a chemokine pool was created based on a publicly available bulk RNA-seq dataset[466]. Using RNA-sequencing data to construct a chemokine pool was a novel strategy employed by the Bhattacharya group[408]. Using a complex chemokine mixture for testing was necessary to overcome the cost- and time-prohibitive limitations of single chemokine chemotaxis assays used in chapters two and three. Streamlining testing to include chemokine pools provided the most robust and physiologically relevant data while allowing for the rapid testing of peptides. Due to the known interactions between chemokines, such as chemokine dimerism and synergism[88], using chemokine pools is a more complex model than single chemokine assays.

RNA-seq data from the dataset GSE226888 was used to identify the chemokines produced by cytokine-stimulated healthy islets from five deceased donors. The cytokines used to stimulate the islets in this dataset were IL-1β and IFN-γ for 24 hours. A substantial overlap is observed when comparing upregulated gene expression between human islets stimulated with IL-1β and IFN-γ[468, 469] and human beta cells from donors with T1D[470]. Therefore, both IL-1β and IFN-γ have been robustly characterised as having a role in T1D.

Using information from chemokine transcripts per million, a chemokine pool was constructed based on ratios dictated by the chemokine abundance in the dataset. Bulk RNA data was used instead of single-cell RNA sequencing data, as single-cell sequencing data does not provide information regarding total protein production by the tissue. Therefore, single-cell RNA sequencing was not suitable for this investigation, as multiple cell types produce chemokines in T1D[330], and this work aimed to reflect the total chemokine microenvironment in T1D. RNA transcript levels do not precisely correlate with protein secretion. Several factors can confound this, including post-transcriptional modification of chemokines[463, 464]. Therefore, the chemokine ratios tested in cell migration assays may not accurately reflect the abundance of chemokines in T1D.

Due to the limitations of using RNA-seq data to estimate chemokine abundance, a proteomic-based strategy was also investigated, and work is ongoing (Appendix). Human deceased-donor islets were cytokine-stimulated, and the supernatant was tested for its ability to elicit $CD8^+$ T-cell migration. The stimulation cocktail selected was 10 ng/mL of IFN-γ, 10 ng/mL of TNF-α, and 2 ng/mL of IL-1β, based on the work by Sarkar *et al*[471]. Stimulation of healthy human islets with TNF-α, IL-1β, and IFN-γ mimics the cytokines used in multiple studies, which are known to induce T1D-relevant chemokine production[323, 324, 466, 471]. A stimulation time of 48 hours was selected from the tested stimulation time course, as 48-hour stimulated samples demonstrated greater migration than those stimulated for 24 hours. Stimulated islet supernatant was analysed to determine the concentration of 40 human chemokines.

Difficulty accessing the arrays due to unavoidable logistical constraints resulted in delays in sending the supernatant for array analysis. This delay precluded the analysis from being included in this thesis. If time had allowed, a proteomic-based pool would have been created and CM1629 tested using the available cell lines. The creation of a proteomic-based chemokine pool remains an avenue for future work.

The chemokines in the RNA-based pool correlate with those chemokines identified as either pathogenic or present in T1D. CXCL10, the most abundant chemokine in the RNA-seq pool, has been robustly identified as a pathogenic chemokine in T1D[322, 323]. Likewise, CXCL9 and CXCL11 are implicated through the upregulated expression of their chemokine receptor, CXCR3, in T1D[321]. CCL5, CCL8, CCL22 and CX3CL1 have been identified from further RNA-seq-based analysis[323]. The presence of the chemokines CXCL1/2/3/5/6/8 is implicated by the trialled (but failed[344]) inhibition of the chemokine receptors CXCR1/2 to prevent beta cell destruction post islet transplantation[342]. Evidence from mouse models has identified the chemokine CXCL16 in NOD mice[472] and CCL2 production by beta cells exacerbated monocyte migration and diabetes development in transgenic models[473]. XCL2 was not available for purchase and was thus excluded from the pool creation. The correlation with previously seen chemokine data increases the confidence that this pool resembles the chemokines present in insulitis.

4.3.2 The Combinatorial Peptide CM1629 Significantly Inhibits $CD8^+$ and $CD4^+$ T-cell Migration

In this chapter, the peptide CM1629 has been identified. Developed from the peptide EB429, CM1629 contains five sequence mutations. The mutations of I4W, T5W, G8Y, G11Y, and S14I have improved the mean potency from 11.36 μM (EB429) to 602 nM (CM1629) using the insulitis pool and $CD8^+$ T-cells. Potency curves provide robust evidence for using the CoSMOS methodology, as transitioning from a single mutation to five mutations improved the potency of CM1629 roughly threefold, from the mean IC50 value of T5W, 1.781 μM, to 602 nM. By converting the IC50 values to pIC50 and comparing pIC50 values of EB429, T5W, and CM1629, step-wise statistically significant improvements can be observed.

Alphafold3 modelling of EB429, T5W, and CM1629 was completed to elucidate the mechanism underlying this significant improvement in potency. Using Arpeggio, SB modelled the interactions between peptides and chemokines. Both T5W and CM1629 have significantly more hydrophobic

interactions with chemokines than parental EB429 at mutation sites introducing tryptophan residues. Hydrophobic interactions are typically enriched in effective ligands[474], suggesting a mechanism behind the improved potency of EB429 compared to CM1629.

CM1629 significantly inhibits the migration of $CD4^+$ T-cells, but does not affect the migration of THP-1 cells or primary monocytes. Therefore, CM1629 appears to work selectively on T-cell recruiting chemokines. In T1D, resident macrophages have been reported to contribute to the inflammatory milieu through antigen presentation to autoreactive T-cells and their accumulation during disease progression[475]. However, inhibiting macrophage migration may be detrimental to health in T1D patients. Resident macrophages promote beta cell proliferation through the upregulation of the protein SMAD7[476]. Data from mouse models suggest that resident macrophages may play a critical role in islet vasculature through VEGF-A[477, 478] and beta cell crosstalk[479]. Specific inhibition of T-cell migration in T1D, whilst not affecting resident macrophages, could offer targeted protection without immunosuppression, positioning CM1629 as a promising therapeutic candidate.

$CD4^+$ T-cells were labelled with antibodies to chemokine receptors available at the time of testing, and were positive for CXCR3, CCR4 and CCR7. The isolation of $CD4^+$ T-cells in this work did not distinguish between subclasses of $CD4^+$ T-cells. As T1D is considered a disease primarily mediated by $CD8^+$ T-cells and Th1 $CD4^+$ T-cells[156, 245] and to confirm that CM1629 blocks Th1 cell migration, future work will focus on isolating a homogenous population of Th1 $CD4^+$ T-cells. This isolation could be achieved using a commercially available Th1 differentiation kit (CDK001, R&D Systems) to prevent the isolation of a heterogeneous $CD4^+$ T-cell population.

Crucially, CM1629 did not elicit any cell death, had no effect on cells in the absence of chemokine, and did not affect non-specific C5a-induced monocyte migration. Such experiments are crucial in pre-clinical drug development to ensure specificity for the intended drug target.

Coupled with T-cell specificity, which may prevent immunosuppression, CM1629 should now progress into *in vivo* models.

All testing in this chapter was completed using an EC50 concentration of the chemokine pool, rather than the previously used EC80 concentration, to reduce assay costs. The chemokine EC80 concentration was initially selected to maintain a robust assay window and was used in previous chapters. Testing of EB429-derived peptides using the chemokine pool strategy reduced the overall number of assays, but it required a large amount of expensive chemokine pools. Therefore, EC50 chemokine pool concentrations were used. While an EC80 chemokine dose is historically used in inhibitor assays to maximise the linear range available on the dose-response curve to detect inhibition, the use of an EC50 concentration is a reasonable compromise[408].

The next step in the development of EB-derived peptide translation to the clinic would include *in vivo* mouse models of inflammation or diabetes. The peptides have thus far been tested against human chemokines. Chemokine sequence homology varies between humans and mice. Therefore, testing is required to ensure the peptides can inhibit mouse chemokines. Previously identified peptides by the Bhattacharya group have been effective in an *in vivo* inflammatory mouse air pouch model[403] and a mouse cardiovascular disease model[480]. Therefore, CM1629 may be effective against mouse chemokines and immune cells, but further testing is required.

4.3.3 Limitations

4.3.3.1 Combinatorial Peptide Cell Death

Three out of the five selected combinatorial peptides resulted in cell death. The peptides CM2627, CM3355, and CM3384 were toxic to $CD8^+$ T-cells, as observed through PI labelling. This cell death was an unexpected result, suggesting that selecting peptides based solely on Δlog2E may not be an effective strategy. Reflecting on peptide sequences and limiting the number of aromatic residues may prevent this. Aromatic residues may increase the potential of peptides to penetrate cell membranes[481-483], potentially contributing to peptide-induced cytotoxicity. An

investigation into the exact mechanism of cell death was beyond the scope of this thesis. This cell death reaffirms the need for peptide characterisation using cell migration and other assays, rather than relying solely on phage display data. It also confirms the hypothesis that mutations cannot be randomly combined with automatic success[408].

4.3.3.2 In-Vitro Models

The main limitation of the work presented in this chapter is that these models cannot fully reflect *in vivo* inflammation or the insulitis environment. CM1629 requires validation in an *in vivo* model, such as an air pouch model, to reflect the complexity of mammalian inflammation. To test whether this peptide can prevent the development of T1D, an NOD mouse model would be the best choice.

4.4 Conclusions

The work illustrated in this chapter characterises the EB429 peptide, CM1629, as a potential therapeutic for T1D. Using a strategy of deducing chemokine abundance from RNA-seq data, CM1629 was tested against cell lines and primary immune cells. Inhibition of $CD8^+$ and $CD4^+$ T-cells was observed with CM1629, whilst no inhibition was observed for monocytes or THP-1 cells. The activity of CM1629, therefore, appears to be T-cell-specific. IC50 curves determined that CM1629 now exhibits potency within the nanomolar range when tested against 20 human chemokines and $CD8^+$ T-cells. Modelling with AlphaFold3 suggests that this increase in potency may be due to the increased number of hydrophobic interactions resulting from peptide mutations. While human islets were cytokine-stimulated, the limited time available meant that the proteomic analysis and testing could not be replicated in this proteomic-based chemokine pool, which will be investigated in future work. The next step for CM1629 testing is *in vivo* models of inflammation and T1D to fully validate the peptide's therapeutic potential. The findings of this chapter strongly support the progression of CM1629 into *in vivo* validation studies.

5. Chapter Five - Discussion, Future Work, and Conclusions

5.1 General Discussion

In autoimmune diseases such as T1D, inappropriate leukocyte recruitment leads to aberrant inflammation and tissue damage[484]. Chemokines drive leukocyte migration to sites of inflammation in T1D[485]. Chemokines, such as CXCL10, drive autoreactive T-cells to the site of inflammation around the islets in the pancreas in T1D[238]. Insulitis, characterised by inflammation surrounding the islets, is a hallmark of T1D[321]. T1D treatments have been revolutionised by targeting T-cells, but they risk immunosuppression. Teplizumab delays the development of T1D by 18 months[292], but there is currently no treatment that prevents the onset of T1D.

The therapeutic targeting of chemokines in inflammatory diseases, although promising[103], has been hindered by the complexity and redundancy of the chemokine network[100]. A pan-chemokine inhibiting protein, specifically targeted to beta cells in mouse models, prevented the development of T1D[115, 330, 331]. However, this chemokine-inhibiting protein was unsuitable for translation as it originated from a herpes virus. Furthermore, the inhibition of the chemokine receptors CXCR1/2 reversed diabetes in an NOD mouse model[342]. Treatment of CXCR1/2 in a clinical trial failed to increase islet survival following islet transplantation[344]. Chemokine redundancy is a proposed reason behind the failure of chemokine targeting in inflammation and in T1D[102, 353]. Therefore, T1D is a disease driven by T-cells, with chemokines playing a crucial role in the disease pathogenesis. As there is an unmet disease burden for patients, targeting chemokines that drive T-cells may be a novel treatment strategy for T1D.

Evasins are chemokine-neutralising proteins found in the saliva of ticks and are injected when a tick bites its host to feed[373]. Evasins bind to CC or CXC chemokines, forming two structurally distinct subclasses. Class A binds to CC chemokines, and class B binds to CXC chemokines[375]. Ticks co-administer many evasins at the bite site, neutralising leukocyte recruitment to allow for undisturbed feeding[116]. Evasins are effective in various *in vivo* mouse models of inflammation, including fibrosis, atherosclerosis, and colitis[395, 399, 480, 486]. Despite this, they have not been translated into human therapeutics due to the risk of immunogenicity as they are large, heavily glycosylated, non-human proteins.

The work established by the Bhattacharya laboratory identified a class A evasin-derived peptide, HD2. In a novel finding, the peptide HD2 exhibited cross-class chemokine inhibition, despite being derived from a class A evasin sequence[76]. To enhance the range of chemokines to which HD2 could bind and improve its pharmacological properties, a peptide improvement pipeline was developed. The Combinatorial Saturation Mutagenesis Optimisation Strategy (CoSMOS) was developed and applied to the HD2 sequence[408]. To validate the mutated peptides, chemokine pools were constructed for use *in vitro* assays. These chemokine pools contained 20 or more chemokines present in disease states, such as RA, as identified by bulk RNA sequencing data[408]. A combinatorial HD2 peptide, termed CM304, demonstrated significantly improved potency over HD2 against chemokine pools that mimicked RA, atherosclerosis and T1D[408]. This work outlined the success of the CoSMOS strategy and demonstrated that promiscuous chemokine-binding peptides could be identified from evasin sequences.

The hypothesis underlying this thesis was that a dual-class chemokine-binding peptide could be identified from a class B evasin sequence. The work in this thesis aimed to identify a dual chemokine class binding peptide from class B evasin sequences using phage display and to characterise peptides of interest using *in vitro* cell migration assays. Combinatorial saturation mutagenesis could then be applied to this peptide to enhance its properties, such as potency.

Finally, any peptides of interest would be validated in an *in vitro* model that recapitulates the chemokines involved in T1D and insulitis.

5.1.1 Chapter Two Findings

In this chapter, phage display screening of the class B evasin library identified a promiscuous cross-chemokine-binding peptide called EB429. EB429 demonstrated binding to CC and CXC chemokines and was selected for validation using *in vitro* cell migration assays. Chemotaxis assays validated that EB429 could inhibit CXC and CC chemokines using $CD8^+$ T-cells. Modelling with AlphaFold3 indicates that EB429 is in proximity to the first β-sheet and the α-helix of CXCL10. Modelling also shows that EB429 is in proximity to the N-loop, N-terminus and third β-sheet of CCL19. This modelling provides a potential mechanism of action for EB429, binding to the chemokine at the site where the chemokine would interact with its respective chemokine receptor. The therapeutic translation of EB429 is currently limited by the micromolar potency against the chemokine CXCL10, identified by inhibitory dose-response curves used to determine IC50 peptide values.

5.1.2 Chapter Three Findings

The results of the previous chapter suggest that the pharmacological properties of EB429 require improvement before it can be considered as a potential chemokine-targeting therapeutic. To improve the properties of the EB429 peptide, the CoSMOS protocol was applied to the EB429 peptide sequence. A mutant EB429 phage library was constructed, with each residue of EB429 mutated to include a degenerate NNK codon. This mutant library encoded all possible EB429 single mutant peptides and was screened in phage display. Single-mutant peptides were identified as having significantly enriched binding to chemokines compared to EB429. Several peptides were selected for validation using single chemokine cell migration assays. EB429 mutant peptides demonstrated significant inhibition of CC and CXC chemokines compared to EB429 and inhibition of a new chemokine. To identify whether combinations of these beneficial

mutations would have further cooperative effects, a combinatorial phage library was constructed and screened in phage display. The 20 best and 20 worst combinatorial mutants were identified. The best combinatorial mutants exhibited enhanced binding to chemokines compared to EB429 and EB429 single mutants, but their functional activity required validation in cell migration assays. More complex assays were required to fully characterise the therapeutic potential of the combinatorial EB429 mutants in a model including multiple disease-related chemokines.

5.1.3 Chapter Four Findings

The results of the previous chapter suggest that EB429-derived combinatorial peptides exhibit enhanced chemokine-binding abilities compared to EB429 single-mutant peptides and may be effective in treating chemokine-driven diseases. T1D was selected as the disease model for peptide characterisation due to T-cell-mediated autoimmunity and the implication of chemokines in disease pathogenesis. To validate the combinatorial peptides *in vitro* before progressing to *in vivo* models, a chemokine pool was constructed to mimic the chemokine profile in T1D. Bulk RNA-seq data from human islets stimulated with cytokines was analysed for chemokine abundance. Using this analysis, the insulitis chemokine pool was created for use in cell migration assays. As RNA-seq may not accurately reflect protein expression, cytokine-stimulated human islets were also pursued as an alternative strategy to allow for proteomic analysis. While several mutant peptides were toxic to cells, CM1629 significantly inhibited the migration of both $CD8^+$ and $CD4^+$ T-cells. CM1629 did not inhibit THP-1 monocytes, indicating T-cell specificity. CM1629 is unlikely to exhibit off-target effects due to the testing performed using the chemotactic protein C5a. Inhibitory dose-response curves demonstrate that the potency of CM1629 has been improved 19-fold compared to EB429 and 3-fold compared to the best single mutant, T5W, validating the CoSMOS protocol. AlphaFold3 modelling of CM1629 in complex with chemokines suggests this increase in potency may be due to an increase in hydrophobic interactions through tryptophan peptide mutations.

5.1.4 Impact of Findings

In summary, the work described in this thesis has identified a peptide series derived from a class B evasin, EB429. This work marks the first chemokine-neutralising peptide to be identified from a class B evasin. This result is novel, as this is the first reported class B evasin-derived sequence capable of inhibiting two chemokine classes. As demonstrated by the improvements in peptide potency, this work validates the CoSMOS protocol for stepwise mutagenesis of peptide sequences. The CoSMOS protocol can be applied to a peptide sequence to engineer an increase in binding to multiple targets, as exemplified by the increase in potency achieved from EB429 to CM1629. The work in this thesis proposes that CM1629 could be developed into a therapeutic for T1D. By specifically targeting T-cell recruiting chemokines with nanomolar potency, CM1629 may circumvent the risks of immunosuppression associated with T1D treatments such as teplizumab. As CM1629 is a potent inhibitor of T-cell chemokines, it may also be effective as a treatment for other T-cell-driven autoimmune diseases, such as RA.

5.2 Future Work

The identification and development of the peptide CM1629, although promising, requires extensive preclinical work before its translation to the clinic can be proposed. The primary areas to consider are converting this peptide into a viable compound for patient administration and designing the pipeline for future assays and *in vivo* testing.

5.2.1 Peptide Improvement Strategies

While peptide-based therapeutics are becoming an increasingly popular drug modality, there are downsides to peptide therapeutics compared to the more widely used monoclonal antibodies or small molecules. Peptides have short half-lives due to rapid renal clearance and enzymatic degradation[439]. Therefore, peptides would require repeated administration if given subcutaneously, which can result in poor patient compliance and discomfort[487]. Other

administration routes are preferred, such as oral delivery, but gastrointestinal degradation and poor intestinal permeability limit this administration[444, 488].

Peptide modifications can be used to enhance the drug-like properties of peptides, making them more desirable from both commercial and patient perspectives (**Table 5.1**). To improve cell membrane permeability, a peptide can be conjugated to a lipid group[489]. Lipidation promotes the binding of a molecule to serum albumin, which has a half-life of approximately 20 days, thereby improving the molecule's half-life[490, 491]. Albumin interacts with FcRn receptors present on the surface of endothelial cells[492], allowing for albumin to be internalised via endocytosis. Internalisation prevents clearance from circulation, and the strong binding between albumin and the FcRn prevents endosomal degradation[493]. Lipidation improved the pharmacokinetic properties of the GLP-1 agonist liraglutide for the treatment of type two diabetes[494].

Conjugating peptides to an antibody can result in a significant increase in half-life by preventing rapid kidney excretion[495]. Coupling a GLP-1 agonist peptide analogue with an anti-GIPR antibody created a weight loss compound, AMG 133, which resulted in significant weight loss when administered subcutaneously once a month in a phase one clinical trial[496]. Coupling peptides to a human Fc-domain has also been trialled to reduce the risk of antibody-dependent cell-mediated cytotoxicity while retaining desirable antibody features[497]. Chemokine-blocking peptides, named BKT120 and BKT130, were coupled to a human immunoglobulin Fc chain, creating a compound known as a peptibody. Conversion from peptide to peptibody increased the compound's *in vitro* activity and resulted in favourable pharmacokinetics *in vivo*[498]. The peptibody was also effective in reducing immune infiltrate and disease severity in mouse models of delayed-type hypersensitivity, arthritis, and multiple sclerosis[498]. PEGylation can improve the half-life of compounds by increasing their solubility, inhibiting proteolytic enzyme cleavage, and reducing renal clearance[499]. PEGylation significantly reduced the biological activity of the drug Pegasys, but due to the dramatic improvement in half-life, it was advanced to the clinic[500].

Table 5.1 – Examples of drug modifications, benefits, drawbacks and exemplar drugs

Drug Modification	Benefits	Drawbacks	Exemplar drug in the clinic/clinical trial
Lipidation	Increased half-life, reduced immunogenicity	Loss of efficacy, toxicity	Semaglutide[501]
Antibody conjugation	Improved efficacy, increased half-life, enhanced tissue penetration	Antibody-dependent cell-mediated toxicity	Adcetris[502]
PEGylation	Increased solubility, increased half-life, enhanced stability, improved delivery	Inconsistent PEG formulation, immunogenicity, complex manufacturing	Zilucoplan[503]
Cyclisation	Increased stability, increase cell membrane permeability	Rapid clearance, reduced selectivity	MK-0616[504]

Using the PeptideCutter tool (Expasy - PeptideCutter) and selecting enzymes and chemicals present in the blood, it was determined that CM1629 contains one cleavage site at the V2 residue, which can be cleaved by neutrophil elastase. To prevent the degradation of CM1629 in the bloodstream, the V2 residue could be methylated to prevent protease recognition. Semaglutide, the GLP-1 agonist for the treatment of type two diabetes and obesity, contains two amino acid substitutions to prevent enzymatic degradation. Alanine at position two has been mutated to 2-aminoisobutyric acid, and lysine at position 28 is mutated to arginine to prevent digestion by DPP4[505]. Cyclisation may also prevent enzymatic degradation and enhance peptide stability[506]. The peptide BK 1.2, an evasin-derived peptide identified by the Bhattacharya group, was cyclised to improve conformational stability[403]. Compared to a linear control peptide, BK 1.2 showed a loss of potency against the chemokine CCL8, from 238 nM to 729 nM.

The use of non-canonical amino acids (ncAAs) could also be explored. The term ncAA refers to an amino acid found in nature, or made synthetically, but not typically present in protein synthesis. ncAA's are typically used to improve protein or peptide properties, such as binding affinity[507]. Selectively sulfating tyrosine residues from the tick evasin ACA-01 improved the binding affinity of the protein and inhibition of chemokine targets[508]. Tyrosine sulfation also

occurs on conserved tyrosine residues in the N-terminal regions of chemokine receptors, thereby increasing receptor binding to chemokines[509]. EVA-1 in complex with CCL3 illustrates how evasins may mimic chemokine receptors by utilising sulfated tyrosine residues. EVA-1 interacts with the same portion of CCL3 that binds to the sulfated tyrosine chemokine receptor N-terminus[388]. Therefore, sulfation of tyrosine residues may be a means by which evasins enhance their binding affinity to chemokines by mimicking the action of chemokine receptors. Sulfation of tyrosine residues on the viral protein UL22A increased the binding affinity of CCL5 300-fold[510]. CCL11-neutralising cyclic peptides containing sulfated tyrosine residues have also been identified[511]. Sulfated tyrosines have been reported to increase the binding affinity of peptides to chemokine targets[512], while studies have demonstrated that this incorporation is not effective in all cases[513]. As CM1629 contains three tyrosine residues, this is a logical next step for investigation.

An alternate strategy to incorporate ncAAs is to use genetic code expansion (GCE) technology[514]. GCE utilises organisms with altered tRNA and blank codons to incorporate ncAAs into the peptides or proteins they produce. Coupled with screening technologies such as phage or mRNA display, GCE can enable the incorporation of over 500 ncAAs. Despite this, GCE can only incorporate one or two ncAAs at a time, and ncAAs are expressed at a lower rate than natural amino acids, resulting in a library with limited diversity[515]. If CM1629 is to be mutated or any of the above peptide improvement strategies applied, the peptide would require validation in cell migration assays to confirm that there has been no significant effect on peptide function.

To better understand the importance of specific residues in the CM1629 sequence and where to modify the peptide sequence, alanine-scanning mutagenesis should be employed on CM1629. Alanine scanning is a commonly used method for site-directed mutagenesis and has been successful in identifying amino acid residues suitable for mutating[516]. Alanine is the amino acid selected for mutations because it is non-polar and lacks bulky side chains[517]. Alanine scanning

can be achieved using the NNK codon to create a mutant phage library, followed by screening the library in phage display, the first step in the CoSMOS protocol.

By screening the mutant phage display library against chemokines, key residues in the CM1629 sequence can be identified. If an amino acid is crucial for the function of CM1629, mutating it to alanine will impact the chemokine binding and, thus, Δlog2E. Amino acids that are suitable sites for mutating will not affect chemokine binding in phage display when mutated to alanine. Alanine mutant CM1629 peptides can then be tested in cell migration assays to validate that the peptides do not affect cell migration compared to CM1629. Thus, sites on the CM1629 peptide sequence that are suitable sites to mutate can be identified, and improvement strategies can be applied. Due to the number of hydrophobic residues that CM1629 possesses, applying modifications that improve *in vivo* solubility should be prioritised, such as PEGylation.

Due to evasins being heavily glycosylated[379], the glycosylation of CM1629 should also be investigated. To do this, CM1629 should be produced in a mammalian cell line, such as HEK-293 cells. The molecular weight of the peptide should then be examined by gel electrophoresis. Glycosylated products appear with a higher than expected molecular weight, and glycosylation can be observed using periodic acid–Schiff staining[379], allowing for the analysis of the glycosylation status of CM1629.

5.2.2 Peptide Targeting

A concern with targeting the chemokine network is the risk of immunosuppression. Chemokines can have dual roles depending on their location. For example, CCL19 is vital for cell migration in secondary lymphoid tissues[518, 519]. However, CCL19 is significantly elevated in the synovial fluid of RA patients compared to controls, implicating the chemokine in RA inflammation[520].

LY3041658 is a monoclonal antibody that targets the chemokine ligands to CXCR1 and CXCR2[363]. LY3041658 is currently being trialled in a Stage 2b clinical trial for a skin condition

known as severe hidradenitis suppurativa. In a previous trial, the treatment group administered LY3041658 reported an increased incidence of gastrointestinal disorders compared to the placebo group. When the trial was converted to an open-label study, infections were more common among the treatment group[521]. As chemokines can have dual roles dependent on their spatial location and context, the risk of immunosuppression with chemokine targeting must be considered for CM1629.

A solution to circumvent the risk of immunosuppression with chemokine-targeting is to couple the peptide to a molecular "zip code"[522]. Utilising a disease- or tissue-specific molecule, a drug can be targeted to the site of inflammation. This targeting enables a higher concentration of the drug to be delivered to the desired site, thereby reducing the likelihood of off-target side effects and enhancing both efficacy and safety. Zip code technology has been successfully employed in cancer therapeutics[522].

Nanobodies may offer a solution. Naturally occurring in camelids, nanobodies are small (12-15 kDa) fragments of the heavy chain of an antibody (**Figure 5.1**). Nanobodies are reported to have the function of antibodies, but as small single molecules[523]. A nanobody targeting TNF-α has been approved for the treatment of RA in Japan, with administration every four weeks[524]. Using phage display, chemokine-binding nanobodies have been identified[523], illustrating the feasibility of this approach.

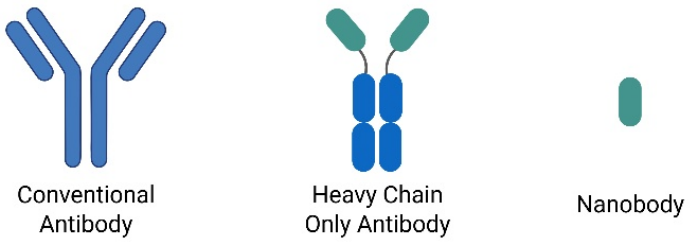

Figure 5.1 – Nanobody structure. Structure of conventional antibodies, heavy chain only antibodies and nanobodies. Figure made in Biorender.

Conjugating CM1629 to a nanobody could provide the benefits associated with antibody coupling alongside peptide targeting. Cyclic peptides have been coupled with an MHC-targeting nanobody[525], providing further rationale for this approach. To target T1D, a pancreas-specific molecule would ensure nanobody accumulation at the site of insulitis. DPP6 is expressed on alpha and beta cells within the pancreas. A DPP6 nanobody has been developed as an imaging agent for pancreatic endocrine cells[526, 527]. Despite this, as T1D progresses and beta cells are lost due to apoptosis, DPP6 expression will decline. Further options include using a GLP-1R-targeting molecule, such as exendin-4[528], or the extracellular protein islet-amyloid polypeptide (IAPP)[529]. As exendin-4 has a slower renal clearance than other peptide sequences, between five and seven hours, coupling to exendin-4 would also benefit half-life[530]. Furthermore, strategies to couple the nanobody and peptide would require intensive investigation and remain an avenue for future work.

5.2.3 In Vivo Models

The next step in the drug development pipeline of CM1629 is to test the efficacy in an *in vivo* model. Air pouch models involve subcutaneously injecting sterile air into the back of a rodent, followed by the injection of an irritant to stimulate inflammation[531]. An anti-inflammatory agent can also be co-administered to test whether it can prevent leukocyte recruitment to the site of injection (**Figure 5.2**). The fluid can be retrieved and analysed by flow cytometry. An air pouch model using zymosan as the irritant was the *in vivo* model used to characterise the effectiveness of the evasin-derived peptide BK1.3[403].

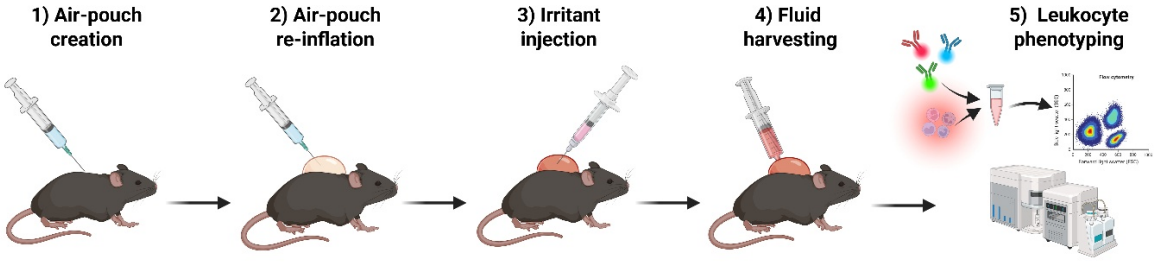

Figure 5.2 – Workflow of an in vivo air pouch model. Air is subcutaneously injected into the back of a mouse on day one, and reinflated on day four. On day seven, the irritant or vehicle control can be injected into the air pouch. Following a 24-hour incubation period, the fluid can be harvested. The fluid can then be analysed by flow cytometry to determine which leukocytes have migrated to the air pouch. Figure made in Biorender.

To test the therapeutic potential of CM1629 in T1D, a mouse chemokine pool that mimics chemokines present in the NOD mouse could be used as the inflammatory agent. A NOD chemokine pool was constructed from the dataset GSE256150 (**Figure 5.3**). This chemokine pool was constructed in the same manner as the insulitis pool described in chapter four, using bulk RNA-sequencing data from the islets of NOD mice at the ages of eight, ten and twelve weeks. Mice aged four and six weeks were excluded from the analysis, as the chemokine pool was not designed to reflect early insulitis. As NOD mice spontaneously develop insulitis, cytokine stimulation was not required to mimic T1D. This chemokine pool will be used as the inflammatory agent in an air pouch model to validate whether CM1629 can inhibit mouse T-cells from migrating to the air pouch.

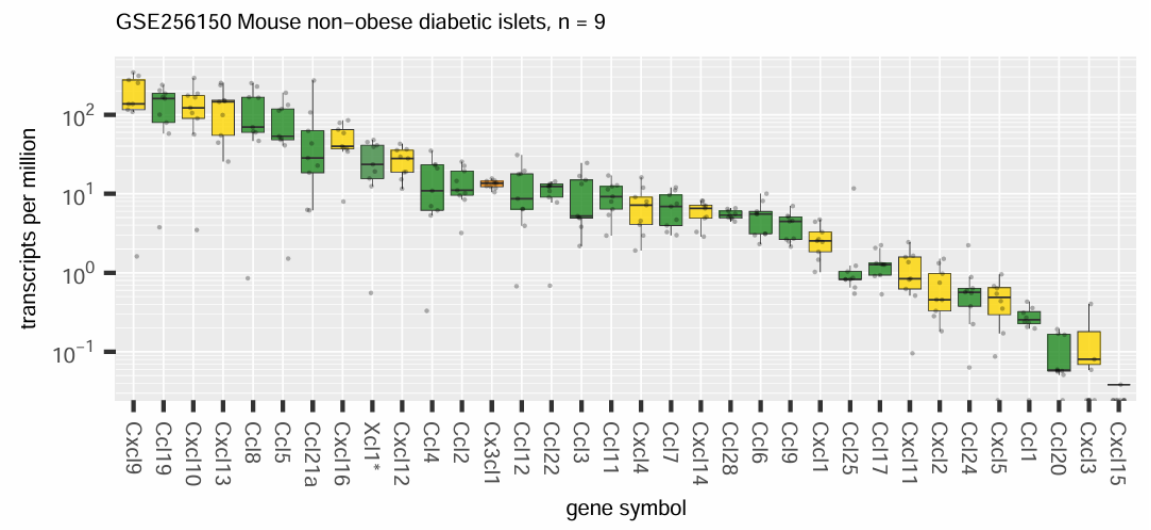

Figure 5.3 – Bulk RNA-seq of chemokine expression in non-obese diabetic mouse islets. Box-whisker plot of chemokine expressed in the islets of non-obese diabetic mice. Information was retrieved from the GEO database, dataset GSE256150. Chemokine genes are shown on the x-axis, and the chemokine transcripts per million are shown on the y-axis. Chemokines are colour-coded by chemokine class. Yellow-shaded chemokines are CXC chemokines, green-shaded chemokines are CC chemokines, and the orange-shaded chemokine is CX3CL1. An asterisk (*) indicates a chemokine that is not available for purchase. Data analysed by SB.

The discrepancy between the human and mouse immune systems has been reported as a reason behind the failure of chemokine-targeting therapies in clinical trials[103] and anti-inflammatory therapies more broadly[532]. The chemokine networks differ between mice and humans[533]. Despite this, evasins can neutralise chemokines in both mice and humans[388]. The success of the evasin-derived BK1.3 in an air-pouch model demonstrates this further[403]. Ticks have evolved chemokine-targeting evasins for multiple species, as they feed on humans, dogs, deer, and mice[534]. Therefore, the species cross specificity of evasin-derived peptides is not entirely unexpected.

Further *in vivo* experiments to explore include toxicological studies, pharmacokinetics, pharmacodynamics, and long-term safety to determine a safe dosage range[535]. Toxicological studies should provide information regarding potential risks to human subjects if CM1629 were to be translated into a phase one clinical trial[536]. The benefits of the aforementioned peptide modifications to improve half-life and peptide stability need to be balanced with *in vivo* safety.

Concentrations determined *in vitro* often do not reflect *in vivo* potency[537], and increasing dosing in mouse models will allow for the determination of the peptide's therapeutic index[538].

5.2.4 Applications in T1D

The desired T1D model for CM1629 testing is the NOD mouse. Despite the issues of therapeutic translation between the NOD mouse and human trials[539], the NOD mouse remains the best option for an *in vivo* T1D model. If CM1629 is successful in air-pouch models, the NOD mouse is the next step for therapeutic translation. CM1629 could also be used to prevent islet destruction following transplantation. If targeted to islets using islet-specific molecules, such as DPP6 or exendin-4, or engineered to be produced by islets or stem cell-derived beta cells, CM1629 could prevent T-cell destruction following transplantation. Such experiments remain an avenue for future work.

CM1629 (or future mutated formulations) could be tested on newly diagnosed T1D patients. Genetic screening of at-risk families allows for patients to be identified when they are in the early stages of disease development[540]. However, screening is not yet standard among the general population and remains a controversial practice due to cost. When patients are diagnosed, they often retain functional beta cell mass and may not require insulin yet[541]. Furthermore, isolated islets from T1D patients regained their ability to release insulin when cultured in vitro, providing evidence that dysfunctional beta cells in insulitis can regain function[231]. If treatment was initiated immediately upon diagnosis, beta cell mass may be preserved by preventing T-cells from migrating to the sites of insulitis. Intervention as early as possible would be pivotal to maintaining beta cell mass. At stage 1 of T1D, where patients present with 2+ autoantibodies but normal glucose levels, the risk of developing stage 3 T1D within 10 years is 70%[542]. This risk then rises to 85% after 15 years[542]. When patients enter stage 2 of T1D, they present with abnormal glucose levels, indicating that the process of beta cell destruction is already underway. Currently, no

treatments are approved for stage 1 of T1D. Therefore, treatment initiation upon stage 2 diagnosis is vital[543].

CM1629 may also be effective if used in tandem with teplizumab. If a chemokine inhibitor were coupled with teplizumab, when effector T-cells regenerate post-treatment, they would not have a chemokine gradient to follow to the site of insulitis. As teplizumab is approved for stage 2 of T1D[294], a chemokine-targeting agent may also be effective at this stage, to prevent further beta cell death and to preserve residual beta cell mass. If administered repeatedly, safety would be paramount to prevent immunosuppression and minimise side effects that could hinder patient compliance. If CM1629 and teplizumab were to be used together, this would complicate the testing of the drug in clinical trials. If both drugs are used together, safety data for both drugs would need to be available, and they would have to be tested in a clinical trial both together and separately. This number of clinical trials would be associated with significant costs and is likely to be prohibitive.

As a peptide that targets T-cell recruiting chemokines specifically, the benefit of CM1629 is not limited to T1D. RA is a disease characterised by T-cell accumulation within the inflamed joint that destroys healthy tissue[544]. Other examples of T-cell diseases are MS[545], myasthenia gravis[546], lupus[547], vasculitis[547], Sjogren's syndrome polymyositis[548], autoimmune hepatitis[549], addison's disease[550], and others[551]. CM1629 may be effective in models of T-cell-driven diseases indicated above, which remains to be investigated.

5.3 Conclusions of the project

The work described in this thesis has identified a T-cell chemokine-inhibiting peptide, CM1629. CM1629 is derived from a class B evasin that was identified by phage display and mutated using the CoSMOS protocol. This work validates the CoSMOS pipeline, and the discovery of a dual chemokine class inhibiting peptide derived from a class B evasin is a novel discovery. CM1629

possesses nanomolar potency against a complex chemokine mixture designed to represent chemokines present in T1D. As T1D is primarily driven by T-cells, the ability of CM1629 to specifically neutralise $CD8^+$ and $CD4^+$ T-cell migration makes CM1629 an intriguing therapeutic candidate for T1D. CM1629 now requires validation *in vivo* and modification to enhance its pharmacological properties, creating a desirable drug candidate.

6. Chapter Six - Materials and Methods

6.1 Materials

6.1.1 Buffers

Table 6.1 – Description of buffers and supplier information.

Buffer	Constituents	Suppliers
Phosphate Buffered Saline (PBS)	8 mM Na_2HPO_4, 2 mM KH_2PO_4, 2.7 mM KCl and 137 mM NaCl, pH 7.5	Sigma-Aldrich
PBSA Buffer	PBS and 0.1% BSA	Sigma-Aldrich
PT Buffer	PBS and 0.05% tween-20	Sigma-Aldrich
Blocking Buffer	PBS and 0.2% BSA	Sigma-Aldrich
PBT Buffer	PBS, 0.2% BSA and 0.05% tween-20	Sigma-Aldrich
10x PBT Buffer	10x PBS, 2% BSA and 0.5% tween-20	Sigma-Aldrich
50x TAE Buffer	24% Tris, 5% acetic acid and 2% EDTA	Fisher Scientific
MACS Buffer	PBS, 0.5% BSA and 2 mM EDTA, pH 7.2	Sigma-Aldrich
10x RBC Lysis Buffer	-	Miltenyi Biotec

6.1.2 Media

Table 6.2 – Description of media and supplier information.

Media	Constituents	Suppliers
LB media	10 g/L tryptone, 5 g/L yeast extract and 10 g/L NaCl, pH 7	Sigma-Aldrich
2YT media	16 g/L tryptone, 10 g/L yeast extract and 5 g/L NaCl, pH 7	Sigma-Aldrich
SOC media	0.5% yeast extract, 2% tryptone, 10 mM NaCl, 2.5 mM KCl, 10 mM $MgSO_4$, 10 mM $MgCl_2$ and 20 mM glucose	Sigma-Aldrich
Biosearch Technologies Recovery Media	-	Fisher Scientific
RPMI Cell Media	RMPI-1640, 10% heat inactivated fetal calf serum and 4 mM L-Glutamine	Sigma-Aldrich
RPMI Cell Migration Media	RMPI-1640, 0.1% protease free BSA, 4 mM L-glutamine and 0.05% DMSO	Sigma-Aldrich
HBSS Cell Migration Media	HBSS, 0.1% protease free BSA and 0.05% DMSO	Sigma-Aldrich
CMRL Cell Migration Media	CMRL 1066 media and 0.05% DMSO	Corning
ImmunoCult™-XF T Cell Expansion Medium	-	STEMCELL Technologies
TexMAC Medium	-	Miltenyi Biotec

6.1.3 General Reagents

General chemicals were purchased from Thermo Fisher, Sigma-Aldrich and Merck. Biotinylated chemokines and C5a were purchased from Almac or Protein Foundry (**Table 6.3)**. Biotinylated chemokines for phage display were reconstituted in PBS at a concentration of 1 µg/µl and stored at –20 °C for up to 12 months. Human chemokines for cell migration assays were purchased from Peprotech, BioLegend or Novus (**Table 6.4**). An 's' at the end of a chemokine name denotes a truncated sequence. All chemokines were reconstituted in PBSA at 10 µM and stored at –20 °C for up to 12 months. Oligonucleotides were purchased from Merck or IDT. Enzymes were obtained from New England Biolabs and Thermo Fisher. Antibodies were purchased from Miltenyi Biotec (**Table 6.5**). Primer sequences were procured from Sigma-Aldrich and Life Technologies (**Table 6.6**).

Table 6.3 – Biotinylated chemoattractants and supplier information

Biotinylated Chemoattractant	Supplier	Code
C5a	Almac	CB-90
CCL1	Almac	CB-07
CCL2	Almac	CB-02
CCL3	Almac	CB-01
CCL4	Almac	CB-23
CCL5	Almac	CB-08
CCL8	Almac	CB-18
CCL11	Almac	CB-03
CCL14s	Protein Foundry	PFP047T
CCL15	Almac	CB-19
CCL17	Almac	CB-16
CCL18	Almac	CB-21
CCL19	Almac	CB-06
CCL20	Almac	CB-05
CCL22	Almac	CB-04
CCL23s	Protein Foundry	PFP058T
CCL25	Almac	CB-15
CCL28	Almac	CB-20
CXCL1	Protein Foundry	PFP029TBL
CXCL5	Protein Foundry	PFP004TBL
CXCL8	Almac	CB-09
CXCL9	Almac	CB-0
CXCL10	Almac	CB-10
CXCL11	Almac	CB-13
CXCL12	Almac	CB-11
CXCL12B	Almac	CB-22
CXCL13	Almac	CB-12
CXCL14	Almac	CB-17
CX3CL1	Almac	CB-14

Table 6.4 – Human chemokines and supplier information.

Human Chemokines	Supplier	Code
CCL1	Peprotech	300-37
CCL2	Peprotech	300-04
CCL3	Peprotech	300-08
CCL4	Peprotech	300-09
CCL5	Peprotech	300-06
CCL7	Peprotech	300-17
CCL8	Peprotech	300-15
CCL11	Peprotech	300-21
CCL13	Peprotech	300-24
CCL14s	Peprotech	300-38B
CCL15	Peprotech	300-43
CCL15s	Novus	NBP2-35043
CCL17	Peprotech	300-30
CCL18	Peprotech	300-34
CCL19	Peprotech	300-29B
CCL20	Peprotech	300-29A
CCL21	Peprotech	300-35A
CCL22	Peprotech	300-36A
CCL23	Peprotech	300-29
CCL23s	BioLegend	587002
CCL24	Peprotech	300-33
CCL25	Peprotech	300-45
CCL26	Peprotech	300-48
CCL27	Peprotech	300-54
CCL28	Peprotech	300-57
CXCL1	Peprotech	300-11
CXCL2	Peprotech	300-39
CXCL3	Peprotech	300-40
CXCL4	Peprotech	300-16
CXCL5	Peprotech	300-22
CXCL6	Peprotech	300-41
CXCL7	Peprotech	300-14
CXCL8	Peprotech	200-08M
CXCL9	Peprotech	300-29
CXCL10	Peprotech	300-12
CXCL11	Peprotech	300-46
CXCL12	Peprotech	300-28A
CXCL13	Peprotech	300-47
CXCL14	Peprotech	300-50
CXCL16	Peprotech	300-55
CX3CL1	Peprotech	300-31

Table 6.5 – Flow cytometry antibodies and supplier information.

Cell Surface Receptor	Antibody Name	Supplier	Code
Control APC	REA Control Antibody (S), human IgG1, APC, REAfinity™	Miltenyi Biotec	130-113-434
Control FITC	REA Control Antibody (S), human IgG1, FITC, REAfinity™	Miltenyi Biotec	130-113-437
CD8	CD8 Antibody, anti-human, FITC, REAfinity™	Miltenyi Biotec	130-110-677
CD4	CD4 Antibody, anti-human, APC, REAfinity™	Miltenyi Biotec	130-113-222
CCR1	CCR1 Antibody, anti-human, APC, REAfinity™	Miltenyi Biotec	130-130-365
CCR2	CCR2 Antibody, anti-human, APC, REAfinity™	Miltenyi Biotec	130-103-830
CCR3	CCR3 Antibody, anti-human, APC, REAfinity™	Miltenyi Biotec	130-123-341
CCR4	CCR4 Antibody, anti-human, APC, REAfinity™	Miltenyi Biotec	130-117-525
CCR5	CCR5 Antibody, anti-human, APC, REAfinity™	Miltenyi Biotec	130-120-057
CCR7	CCR7 Antibody, anti-human, APC, REAfinity™	Miltenyi Biotec	130-120-466
CXCR3	CXCR3 Antibody, anti-human, APC, REAfinity™	Miltenyi Biotec	130-120-450

Table 6.6 – Primer names, sequences, and supplier information.

Primer	Sequence	Supplier
pRSTOP4Nsi_fwd	5'-GGAGGCGCCGAGGGTGAC	Sigma-Aldrich
pRSTOP4Nsi_rev	5'-ATAGGCATTTGTAGCAATAGAAAAAACGAACATAGATGCAAG	Sigma-Aldrich
oligo_fwd	5'-CTATTGCTACAAATGCCTATGCAGCCTCTTCATCTGGC	Sigma-Aldrich
oligo_rev2	5'- TCGTCACCCTCGGCGCCTCCTCCGGATCCTCCACC	Sigma-Aldrich
Genewiz4_fwd	5'-ACACTCTTTCCCTACACGACGCTCTTCCGATCTCTAGCGCTATGCCTATGCAGCCTCTTCA	Life Technologies
Genewiz4_rev	5'-GACTGGAGTTCAGACGTGTGCTCTTCCGATCTCGTCTGCGATGACAACAACCATCGCCCA	Life Technologies

6.1.4 Plasmids

Plasmids for protein expression were produced by SB using the plasmid pHLSec and an In-Fusion cloning kit (Takara)[76]. Sequences contained the protein sequence of interest with an N-terminal

His-tag. Samples were sent to Azenta/GeneWiz to confirm plasmid sequences and were analysed using their Sanger sequencing protocol.

6.1.5 Cell Lines

All cell lines were incubated in a humidified incubator at 37 °C and 5% CO_2 and tested monthly for mycoplasma using a MycoAlert kit (LT07-318, Lonza). Human $CD8^+$ and $CD4^+$ T-cells were isolated, activated, expanded and cryopreserved as described below (**Section 6.13 and Section 6.14**) and were allowed to recover for 24 hours before every experiment. THP-1 cells were obtained from ECACC (88081201) and maintained at a 0.2/0.3 x 10^6 cells/mL density in RPMI cell media.

6.1.6 Proteins

KK, PM, SC or EW produced evasin proteins. Proteins were expressed in HEK293F cells. Proteins were resuspended in PBS supplemented with 5% DMSO (D4540, Sigma-Aldrich) and stored at –20 °C.

6.1.7 Peptides

Peptides were acquired from GenScript (**Table 6.7**). Peptides were synthesised using Fmoc solid-phase synthesis, with >95% purity and a C-terminal amide. The supplier performed LC-MS to confirm the molecular weight of the peptides. Peptides arrived lyophilised and were dissolved in 100% DMSO for 30 minutes at room temperature. PBS was then added to bring the DMSO concentration to 5%. Peptides were then stored at 1000 µM aliquots at –20 °C. Scrambled peptide sequences were designed by SB using the R package stringu_1.7.6 and function stri_rand_shuffle. WT peptide sequences were shuffled 50 times, and the peptide with the largest string distance to the WT sequence was selected by the R package stringdist_0.9.8.

Table 6.7 – Peptides and their sequences

Peptide Name	Peptide Sequence	Parental Peptide or Evasin
EB429	CVEITYFGDFGDPSQD	E1096_IXORI
EB429 SCR	GFDYEFCVDQSGTPDI	E1096_IXORI
EB429 T5W	CVEIWYFGDFGDPSQD	EB429
EB429 G11Y	CVEITYFGDFYDPSQD	EB429
EB429 P13W	CVEITYFGDFGDWSQD	EB429
EB429 D16W	CVEITYFGDFGDPSQW	EB429
CM1629	CVEWWYFYDFYDPIQD	EB429
CM2617	CVEIWYFGGWGDWIFD	EB429
CM3355	CVEWWYFYDFYYWSFW	EB429
CM3384	CVEYWYFYDFYYWIQW	EB429
CM3583	CVEYWYFYDWGYWIQW	EB429
CM1629 SCR	YIYDDQEFWPDWCYFV	EB429

6.2 Methods

6.2.1 Ethical Approval

Peripheral blood mononuclear cells were isolated from leukocyte cones. Granulocytes, monocytes, and lymphocytes were harvested from buffy coats. Both blood products were purchased from NHS Blood Transfusion Services, CUREC1 approval R75963/RE001. Deceased donor human islets were obtained from isolation centres in San Raffaele in Milan, with written informed consent from next of kin and approval from their ethics committee. Human islets were procured from the Alberta Diabetes Institute in Canada, with approval from the Human Research Ethics Board (reference Pro00013094 and Pro00001754). A final source of islets was obtained from Oxford University's Human Islet Isolation Facility, with ethical approval from Oxford's Research Ethics Committee (reference 09/H0695/2) and written informed consent from the donor's relatives.

6.2.2 Phage Display Library Design

Phage libraries were designed by SB, utilising wild-type class B evasins to inform the design of nucleotide sequences. The nucleotide sequences were codon-optimised for expression in *E. coli*

using GeneDesigner 1.0 with the following settings: RNA destabilisation, a codon bias threshold of 0.1, removal of splicing, prokaryotic ribosomal binding sites, Shine-Dalgarno sequences, optimisation of the 5' structure, and removal of repeats. Cysteine residues were mutated to Alanine and Serine to prevent disulphide bond formation. Codon optimisation was then repeated for these mutated sequences. Oligonucleotides (81-mer) were designed to encode 16-amino acid hexadecapeptides. Each oligonucleotide was designed to encode an overlapping peptide library with a single amino acid shift covering the entire length of the parental evasins. Each oligonucleotide was designed to have the sequences 5'-GCAGCCTCTTCATCTGGC, and GGTGGAGGATCCGGA-3' flanking either end to allow for cloning and amplification. The 4,439 oligonucleotide sequences encoding the peptides were synthesised as a pool on a 12K chip by Genescript.

6.2.3 Phage Display Library Construction

6.2.3.1 pRSTOP4 Plasmid Generation

A prSTOP4 plasmid was donated by Dr Sachdev Sidhu from the University of Toronto and had been previously modified to include an NsiI restriction site. This plasmid was amplified using the primers pRSTOP4Nsi_fwd and pRSTOP4Nsi_rev and a Q5 high-fidelity DNA polymerase in a 50 µL reaction (**Tables 6.8 and 6.9**). Following PCR, the samples were run on a 2% TAE gel (Agarose, (A9539-500G, Sigma-Aldrich), and 1x TAE buffer supplemented with 1% ethidium bromide (15585011, Thermo Fisher) for 60 minutes at 120 V. A previously made PCR product was used as a positive control and a water control was used as a negative control. Gels were visualised under UV light using a Bio-Rad ChemiDoc imaging system. The pRSTOP4 PCR product was cleaned using a Monarch PCR and DNA Clean-up Kit (5 µg, T1030, NEB) and quantified using a Nanodrop Spectophotometer (Model ND-1000) to determine the 260/280 ratio. The concentration was determined using a Qubit dsDNA Quantification high-sensitivity kit (Q3281, Thermo Fisher) with a Qubit Fluorometer (Model 2.0).

6.2.3.2 Oligonucleotide Pool Amplification and HiFi Assembly

The 12K Genescript oligonucleotide pool was amplified using the primers oligo_fwd and oligo_rev2, 10ng of the oligonucleotide pool, and a Q5 high-fidelity DNA polymerase (**Tables 6.8 and 6.9**). To maximise library coverage, three 50 µL reactions were created and combined, and the samples were visualised and quantified as described (**Section 6.2.3.1**). The oligonucleotide PCR product was cloned into the prSTOP4NsiI plasmid using a NEB Builder HiFi kit (E5520, NEB). 100 ng of the pRSTOP4 product was combined with 5 ng of the oligonucleotide pool and 10 µL of HiFi assembly mixture. The reactions were incubated at 50 °C for 60 minutes. Four reactions were created and combined to maximise library coverage. The HiFi assembled prSTOP4 phagemid vector was precipitated overnight at –20 °C.

6.2.3.3 Determination of Transformation and Insert Incorporation Efficiency

The pooled DNA was transformed into electrocompetent ElectroMAX™ DH5α-E ™ cells (11319019, Invitrogen). DH5α-E cells were thawed on ice, and 20 µL of the cells was combined per reaction with 5 ng of DNA. The cell and DNA mixture was pipetted into a chilled 1 mm cuvette. Electroporation was performed using the following conditions: 2.0 kV, 200 Ω, and 25 µF, with a Bio-Rad GenePulser Xcell. To the cell DNA mixture, 1 mL of room-temperature SOC medium was added immediately after electroporation. Cell recovery was performed for 60 minutes at 37 °C with shaking at 225 RPM. Transformation efficiency was determined by plating out 100 µL of 1:10, 1:100 and 1:1000 dilutions onto LB plates supplemented with 100 µg/mL carbenicillin (C9231, Sigma-Aldrich). Ten colonies were picked to determine insert incorporation efficiency, and a 25 µL PCR reaction using the OneTaq polymerase was set up (**Tables 2.8 and 2.9**). Clones with an insert were identified at 271 bp, and clones missing inserts were identified at 241 bp. Clones with an insert were then grown overnight in 5 mL LB media supplemented with 100 µg/mL carbenicillin, shaking at 225 RPM at 37 °C. Following miniprep using a QIAprep spin miniprep kit (27104, Qiagen), the samples were sent for sequencing and analysed using a Sanger sequencing protocol

provided by the service supplier (Azenta/GeneWiz). Insert incorporation efficiency was determined by calculating the ratio of clones that contained the correct insert sequences.

6.2.3.4 Transformation and DNA Extraction

The transformation efficiency and insert incorporation efficiency were assessed to ensure complete coverage of the peptides within the library. To ensure adequate coverage of all peptides, the number of peptide inserts in the library was multiplied by 30 and multiplied by the insert incorporation efficiency. A test transformation was performed to determine the transformation efficiency and the required plating serial dilution to avoid a bacterial lawn. Any subsequent transformation that was lower than the expected transformation efficiency was rejected. Plates were also rejected if the colonies were overgrown. The DNA from all transformation plates was harvested and combined using a GeneJet Plasmid Maxiprep Kit (K0491, Thermo Scientific) and quantified as described **(Section 6.2.3.1)**.

6.2.3.5 Phage Generation

The combined plasmid DNA was transformed into electrocompetent SS320 phage display cells (60512, Lucigen). SS320 cells were thawed on ice, and 20 µL of the cells was combined with 1 µL of 100 ng/mL of DNA. The mixture was pipetted into a chilled 1 mm cuvette. Electroporation was performed under the following conditions: 1.8 kV, 600 Ω, and 10 µF. Immediately after electroporation, cells were resuspended in 1 mL of Biosearch Technologies Recovery media (NC9996840, Fisher Scientific) per electroporation and supplemented with 100 µL of 10^{11} CFU/mL M13KO7 helper phage (N0315S, NEB). Cells were recovered at 37 °C, 220 RPM for 60 minutes. Onto an LB agar plate supplemented with 100 µg/mL of carbenicillin, 100 µL of the recovered culture was plated to ensure successful electroporation. The remaining recovery culture was added to 2YT medium supplemented with 50 µg/mL carbenicillin and 25 µg/mL kanamycin (K1377, Sigma-Aldrich) and grown overnight at 37 °C with shaking at 220 RPM. The assembled phage was precipitated from the culture by adding 22.5 mL of supernatant to 4.5 mL

of 20 % PEG 8000 (89510, Sigma-Aldrich) supplemented with 2.5 M NaCl (S9625, Sigma-Aldrich) and incubated on ice for 30 minutes. The phage was centrifuged at 10,000 RPM at 4°C for 10 minutes and resuspended in 1 mL of PBT. The phage library was then stored at 4°C, and a sample was deposited at –20°C for long-term storage.

6.2.3.6 Phage Library Quality Control

The phage library was quantified using a nanodrop at 269 and 320 nm. Briefly, the phage library was tested at various dilutions, including neat and 1:2, 1:5, 1:10, 1:50 and 1:100. This was done to ensure consistency. Virions/mL were calculated (**Figure 6.1**). Phage functionality was tested by completing a phage titration. Before the experiment, One Shot™ OmniMAX™ 2 T1^{R} Chemically Competent *E. coli* (C854003, Invitrogen) was streaked onto an LB agar plate supplemented with 5 µg/mL tetracycline. Omnimax colonies were picked and grown to an OD_{600} of approximately 0.6 in 2YT medium supplemented with 5 µg/mL tetracycline. 500 µL of omnimax was combined with 4.5 mL of top agar (7.5 g/L of agar in LB media) and poured onto an LB agar plate supplemented with 50 µg/mL carbenicillin. The phage library was diluted (5 µL into 45 µL of PBT) ten times, creating a series of dilutions from 10^{-1} to 10^{-10}. 10 µL of each dilution was spotted onto the plate, and the plate was imaged after overnight incubation at 37 °C.

$$\frac{(A_{269} - A_{320}) \times 6 \times 10^{16}}{Vector\ size\ (bp)} = Virions/mL$$

Figure 6.1 – Equation for phage library quantification

Table 6.8 – PCR components and concentrations

PCR Type	Components	Percentage of final reaction volume	Final concentration
Q5 Polymerase	5X Q5 Reaction buffer	20%	1x
	10 mM dNTPs	2%	200 µM
	10 µM FP	5%	0.5 µM
	10 µM RP	5%	0.5 µM
	Q5 High-Fidelity Polymerase	1%	1.0 units per PCR
	Template DNA	2-4%	Dependent on reaction
	Nuclease-free H_2O	Up to required volume	N/A
OneTaq Polymerase	5X OneTaq Standard Reaction buffer	20%	1x
	10 mM dNTPs	2%	200 µM
	10 µM FP	2%	0.5 µM
	10 µM RP	2%	0.5 µM
	OneTaq DNA Polymerase	0.5%	1.25 units per PCR
	Template DNA	10%	Dependent on reaction
	Nuclease-free H_2O	Up to required volume	N/A

Table 6.9 – PCR thermocycler settings

PCR Type	Step	Temperature (°C)	Time (seconds)
Q5 Polymerase	Initial denaturation	98	30
	20/25 cycles	98	10
		60	30
		72	30 to 180
	Final extension	72	120
	Hold	4-10	Indefinite
OneTaq Polymerase	Initial denaturation	94	30
	20 cycles	94	15
		65	30
		68	30
	Final extension	68	300
	Hold	4-10	Indefinite

6.2.4 Saturation Mutagenesis Design and Construction

Oligonucleotides were designed with an NNK codon replacing each of the 16 amino acid residues of EB429 (Genscript). To allow for amplification, oligonucleotides were designed to contain the sequences 5'-GCAGCCTCTTCATCTGGC, and GGTGGAGGATCCGGA-3'. The 16 oligonucleotides

were individually amplified using the primers oligo_fwd and oligo_rev2, using the Q5 high-fidelity DNA polymerase. The PCR products were pooled and cloned into pRSTOP4Nsi. The remaining steps of constructing the mutant EB429 library (designated as EB429X) were performed as described **(Section 6.2.3)**.

6.2.5 Phage Display Library Screening

Phage display screening experiments were performed against multiple chemokine targets in parallel, in 96-well plates (655180, Greiner Bio-One). All washing steps were performed using a 96-well magnetic separator. Biotinylated C5a was used as a negative control to prevent non-specific binding throughout the experiment. Streptavidin-coated beads (Dynabeads™ M-280, 11205D, Invitrogen) were washed with 5 µl in 200 µL of PBS. The streptavidin beads were incubated with 1 µg of biotinylated chemoattractants in 100 µl of PBS (P4417, Sigma-Aldrich) at 4 °C overnight, with shaking at 250 RPM. Unbound chemoattractants were washed off with 200 µL of blocking buffer, and plate contents were transferred to a new 96-well plate. The plate was then blocked in 200 µL of blocking buffer at room temperature for two hours, shaking at 250 RPM. Following blocking, the plate was washed four times with 200 µL of PT buffer, and the plate contents were transferred to a new plate. Phage libraries were diluted to 10^{10} CFU/mL, and 100 µL/well was added to the chemokine-bound beads. The library was incubated with the chemoattractant-bound beads for two hours at room temperature, shaking at 250 RPM. To remove unbound phage, the beads were washed 15 times with 200 µL PT buffer and transferred to a new 96-well plate. The phage was eluted by adding 100 µL of Omnimax *E. coli*, in 2YT media supplemented with 50 µg/mL of kanamycin, when the bacteria had reached an optical density (OD) between 0.4 and 0.8. The beads and Omnimax were incubated at 37 °C for 30 minutes with shaking at 220 RPM. 10 µL of 10^{10} CFU/mL M13K07 helper phage was added and incubated for 45 minutes at 37 °C, with 220 RPM shaking. The cells were transferred to a 96-deep-well plate (CLS3960, Corning) in 1 mL 2YT medium supplemented with 150 µg/mL carbenicillin and 75

µg/mL kanamycin. Following an overnight incubation with shaking at 220 RPM at 37 °C, the plate was centrifuged at 2000 g for 30 minutes at 4 °C. 540 µL of supernatant was transferred to a new deep-well plate containing 60 µL of 10x PBT for storage at 4 °C. Phage display screening was repeated for three rounds of selection. The same method was applied on the subsequent days, using the phage produced from the previous day and stored in 10x PBT at 4 °C.

6.2.6 Next Generation Sequencing

Phage that had been successfully selected were amplified using the Genewiz4_fwd and Genewiz4_rev primers (Life Technologies) and a OneTaq polymerase (**Tables 2.8 and 2.9).** The positive control was the library used in the phage display experiment, and the empty pRSTOP4 vector served as the negative control. The PCR products were quantified using the Qubit dsDNA Quantitation High Sensitivity kit, and the 260/280 ratio was determined using a nanodrop. 25 µL of each sample at 20 ng/mL was sent to Azenta/GeneWiz and analysed using their Amplicon EZ protocol.

6.2.7 Next-Generation Sequencing Analysis

Analysis of next-generation sequencing was performed by SB (**Figure 6.2**). Sequences containing both forward and reverse demultiplexing regions and constant regions were analysed to identify insert sequences (**Table 6.10**). Reads with ambiguous or non-identical insert sequences or incorrect insert size (not 48 nucleotides) or not coding for peptide sequences present in the designed library were excluded. Insert peptide sequences were counted and frequency determined. Following selection, enrichment (E) was calculated as the ratio of output to input peptide frequencies and expressed as log2E. Where proportion of count in input library was not available it was replaced with the lowest input proportion in the experiment rather than replacing it with 0. This is needed to avoid a value of E that is infinity. Peptides that showed binding to control (C5A, log2E>0) were excluded from downstream analysis.

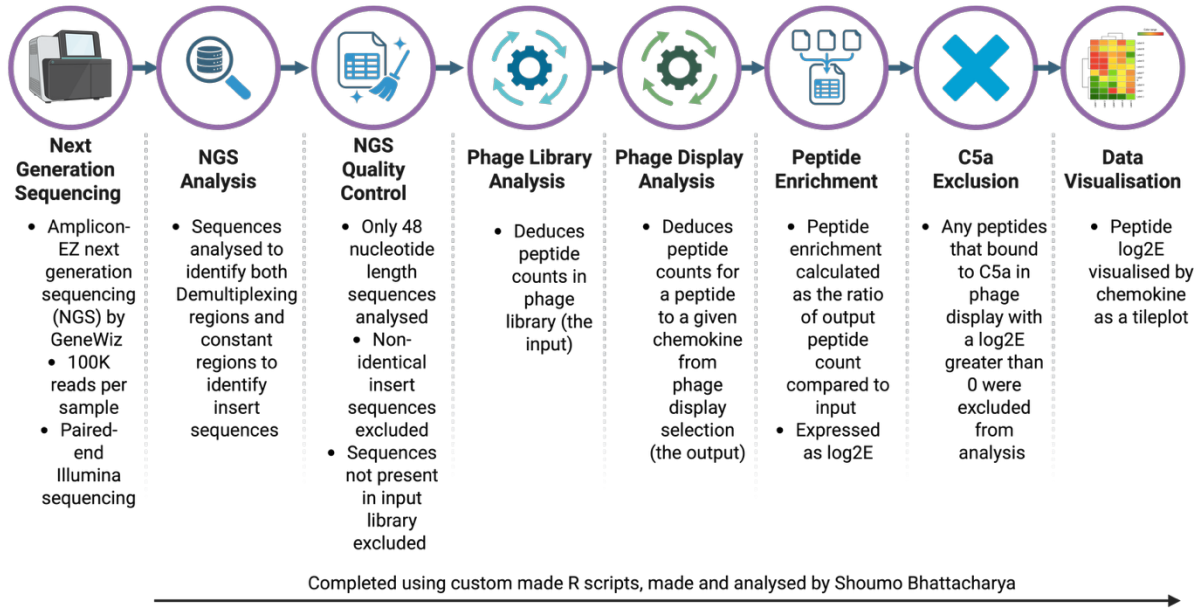

Figure 6.2 – Overview of phage display analysis. Paired-end illumina next generation sequencing (NGS) was used to analyse phage display data. NGS analysis identified insert sequences that contained both demultiplexing regions and constant regions. Quality control steps ensured only inserts of the correct size, and those present in the input library were analysed. Phage library analysis determined peptide frequency in the 'input' library. Phage display analysis determined peptide frequency in the 'output'. Peptide enrichement in phage display could then be calculated as the ratio of output peptide frequency to the input, expressed as log2E. Any peptides that bound to the negative control protein C5a with a log2E greater than 0 were excluded from analysis. Peptide enrichment could then be visualised in a tileplot. All analysis steps were completed by Shoumo Bhattacharya using custom made R scripts. Figure made in Biorender.

Table 6.10 – Demultiplexing regions required for analysis of sequences by NGS

Demultiplexing and constant regions required for NGS sequencing analysis
5'-CTAGCGCT
5'-CGCAGACG
5'-ATGCCTATGCAGCCTCTTCATCTGGC
5'-GGTGGAGGATCCGGAGGAGGCGCCGAGGGTGACGATCCCGCAAAAGCGGCCTTTAACTCCCTGCAAGCCTCAGCGACCGAATATATCGGTTATGCGTGGGCGATGGTTGTTGTCAT

6.2.8 Combinatorial Mutagenesis Design and Construction

Point mutations were selected as described previously using an algorithm that optimizes CC and CXnC improving mutations separately[408]. At each peptide position the mutation giving the highest mean Δlog2E and the highest peak Δlog2E were identified using a threshold 5 for peak Δlog2E, and a threshold of 0.55 for mean Δlog2E, and then selected the top 10 mutations (arranged by mean Δlog2E and peak Δlog2E) for CC and top 12 mutations for CXnC chemokines.

This resulted in a total of 16 mutations. We generated all possible combinations of these mutations, added the parental and scrambled parental sequence, and reverse translated the peptides to generate 3777 oligonucleotide sequences using R package reversetranslate_1.0.0, with ecoli_tbl and model ="gc_biased". Oligonucleotides were synthesized as a pool (Genscript, 12K chip) and cloned into plasmid prSTOP4Nsi as described above. Library quality was assessed by NGS AmpliconEZ (100,000 reads), and 3418 of 3777 inserts were identified. For the combinatorial library phage display screen, adjusted counts for input and output libraries were generated from raw counts by adding 1 to all counts to avoid division by zero, and frequency determined. Enrichment (E) was calculated as ratio of output to input peptide frequencies and expressed as log2E. Deltalog2E was calculated as the difference between log2E of peptide and that of parental EB429. Peptides that showed binding to control (C5A, log2E>0) were excluded from downstream analysis.

6.2.9 Bulk RNA-sequencing Analysis

Analysis was performed by SB (**Figure 6.3**)[408]. Raw counts were downloaded from the GEO database and were converted to transcripts per million (tpm). Tpm was selected over RPKM as Tpm corrects for gene length, sequencing depth biases, and the proportion of reads that map to each gene in each sample. Mean tpm was calculated using the number of samples available for each chemokine in the dataset (**Table 6.10**). To construct a 10 μM chemokine pool, the abundance of each chemokine (as measured by the mean tpm) was converted to the relative amount of each chemokine at 10 μM.

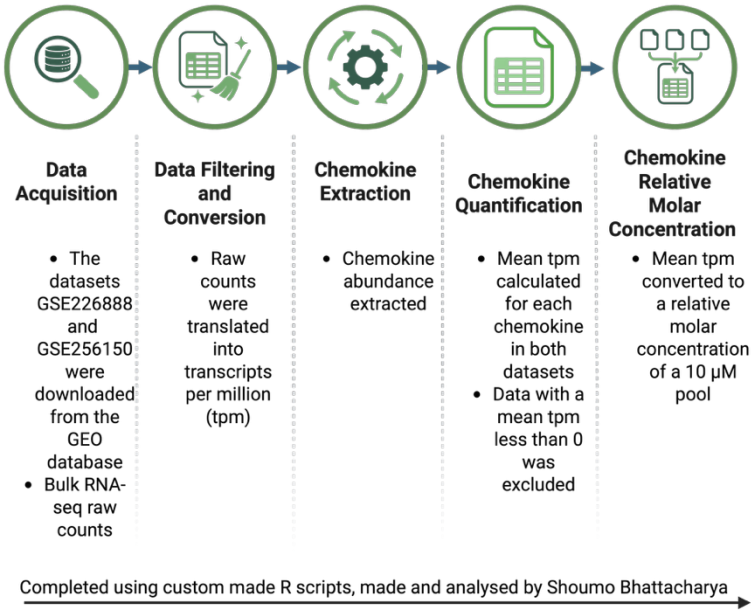

Figure 6.3 – Overview of RNA-seq analysis. Bulk-RNA sequencing datasets were downloaded from the GEO database. Raw counts were translated to transcripts per million (tpm). Chemokine abundance was extracted, and mean tpm was calculated for each chemokine. Relative chemokine molar concentrations were calculated per dataset. All analysis steps were completed by Shoumo Bhattacharya using custom made R scripts. Figure made in Biorender.

Table 6.11 – Dataset information for RNA-seq guided chemokine pool construction

GEO Accession	Species	Description	Sample ID
GSE226888	Homo sapiens	Healthy human isolated pancreatic islets stimulated ex vivo with cytokines. N=5.	GSM7086403
			GSM7086404
			GSM7086405
			GSM7086406
			GSM7086407

6.2.10 Human Islet Stimulation

Human islets were cultured in CMRL 1066 medium (99603CV, Corning) supplemented with 1% foetal calf serum (FCS) and 100 µg/mL penicillin and streptomycin at 5% CO_2 and 37 °C. 150/200 islets per condition were stimulated in 2 mL of the supplemented CMRL 1066. Samples were stimulated with 10 ng/mL of IFN-γ, 10 ng/mL of TNF-α, and 2 ng/mL of IL-1β, with an unstimulated matched time point. The time points trialled were 24, 48, 72 and 96 hours. Cytokines were replenished every 48 hours. Following stimulation, samples were decellularised by centrifugation twice for 15 minutes at 2500 g. Samples were frozen in 250 µl aliquots at –80 °C.

6.2.11 Quantibody

Custom Quantibody Human Chemokine Antibody Arrays for the chemokines CXCL1, CXCL2, CXCL12α, CXCL12β, CXCL14, CXCL16 and CX3CL1 (QAH-CUST, RayBiotech) and Quantibody Human Cytokine Antibody Arrays (Q2000, RayBiotech) were equilibrated at room temperature for 30 minutes. All buffers and standards were prepared according to the manufacturer's instructions, including the cytokine standard dilutions. Arrays were then air-dried for 2 hours and blocked for 30 minutes in 100 µL of sample diluent buffer on a rocking shaker. Conditioned media samples for analysis were diluted 1:2 with sample dilution buffer, and 100 µL was added to each well. Wells were incubated overnight on a rocking shaker at 4 °C. Wells were washed with 150 µL of 1x wash buffer I for 5 minutes on a rocking shaker, 5 times. Wells were washed twice with 150 µL of 1x wash buffer II for 5 minutes on a rocking shaker. 80 µL of the biotinylated detection antibody cocktail was added to each well for 2 hours. Washes were then repeated, 5 times with 150 µL of 1x wash buffer, and then twice with 150 µL of 1x wash buffer II, for 5 minutes each on a rocking shaker. 80 µL of the Cy3 equivalent dye, conjugated to streptavidin, was added to each well and incubated for one hour in the dark. Samples were washed 5 times with 150 µL of 1x wash buffer, for 5 minutes each time on a rocking shaker. The arrays were removed from their gasket, placed into the slide washing containers, and covered in 1x wash buffer I. The slides were washed for 15 minutes with gentle shaking, and the process was repeated for 5 minutes with 1x wash buffer II. Slides were air-dried and sent to RayBiotech for slide scanning and data extraction. Cytokine and chemokine quantities were returned in pg/mL to ng/mL based on linear regression of the standard curves included in the samples.

6.2.12 Human Lymphocyte, Monocyte and Granulocyte Isolation

Buffy coat blood samples were procured from NHS BT. Red blood cells were depleted using 1 mL of HetaSep (07806, Stemcell Technologies) per 5 mL of buffy coat, and the samples were incubated for 15-25 minutes at 37 °C. The top layer of the buffy coat was collected, and cells were

washed in MACS buffer. Following a 10-minute treatment with 1x RBC lysis buffer (170-080-033, Miltenyi Biotec) to remove the remaining RBCs, cells were centrifuged and resuspended in MACS buffer. Granulocytes, monocytes, and lymphocytes were then counted based on FSC-H and SSC-H parameters using the Attune Nxt Flow Cytometer and previously defined gate settings for granularity and size[408].

6.2.13 Human CD8⁺ T-cell Isolation, Activation and Expansion

Leukocyte cones were procured from NHS BT. Peripheral blood mononuclear cells (PBMCs) were purified by lysing the RBCs twice, with 1x RBC lysis buffer for 10 minutes and spinning at 1400 RPM for a further 10 minutes. PBMCs were strained through a 70 µM filter and resuspended in ~5 mL MACS buffer. 100 x 10^6 cells/mL were added to 100 µL of both biotin-antibody cocktail and streptavidin nanobeads (B305145, MojoSort) for 15 minutes, respectively. The cell mixture was placed in a magnet (480019, MojoSort) for 5 minutes twice, and the cells of interest were poured out. 1 x 10^6/mL isolated CD8⁺ cells were resuspended in ImmunoCult™-XF T Cell Expansion Medium (10981, Stemcell Technologies), supplemented with 10 ng/µL human IL-2 (200-02-10, Peprotech), 25 µL/mL anti-CD3/anti-CD28 T-cell activator (10991, Stemcell Technologies) and 1% penicillin-streptomycin for activation. Activation occurred for 10 to 13 days, with cells being passaged every 2 to 3 days in TexMACS medium (130-097-196, Miltenyi Biotec) supplemented with 10 ng/µL human IL-2. Following successful labelling for CD8⁺ and CXCR3, cells were aliquoted to 20 x 10^6 cells/mL in TexMACS supplemented with 10% DMSO and stored at –80°C. Cells were subsequently moved to vapour phase nitrogen for long- term storage.

6.2.14 Human CD4⁺ T-cell Isolation, Activation and Expansion

Human CD4⁺ cells were isolated as described (**Section 2.2.14**) with the adjustments described. CD4⁺ cells were isolated with the CD4⁺ isolation kit (480010, Mojosort). To activate the CD4⁺ T-cells, ImmunoCult activation was supplemented with 10 ng/µL human IL-12 (200-12H-10, Peprotech) and 10 ng/µL IL-2. Every 2/3 days, cells were passaged in TexMACS medium

supplemented with 10 ng/µL human IL-2 and 10 ng/µL human IL-12. Following successful labelling of $CD4^+$ cells, cells were cryopreserved as described.

6.2.15 Cell Surface Labelling

Cells were labelled using a variety of antibodies to identify relevant cell markers and chemokine receptors. Antibodies used were allophycocyanin (APC) or FITC conjugated. For all samples, a negative control sample was run using a control APC or a control FITC antibody. 100,000 cells were centrifuged for 2 minutes at 5000 RPM and resuspended in 100 µL of MACS buffer. 2 µL of antibody or control APC/FITC antibody was added to the cells and samples were incubated in the dark for 10 minutes at 4°C. Cells were centrifuged for 2 minutes at 5000 RPM and resuspended in 500 µL of MACS buffer. Relevant fluorescence intensities of the samples were determined by gating 10,000 cells on the Attune Nxt Flow Cytometer using previously defined gate settings.

6.2.16 Propidium Iodide Staining

Propidium iodide (PI) staining was used to determine cellular membrane integrity and cell viability. 0.1 x 10^6 cells were incubated with 10 µM of peptide for 2 hours. For each experiment, a cell-only control was incubated for the same time and boiled to kill the cells. This sample of non-viable cells can then act as a control for fluorescence intensity gating. Two drops of PI (R37169, Invitrogen) was added to each sample. Samples were incubated for 15 minutes at room temperature. Relevant fluorescence intensities of the samples were determined by gating 10,000 cells on the Attune Nxt Flow Cytometer using previously defined gate settings.

6.2.17 Cell Migration Assays

6.2.17.1 Human $CD8^+$ and $CD4^+$ T-cells

24 hours prior to use in cell migration assays, $CD8^+$ and $CD4^+$ cells were recovered in TexMACS at 0.3x10^6 cells/mL and incubated at 37 °C in 5% CO_2. 3-micron transwell plates (3385, Corning) were used for T-cell assays. 150 µL of HBSS migration media was added to the bottom chamber

alone, or supplemented with chemokine, with or without peptide. To the top chamber, 100,000 cells per well were added in 50 µL of HBSS migration media. The T-cell assays were incubated for two hours at 37 °C in 5% CO_2.

6.2.17.2 Human granulocytes, monocytes, and lymphocytes

3-micron transwell plates were used for granulocyte, monocyte, and lymphocyte assays. To the bottom well, 150 µL HBSS migration media with peptides and chemokines used for the relevant experiment was added. In the top chamber, 100,000 monocytes were added to 50 µL of HBSS migration media. Buffy coat assays were incubated for 2 hours at 37 °C in 5% CO_2.

6.2.17.3 THP-1 cells

THP-1 assays were performed using 5-micron transwell plates (3387, Corning). To the bottom chamber, 150 µL of RPMI migration media was added, combined with relevant chemokines and peptides. 300,000 cells per well were added to the top chamber in 50 µL of RPMI migration media. THP-1 migration assays were incubated for 4 hours at 37 °C in 5% CO_2.

6.2.18 Analysis of Cell Migration Experiments

Following the designated incubation length, the migration plate was shaken for 10 minutes at 850 RPM, and 150 µL of media from the bottom of the cell migration plate was added to a 96-well round-bottom plate (353910, Falcon) containing 50 µL of the migration media. An attune NxT Flow Cytometer Plate Reader with Cytkick autosampler (Thermo Fisher) was used to determine cell counts based on FSC-H and SSC-H parameters. All cell types had previously defined gate settings[76, 408]. Unless otherwise indicated, all experiments include 3 technical and 3 biological replicates. Individual data points indicate the normalised values of 3 biological replicates.

6.2.18.1 Dose-Response Curves

Dose-response curves were used to determine effective concentrations (EC) of the chemoattractant. The EC80 or EC50 is the chemokine concentration required to cause 80% or

50% of the maximal observed migration, respectively. EC values were calculated using GraphPad Prism, fitting an agonist response curve with 3 parameters.

6.2.18.2 Single-Concentration Inhibition Assays

Single-concentration inhibition assays were used to determine a peptide's effectiveness in inhibiting migration of a cell type to a chemokine or chemokine mixture. Chemokines or chemokine pools at their EC50/80 concentration were mixed with a peptide at a final concentration of 10 µM. All peptides were tested at a concentration of 10 µM unless otherwise stated. All peptides contained 0.05% DMSO, which was added to all media to standardise assay conditions. The chemokine and peptides were pre-incubated together for 30 minutes at 37 °C and 5% CO_2 before plating. Graphs were plotted using GraphPad Prism. Cell migration was normalised to 1,000 by taking the mean value of cells migrating to the EC50/80 chemokine concentration.

6.2.18.3 IC50 curves

IC50 curves were used to determine a peptide's potency. IC50 curves were performed by pre-incubating decreasing concentrations of a peptide with an EC80/50 of chemokine for 30 minutes at 37 °C before plating. Peptide IC50 values were calculated using GraphPad Prism, fitting an inhibitor dose-response curve with 3 parameters fixing the bottom of the curve to 0[408]. The mean IC50 value was then calculated over the three biological replicate experiments. Cell migration was normalised to 1,000 by taking the mean value of cells migrating to the EC50/80 chemokine concentration. To allow for comparison of IC50 values, pIC50 was calculated as the negative $\log_{10}$ of IC50[408].

6.2.19 AlphaFold3 Modelling

Chemokine models with either chemokine receptors or peptides were generated using the AlphaFold3 webserver[433]. Chemokine receptor sequences were identified using the IUPHAR database[68]. The output of the webserver was downloaded, and the highest-ranking model was

visualised using PyMOL version 3.1.4.1. The PyMOL 'distance' command was used to determine areas on chemokines within a 5 angstrom distance from a peptide/chemokine receptor.

Modelling of peptide:chemokine inter-chain interactions was performed by SB. Protein sequences were converted into JSON files for submission to the AlphaFold3 webserver. Arpeggio[552] was utilised to extract the inter-chain interactions and inter-residue distance of the highest-ranking model. All modelling was performed in accordance with AlphaFold3's terms and conditions[408, 433].

6.2.20 Statistical Information

Graphs were plotted using GraphPad Prism 10.4.2. Summary statistics were calculated in GraphPad, and statistical significance was calculated using a one-way ANOVA followed by a two-sided Dunnett's test for multiple comparisons[553]. The statistical significance of cell-only values and EC50/80 values are not shown. The P-value (the probability of a type I error) was adjusted for multiple comparisons and set at a threshold of $P < 0.05$. Asterisks indicate the following: ****$p \leq 0.0001$, ***$p \leq 0.001$, **$p \leq 0.01$, *$p \leq 0.05$.

7. Chapter Seven - Appendix

7.1 Cytokine Stimulation of Human Islets and Supernatant Testing

Human islets were procured, cultured and stimulated with the chemokines IFN-γ, IL-1β and TNF-α (**Figure 7.1**). The supernatant of islet batches was tested for its ability to induce $CD8^+$ migration in cell migration assays (**Figure 7.2**). Supernatant testing was performed to determine whether the cytokine stimulation was successful. The negative control was the supernatant of unstimulated time- and donor-matched islets. To confirm that the migration observed by the islet supernatant was due to chemokine production, the triple warhead evasin protein P1834 was used in combination with the cytokine-stimulated supernatant. Collating donor samples, testing with P1834 significantly inhibited $CD8^+$ T-cell migration to the 48 hour stimulated islet supernatant (**Figure 7.3**). Stimulated samples were sent for analysis using Quantibody multiplex ELISA arrays.

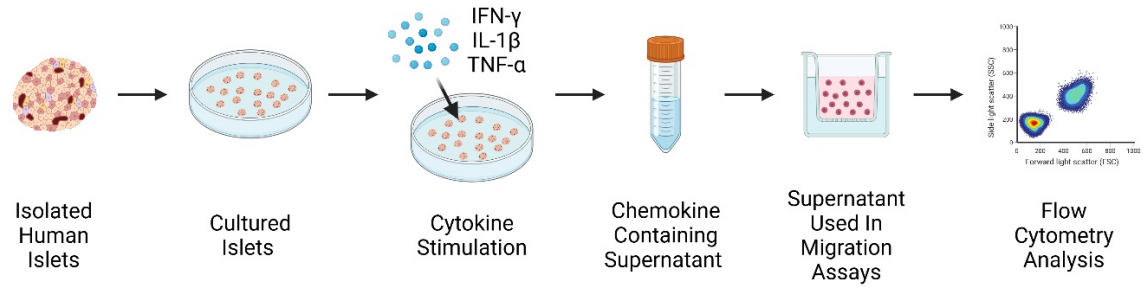

Figure 7.1 – Pipeline of human islet stimulation. Isolated human islets are procured and cultured. Islets are stimulated with the cytokines IFN-γ, IL-1β and TNF-α, with a time-matched unstimulated control. Following the time course of stimulation, islet samples are centrifuged to isolate the chemokine-containing supernatant. The chemokine-containing supernatant is then used in cell migration assays with $CD8^+$ T-cells, and the experimental output is analysed using flow cytometry. Figure made in Biorender.

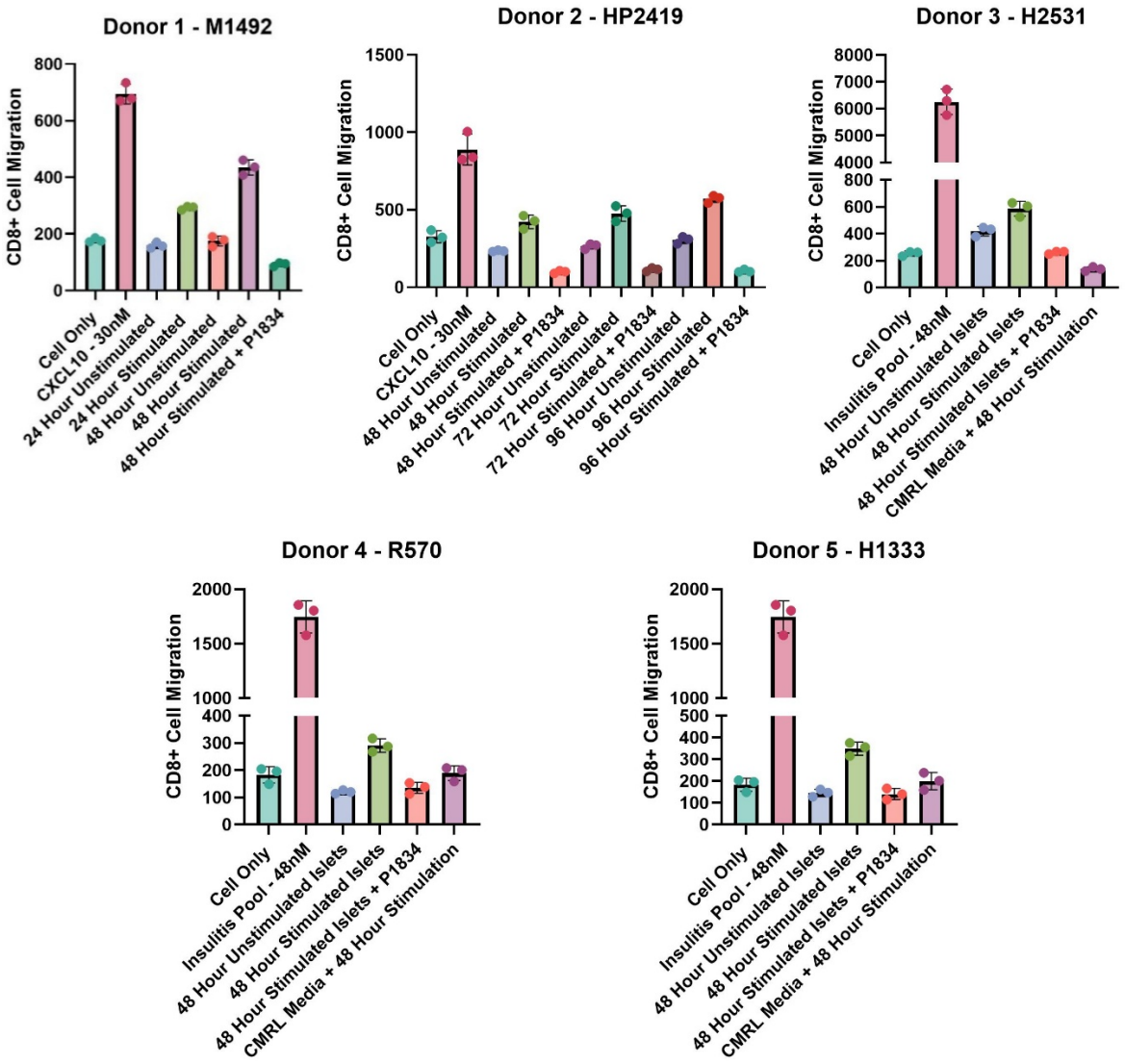

Figure 7.2 – Effect of cytokine-stimulated islet supernatant on CD8⁺ T-cell migration. Bar charts with standard deviation error bars depicting the effect of islet supernatant to induce CD8⁺ T-cell migration. All experiments were performed as technical replicates. The Y-axis shows CD8⁺ cell migration. The X-axis shows experimental constituents. P1834 was tested at a final concentration of 10 μM.

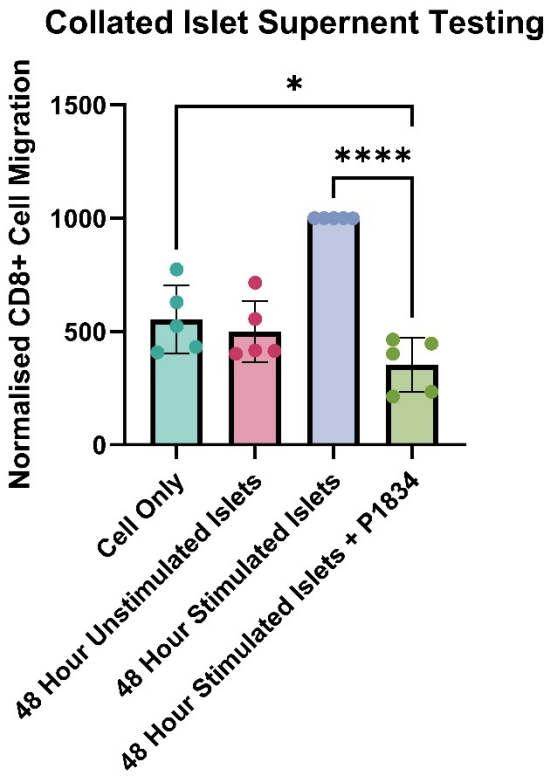

Figure 7.3 – Collated effect of cytokine-stimulated islet supernatant on CD8⁺ T-cell migration. Bar charts with standard deviation error bars depicting the effect of islet supernatant to induce CD8⁺ T-cell migration. The experiment was performed as three technical replicates and three biological replicates. Individual data points indicate mean values of technical replicates per experiment. Cell migration values were normalised to the mean value of migrated cell counts to the 48 hour stimulated islets and set to 1000 cells, as indicated on the Y-axis. The X-axis shows experimental constituents. P1834 was tested at a final concentration of 10 μM. The statistical significance was calculated compared to the cell migration of 48 hour stimulated islets using a one-way ANOVA and a Dunnett's test for multiple comparisons. Asterisks indicate the following: ****p ≤ 0.0001, ***p ≤ 0.001, **p ≤ 0.01, *p ≤ 0.05.

Bibliography

1) Punchard NA, Whelan CJ, Adcock I. The Journal of Inflammation. J Inflamm (Lond). 2004;1(1):1.

2) Tracy RP. The Five Cardinal Signs of Inflammation: Calor, Dolor, Rubor, Tumor ... and Penuria (Apologies to Aulus Cornelius Celsus, De Medicina, C. A.D. 25). The Journals of Gerontology: Series A. 2006;61(10):1051-52.

3) Kumar R, Clermont G, Vodovotz Y, Chow CC. The Dynamics of Acute Inflammation. Journal of theoretical biology. 2004;230(2):145-55.

4) Medzhitov R. Origin and Physiological Roles of Inflammation. Nature. 2008;454(7203):428-35.

5) Li J, Xiao C, Li C, He J. Tissue-Resident Immune Cells: From Defining Characteristics to Roles in Diseases. Signal Transduction and Targeted Therapy. 2025;10(1):12.

6) Ma M, Jiang W, Zhou R. Damps and Damp-Sensing Receptors in Inflammation and Diseases. Immunity. 2024;57(4):752-71.

7) Carty M, Guy C, Bowie AG. Detection of Viral Infections by Innate Immunity. Biochemical Pharmacology. 2021;183:114316.

8) Bianchi ME. Damps, Pamps and Alarmins: All We Need to Know About Danger. Journal of Leukocyte Biology. 2007;81(1):1-5.

9) Murphy K, Weaver C. Janeway's Immunobiology: Garland science; 2016.

10) Tang D, Kang R, Coyne CB, Zeh HJ, Lotze MT. Pamp S and Damp S: Signal 0s That Spur Autophagy and Immunity. Immunological reviews. 2012;249(1):158-75.

11) Kawai T, Akira S. The Roles of Tlrs, Rlrs and Nlrs in Pathogen Recognition. International Immunology. 2009;21(4):317-37.

12) Creagh EM. Caspase Crosstalk: Integration of Apoptotic and Innate Immune Signalling Pathways. Trends in immunology. 2014;35(12):631-40.

13) Newton K, Dixit VM. Signaling in Innate Immunity and Inflammation. Cold Spring Harbor perspectives in biology. 2012;4(3):a006049.

14) Jutel M, Akdis M, Akdis CA. Histamine, Histamine Receptors and Their Role in Immune Pathology. Clinical & Experimental Allergy. 2009;39(12):1786-800.

15) Rubinstein M, Dinarello CA, Oppenheim JJ, Hertzog P. Recent Advances in Cytokines, Cytokine Receptors and Signal Transduction. Cytokine & growth factor reviews. 1998;9(2):175-81.

16) Stenger S, Röllinghoff M. Role of Cytokines in the Innate Immune Response to Intracellular Pathogens. Annals of the rheumatic diseases. 2001;60(suppl 3):iii43-iii46.

17) Hamilton JA. Colony-Stimulating Factors in Inflammation and Autoimmunity. Nature Reviews Immunology. 2008;8(7):533-44.

18) Mantovani A, Dinarello CA, Molgora M, Garlanda C. Interleukin-1 and Related Cytokines in the Regulation of Inflammation and Immunity. Immunity. 2019;50(4):778-95.

19) Van Loo G, Bertrand MJ. Death by Tnf: A Road to Inflammation. Nature Reviews Immunology. 2023;23(5):289-303.

20) Rauch I, Müller M, Decker T. The Regulation of Inflammation by Interferons and Their Stats. Jak-stat. 2013;2(1):e23820.

21) Chen K, Bao Z, Tang P, Gong W, Yoshimura T, Wang JM. Chemokines in Homeostasis and Diseases. Cell Mol Immunol. 2018;15(4):324-34.

22) Johnston B, Butcher EC, editors. Chemokines in Rapid Leukocyte Adhesion Triggering and Migration. Seminars in immunology; 2002: Elsevier.

23) Langer HF, Chavakis T. Leukocyte–Endothelial Interactions in Inflammation. Journal of cellular and molecular medicine. 2009;13(7):1211-20.

24) Leick M, Azcutia V, Newton G, Luscinskas FW. Leukocyte Recruitment in Inflammation: Basic Concepts and New Mechanistic Insights Based on New Models and Microscopic Imaging Technologies. Cell and tissue research. 2014;355(3):647-56.
25) Ivetic A, Hoskins Green HL, Hart SJ. L-Selectin: A Major Regulator of Leukocyte Adhesion, Migration and Signaling. Frontiers in Immunology. 2019;10:1068.
26) Guo J, Xu Z, Gunderson RC, Xu B, Michie SA. Lfa-1/Icam-1 Adhesion Pathway Mediates the Homeostatic Migration of Lymphocytes from Peripheral Tissues into Lymph Nodes through Lymphatic Vessels. Biomolecules. 2023;13(8):1194.
27) Petri B, Bixel MG. Molecular Events During Leukocyte Diapedesis. The FEBS Journal. 2006;273(19):4399-407.
28) DeLeo FR, Allen L-AH. Phagocytosis and Neutrophil Extracellular Traps. Faculty reviews. 2020;9:25.
29) Kelly M, Hwang JM, Kubes P. Modulating Leukocyte Recruitment in Inflammation. Journal of Allergy and Clinical Immunology. 2007;120(1):3-10.
30) Ortega-Gómez A, Perretti M, Soehnlein O. Resolution of Inflammation: An Integrated View. EMBO molecular medicine. 2013;5(5):661-74.
31) Serhan CN, Brain SD, Buckley CD, Gilroy DW, Haslett C, O'Neill LA, Perretti M, Rossi AG, Wallace JL. Resolution of Inflammation: State of the Art, Definitions and Terms. FASEB journal: official publication of the Federation of American Societies for Experimental Biology. 2007;21(2):325.
32) Fu Z, Thorpe M, Alemayehu R, Roy A, Kervinen J, de Garavilla L, Åbrink M, Hellman L. Highly Selective Cleavage of Cytokines and Chemokines by the Human Mast Cell Chymase and Neutrophil Cathepsin G. The Journal of Immunology. 2017;198(4):1474-83.
33) Gilroy D, De Maeyer R, editors. New Insights into the Resolution of Inflammation. Seminars in immunology; 2015: Elsevier.
34) Lawrence T, Gilroy DW. Chronic Inflammation: A Failure of Resolution? International journal of experimental pathology. 2007;88(2):85-94.
35) Furman D, Campisi J, Verdin E, Carrera-Bastos P, Targ S, Franceschi C, Ferrucci L, Gilroy DW, Fasano A, et al. Chronic Inflammation in the Etiology of Disease across the Life Span. Nature medicine. 2019;25(12):1822-32.
36) Manabe I. Chronic Inflammation Links Cardiovascular, Metabolic and Renal Diseases. Circulation Journal. 2011;75(12):2739-48.
37) Ehlers S, Kaufmann SH. Infection, Inflammation, and Chronic Diseases: Consequences of a Modern Lifestyle. Trends in immunology. 2010;31(5):184-90.
38) Pawelec G, Goldeck D, Derhovanessian E. Inflammation, Ageing and Chronic Disease. Current opinion in immunology. 2014;29:23-28.
39) Simmonds M, Gough S. Genetic Insights into Disease Mechanisms of Autoimmunity. British medical bulletin. 2005;71(1):93-113.
40) Gallegos AM, Bevan MJ. Central Tolerance: Good but Imperfect. Immunological reviews. 2006;209(1):290-96.
41) Morris PJ, Wood KJ, Sprent J, Kishimoto H. The Thymus and Central Tolerance. Philosophical Transactions of the Royal Society of London Series B: Biological Sciences. 2001;356(1409):609-16.
42) Waldmann H. Mechanisms of Immunological Tolerance. Clinical biochemistry. 2016;49(4-5):324-28.
43) Danke NA, Koelle DM, Yee C, Beheray S, Kwok WW. Autoreactive T Cells in Healthy Individuals. The Journal of Immunology. 2004;172(10):5967-72.
44) Sakaguchi S, Yamaguchi T, Nomura T, Ono M. Regulatory T Cells and Immune Tolerance. Cell. 2008;133(5):775-87.
45) Mueller DL. Mechanisms Maintaining Peripheral Tolerance. Nature Immunology. 2010;11(1):21-27.

46) Mezgebu E, Aliy A, Worku T. Autoimmunity and Immune Tolerance: A Review. Microbiol Res Int. 2023;11:23-25.
47) Hocking AM, Buckner JH. Genetic Basis of Defects in Immune Tolerance Underlying the Development of Autoimmunity. Frontiers in Immunology. 2022;13:972121.
48) Skapenko A, Leipe J, Lipsky PE, Schulze-Koops H. The Role of the T Cell in Autoimmune Inflammation. Arthritis Research & Therapy. 2005;7(2):S4.
49) Palmer E. Negative Selection—Clearing out the Bad Apples from the T-Cell Repertoire. Nature Reviews Immunology. 2003;3(5):383-91.
50) Özkan AMG, Güray ÇG. A Mediterranean: Myrtus Communis L.(Myrtle). Plants and Culture: Seeds of the Cultural Heritage of Europe, Morel JP, Mercuri AM (eds) Edipuglia: Bari. 2009:159-68.
51) Buring SD, Cook N, Richard Doll F, Đberlein K, Mathew-Roth JMMM, Mayrent SL, MD FES, Stampfer MJ, Stubblefield F, et al. Lthough Chewing Willow Bark, Which Has Aspirin-Like Propertics, Was Prescribed for Pain Relief by Hippocrates in the Fifth Century Ec, the Possible Role of Aspirin in Reducing the Risk of Cardio. vascular.129:35.
52) Jack DB. One Hundred Years of Aspirin. The Lancet. 1997;350(9075):437-39.
53) Davis A, Robson J. The Dangers of Nsaids: Look Both Ways. The British journal of general practice. 2016;66(645):172.
54) Brennan R, Wazaify M, Shawabkeh H, Boardley I, McVeigh J, Van Hout MC. A Scoping Review of Non-Medical and Extra-Medical Use of Non-Steroidal Anti-Inflammatory Drugs (Nsaids). Drug Safety. 2021;44:917-28.
55) Leung YY, Hui LLY, Kraus VB, editors. Colchicine—Update on Mechanisms of Action and Therapeutic Uses. Seminars in arthritis and rheumatism; 2015: Elsevier.
56) Ericson-Neilsen W, Kaye AD. Steroids: Pharmacology, Complications, and Practice Delivery Issues. Ochsner J. 2014;14(2):203-7.
57) Manson SC, Brown RE, Cerulli A, Vidaurre CF. The Cumulative Burden of Oral Corticosteroid Side Effects and the Economic Implications of Steroid Use. Respir Med. 2009;103(7):975-94.
58) Colobran R, Pujol-Borrell R, Armengol MP, Juan M. The Chemokine Network. I. How the Genomic Organization of Chemokines Contains Clues for Deciphering Their Functional Complexity. Clinical & Experimental Immunology. 2007;148(2):208-17.
59) Zlotnik A, Yoshie O. The Chemokine Superfamily Revisited. Immunity. 2012;36(5):705-16.
60) Turner MD, Nedjai B, Hurst T, Pennington DJ. Cytokines and Chemokines: At the Crossroads of Cell Signalling and Inflammatory Disease. Biochim Biophys Acta. 2014;1843(11):2563-82.
61) Youn B-S, Mantel C, Broxmeyer Hal E. Chemokines, Chemokine Receptors and Hematopoiesis. Immunological reviews. 2000;177(1):150-74.
62) Janssens R, Struyf S, Proost P. The Unique Structural and Functional Features of Cxcl12. Cell Mol Immunol. 2018;15(4):299-311.
63) Wu T, Yang W, Sun A, Wei Z, Lin Q. The Role of Cxc Chemokines in Cancer Progression. Cancers (Basel). 2022;15(1).
64) Hughes CE, Nibbs RJB. A Guide to Chemokines and Their Receptors. Febs j. 2018;285(16):2944-71.
65) Miller MC, Mayo KH. Chemokines from a Structural Perspective. International journal of molecular sciences. 2017;18(10):2088.
66) Bachelerie F, Ben-Baruch A, Burkhardt AM, Combadiere C, Farber JM, Graham GJ, Horuk R, Sparre-Ulrich AH, Locati M, et al. International Union of Basic and Clinical Pharmacology. [Corrected]. Lxxxix. Update on the Extended Family of Chemokine Receptors and Introducing a New Nomenclature for Atypical Chemokine Receptors. Pharmacol Rev. 2014;66(1):1-79.

67) Gangele K, Jamsandekar M, Mishra A, Poluri KM. Unraveling the Evolutionary Origin of Elr Motif Using Fish Cxc Chemokine Cxcl8. Fish & shellfish immunology. 2019;93:17-27.
68) Harding SD, Sharman JL, Faccenda E, Southan C, Pawson AJ, Ireland S, Gray AJG, Bruce L, Alexander SPH, et al. The Iuphar/Bps Guide to Pharmacology in 2018: Updates and Expansion to Encompass the New Guide to Immunopharmacology. Nucleic Acids Res. 2018;46(D1):D1091-d106.
69) Kufareva I, Gustavsson M, Zheng Y, Stephens BS, Handel TM. What Do Structures Tell Us About Chemokine Receptor Function and Antagonism? Annu Rev Biophys. 2017;46:175-98.
70) Zweemer AJM, Toraskar J, Heitman LH, Ijzerman AP. Bias in Chemokine Receptor Signalling. Trends in immunology. 2014;35(6):243-52.
71) Bonecchi R, Graham GJ. Atypical Chemokine Receptors and Their Roles in the Resolution of the Inflammatory Response. Frontiers in Immunology. 2016;Volume 7 - 2016.
72) Borroni EM, Mantovani A, Locati M, Bonecchi R. Chemokine Receptors Intracellular Trafficking. Pharmacology & therapeutics. 2010;127(1):1-8.
73) Johnson Z, Proudfoot AE, Handel TM. Interaction of Chemokines and Glycosaminoglycans: A New Twist in the Regulation of Chemokine Function with Opportunities for Therapeutic Intervention. Cytokine Growth Factor Rev. 2005;16(6):625-36.
74) Graham GJ, Handel TM, Proudfoot AEI. Leukocyte Adhesion: Reconceptualizing Chemokine Presentation by Glycosaminoglycans. Trends Immunol. 2019;40(6):472-81.
75) Proudfoot AE, Handel TM, Johnson Z, Lau EK, LiWang P, Clark-Lewis I, Borlat F, Wells TN, Kosco-Vilbois MH. Glycosaminoglycan Binding and Oligomerization Are Essential for the in Vivo Activity of Certain Chemokines. Proceedings of the National Academy of Sciences. 2003;100(4):1885-90.
76) Vales S, Kryukova J, Chandra S, Smagurauskaite G, Payne M, Clark CJ, Hafner K, Mburu P, Denisov S, et al. Discovery and Pharmacophoric Characterization of Chemokine Network Inhibitors Using Phage-Display, Saturation Mutagenesis and Computational Modelling. Nature Communications. 2023;14(1):5763.
77) Ridley AJ, Ou Y, Karlsson R, Pun N, Birchenough HL, Mulholland IZ, Birch ML, MacDonald AS, Jowitt TA, et al. Chemokines Form Complex Signals During Inflammation and Disease That Can Be Decoded by Extracellular Matrix Proteoglycans. Science Signaling. 2023;16(810):eadf2537.
78) Wolkenhauer O, Muir A. The Complexity of Cell-Biological Systems. Philosophy of Complex Systems: Elsevier; 2011. p. 355-85.
79) D'Agostino G, García-Cuesta EM, Gomariz RP, Rodríguez-Frade JM, Mellado M. The Multilayered Complexity of the Chemokine Receptor System. Biochemical and Biophysical Research Communications. 2020;528(2):347-58.
80) Elsen M, Visser-Wijnveen GJ, Van Der Rijst RM, Van Driel JH. How to Strengthen the Connection between Research and Teaching in Undergraduate University Education. Higher Education Quarterly. 2009;63(1):64-85.
81) Saha S, Sano FK, Sharma S, Ganguly M, Mishra S, Dalal A, Akasaka H, Kobayashi TA, Zaidi N, et al. Molecular Basis of Promiscuous Chemokine Binding and Structural Mimicry at the C-X-C Chemokine Receptor, Cxcr2. Mol Cell. 2025;85(5):976-88.e9.
82) Zernecke A, Weber C. Chemokines in the Vascular Inflammatory Response of Atherosclerosis. Cardiovasc Res. 2010;86(2):192-201.
83) Elemam NM, Hannawi S, Maghazachi AA. Role of Chemokines and Chemokine Receptors in Rheumatoid Arthritis. Immunotargets Ther. 2020;9:43-56.
84) Bhattacharya S, Kawamura A. Using Evasins to Target the Chemokine Network in Inflammation. Adv Protein Chem Struct Biol. 2020;119:1-38.
85) Von Hundelshausen P, Agten SM, Eckardt V, Blanchet X, Schmitt MM, Ippel H, Neideck C, Bidzhekov K, Leberzammer J, et al. Chemokine Interactome Mapping Enables Tailored

Intervention in Acute and Chronic Inflammation. Science translational medicine. 2017;9(384):eaah6650.
86) Budean D, Almeida-Hernández Y, Pandey J, Pérez JM, Sánchez García E, Haglund E. Exploring Chemokine Homodimer Stability: Structural Insights into Cxc and Cc Interfaces. Biophysica. 2024;4(4):561-72.
87) Mayo KH, Roongta V, Ilyina E, Milius R, Barker S, Quinlan C, La Rosa G, Daly TJ. Nmr Solution Structure of the 32-Kda Platelet Factor 4 Elr-Motif N-Terminal Chimera: A Symmetric Tetramer. Biochemistry. 1995;34(36):11399-409.
88) Gouwy M, Struyf S, Proost P, Van Damme J. Synergy in Cytokine and Chemokine Networks Amplifies the Inflammatory Response. Cytokine & growth factor reviews. 2005;16(6):561-80.
89) Gouwy M, Schiraldi M, Struyf S, Van Damme J, Uguccioni M. Possible Mechanisms Involved in Chemokine Synergy Fine Tuning the Inflammatory Response. Immunology letters. 2012;145(1-2):10-14.
90) Proudfoot AE, Uguccioni M. Modulation of Chemokine Responses: Synergy and Cooperativity. Frontiers in Immunology. 2016;7:183.
91) Mortier A, Van Damme J, Proost P. Regulation of Chemokine Activity by Posttranslational Modification. Pharmacology & therapeutics. 2008;120(2):197-217.
92) Barker CE, Thompson S, O'boyle G, Lortat-Jacob H, Sheerin NS, Ali S, Kirby JA. Ccl2 Nitration Is a Negative Regulator of Chemokine-Mediated Inflammation. Scientific Reports. 2017;7(1):44384.
93) Loos T, Mortier A, Gouwy M, Ronsse I, Put W, Lenaerts J-P, Van Damme J, Proost P. Citrullination of Cxcl10 and Cxcl11 by Peptidylarginine Deiminase: A Naturally Occurring Posttranslational Modification of Chemokines and New Dimension of Immunoregulation. Blood, The Journal of the American Society of Hematology. 2008;112(7):2648-56.
94) Denney H, Clench MR, Woodroofe MN. Cleavage of Chemokines Ccl2 and Cxcl10 by Matrix Metalloproteinases-2 and-9: Implications for Chemotaxis. Biochemical and Biophysical Research Communications. 2009;382(2):341-47.
95) Starr AE, Dufour A, Maier J, Overall CM. Biochemical Analysis of Matrix Metalloproteinase Activation of Chemokines Ccl15 and Ccl23 and Increased Glycosaminoglycan Binding of Ccl16. Journal of Biological Chemistry. 2012;287(8):5848-60.
96) Kitano H. Biological Robustness. Nature Reviews Genetics. 2004;5(11):826-37.
97) Aleotti A, Goulty M, Lewis C, Giorgini F, Feuda R. The Origin, Evolution, and Molecular Diversity of the Chemokine System. Life Science Alliance. 2024;7(3).
98) Stephens JC, Reich DE, Goldstein DB, Shin HD, Smith MW, Carrington M, Winkler C, Huttley GA, Allikmets R, et al. Dating the Origin of the Ccr5-Δ32 Aids-Resistance Allele by the Coalescence of Haplotypes. The American Journal of Human Genetics. 1998;62(6):1507-15.
99) McDermott DH, Fong AM, Yang Q, Sechler JM, Cupples LA, Merrell MN, Wilson PW, D'Agostino RB, O'Donnell CJ, et al. Chemokine Receptor Mutant Cx3cr1-M280 Has Impaired Adhesive Function and Correlates with Protection from Cardiovascular Disease in Humans. The Journal of clinical investigation. 2003;111(8):1241-50.
100) Whitacre JM. Biological Robustness: Paradigms, Mechanisms, and Systems Principles. Front Genet. 2012;3:67.
101) Mantovani A, editor Redundancy and Robustness Versus Division of Labour and Specialization in Innate Immunity. Seminars in immunology; 2018: Elsevier.
102) Mantovani A. The Chemokine System: Redundancy for Robust Outputs. Immunology today. 1999;20(6):254-57.
103) Solari R, Pease JE, Begg M. "Chemokine Receptors as Therapeutic Targets: Why Aren't There More Drugs?". European Journal of Pharmacology. 2015;746:363-67.

104) Dyer DP. Understanding the Mechanisms That Facilitate Specificity, Not Redundancy, of Chemokine-Mediated Leukocyte Recruitment. Immunology. 2020;160(4):336-44.
105) Dyer DP, Medina-Ruiz L, Bartolini R, Schuette F, Hughes CE, Pallas K, Vidler F, Macleod MK, Kelly CJ, et al. Chemokine Receptor Redundancy and Specificity Are Context Dependent. Immunity. 2019;50(2):378-89. e5.
106) Metzemaekers M, Vanheule V, Janssens R, Struyf S, Proost P. Overview of the Mechanisms That May Contribute to the Non-Redundant Activities of Interferon-Inducible Cxc Chemokine Receptor 3 Ligands. Frontiers in Immunology. 2018;8:1970.
107) Graham JB, Swarts JL, Mooney M, Choonoo G, Jeng S, Miller DR, Ferris MT, McWeeney S, Lund JM. Extensive Homeostatic T Cell Phenotypic Variation within the Collaborative Cross. Cell reports. 2017;21(8):2313-25.
108) Graham JB, Swarts JL, Leist SR, Schäfer A, Bell TA, Hock P, Farrington J, Shaw GD, Ferris MT, et al. Unique Immune Profiles in Collaborative Cross Mice Linked to Survival and Viral Clearance Upon Infection. Iscience. 2024;27(3).
109) Hsieh M-F, Lai S-L, Chen J-P, Sung J-M, Lin Y-L, Wu-Hsieh BA, Gerard C, Luster A, Liao F. Both Cxcr3 and Cxcl10/Ifn-Inducible Protein 10 Are Required for Resistance to Primary Infection by Dengue Virus. The Journal of Immunology. 2006;177(3):1855-63.
110) Tao L, Reese TA. Making Mouse Models That Reflect Human Immune Responses. Trends in immunology. 2017;38(3):181-93.
111) Beura LK, Hamilton SE, Bi K, Schenkel JM, Odumade OA, Casey KA, Thompson EA, Fraser KA, Rosato PC, et al. Normalizing the Environment Recapitulates Adult Human Immune Traits in Laboratory Mice. Nature. 2016;532(7600):512-16.
112) Gerba CP. Environmentally Transmitted Pathogens. Environmental Microbiology: Elsevier; 2009. p. 445-84.
113) Sanz J, Randolph HE, Barreiro LB. Genetic and Evolutionary Determinants of Human Population Variation in Immune Responses. Current Opinion in Genetics & Development. 2018;53:28-35.
114) Smith P, Fallon RE, Mangan NE, Walsh CM, Saraiva M, Sayers JR, McKenzie AN, Alcami A, Fallon PG. Schistosoma Mansoni Secretes a Chemokine Binding Protein with Antiinflammatory Activity. J Exp Med. 2005;202(10):1319-25.
115) Parry CM, Simas JP, Smith VP, Stewart CA, Minson AC, Efstathiou S, Alcami A. A Broad Spectrum Secreted Chemokine Binding Protein Encoded by a Herpesvirus. J Exp Med. 2000;191(3):573-8.
116) Bhusal RP, Eaton JRO, Chowdhury ST, Power CA, Proudfoot AEI, Stone MJ, Bhattacharya S. Evasins: Tick Salivary Proteins That Inhibit Mammalian Chemokines. Trends in Biochemical Sciences. 2020;45(2):108-22.
117) Ferrannini E, Mari A. Beta Cell Function and Its Relation to Insulin Action in Humans: A Critical Appraisal. Diabetologia. 2004;47(5):943-56.
118) Roche EF, Menon A, Gill D, Hoey H. Clinical Presentation of Type 1 Diabetes. Pediatric diabetes. 2005;6(2):75-78.
119) Barnett R. Type 1 Diabetes. The Lancet. 2018;391(10117):195.
120) Mameli C, Mazzantini S, Nasr MB, Fiorina P, Scaramuzza AE, Zuccotti GV. Explaining the Increased Mortality in Type 1 Diabetes. World journal of diabetes. 2015;6(7):889.
121) Garg R, Hurwitz S, Turchin A, Trivedi A. Hypoglycemia, with or without Insulin Therapy, Is Associated with Increased Mortality among Hospitalized Patients. Diabetes care. 2013;36(5):1107-10.
122) Skrivarhaug T, Bangstad H-J, Stene L, Sandvik L, Hanssen K, Joner G. Long-Term Mortality in a Nationwide Cohort of Childhood-Onset Type 1 Diabetic Patients in Norway. Diabetologia. 2006;49:298-305.

123) Patterson CC, Dahlquist G, Harjutsalo V, Joner G, Feltbower RG, Svensson J, Schober E, Gyürüs E, Castell C, et al. Early Mortality in Eurodiab Population-Based Cohorts of Type 1 Diabetes Diagnosed in Childhood since 1989. Diabetologia. 2007;50:2439-42.

124) Feltbower RG, Bodansky HJ, Patterson CC, Parslow RC, Stephenson CR, Reynolds C, McKinney PA. Acute Complications and Drug Misuse Are Important Causes of Death for Children and Young Adults with Type 1 Diabetes: Results from the Yorkshire Register of Diabetes in Children and Young Adults. Diabetes care. 2008;31(5):922-26.

125) Wasag DR, Gregory JW, Dayan C, Harvey JN. Excess All-Cause Mortality before Age 30 in Childhood Onset Type 1 Diabetes: Data from the Brecon Group Cohort in Wales. Archives of disease in childhood. 2018;103(1):44-48.

126) Karges B, Rosenbauer J, Holterhus P-M, Beyer P, Seithe H, Vogel C, Boeckmann A, Peters D, Müther S, et al. Hospital Admission for Diabetic Ketoacidosis or Severe Hypoglycemia in 31 330 Young Patients with Type 1 Diabetes. European journal of endocrinology. 2015;173(3):341-50.

127) Olson JC, Edmundowicz D, Becker DJ, Kuller LH, Orchard TJ. Coronary Calcium in Adults with Type 1 Diabetes: A Stronger Correlate of Clinical Coronary Artery Disease in Men Than in Women. Diabetes. 2000;49(9):1571-78.

128) Gubitosi-Klug R, Gao X, Pop-Busui R, de Boer IH, White N, Aiello LP, Miller R, Palmer J, Tamborlane W, et al. Associations of Microvascular Complications with the Risk of Cardiovascular Disease in Type 1 Diabetes. Diabetes care. 2021;44(7):1499-505.

129) Livingstone SJ, Levin D, Looker HC, Lindsay RS, Wild SH, Joss N, Leese G, Leslie P, McCrimmon RJ, et al. Estimated Life Expectancy in a Scottish Cohort with Type 1 Diabetes, 2008-2010. Jama. 2015;313(1):37-44.

130) Huo L, Harding JL, Peeters A, Shaw JE, Magliano DJ. Life Expectancy of Type 1 Diabetic Patients During 1997-2010: A National Australian Registry-Based Cohort Study. Diabetologia. 2016;59(6):1177-85.

131) Patterson CC, Karuranga S, Salpea P, Saeedi P, Dahlquist G, Soltesz G, Ogle GD. Worldwide Estimates of Incidence, Prevalence and Mortality of Type 1 Diabetes in Children and Adolescents: Results from the International Diabetes Federation Diabetes Atlas, 9th Edition. Diabetes Research and Clinical Practice. 2019;157:107842.

132) Ogle GD, James S, Dabelea D, Pihoker C, Svennson J, Maniam J, Klatman EL, Patterson CC. Global Estimates of Incidence of Type 1 Diabetes in Children and Adolescents: Results from the International Diabetes Federation Atlas, 10th Edition. Diabetes Research and Clinical Practice. 2022;183:109083.

133) Maahs DM, West NA, Lawrence JM, Mayer-Davis EJ. Epidemiology of Type 1 Diabetes. Endocrinol Metab Clin North Am. 2010;39(3):481-97.

134) Pociot F, Lernmark Å. Genetic Risk Factors for Type 1 Diabetes. Lancet. 2016;387(10035):2331-39.

135) Patterson CC, Harjutsalo V, Rosenbauer J, Neu A, Cinek O, Skrivarhaug T, Rami-Merhar B, Soltesz G, Svensson J, et al. Trends and Cyclical Variation in the Incidence of Childhood Type 1 Diabetes in 26 European Centres in the 25 year Period 1989-2013: A Multicentre Prospective Registration Study. Diabetologia. 2019;62(3):408-17.

136) Gregory GA, Robinson TIG, Linklater SE, Wang F, Colagiuri S, de Beaufort C, Donaghue KC, Harding JL, Wander PL, et al. Global Incidence, Prevalence, and Mortality of Type 1 Diabetes in 2021 with Projection to 2040: A Modelling Study. The Lancet Diabetes & Endocrinology. 2022;10(10):741-60.

137) Krogvold L, Edwin B, Buanes T, Ludvigsson J, Korsgren O, Hyöty H, Frisk G, Hanssen KF, Dahl-Jørgensen K. Pancreatic Biopsy by Minimal Tail Resection in Live Adult Patients at the Onset of Type 1 Diabetes: Experiences from the Divid Study. Diabetologia. 2014;57(4):841-43.

138) Delovitch TL, Singh B. The Nonobese Diabetic Mouse as a Model of Autoimmune Diabetes: Immune Dysregulation Gets the Nod. Immunity. 1997;7(6):727-38.
139) Driver JP, Serreze DV, Chen Y-G. Mouse Models for the Study of Autoimmune Type 1 Diabetes: A Nod to Similarities and Differences to Human Disease. Seminars in Immunopathology. 2011;33(1):67-87.
140) Wicker LS, Clark J, Fraser HI, Garner VE, Gonzalez-Munoz A, Healy B, Howlett S, Hunter K, Rainbow D, et al. Type 1 Diabetes Genes and Pathways Shared by Humans and Nod Mice. Journal of Autoimmunity. 2005;25:29-33.
141) Solomon M, Sarvetnick N. The Pathogenesis of Diabetes in the Nod Mouse. Advances in immunology. 2004;84:239-64.
142) Trudeau JD, Kelly-Smith C, Verchere CB, Elliott JF, Dutz JP, Finegood DT, Santamaria P, Tan R. Prediction of Spontaneous Autoimmune Diabetes in Nod Mice by Quantification of Autoreactive T Cells in Peripheral Blood. The Journal of clinical investigation. 2003;111(2):217-23.
143) Haskins K, McDuffie M. Acceleration of Diabetes in Young Nod Mice with a Cd4+ Islet-Specific T Cell Clone. Science. 1990;249(4975):1433-6.
144) Chatenoud L, Thervet E, Primo J, Bach J-F. Anti-Cd3 Antibody Induces Long-Term Remission of Overt Autoimmunity in Nonobese Diabetic Mice. Proceedings of the National Academy of Sciences. 1994;91(1):123-27.
145) Herold KC, Gitelman SE, Ehlers MR, Gottlieb PA, Greenbaum CJ, Hagopian W, Boyle KD, Keyes-Elstein L, Aggarwal S, et al. Teplizumab (Anti-Cd3 Mab) Treatment Preserves C-Peptide Responses in Patients with New-Onset Type 1 Diabetes in a Randomized Controlled Trial: Metabolic and Immunologic Features at Baseline Identify a Subgroup of Responders. Diabetes. 2013;62(11):3766-74.
146) Kikutani H, Makino S. The Murine Autoimmune Diabetes Model: Nod and Related Strains. Advances in immunology. 1992;51:285-322.
147) Rivera J, Tessarollo L. Genetic Background and the Dilemma of Translating Mouse Studies to Humans. Immunity. 2008;28(1):1-4.
148) Mestas J, Hughes CC. Of Mice and Not Men: Differences between Mouse and Human Immunology. The Journal of Immunology. 2004;172(5):2731-38.
149) Medina A, Parween S, Ullsten S, Vishnu N, Siu YT, Quach M, Bennet H, Balhuizen A, Åkesson L, et al. Early Deficits in Insulin Secretion, Beta Cell Mass and Islet Blood Perfusion Precede Onset of Autoimmune Type 1 Diabetes in Biobreeding Rats. Diabetologia. 2018;61(4):896-905.
150) Furman BL. Streptozotocin-Induced Diabetic Models in Mice and Rats. Current Protocols in Pharmacology. 2015;70(1):5.47. 1-5.47. 20.
151) Campbell-Thompson M, Wasserfall C, Kaddis J, Albanese-O'Neill A, Staeva T, Nierras C, Moraski J, Rowe P, Gianani R, et al. Network for Pancreatic Organ Donors with Diabetes (Npod): Developing a Tissue Biobank for Type 1 Diabetes. Diabetes/Metabolism Research and Reviews. 2012;28(7):608-17.
152) Bruni A, Gala-Lopez B, Pepper AR, Abualhassan NS, Shapiro AJ. Islet Cell Transplantation for the Treatment of Type 1 Diabetes: Recent Advances and Future Challenges. Diabetes, metabolic syndrome and obesity: targets and therapy. 2014:211-23.
153) Bhonde R, Shukla R, Kanitkar M, Shukla R, Banerjee M, Datar S. Isolated Islets in Diabetes Research. Indian Journal of Medical Research. 2007;125(3):425-40.
154) Eizirik DL, Colli ML, Ortis F. The Role of Inflammation in Insulitis and Beta-Cell Loss in Type 1 Diabetes. Nat Rev Endocrinol. 2009;5(4):219-26.
155) Colli ML, Szymczak F, Eizirik DL. Molecular Footprints of the Immune Assault on Pancreatic Beta Cells in Type 1 Diabetes. Frontiers in endocrinology. 2020;11:568446.

156) Varela-Calvino R, Calviño-Sampedro C, Gómez-Touriño I, Cordero OJ. Apportioning Blame: Autoreactive Cd4+ and Cd8+ T Cells in Type 1 Diabetes. Archivum Immunologiae et Therapiae Experimentalis. 2017;65(4):275-84.
157) Krischer JP, Lynch KF, Schatz DA, Ilonen J, Lernmark Å, Hagopian WA, Rewers MJ, She J-X, Simell OG, et al. The 6 Year Incidence of Diabetes-Associated Autoantibodies in Genetically at-Risk Children: The Teddy Study. Diabetologia. 2015;58:980-87.
158) Ziegler A-G, Bonifacio E, Group B-BS. Age-Related Islet Autoantibody Incidence in Offspring of Patients with Type 1 Diabetes. Diabetologia. 2012;55:1937-43.
159) Evans-Molina C, Sims EK, DiMeglio LA, Ismail HM, Steck AK, Palmer JP, Krischer JP, Geyer S, Xu P, et al. B Cell Dysfunction Exists More Than 5 Years before Type 1 Diabetes Diagnosis. JCI Insight. 2018;3(15).
160) Madsbad S, Faber O, Binder C, McNair P, Christiansen C, Transbøl I. Prevalence of Residual Beta-Cell Function in Insulin-Dependent Diabetics in Relation to Age at Onset and Duration of Diabetes. Diabetes. 1978;27(Supplement_1):262-64.
161) Klinke DJ. Extent of Beta Cell Destruction Is Important but Insufficient to Predict the Onset of Type 1 Diabetes Mellitus. PLOS ONE. 2008;3(1):e1374.
162) Leete P, Willcox A, Krogvold L, Dahl-Jørgensen K, Foulis AK, Richardson SJ, Morgan NG. Differential Insulitic Profiles Determine the Extent of B-Cell Destruction and the Age at Onset of Type 1 Diabetes. Diabetes. 2016;65(5):1362-69.
163) Agner T, Damm P, Binder C. Remission in Iddm: Prospective Study of Basal C-Peptide and Insulin Dose in 268 Consecutive Patients. Diabetes care. 1987;10(2):164-69.
164) Redondo MJ, Morgan NG. Heterogeneity and Endotypes in Type 1 Diabetes Mellitus. Nature Reviews Endocrinology. 2023;19(9):542-54.
165) Jacobsen LM, Felton JL, Nathan BM, Speake C, Krischer J, Herold KC. Type 1 Diabetes Trialnet: Leading the Charge in Disease Prediction, Prevention, and Immunotherapeutic Mechanistic Understanding. Diabetes care. 2025;48(7):1112-24.
166) Bonifacio E, Beyerlein A, Hippich M, Winkler C, Vehik K, Weedon MN, Laimighofer M, Hattersley AT, Krumsiek J, et al. Genetic Scores to Stratify Risk of Developing Multiple Islet Autoantibodies and Type 1 Diabetes: A Prospective Study in Children. PLoS medicine. 2018;15(4):e1002548.
167) Clements GB, Galbraith DN, Taylor KW. Coxsackie B Virus Infection and Onset of Childhood Diabetes. Lancet. 1995;346(8969):221-3.
168) Eizirik DL, Cardozo AK, Cnop M. The Role for Endoplasmic Reticulum Stress in Diabetes Mellitus. Endocr Rev. 2008;29(1):42-61.
169) Ilonen J, Lempainen J, Veijola R. The Heterogeneous Pathogenesis of Type 1 Diabetes Mellitus. Nature Reviews Endocrinology. 2019;15(11):635-50.
170) Noble JA, Valdes AM. Genetics of the Hla Region in the Prediction of Type 1 Diabetes. Current diabetes reports. 2011;11:533-42.
171) Horton R, Wilming L, Rand V, Lovering RC, Bruford EA, Khodiyar VK, Lush MJ, Povey S, Talbot Jr CC, et al. Gene Map of the Extended Human Mhc. Nature Reviews Genetics. 2004;5(12):889-99.
172) Knight SC, Stagg AJ. Antigen-Presenting Cell Types. Current opinion in immunology. 1993;5(3):374-82.
173) Zernich D, Purcell AW, Macdonald WA, Kjer-Nielsen L, Ely LK, Laham N, Crockford T, Mifsud NA, Bharadwaj M, et al. Natural Hla Class I Polymorphism Controls the Pathway of Antigen Presentation and Susceptibility to Viral Evasion. The Journal of experimental medicine. 2004;200(1):13-24.
174) Noble JA, Valdes AM, Cook M, Klitz W, Thomson G, Erlich HA. The Role of Hla Class Ii Genes in Insulin-Dependent Diabetes Mellitus: Molecular Analysis of 180 Caucasian, Multiplex Families. American journal of human genetics. 1996;59(5):1134.

175) Neefjes J, Jongsma ML, Paul P, Bakke O. Towards a Systems Understanding of Mhc Class I and Mhc Class Ii Antigen Presentation. Nature Reviews Immunology. 2011;11(12):823-36.
176) Caillat-Zucman S. Molecular Mechanisms of Hla Association with Autoimmune Diseases. Tissue Antigens. 2009;73(1):1-8.
177) Girdhar K, Huang Q, Chow I-T, Vatanen T, Brady C, Raisingani A, Autissier P, Atkinson MA, Kwok WW, et al. A Gut Microbial Peptide and Molecular Mimicry in the Pathogenesis of Type 1 Diabetes. Proceedings of the National Academy of Sciences. 2022;119(31):e2120028119.
178) Afonso G, Mallone R. Infectious Triggers in Type 1 Diabetes: Is There a Case for Epitope Mimicry? Diabetes, Obesity and Metabolism. 2013;15(s3):82-88.
179) Noble JA, Valdes AM, Varney MD, Carlson JA, Moonsamy P, Fear AL, Lane JA, Lavant E, Rappner R, et al. Hla Class I and Genetic Susceptibility to Type 1 Diabetes: Results from the Type 1 Diabetes Genetics Consortium. Diabetes. 2010;59(11):2972-79.
180) Pugliese A, Zeller M, Fernandez A, Jr., Zalcberg LJ, Bartlett RJ, Ricordi C, Pietropaolo M, Eisenbarth GS, Bennett ST, et al. The Insulin Gene Is Transcribed in the Human Thymus and Transcription Levels Correlated with Allelic Variation at the Ins Vntr-Iddm2 Susceptibility Locus for Type 1 Diabetes. Nat Genet. 1997;15(3):293-7.
181) Vafiadis P, Bennett ST, Todd JA, Nadeau J, Grabs R, Goodyer CG, Wickramasinghe S, Colle E, Polychronakos C. Insulin Expression in Human Thymus Is Modulated by Ins Vntr Alleles at the Iddm2 Locus. Nature genetics. 1997;15(3):289-92.
182) Šabanović K. Genetic Background of Type 1 Diabetes Mellitus: A Review. Bioengineering Studies. 2023;4(2):34-45.
183) Sharp SA, Rich SS, Wood AR, Jones SE, Beaumont RN, Harrison JW, Schneider DA, Locke JM, Tyrrell J, et al. Development and Standardization of an Improved Type 1 Diabetes Genetic Risk Score for Use in Newborn Screening and Incident Diagnosis. Diabetes care. 2019;42(2):200-07.
184) Mameli C, Triolo TM, Chiarelli F, Rewers M, Zuccotti G, Simmons KM. Lessons and Gaps in the Prediction and Prevention of Type 1 Diabetes. Pharmacological Research. 2023;193:106792.
185) Knip M, Veijola R, Virtanen SM, Hyoty H, Vaarala O, Akerblom HK. Environmental Triggers and Determinants of Type 1 Diabetes. Diabetes. 2005;54(suppl_2):S125-S36.
186) Söderström U, Aman J, Hjern A. Being Born in Sweden Increases the Risk for Type 1 Diabetes - a Study of Migration of Children to Sweden as a Natural Experiment. Acta Paediatr. 2012;101(1):73-7.
187) Oilinki T, Otonkoski T, Ilonen J, Knip M, Miettinen P. Prevalence and Characteristics of Diabetes among Somali Children and Adolescents Living in Helsinki, Finland. Pediatric diabetes. 2012;13(2):176-80.
188) Peled A, Gordon B, Twig G, Mendlovic J, Derazne E, Lisnyansky M, Raz I, Afek A. Immigration to Israel During Childhood Is Associated with Diabetes at Adolescence: A Study of 2.7 Million Adolescents. Diabetologia. 2017;60:2226-30.
189) Jacobsen L, Schatz D. Current and Future Efforts toward the Prevention of Type 1 Diabetes. Pediatric diabetes. 2016;17:78-86.
190) Verduci E, Mameli C, Amatruda M, Petitti A, Vizzuso S, El Assadi F, Zuccotti G, Alabduljabbar S, Terranegra A. Early Nutrition and Risk of Type 1 Diabetes: The Role of Gut Microbiota. Frontiers in Nutrition. 2020;7:612377.
191) Hamilton-Williams EE, Lorca GL, Norris JM, Dunne JL. A Triple Threat? The Role of Diet, Nutrition, and the Microbiota in T1d Pathogenesis. Frontiers in Nutrition. 2021;8:600756.
192) Friman G, Fohlman J, Frisk G, Diderholm H, Ewald U, Kobbah M, Tuvemo T. An Incidence Peak of Juvenile Diabetes. Relation to Coxsackie B Virus Immune Response. Acta Paediatr Scand Suppl. 1985;320:14-9.

193) Laitinen OH, Honkanen H, Pakkanen O, Oikarinen S, Hankaniemi MM, Huhtala H, Ruokoranta T, Lecouturier V, André P, et al. Coxsackievirus B1 Is Associated with Induction of B-Cell Autoimmunity That Portends Type 1 Diabetes. Diabetes. 2014;63(2):446-55.
194) Oikarinen S, Tauriainen S, Hober D, Lucas B, Vazeou A, Sioofy-Khojine A, Bozas E, Muir P, Honkanen H, et al. Virus Antibody Survey in Different European Populations Indicates Risk Association between Coxsackievirus B1 and Type 1 Diabetes. Diabetes. 2014;63(2):655-62.
195) Craig ME, Nair S, Stein H, Rawlinson WD. Viruses and Type 1 Diabetes: A New Look at an Old Story. Pediatr Diabetes. 2013;14(3):149-58.
196) Ylipaasto P, Klingel K, Lindberg AM, Otonkoski T, Kandolf R, Hovi T, Roivainen M. Enterovirus Infection in Human Pancreatic Islet Cells, Islet Tropism in Vivo and Receptor Involvement in Cultured Islet Beta Cells. Diabetologia. 2004;47(2):225-39.
197) Dahlquist G. Can We Slow the Rising Incidence of Childhood-Onset Autoimmune Diabetes? The Overload Hypothesis. Diabetologia. 2006;49(1):20-24.
198) Stene LC, Rewers M. Immunology in the Clinic Review Series; Focus on Type 1 Diabetes and Viruses: The Enterovirus Link to Type 1 Diabetes: Critical Review of Human Studies. Clinical and Experimental Immunology. 2012;168(1):12-23.
199) Kawasaki E. Anti-Islet Autoantibodies in Type 1 Diabetes. International journal of molecular sciences. 2023;24(12):10012.
200) Winter WE, Pittman DL, Jialal I. Practical Clinical Applications of Islet Autoantibody Testing in Type 1 Diabetes. The Journal of Applied Laboratory Medicine. 2022;7(1):197-205.
201) Yu L, Zhao Z, Steck AK. T1d Autoantibodies: Room for Improvement? Current Opinion in Endocrinology, Diabetes and Obesity. 2017;24(4).
202) Hämäläinen AM, Savola K, Kulmala PK, Koskela P, Akerblom HK, Knip M. Disease-Associated Autoantibodies During Pregnancy and at Birth in Families Affected by Type 1 Diabetes. Clin Exp Immunol. 2001;126(2):230-5.
203) Harjutsalo V, Reunanen A, Tuomilehto J. Differential Transmission of Type 1 Diabetes from Diabetic Fathers and Mothers to Their Offspring. Diabetes. 2006;55(5):1517-24.
204) Campbell-Thompson ML, Atkinson MA, Butler AE, Chapman NM, Frisk G, Gianani R, Giepmans BN, von Herrath MG, Hyöty H, et al. The Diagnosis of Insulitis in Human Type 1 Diabetes. Diabetologia. 2013;56(11):2541-43.
205) Imagawa A, Hanafusa T, Tamura S, Moriwaki M, Itoh N, Yamamoto K, Iwahashi H, Yamagata K, Waguri M, et al. Pancreatic Biopsy as a Procedure for Detecting in Situ Autoimmune Phenomena in Type 1 Diabetes: Close Correlation between Serological Markers and Histological Evidence of Cellular Autoimmunity. Diabetes. 2001;50(6):1269-73.
206) In't Veld P. Insulitis in Human Type 1 Diabetes: The Quest for an Elusive Lesion. Islets. 2011;3(4):131-38.
207) Pipeleers D, Ling Z. Pancreatic Beta Cells in Insulin-Dependent Diabetes. Diabetes Metabolism Reviews. 1992;8:209-09.
208) Löhr M, Klöppel G. Residual Insulin Positivity and Pancreatic Atrophy in Relation to Duration of Chronic Type 1 (Insulin-Dependent) Diabetes Mellitus and Microangiopathy. Diabetologia. 1987;30:757-62.
209) Keenan HA, Sun JK, Levine J, Doria A, Aiello LP, Eisenbarth G, Bonner-Weir S, King GL. Residual Insulin Production and Pancreatic B-Cell Turnover after 50 Years of Diabetes: Joslin Medalist Study. Diabetes. 2010;59(11):2846-53.
210) Foulis A, Liddle C, Farquharson M, Richmond J, Weir R. The Histopathology of the Pancreas in Type I (Insulin-Dependent) Diabetes Mellitus: A 25-Year Review of Deaths in Patients under 20 Years of Age in the United Kingdom. Diabetologia. 1986;29:267-74.
211) Gepts W, De Mey J. Islet Cell Survival Determined by Morphology an Immunocytochemical Study of the Islets of Langerhans in Juvenile Diabetes Mellitus. Diabetes. 1978;27(Supplement_1):251-61.

212) In't Veld P, Marichal M. Microscopic Anatomy of the Human Islet of Langerhans. Adv Exp Med Biol. 2010;654:1-19.
213) Atkinson MA, Leiter EH. The Nod Mouse Model of Type 1 Diabetes: As Good as It Gets? Nature medicine. 1999;5(6):601-04.
214) Homo-Delarche F, Drexhage HA. Immune Cells, Pancreas Development, Regeneration and Type 1 Diabetes. Trends in immunology. 2004;25(5):222-29.
215) Hultcrantz M, Hühn MH, Wolf M, Olsson A, Jacobson S, Williams BR, Korsgren O, Flodström-Tullberg M. Interferons Induce an Antiviral State in Human Pancreatic Islet Cells. Virology. 2007;367(1):92-101.
216) Dogusan Z, Garcia M, Flamez D, Alexopoulou L, Goldman M, Gysemans C, Mathieu C, Libert C, Eizirik DL, et al. Double-Stranded Rna Induces Pancreatic B-Cell Apoptosis by Activation of the Toll-Like Receptor 3 and Interferon Regulatory Factor 3 Pathways. Diabetes. 2008;57(5):1236-45.
217) Rasschaert J, Ladrière L, Urbain M, Dogusan Z, Katabua B, Sato S, Akira S, Gysemans C, Mathieu C, et al. Toll-Like Receptor 3 and Stat-1 Contribute to Double-Stranded Rna+ Interferon-Γ-Induced Apoptosis in Primary Pancreatic B-Cells. Journal of Biological Chemistry. 2005;280(40):33984-91.
218) Liu D, Cardozo AK, Darville MI, Eizirik DcL. Double-Stranded Rna Cooperates with Interferon-Γ and Il-1β to Induce Both Chemokine Expression and Nuclear Factor-Kb-Dependent Apoptosis in Pancreatic B-Cells: Potential Mechanisms for Viral-Induced Insulitis and B-Cell Death in Type 1 Diabetes Mellitus. Endocrinology. 2002;143(4):1225-34.
219) Liu D, Darville M, Eizirik DcL. Double-Stranded Ribonucleic Acid (Rna) Induces B-Cell Fas Messenger Rna Expression and Increases Cytokine-Induced B-Cell Apoptosis. Endocrinology. 2001;142(6):2593-99.
220) Marhfour I, Lopez XM, Lefkaditis D, Salmon I, Allagnat F, Richardson SJ, Morgan NG, Eizirik DL. Expression of Endoplasmic Reticulum Stress Markers in the Islets of Patients with Type 1 Diabetes. Diabetologia. 2012;55(9):2417-20.
221) Brozzi F, Eizirik DL. Er Stress and the Decline and Fall of Pancreatic Beta Cells in Type 1 Diabetes. Ups J Med Sci. 2016;121(2):133-9.
222) Eizirik DL, Miani M, Cardozo AK. Signalling Danger: Endoplasmic Reticulum Stress and the Unfolded Protein Response in Pancreatic Islet Inflammation. Diabetologia. 2013;56(2):234-41.
223) Scheuner D, Kaufman RJ. The Unfolded Protein Response: A Pathway That Links Insulin Demand with B-Cell Failure and Diabetes. Endocrine Reviews. 2008;29(3):317-33.
224) Li Y, Sun F, Yue T-T, Wang F-X, Yang C-L, Luo J-H, Rong S-J, Xiong F, Zhang S, et al. Revisiting the Antigen-Presenting Function of B Cells in T1d Pathogenesis. Frontiers in Immunology. 2021;12:690783.
225) Eizirik DL, Kutlu B, Rasschaert J, Darville M, Cardozo AK. Use of Microarray Analysis to Unveil Transcription Factor and Gene Networks Contributing to B Cell Dysfunction and Apoptosis. Annals of the New York Academy of Sciences. 2003;1005(1):55-74.
226) Eizirik DL, Colli ML. Revisiting the Role of Inflammation in the Loss of Pancreatic B-Cells in T1dm. Nature Reviews Endocrinology. 2020;16(11):611-12.
227) Pugliese A. Autoreactive T Cells in Type 1 Diabetes. The Journal of clinical investigation. 2017;127(8):2881-91.
228) Todd JA, Walker NM, Cooper JD, Smyth DJ, Downes K, Plagnol V, Bailey R, Nejentsev S, Field SF, et al. Robust Associations of Four New Chromosome Regions from Genome-Wide Analyses of Type 1 Diabetes. Nature genetics. 2007;39(7):857-64.
229) Strandell E, Eizirik DL, Sandler S. Reversal of Beta-Cell Suppression in Vitro in Pancreatic Islets Isolated from Nonobese Diabetic Mice During the Phase Preceding Insulin-Dependent Diabetes Mellitus. The Journal of clinical investigation. 1990;85(6):1944-50.

230) Brissova M, Haliyur R, Saunders D, Shrestha S, Dai C, Blodgett DM, Bottino R, Campbell-Thompson M, Aramandla R, et al. A Cell Function and Gene Expression Are Compromised in Type 1 Diabetes. Cell Rep. 2018;22(10):2667-76.

231) Krogvold L, Skog O, Sundström G, Edwin B, Buanes T, Hanssen KF, Ludvigsson J, Grabherr M, Korsgren O, et al. Function of Isolated Pancreatic Islets from Patients at Onset of Type 1 Diabetes: Insulin Secretion Can Be Restored after Some Days in a Nondiabetogenic Environment in Vitro: Results from the Divid Study. Diabetes. 2015;64(7):2506-12.

232) Itoh N, Hanafusa T, Miyazaki A, Miyagawa J-i, Yamagata K, Yamamoto K, Waguri M, Imagawa A, Tamura S, et al. Mononuclear Cell Infiltration and Its Relation to the Expression of Major Histocompatibility Complex Antigens and Adhesion Molecules in Pancreas Biopsy Specimens from Newly Diagnosed Insulin-Dependent Diabetes Mellitus Patients. The Journal of clinical investigation. 1993;92(5):2313-22.

233) Bruggeman Y, Martens P-J, Sassi G, Viaene M, Wasserfall CH, Mathieu C, Gysemans C. Footprint of Pancreas Infiltrating and Circulating Immune Cells Throughout Type 1 Diabetes Development. Frontiers in endocrinology. 2023;Volume 14 - 2023.

234) Sun F, Yang CL, Wang FX, Rong SJ, Luo JH, Lu WY, Yue TT, Wang CY, Liu SW. Pancreatic Draining Lymph Nodes (Plns) Serve as a Pathogenic Hub Contributing to the Development of Type 1 Diabetes. Cell Biosci. 2023;13(1):156.

235) Fabien N, Bergerot I, Maguer-Satta V, Orgiazzi J, Thivolet C. Pancreatic Lymph Nodes Are Early Targets of T Cells During Adoptive Transfer of Diabetes in Nod Mice. Journal of Autoimmunity. 1995;8(3):323-34.

236) Höglund P, Mintern J, Waltzinger C, Heath W, Benoist C, Mathis D. Initiation of Autoimmune Diabetes by Developmentally Regulated Presentation of Islet Cell Antigens in the Pancreatic Lymph Nodes. The Journal of experimental medicine. 1999;189(2):331-39.

237) Bender C, Rodriguez-Calvo T, Amirian N, Coppieters KT, von Herrath MG. The Healthy Exocrine Pancreas Contains Preproinsulin-Specific Cd8 T Cells That Attack Islets in Type 1 Diabetes. Science advances. 2020;6(42):eabc5586.

238) Bender C, Christen S, Scholich K, Bayer M, Pfeilschifter JM, Hintermann E, Christen U. Islet-Expressed Cxcl10 Promotes Autoimmune Destruction of Islet Isografts in Mice with Type 1 Diabetes. Diabetes. 2017;66(1):113-26.

239) Richardson SJ, Rodriguez-Calvo T, Gerling IC, Mathews CE, Kaddis JS, Russell MA, Zeissler M, Leete P, Krogvold L, et al. Islet Cell Hyperexpression of Hla Class I Antigens: A Defining Feature in Type 1 Diabetes. Diabetologia. 2016;59(11):2448-58.

240) Trivedi P, Graham KL, Krishnamurthy B, Fynch S, Slattery RM, Kay TW, Thomas HE. Perforin Facilitates Beta Cell Killing and Regulates Autoreactive Cd8+ T-Cell Responses to Antigen in Mouse Models of Type 1 Diabetes. Immunology and cell biology. 2016;94(4):334-41.

241) Herrera PL, Harlan DM, Vassalli P. A Mouse Cd8 T Cell-Mediated Acute Autoimmune Diabetes Independent of the Perforin and Fas Cytotoxic Pathways: Possible Role of Membrane Tnf. Proceedings of the National Academy of Sciences. 2000;97(1):279-84.

242) Thomas HE, Kay T. How Beta Cells Die in Type 1 Diabetes. Molecular Pathology of Type 1 Diabetes Mellitus. 2001;4:143.

243) Zhang Y, O'Brien B, Trudeau J, Tan R, Santamaria P, Dutz JP. In Situ B Cell Death Promotes Priming of Diabetogenic Cd8 T Lymphocytes. The Journal of Immunology. 2002;168(3):1466-72.

244) Espinosa-Carrasco G, Le Saout C, Fontanaud P, Stratmann T, Mollard P, Schaeffer M, Hernandez J. Cd4+ T Helper Cells Play a Key Role in Maintaining Diabetogenic Cd8+ T Cell Function in the Pancreas. Frontiers in Immunology. 2018;Volume 8 - 2017.

245) Walker LS, von Herrath M. Cd4 T Cell Differentiation in Type 1 Diabetes. Clinical & Experimental Immunology. 2016;183(1):16-29.

246) Haskins K, Cooke A. Cd4 T Cells and Their Antigens in the Pathogenesis of Autoimmune Diabetes. Current opinion in immunology. 2011;23(6):739-45.

247) Coppieters KT, Dotta F, Amirian N, Campbell PD, Kay TW, Atkinson MA, Roep BO, von Herrath MG. Demonstration of Islet-Autoreactive Cd8 T Cells in Insulitic Lesions from Recent Onset and Long-Term Type 1 Diabetes Patients. Journal of Experimental Medicine. 2012;209(1):51-60.

248) Pathiraja V, Kuehlich JP, Campbell PD, Krishnamurthy B, Loudovaris T, Coates PT, Brodnicki TC, O'Connell PJ, Kedzierska K, et al. Proinsulin-Specific, Hla-Dq8, and Hla-Dq8-Transdimer-Restricted Cd4+ T Cells Infiltrate Islets in Type 1 Diabetes. Diabetes. 2015;64(1):172-82.

249) Vendrame F, Pileggi A, Laughlin E, Allende G, Martin-Pagola A, Molano RD, Diamantopoulos S, Standifer N, Geubtner K, et al. Recurrence of Type 1 Diabetes after Simultaneous Pancreas-Kidney Transplantation, Despite Immunosuppression, Is Associated with Autoantibodies and Pathogenic Autoreactive Cd4 T-Cells. Diabetes. 2010;59(4):947-57.

250) Christianson SW, Shultz LD, Leiter EH. Adoptive Transfer of Diabetes into Immunodeficient Nod-Scid/Scid Mice: Relative Contributions of Cd4+ and Cd8+ T-Cells from Diabetic Versus Prediabetic Nod.Non-Thy-1a Donors. Diabetes. 1993;42(1):44-55.

251) Wong FS, Visintin I, Wen L, Flavell RA, Janeway CA, Jr. Cd8 T Cell Clones from Young Nonobese Diabetic (Nod) Islets Can Transfer Rapid Onset of Diabetes in Nod Mice in the Absence of Cd4 Cells. Journal of Experimental Medicine. 1996;183(1):67-76.

252) Edouard P, Hiserodt JC, Plamondon C, Poussier P. Cd8+ T-Cells Are Required for Adoptive Transfer of the Bb Rat Diabetic Syndrome. Diabetes. 1993;42(3):390-97.

253) Serreze DV, Leiter EH, Christianson GJ, Greiner D, Roopenian DC. Major Histocompatibility Complex Class I-Deficient Nod-B2m Null Mice Are Diabetes and Insulitis Resistant. Diabetes. 1994;43(3):505-09.

254) Wicker LS, Leiter EH, Todd JA, Renjilian RJ, Peterson E, Fischer PA, Podolin PL, Zijlstra M, Jaenisch R, et al. B2-Microglobulin–Deficient Nod Mice Do Not Develop Insulitis or Diabetes. Diabetes. 1994;43(3):500-04.

255) Lind M, Svensson A-M, Kosiborod M, Gudbjörnsdottir S, Pivodic A, Wedel H, Dahlqvist S, Clements M, Rosengren A. Glycemic Control and Excess Mortality in Type 1 Diabetes. New England Journal of Medicine. 2014;371(21):1972-82.

256) Warshauer JT, Bluestone JA, Anderson MS. New Frontiers in the Treatment of Type 1 Diabetes. Cell metabolism. 2020;31(1):46-61.

257) Palmer JP, Fleming GA, Greenbaum CJ, Herold KC, Jansa LD, Kolb H, Lachin JM, Polonsky KS, Pozzilli P, et al. C-Peptide Is the Appropriate Outcome Measure for Type 1 Diabetes Clinical Trials to Preserve B-Cell Function: Report of an Ada Workshop, 21–22 October 2001. Diabetes. 2004;53(1):250-64.

258) Diabetes Prevention Program Research G. Hba1c as a Predictor of Diabetes and as an Outcome in the Diabetes Prevention Program: A Randomized Clinical Trial. Diabetes care. 2014;38(1):51-58.

259) Ehlers MR. Strategies for Clinical Trials in Type 1 Diabetes. Journal of Autoimmunity. 2016;71:88-96.

260) Control D, Group CTR. The Effect of Intensive Treatment of Diabetes on the Development and Progression of Long-Term Complications in Insulin-Dependent Diabetes Mellitus. New England Journal of Medicine. 1993;329(14):977-86.

261) Weinstock RS, Xing D, Maahs DM, Michels A, Rickels MR, Peters AL, Bergenstal RM, Harris B, DuBose SN, et al. Severe Hypoglycemia and Diabetic Ketoacidosis in Adults with Type 1 Diabetes: Results from the T1d Exchange Clinic Registry. The Journal of Clinical Endocrinology & Metabolism. 2013;98(8):3411-19.

262) Kłak A, Mańczak M, Owoc J, Olszewski R. Impact of Continuous Glucose Monitoring on Improving Emotional Well-Being among Adult People with Type 1 Diabetes Mellitus: A Systematic Review and Meta-Analysis. Polish Arch Intern Med. 2021;131(9):808-18.

263) Perkins BA, Sherr JL, Mathieu C. Type 1 Diabetes Glycemic Management: Insulin Therapy, Glucose Monitoring, and Automation. Science. 2021;373(6554):522-27.
264) Aschner P, Horton E, Leiter L, Munro N, Skyler J, Management* GPfED. Practical Steps to Improving the Management of Type 1 Diabetes: Recommendations from the Global Partnership for Effective Diabetes Management. International journal of clinical practice. 2010;64(3):305-15.
265) Mathieu C, Gillard P, Benhalima K. Insulin Analogues in Type 1 Diabetes Mellitus: Getting Better All the Time. Nature Reviews Endocrinology. 2017;13(7):385-99.
266) Ryan EA, Bigam D, Shapiro AJ. Current Indications for Pancreas or Islet Transplant. Diabetes, Obesity and Metabolism. 2006;8(1):1-7.
267) Shapiro AJ. State of the Art of Clinical Islet Transplantation and Novel Protocols of Immunosuppression. Current diabetes reports. 2011;11(5):345-54.
268) Berney T, Ferrari-Lacraz S, Bühler L, Oberholzer J, Marangon N, Philippe J, Villard J, Morel P. Long-Term Insulin-Independence after Allogeneic Islet Transplantation for Type 1 Diabetes: Over the 10-Year Mark. American journal of transplantation. 2009;9(2):419-23.
269) Foster ED, Bridges ND, Feurer ID, Eggerman TL, Hunsicker LG, Alejandro R. Improved Health-Related Quality of Life in a Phase 3 Islet Transplantation Trial in Type 1 Diabetes Complicated by Severe Hypoglycemia. Diabetes care. 2018;41(5):1001-08.
270) Ricordi C, Strom TB. Clinical Islet Transplantation: Advances and Immunological Challenges. Nature Reviews Immunology. 2004;4(4):259-68.
271) Komatsu H, Kandeel F, Mullen Y. Impact of Oxygen on Pancreatic Islet Survival. Pancreas. 2018;47(5):533-43.
272) Kale A, Rogers NM. No Time to Die—How Islets Meet Their Demise in Transplantation. Cells. 2023;12(5):796.
273) Shapiro AJ. Islet Transplantation in Type 1 Diabetes: Ongoing Challenges, Refined Procedures, and Long-Term Outcome. The review of diabetic studies: RDS. 2013;9(4):385.
274) Bellin MD, Barton FB, Heitman A, Harmon J, Kandaswamy R, Balamurugan A, Sutherland D, Alejandro R, Hering B. Potent Induction Immunotherapy Promotes Long-Term Insulin Independence after Islet Transplantation in Type 1 Diabetes. American journal of transplantation. 2012;12(6):1576-83.
275) Monti P, Scirpoli M, Maffi P, Ghidoli N, De Taddeo F, Bertuzzi F, Piemonti L, Falcone M, Secchi A, et al. Islet Transplantation in Patients with Autoimmune Diabetes Induces Homeostatic Cytokines That Expand Autoreactive Memory T Cells. The Journal of clinical investigation. 2008;118(5):1806-14.
276) Fujikura J, Anazawa T, Toyoda T, Ito R, Kimura Y, Yabe D. Toward a Cure for Diabetes: Ipsc and Esc-Derived Islet Cell Transplantation Trials. Journal of Diabetes Investigation. 2025;16(3):384-88.
277) Rickels MR, Witkowski P, Reichman TW, De Koning EJ, Markmann JF, Odorico JS, Wijkstrom M, Kean LS, Mathieu C, et al. 140-Or: Durable Glycemic Control and Elimination of Exogenous Insulin Use with Vx-880 in Patients with Type 1 Diabetes (T1d)—Vx-880-101 (Forward). Diabetes. 2025;74(Supplement_1):140-OR.
278) Keymeulen B, De Groot K, Jacobs-Tulleneers-Thevissen D, Thompson DM, Bellin MD, Kroon EJ, Daniels M, Wang R, Jaiman M, et al. Encapsulated Stem Cell–Derived B Cells Exert Glucose Control in Patients with Type 1 Diabetes. Nature Biotechnology. 2024;42(10):1507-14.
279) Millman JR, Xie C, Van Dervort A, Gürtler M, Pagliuca FW, Melton DA. Generation of Stem Cell-Derived B-Cells from Patients with Type 1 Diabetes. Nature Communications. 2016;7(1):11463.
280) van Megen KM, van't Wout E-JT, Forman SJ, Roep BO. A Future for Autologous Hematopoietic Stem Cell Transplantation in Type 1 Diabetes. Frontiers in Immunology. 2018;9:690.

281) Vegas AJ, Veiseh O, Gürtler M, Millman JR, Pagliuca FW, Bader AR, Doloff JC, Li J, Chen M, et al. Long-Term Glycemic Control Using Polymer-Encapsulated Human Stem Cell–Derived Beta Cells in Immune-Competent Mice. Nature medicine. 2016;22(3):306-11.

282) Viviano KR. Glucocorticoids, Cyclosporine, Azathioprine, Chlorambucil, and Mycophenolate in Dogs and Cats: Clinical Uses, Pharmacology, and Side Effects. Veterinary Clinics: Small Animal Practice. 2022;52(3):797-817.

283) Feutren G, Assan R, Karsenty G, Du Rostu H, Sirmai J, Papoz L, Vialettes B, Vexiau P, Rodier M, et al. Cyclosporin Increases the Rate and Length of Remissions in Insulin-Dependent Diabetes of Recent Onset: Results of a Multicentre Double-Blind Trial. The Lancet. 1986;328(8499):119-24.

284) Couri CE, Oliveira MC, Stracieri AB, Moraes DA, Pieroni F, Barros GM, Madeira MIA, Malmegrim KC, Foss-Freitas MC, et al. C-Peptide Levels and Insulin Independence Following Autologous Nonmyeloablative Hematopoietic Stem Cell Transplantation in Newly Diagnosed Type 1 Diabetes Mellitus. Jama. 2009;301(15):1573-79.

285) Malmegrim KC, De Azevedo JT, Arruda LC, Abreu JR, Couri CE, De Oliveira GL, Palma PV, Scortegagna GT, Stracieri AB, et al. Immunological Balance Is Associated with Clinical Outcome after Autologous Hematopoietic Stem Cell Transplantation in Type 1 Diabetes. Frontiers in Immunology. 2017;8:167.

286) Bretzel R, Brandhorst D, Brandhorst H, Eckhard M, Ernst W, Friemann S, Rau W, Weimar B, Rauber K, et al. Improved Survival of Intraportal Pancreatic Islet Cell Allografts in Patients with Type-1 Diabetes Mellitus by Refined Peritransplant Management. Journal of Molecular Medicine. 1999;77:140-43.

287) Shapiro AJ, Ricordi C, Hering BJ, Auchincloss H, Lindblad R, Robertson RP, Secchi A, Brendel MD, Berney T, et al. International Trial of the Edmonton Protocol for Islet Transplantation. New England Journal of Medicine. 2006;355(13):1318-30.

288) Hyder A, Laue C, Schrezenmeir J. Effect of the Immunosuppressive Regime of Edmonton Protocol on the Long-Term in Vitro Insulin Secretion from Islets of Two Different Species and Age Categories. Toxicology in vitro. 2005;19(4):541-46.

289) Carvalho T. Fda Approves First Drug to Delay Type 1 Diabetes. Nat Med. 2023;29(2):280.

290) Urbano F, Farella I, Brunetti G, Faienza MF. Pediatric Type 1 Diabetes: Mechanisms and Impact of Technologies on Comorbidities and Life Expectancy. International journal of molecular sciences. 2023;24(15):11980.

291) Chavan T, Waghamare S, Kokare S, Madake A. Advanced Treatment of Type 1 Diabetes with Teplizumab: Mechanism and Clinical Efficacy. Asian Journal of Medical Principles and Clinical Practice. 2025;8(1):1-11.

292) Perdigoto AL, Preston-Hurlburt P, Clark P, Long SA, Linsley PS, Harris KM, Gitelman SE, Greenbaum CJ, Gottlieb PA, et al. Treatment of Type 1 Diabetes with Teplizumab: Clinical and Immunological Follow-up after 7 years from Diagnosis. Diabetologia. 2019;62(4):655-64.

293) Hagopian W, Ferry Jr RJ, Sherry N, Carlin D, Bonvini E, Johnson S, Stein KE, Koenig S, Daifotis AG, et al. Teplizumab Preserves C-Peptide in Recent-Onset Type 1 Diabetes: Two-Year Results from the Randomized, Placebo-Controlled Protégé Trial. Diabetes. 2013;62(11):3901-08.

294) Ramos EL, Dayan CM, Chatenoud L, Sumnik Z, Simmons KM, Szypowska A, Gitelman SE, Knecht LA, Niemoeller E, et al. Teplizumab and B-Cell Function in Newly Diagnosed Type 1 Diabetes. New England Journal of Medicine. 2023;389(23):2151-61.

295) Herold KC, Bundy BN, Long SA, Bluestone JA, DiMeglio LA, Dufort MJ, Gitelman SE, Gottlieb PA, Krischer JP, et al. An Anti-Cd3 Antibody, Teplizumab, in Relatives at Risk for Type 1 Diabetes. New England Journal of Medicine. 2019;381(7):603-13.

296) Herold K, Gitelman S, Willi S, Gottlieb P, Waldron-Lynch F, Devine L, Sherr J, Rosenthal S, Adi S, et al. Teplizumab Treatment May Improve C-Peptide Responses in Participants with

Type 1 Diabetes after the New-Onset Period: A Randomised Controlled Trial. Diabetologia. 2013;56:391-400.

297) Haller MJ, Schatz DA, Skyler JS, Krischer JP, Bundy BN, Miller JL, Atkinson MA, Becker DJ, Baidal D, et al. Low-Dose Anti-Thymocyte Globulin (Atg) Preserves B-Cell Function and Improves Hba1c in New-Onset Type 1 Diabetes. Diabetes care. 2018;41(9):1917-25.

298) Jacobsen LM, Bundy BN, Greco MN, Schatz DA, Atkinson MA, Brusko TM, Mathews CE, Herold KC, Gitelman SE, et al. Comparing Beta Cell Preservation across Clinical Trials in Recent-Onset Type 1 Diabetes. Diabetes Technology & Therapeutics. 2020;22(12):948-53.

299) Rachid O, Osman A, Abdi R, Haik Y. Ctla4-Ig (Abatacept): A Promising Investigational Drug for Use in Type 1 Diabetes. Expert Opinion on Investigational Drugs. 2020;29(3):221-36.

300) Russell WE, Bundy BN, Anderson MS, Cooney LA, Gitelman SE, Goland RS, Gottlieb PA, Greenbaum CJ, Haller MJ, et al. Abatacept for Delay of Type 1 Diabetes Progression in Stage 1 Relatives at Risk: A Randomized, Double-Masked, Controlled Trial. Diabetes care. 2023;46(5):1005-13.

301) Pescovitz MD, Greenbaum CJ, Bundy B, Becker DJ, Gitelman SE, Goland R, Gottlieb PA, Marks JB, Moran A, et al. B-Lymphocyte Depletion with Rituximab and B-Cell Function: Two-Year Results. Diabetes care. 2014;37(2):453-59.

302) Serr I, Drost F, Schubert B, Daniel C. Antigen-Specific Treg Therapy in Type 1 Diabetes–Challenges and Opportunities. Frontiers in Immunology. 2021;12:712870.

303) Bluestone JA, Buckner JH, Fitch M, Gitelman SE, Gupta S, Hellerstein MK, Herold KC, Lares A, Lee MR, et al. Type 1 Diabetes Immunotherapy Using Polyclonal Regulatory T Cells. Science translational medicine. 2015;7(315):315ra189-315ra189.

304) Dong S, Hiam-Galvez KJ, Mowery CT, Herold KC, Gitelman SE, Esensten JH, Liu W, Lares AP, Leinbach AS, et al. The Effect of Low-Dose Il-2 and Treg Adoptive Cell Therapy in Patients with Type 1 Diabetes. JCI Insight. 2021;6(18).

305) Zieliński M, Żalińska M, Iwaszkiewicz-Grześ D, Gliwiński M, Hennig M, Jaźwińska-Curyłło A, Kamińska H, Sakowska J, Wołoszyn-Durkiewicz A, et al. Combined Therapy with Cd4+ Cd25highcd127− T Regulatory Cells and Anti-Cd20 Antibody in Recent-Onset Type 1 Diabetes Is Superior to Monotherapy: Randomized Phase I/Ii Trial. Diabetes, Obesity and Metabolism. 2022;24(8):1534-43.

306) Bazile C, Abdel Malik MM, Ackeifi C, Anderson RL, Beck RW, Donath MY, Dutta S, Hedrick JA, Karpen SR, et al. Tnf-A Inhibitors for Type 1 Diabetes: Exploring the Path to a Pivotal Clinical Trial. Frontiers in Immunology. 2024;15:1470677.

307) Rigby MR, Hayes B, Li Y, Vercruysse F, Hedrick JA, Quattrin T. Two-Year Follow-up from the T1ger Study: Continued Off-Therapy Metabolic Improvements in Children and Young Adults with New-Onset T1d Treated with Golimumab and Characterization of Responders. Diabetes care. 2022;46(3):561-69.

308) Waibel M, Wentworth JM, So M, Couper JJ, Cameron FJ, MacIsaac RJ, Atlas G, Gorelik A, Litwak S, et al. Baricitinib and B-Cell Function in Patients with New-Onset Type 1 Diabetes. New England Journal of Medicine. 2023;389(23):2140-50.

309) Gitelman SE, Bundy BN, Ferrannini E, Lim N, Blanchfield JL, DiMeglio LA, Felner EI, Gaglia JL, Gottlieb PA, et al. Imatinib Therapy for Patients with Recent-Onset Type 1 Diabetes: A Multicentre, Randomised, Double-Blind, Placebo-Controlled, Phase 2 Trial. The Lancet Diabetes & Endocrinology. 2021;9(8):502-14.

310) Hu C-y, Rodriguez-Pinto D, Du W, Ahuja A, Henegariu O, Wong FS, Shlomchik MJ, Wen L. Treatment with Cd20-Specific Antibody Prevents and Reverses Autoimmune Diabetes in Mice. The Journal of clinical investigation. 2007;117(12):3857-67.

311) Zhao Y, Lin B, Darflinger R, Zhang Y, Holterman MJ, Skidgel RA. Human Cord Blood Stem Cell-Modulated Regulatory T Lymphocytes Reverse the Autoimmune-Caused Type 1 Diabetes in Nonobese Diabetic (Nod) Mice. PLOS ONE. 2009;4(1):e4226.

312) Christen U, Kimmel R. Chemokines as Drivers of the Autoimmune Destruction in Type 1 Diabetes: Opportunity for Therapeutic Intervention in Consideration of an Optimal Treatment Schedule. Frontiers in endocrinology. 2020;11:591083.

313) Hanifi-Moghaddam P, Kappler S, Seissler J, Müller-Scholze S, Martin S, Roep BO, Strassburger K, Kolb H, Schloot NC. Altered Chemokine Levels in Individuals at Risk of Type 1 Diabetes Mellitus. Diabet Med. 2006;23(2):156-63.

314) Nicoletti F, Conget I, Di Mauro M, Di Marco R, Mazzarino M, Bendtzen K, Messina A, Gomis R. Serum Concentrations of the Interferon-Γ-Inducible Chemokine Ip-10/Cxcl10 Are Augmented in Both Newly Diagnosed Type I Diabetes Mellitus Patients and Subjects at Risk of Developing the Disease. Diabetologia. 2002;45:1107-10.

315) Shimada A, Morimoto J, Kodama K, Suzuki R, Oikawa Y, Funae O, Kasuga A, Saruta T, Narumi S. Elevated Serum Ip-10 Levels Observed in Type 1 Diabetes. Diabetes care. 2001;24(3):510-15.

316) Pfleger C, Kaas A, Hansen L, Alizadeh B, Hougaard P, Holl R, Kolb H, Roep BO, Mortensen HB, et al. Relation of Circulating Concentrations of Chemokine Receptor Ccr5 Ligands to C-Peptide, Proinsulin and Hba1c and Disease Progression in Type 1 Diabetes. Clinical immunology. 2008;128(1):57-65.

317) Carrero JA, Calderon B, Towfic F, Artyomov MN, Unanue ER. Defining the Transcriptional and Cellular Landscape of Type 1 Diabetes in the Nod Mouse. PLOS ONE. 2013;8(3):e59701.

318) Christen U, McGavern DB, Luster AD, von Herrath MG, Oldstone MBA. Among Cxcr3 Chemokines, Ifn-Γ-Inducible Protein of 10 Kda (Cxc Chemokine Ligand (Cxcl) 10) but Not Monokine Induced by Ifn-Γ (Cxcl9) Imprints a Pattern for the Subsequent Development of Autoimmune Disease 1. The Journal of Immunology. 2003;171(12):6838-45.

319) Frigerio S, Junt T, Lu B, Gerard C, Zumsteg U, Holländer GA, Piali L. Beta Cells Are Responsible for Cxcr3-Mediated T-Cell Infiltration in Insulitis. Nat Med. 2002;8(12):1414-20.

320) Antonelli A, Fallahi P, Ferrari S, Pupilli C, d'Annunzio G, Lorini R, Vanelli M, Ferrannini E. Serum Th1 (Cxcl10) and Th2 (Ccl2) Chemokine Levels in Children with Newly Diagnosed Type 1 Diabetes: A Longitudinal Study. Diabetic medicine. 2008;25(11):1349-53.

321) Roep BO, Kleijwegt FS, van Halteren AG, Bonato V, Boggi U, Vendrame F, Marchetti P, Dotta F. Islet Inflammation and Cxcl10 in Recent-Onset Type 1 Diabetes. Clin Exp Immunol. 2010;159(3):338-43.

322) Uno S, Imagawa A, Saisho K, Okita K, Iwahashi H, Hanafusa T, Shimomura I. Expression of Chemokines, Cxc Chemokine Ligand 10 (Cxcl10) and Cxcr3 in the Inflamed Islets of Patients with Recent-Onset Autoimmune Type 1 Diabetes. Endocr J. 2010;57(11):991-6.

323) Sarkar SA, Lee CE, Victorino F, Nguyen TT, Walters JA, Burrack A, Eberlein J, Hildemann SK, Homann D. Expression and Regulation of Chemokines in Murine and Human Type 1 Diabetes. Diabetes. 2012;61(2):436-46.

324) Sarkar S, Kutlu B, Velmurugan K, Kizaka-Kondoh S, Lee C, Wong R, Valentine A, Davidson H, Hutton J, et al. Cytokine-Mediated Induction of Anti-Apoptotic Genes That Are Linked to Nuclear Factor Kappa-B (Nf-Kb) Signalling in Human Islets and in a Mouse Beta Cell Line. Diabetologia. 2009;52:1092-101.

325) Zhang R, Jin Y, Chang C, Xu L, Bian Y, Shen Y, Sun Y, Sun S, Schrodi SJ, et al. Rna-Seq and Network Analysis Reveal Unique Chemokine Activity Signatures in the Synovial Tissue of Patients with Rheumatoid Arthritis. Frontiers in Medicine. 2022;Volume 9 - 2022.

326) Chen MC, Proost P, Gysemans C, Mathieu C, Eizirik DL. Monocyte Chemoattractant Protein-1 Is Expressed in Pancreatic Islets from Prediabetic Nod Mice and in Interleukin-1 Beta-Exposed Human and Rat Islet Cells. Diabetologia. 2001;44(3):325-32.

327) Bradley LM, Asensio VC, Schioetz LK, Harbertson J, Krahl T, Patstone G, Woolf N, Campbell IL, Sarvetnick N. Islet-Specific Th1, but Not Th2, Cells Secrete Multiple Chemokines and Promote Rapid Induction of Autoimmune Diabetes. J Immunol. 1999;162(5):2511-20.

328) Van Belle T, Taylor P, Von Herrath M. Mouse Models for Type 1 Diabetes. Drug Discovery Today: Disease Models. 2009;6(2):41-45.

329) Yoshimatsu G, Kunnathodi F, Saravanan PB, Shahbazov R, Chang C, Darden CM, Zurawski S, Boyuk G, Kanak MA, et al. Pancreatic B-Cell–Derived Ip-10/Cxcl10 Isletokine Mediates Early Loss of Graft Function in Islet Cell Transplantation. Diabetes. 2017;66(11):2857-67.

330) Martin AP, Alexander-Brett JM, Canasto-Chibuque C, Garin A, Bromberg JS, Fremont DH, Lira SA. The Chemokine Binding Protein M3 Prevents Diabetes Induced by Multiple Low Doses of Streptozotocin1. The Journal of Immunology. 2007;178(7):4623-31.

331) Martin AP, Grisotto MG, Canasto-Chibuque C, Kunkel SL, Bromberg JS, Furtado GC, Lira SA. Islet Expression of M3 Uncovers a Key Role for Chemokines in the Development and Recruitment of Diabetogenic Cells in Nod Mice. Diabetes. 2008;57(2):387-94.

332) Nibbs RJ, Wylie SM, Pragnell IB, Graham GJ. Cloning and Characterization of a Novel Murine B Chemokine Receptor, D6: Comparison to Three Other Related Macrophage Inflammatory Protein-1α Receptors, Ccr-1, Ccr-3, and Ccr-5. Journal of Biological Chemistry. 1997;272(19):12495-504.

333) Lin G-J, Huang S-H, Chen Y-W, Hueng D-Y, Chia W-T, Chien M-W, Yen B, Sytwu H-K. Transgenic Expression of Murine Chemokine Decoy Receptor D6 by Islets Reveals the Role of Inflammatory Cc Chemokines in the Development of Autoimmune Diabetes in Nod Mice. Diabetologia. 2011;54(7):1777-87.

334) Ablamunits V, Henegariu O, Hansen JB, Opare-Addo L, Preston-Hurlburt P, Santamaria P, Mandrup-Poulsen T, Herold KC. Synergistic Reversal of Type 1 Diabetes in Nod Mice with Anti-Cd3 and Interleukin-1 Blockade: Evidence of Improved Immune Regulation. Diabetes. 2012;61(1):145-54.

335) Hu C, Ding H, Zhang X, Wong FS, Wen L. Combination Treatment with Anti-Cd20 and Oral Anti-Cd3 Prevents and Reverses Autoimmune Diabetes. Diabetes. 2013;62(8):2849-58.

336) Lasch S, Müller P, Bayer M, Pfeilschifter JM, Luster AD, Hintermann E, Christen U. Anti-Cd3/Anti-Cxcl10 Antibody Combination Therapy Induces a Persistent Remission of Type 1 Diabetes in Two Mouse Models. Diabetes. 2015;64(12):4198-211.

337) Du Y, Deng W, Wang Z, Ning M, Zhang W, Zhou Y, Lo EH, Xing C. Differential Subnetwork of Chemokines/Cytokines in Human, Mouse, and Rat Brain Cells after Oxygen-Glucose Deprivation. J Cereb Blood Flow Metab. 2017;37(4):1425-34.

338) Planas R, Carrillo J, Sanchez A, de Villa MC, Nuñez F, Verdaguer J, James RF, Pujol-Borrell R, Vives-Pi M. Gene Expression Profiles for the Human Pancreas and Purified Islets in Type 1 Diabetes: New Findings at Clinical Onset and in Long-Standing Diabetes. Clin Exp Immunol. 2010;159(1):23-44.

339) Stroo I, Stokman G, Teske GJ, Raven A, Butter LM, Florquin S, Leemans JC. Chemokine Expression in Renal Ischemia/Reperfusion Injury Is Most Profound During the Reparative Phase. International Immunology. 2010;22(6):433-42.

340) Citro A, Valle A, Cantarelli E, Mercalli A, Pellegrini S, Liberati D, Daffonchio L, Kastsiuchenka O, Ruffini PA, et al. Cxcr1/2 Inhibition Blocks and Reverses Type 1 Diabetes in Mice. Diabetes. 2015;64(4):1329-40.

341) Piemonti L, Keymeulen B, Gillard P, Linn T, Bosi E, Rose L, Pozzilli P, Giorgino F, Cossu E, et al. Ladarixin, an Inhibitor of the Interleukin-8 Receptors Cxcr1 and Cxcr2, in New-Onset Type 1 Diabetes: A Multicentre, Randomized, Double-Blind, Placebo-Controlled Trial. Diabetes, Obesity and Metabolism. 2022;24(9):1840-49.

342) Citro A, Cantarelli E, Maffi P, Nano R, Melzi R, Mercalli A, Dugnani E, Sordi V, Magistretti P, et al. Cxcr1/2 Inhibition Enhances Pancreatic Islet Survival after Transplantation. The Journal of clinical investigation. 2012;122(10):3647-51.

343) Citro A, Cantarelli E, Pellegrini S, Dugnani E, Piemonti L. Anti-Inflammatory Strategies in Intrahepatic Islet Transplantation: A Comparative Study in Preclinical Models. Transplantation. 2018;102(2):240-48.
344) Maffi P, Lundgren T, Tufveson G, Rafael E, Shaw JA, Liew A, Saudek F, Witkowski P, Golab K, et al. Targeting Cxcr1/2 Does Not Improve Insulin Secretion after Pancreatic Islet Transplantation: A Phase 3, Double-Blind, Randomized, Placebo-Controlled Trial in Type 1 Diabetes. Diabetes care. 2020;43(4):710-18.
345) Proudfoot AEI. Chemokine Receptors: Multifaceted Therapeutic Targets. Nature Reviews Immunology. 2002;2(2):106-15.
346) Lieberman-Blum SS, Fung HB, Bandres JC. Maraviroc: A Ccr5-Receptor Antagonist for the Treatment of Hiv-1 Infection. Clinical Therapeutics. 2008;30(7):1228-50.
347) Dorr P, Westby M, Dobbs S, Griffin P, Irvine B, Macartney M, Mori J, Rickett G, Smith-Burchnell C, et al. Maraviroc (Uk-427,857), a Potent, Orally Bioavailable, and Selective Small-Molecule Inhibitor of Chemokine Receptor Ccr5 with Broad-Spectrum Anti-Human Immunodeficiency Virus Type 1 Activity. Antimicrob Agents Chemother. 2005;49(11):4721-32.
348) De Clercq E. Mozobil® (Plerixafor, Amd3100), 10 Years after Its Approval by the Us Food and Drug Administration. Antiviral Chemistry and Chemotherapy. 2019;27:2040206619829382.
349) Kim YH, Bagot M, Pinter-Brown L, Rook AH, Porcu P, Horwitz SM, Whittaker S, Tokura Y, Vermeer M, et al. Mogamulizumab Versus Vorinostat in Previously Treated Cutaneous T-Cell Lymphoma (Mavoric): An International, Open-Label, Randomised, Controlled Phase 3 Trial. The Lancet Oncology. 2018;19(9):1192-204.
350) Szekanecz Z, Koch AE. Successes and Failures of Chemokine-Pathway Targeting in Rheumatoid Arthritis. Nat Rev Rheumatol. 2016;12(1):5-13.
351) Valeta-Magara A, Gadi A, Volta V, Walters B, Arju R, Giashuddin S, Zhong H, Schneider RJ. Inflammatory Breast Cancer Promotes Development of M2 Tumor-Associated Macrophages and Cancer Mesenchymal Cells through a Complex Chemokine Network. Cancer Research. 2019;79(13):3360-71.
352) Brandes M, Klauschen F, Kuchen S, Germain RN. A Systems Analysis Identifies a Feedforward Inflammatory Circuit Leading to Lethal Influenza Infection. Cell. 2013;154(1):197-212.
353) Schall TJ, Proudfoot AEI. Overcoming Hurdles in Developing Successful Drugs Targeting Chemokine Receptors. Nature Reviews Immunology. 2011;11(5):355-63.
354) Qin L, Kufareva I, Holden LG, Wang C, Zheng Y, Zhao C, Fenalti G, Wu H, Han GW, et al. Crystal Structure of the Chemokine Receptor Cxcr4 in Complex with a Viral Chemokine. Science. 2015;347(6226):1117-22.
355) Zipp F, Hartung H, Hillert J, Schimrigk S, Trebst C, Stangel M, Infante-Duarte C, Jakobs P, Wolf C, et al. Blockade of Chemokine Signaling in Patients with Multiple Sclerosis. Neurology. 2006;67(10):1880-83.
356) Liang M, Mallari C, Rosser M, Ng HP, May K, Monahan S, Bauman JG, Islam I, Ghannam A, et al. Identification and Characterization of a Potent, Selective, and Orally Active Antagonist of the Cc Chemokine Receptor-1. Journal of Biological Chemistry. 2000;275(25):19000-08.
357) Anders H-J, Vielhauer V, Frink M, Linde Y, Cohen CD, Blattner SM, Kretzler M, Strutz F, Mack M, et al. A Chemokine Receptor Ccr-1 Antagonist Reduces Renal Fibrosis after Unilateral Ureter Ligation. The Journal of clinical investigation. 2002;109(2):251-59.
358) Xiu Y, Wong CP, Bouaziz J-D, Hamaguchi Y, Wang Y, Pop SM, Tisch RM, Tedder TF. B Lymphocyte Depletion by Cd20 Monoclonal Antibody Prevents Diabetes in Nonobese Diabetic Mice Despite Isotype-Specific Differences in Fcγr Effector Functions. The Journal of Immunology. 2008;180(5):2863-75.

359) Chatenoud L, Primo J, Bach J-F. Cd3 Antibody-Induced Dominant Self Tolerance in Overtly Diabetic Nod Mice. Journal of immunology (Baltimore, Md: 1950). 1997;158(6):2947-54.
360) Herold KC, Hagopian W, Auger JA, Poumian-Ruiz E, Taylor L, Donaldson D, Gitelman SE, Harlan DM, Xu D, et al. Anti-Cd3 Monoclonal Antibody in New-Onset Type 1 Diabetes Mellitus. New England Journal of Medicine. 2002;346(22):1692-98.
361) Herold KC, Gitelman SE, Masharani U, Hagopian W, Bisikirska B, Donaldson D, Rother K, Diamond B, Harlan DM, et al. A Single Course of Anti-Cd3 Monoclonal Antibody Hokt3γ1 (Ala-Ala) Results in Improvement in C-Peptide Responses and Clinical Parameters for at Least 2 Years after Onset of Type 1 Diabetes. Diabetes. 2005;54(6):1763-69.
362) Keymeulen B, Vandemeulebroucke E, Ziegler AG, Mathieu C, Kaufman L, Hale G, Gorus F, Goldman M, Walter M, et al. Insulin Needs after Cd3-Antibody Therapy in New-Onset Type 1 Diabetes. New England Journal of Medicine. 2005;352(25):2598-608.
363) Boyles JS, Beidler CB, Strifler BA, Girard DS, Druzina Z, Durbin JD, Swearingen ML, Lee LN, Kikly K, et al. Discovery and Characterization of a Neutralizing Pan-Elr+Cxc Chemokine Monoclonal Antibody. MAbs. 2020;12(1):1831880.
364) Nagata N, Chen G, Xu L, Ando H. An Update on the Chemokine System in the Development of Nafld. Medicina. 2022;58(6):761.
365) Camba-Gomez M, Arosa L, Gualillo O, Conde-Aranda J. Chemokines and Chemokine Receptors in Inflammatory Bowel Disease: Recent Findings and Future Perspectives. Drug Discovery Today. 2022;27(4):1167-75.
366) Rot FRD-MA. A. Ccr7 and Its Ligands: Balancing Immunity and Tolerance. Nat Rev Immunol. 2008;8:362-71.
367) Aliberti J, Valenzuela JG, Carruthers VB, Hieny S, Andersen J, Charest H, e Sousa CR, Fairlamb A, Ribeiro JM, et al. Molecular Mimicry of a Ccr5 Binding-Domain in the Microbial Activation of Dendritic Cells. Nature Immunology. 2003;4(5):485-90.
368) Waxman L, Smith DE, Arcuri KE, Vlasuk GP. Tick Anticoagulant Peptide (Tap) Is a Novel Inhibitor of Blood Coagulation Factor Xa. Science. 1990;248(4955):593-96.
369) Francischetti IM, Valenzuela JG, Andersen JF, Mather TN, Ribeiro JM. Ixolaris, a Novel Recombinant Tissue Factor Pathway Inhibitor (Tfpi) from the Salivary Gland of the Tick, Ixodes Scapularis: Identification of Factor X and Factor Xa as Scaffolds for the Inhibition of Factor Viia/Tissue Factor Complex. Blood. 2002;99(10):3602-12.
370) Xian T, Cao M, Chen K, Zhao W, Liu Y, Yao W, Guang H, Yang Y, Su M, et al. Identification of a Novel Protein Hq023 of the Hard Tick Haemaphysalis Qinghaiensis and Preliminary Evaluation of Its Analgesic Effect in Mice Model. Parasitology International. 2024;103:102933.
371) Fredslund F, Laursen NS, Roversi P, Jenner L, Oliveira CLP, Pedersen JS, Nunn MA, Lea SM, Discipio R, et al. Structure of and Influence of a Tick Complement Inhibitor on Human Complement Component 5. Nature Immunology. 2008;9(7):753-60.
372) Paveglio SA, Allard J, Mayette J, Whittaker LA, Juncadella I, Anguita J, Poynter ME. The Tick Salivary Protein, Salp15, Inhibits the Development of Experimental Asthma. J Immunol. 2007;178(11):7064-71.
373) Francischetti IM, Sa-Nunes A, Mans BJ, Santos IM, Ribeiro JM. The Role of Saliva in Tick Feeding. Front Biosci (Landmark Ed). 2009;14(6):2051-88.
374) Bhattacharya S, Nuttall PA. Phylogenetic Analysis Indicates That Evasin-Like Proteins of Ixodid Ticks Fall into Three Distinct Classes. Front Cell Infect Microbiol. 2021;11:769542.
375) Déruaz M, Frauenschuh A, Alessandri AL, Dias JoM, Coelho FM, Russo RC, Ferreira BR, Graham GJ, Shaw JP, et al. Ticks Produce Highly Selective Chemokine Binding Proteins with Antiinflammatory Activity. Journal of Experimental Medicine. 2008;205(9):2019-31.
376) Denisov SS, Dijkgraaf I. Immunomodulatory Proteins in Tick Saliva from a Structural Perspective. Frontiers in Cellular and Infection Microbiology. 2021;Volume 11 - 2021.

377) Denisov SS, Ramírez-Escudero M, Heinzmann AC, Ippel JH, Dawson PE, Koenen RR, Hackeng TM, Janssen BJ, Dijkgraaf I. Structural Characterization of Anti-Ccl5 Activity of the Tick Salivary Protein Evasin-4. Journal of Biological Chemistry. 2020;295(42):14367-78.

378) Dias JM, Losberger C, Déruaz M, Power CA, Proudfoot AE, Shaw JP. Structural Basis of Chemokine Sequestration by a Tick Chemokine Binding Protein: The Crystal Structure of the Complex between Evasin-1 and Ccl3. PLOS ONE. 2009;4(12):e8514.

379) Lee AW, Deruaz M, Lynch C, Davies G, Singh K, Alenazi Y, Eaton JRO, Kawamura A, Shaw J, et al. A Knottin Scaffold Directs the Cxc-Chemokine-Binding Specificity of Tick Evasins. J Biol Chem. 2019;294(29):11199-212.

380) Denisov SS, Ippel JH, Heinzmann ACA, Koenen RR, Ortega-Gomez A, Soehnlein O, Hackeng TM, Dijkgraaf I. Tick Saliva Protein Evasin-3 Modulates Chemotaxis by Disrupting Cxcl8 Interactions with Glycosaminoglycans and Cxcr2. J Biol Chem. 2019;294(33):12370-79.

381) Bonvin P, Power CA, Proudfoot AE. Evasins: Therapeutic Potential of a New Family of Chemokine-Binding Proteins from Ticks. Frontiers in Immunology. 2016;7:208.

382) James LC, Roversi P, Tawfik DS. Antibody Multispecificity Mediated by Conformational Diversity. Science. 2003;299(5611):1362-67.

383) Aharoni A, Gaidukov L, Khersonsky O, Gould SM, Roodveldt C, Tawfik DS. The'evolvability'of Promiscuous Protein Functions. Nature genetics. 2005;37(1):73-76.

384) Sethi DK, Agarwal A, Manivel V, Rao KV, Salunke DM. Differential Epitope Positioning within the Germline Antibody Paratope Enhances Promiscuity in the Primary Immune Response. Immunity. 2006;24(4):429-38.

385) Hajnická V, Kocáková P, Sláviková M, Slovák M, Gasperík J, Fuchsberger N, Nuttall PA. Anti-Interleukin-8 Activity of Tick Salivary Gland Extracts. Parasite Immunol. 2001;23(9):483-9.

386) Hajnická V, Vancová I, Kocáková P, Slovák M, Gasperík J, Sláviková M, Hails RS, Labuda M, Nuttall PA. Manipulation of Host Cytokine Network by Ticks: A Potential Gateway for Pathogen Transmission. Parasitology. 2005;130(Pt 3):333-42.

387) Frauenschuh A, Power CA, Déruaz M, Ferreira BR, Silva JS, Teixeira MM, Dias JM, Martin T, Wells TNC, et al. Molecular Cloning and Characterization of a Highly Selective Chemokine-Binding Protein from the Tick Rhipicephalus Sanguineus. J Biol Chem. 2007;282(37):27250-58.

388) Dias JM, Losberger C, Déruaz M, Power CA, Proudfoot AEI, Shaw JP. Structural Basis of Chemokine Sequestration by a Tick Chemokine Binding Protein: The Crystal Structure of the Complex between Evasin-1 and Ccl3. PLOS ONE. 2010;4(12):e8514.

389) Singh K, Davies G, Alenazi Y, Eaton JRO, Kawamura A, Bhattacharya S. Yeast Surface Display Identifies a Family of Evasins from Ticks with Novel Polyvalent Cc Chemokine-Binding Activities. Scientific Reports. 2017;7(1):4267.

390) Hayward J, Sanchez J, Perry A, Huang C, Valle MR, Canals M, Payne RJ, Stone MJ. Ticks from Diverse Genera Encode Chemokine-Inhibitory Evasin Proteins. Journal of Biological Chemistry. 2017;292(38):15670-80.

391) Eaton JRO, Alenazi Y, Singh K, Davies G, Geis-Asteggiante L, Kessler B, Robinson CV, Kawamura A, Bhattacharya S. The N-Terminal Domain of a Tick Evasin Is Critical for Chemokine Binding and Neutralization and Confers Specific Binding Activity to Other Evasins. J Biol Chem. 2018;293(16):6134-46.

392) Aryal P, Devkota SR, Jeevarajah D, Law R, Payne RJ, Bhusal RP, Stone MJ. Swapping N-Terminal Regions among Tick Evasins Reveals Cooperative Interactions Influencing Chemokine Binding and Selectivity. Journal of Biological Chemistry. 2022;298(10).

393) Alenazi Y, Singh K, Davies G, Eaton JRO, Elders P, Kawamura A, Bhattacharya S. Genetically Engineered Two-Warhead Evasins Provide a Method to Achieve Precision Targeting of Disease-Relevant Chemokine Subsets. Scientific Reports. 2018;8(1):6333.

394) Castor MG, Rezende B, Resende CB, Alessandri AL, Fagundes CT, Sousa LP, Arantes RM, Souza DG, Silva TA, et al. The Ccl3/Macrophage Inflammatory Protein-1alpha-Binding Protein Evasin-1 Protects from Graft-Versus-Host Disease but Does Not Modify Graft-Versus-Leukemia in Mice. J Immunol. 2010;184(5):2646-54.

395) Russo RC, Alessandri AL, Garcia CC, Cordeiro BF, Pinho V, Cassali GD, Proudfoot AEI, Teixeira MM. Therapeutic Effects of Evasin-1, a Chemokine Binding Protein, in Bleomycin-Induced Pulmonary Fibrosis. American Journal of Respiratory Cell and Molecular Biology. 2011;45(1):72-80.

396) Montecucco F, Lenglet S, Braunersreuther V, Pelli G, Pellieux C, Montessuit C, Lerch R, Deruaz M, Proudfoot AE, et al. Single Administration of the Cxc Chemokine-Binding Protein Evasin-3 During Ischemia Prevents Myocardial Reperfusion Injury in Mice. Arteriosclerosis, Thrombosis, and Vascular Biology. 2010;30(7):1371-77.

397) Montecucco F, Mach F, Lenglet S, Vonlaufen A, Gomes Quinderé AL, Pelli G, Burger F, Galan K, Dallegri F, et al. Treatment with Evasin-3 Abrogates Neutrophil-Mediated Inflammation in Mouse Acute Pancreatitis. European journal of clinical investigation. 2014;44(10):940-50.

398) Braunersreuther V, Montecucco F, Pelli G, Galan K, Proudfoot AE, Belin A, Vuilleumier N, Burger F, Lenglet S, et al. Treatment with the Cc Chemokine-Binding Protein Evasin-4 Improves Post-Infarction Myocardial Injury and Survival in Mice. Thrombosis and haemostasis. 2013;110(10):807-25.

399) Vieira AT, Fagundes CT, Alessandri AL, Castor MG, Guabiraba R, Borges VO, Silveira KD, Vieira EL, Gonçalves JL, et al. Treatment with a Novel Chemokine-Binding Protein or Eosinophil Lineage-Ablation Protects Mice from Experimental Colitis. Am J Pathol. 2009;175(6):2382-91.

400) Koh CY, Kini RM. From Snake Venom Toxins to Therapeutics--Cardiovascular Examples. Toxicon. 2012;59(4):497-506.

401) Fox JW, Serrano SM. Approaching the Golden Age of Natural Product Pharmaceuticals from Venom Libraries: An Overview of Toxins and Toxin-Derivatives Currently Involved in Therapeutic or Diagnostic Applications. Curr Pharm Des. 2007;13(28):2927-34.

402) Lee BS, Huang JS, Jayathilaka LP, Lee J, Gupta S. Antibody Production with Synthetic Peptides. Methods Mol Biol. 2016;1474:25-47.

403) Darlot B, Eaton JR, Geis-Asteggiante L, Yakala GK, Karuppanan K, Davies G, Robinson CV, Kawamura A, Bhattacharya S. Engineered Anti-Inflammatory Peptides Inspired by Mapping an Evasin–Chemokine Interaction. Journal of Biological Chemistry. 2020;295(32):10926-39.

404) Jaroszewicz W, Morcinek-Orłowska J, Pierzynowska K, Gaffke L, Węgrzyn G. Phage Display and Other Peptide Display Technologies. FEMS Microbiology Reviews. 2021;46(2).

405) Prudent R, Annis DA, Dandliker PJ, Ortholand J-Y, Roche D. Exploring New Targets and Chemical Space with Affinity Selection-Mass Spectrometry. Nature Reviews Chemistry. 2021;5(1):62-71.

406) Koch P, Schmitt S, Heynisch A, Gumpinger A, Wüthrich I, Gysin M, Shcherbakov D, Hobbie SN, Panke S, et al. Optimization of the Antimicrobial Peptide Bac7 by Deep Mutational Scanning. BMC biology. 2022;20(1):114.

407) Linciano S, Pluda S, Bacchin A, Angelini A. Molecular Evolution of Peptides by Yeast Surface Display Technology. MedChemComm. 2019;10(9):1569-80.

408) Kryukova J, Vales S, Payne M, Smagurauskaite G, Chandra S, Clark CJ, Davies G, Bhattacharya S. Development of Chemokine Network Inhibitors Using Combinatorial Saturation Mutagenesis. Communications Biology. 2025;8(1):549.

409) Nov Y. When Second Best Is Good Enough: Another Probabilistic Look at Saturation Mutagenesis. Appl Environ Microbiol. 2012;78(1):258-62.
410) Lodowski DT, Palczewski K. Chemokine Receptors and Other G Protein-Coupled Receptors. Curr Opin HIV AIDS. 2009;4(2):88-95.
411) Coperchini F, Chiovato L, Croce L, Magri F, Rotondi M. The Cytokine Storm in Covid-19: An Overview of the Involvement of the Chemokine/Chemokine-Receptor System. Cytokine & growth factor reviews. 2020;53:25-32.
412) Vela M, Aris M, Llorente M, Garcia-Sanz JA, Kremer L. Chemokine Receptor-Specific Antibodies in Cancer Immunotherapy: Achievements and Challenges. Frontiers in Immunology. 2015;6.
413) Russo RC, Alessandri AL, Garcia CC, Cordeiro BF, Pinho V, Cassali GD, Proudfoot AE, Teixeira MM. Therapeutic Effects of Evasin-1, a Chemokine Binding Protein, in Bleomycin-Induced Pulmonary Fibrosis. Am J Respir Cell Mol Biol. 2011;45(1):72-80.
414) Mohs A, Kuttkat N, Reißing J, Zimmermann HW, Sonntag R, Proudfoot A, Youssef SA, de Bruin A, Cubero FJ, et al. Functional Role of Ccl5/Rantes for Hcc Progression During Chronic Liver Disease. Journal of Hepatology. 2017;66(4):743-53.
415) Copin J-C, da Silva RF, Fraga-Silva RA, Capettini L, Quintao S, Lenglet Sb, Pelli G, Galan K, Burger F, et al. Treatment with Evasin-3 Reduces Atherosclerotic Vulnerability for Ischemic Stroke, but Not Brain Injury in Mice. Journal of Cerebral Blood Flow & Metabolism. 2013;33(4):490-98.
416) Muttenthaler M, King GF, Adams DJ, Alewood PF. Trends in Peptide Drug Discovery. Nature Reviews Drug Discovery. 2021;20(4):309-25.
417) Wang L, Wang N, Zhang W, Cheng X, Yan Z, Shao G, Wang X, Wang R, Fu C. Therapeutic Peptides: Current Applications and Future Directions. Signal Transduction and Targeted Therapy. 2022;7(1):48.
418) Erak M, Bellmann-Sickert K, Els-Heindl S, Beck-Sickinger AG. Peptide Chemistry Toolbox - Transforming Natural Peptides into Peptide Therapeutics. Bioorg Med Chem. 2018;26(10):2759-65.
419) Gao Y, Joshi M, Zhao Z, Mitragotri S. Pegylated Therapeutics in the Clinic. Bioengineering & Translational Medicine. 2024;9(1):e10600.
420) Hamzeh-Mivehroud M, Alizadeh AA, Morris MB, Bret Church W, Dastmalchi S. Phage Display as a Technology Delivering on the Promise of Peptide Drug Discovery. Drug Discovery Today. 2013;18(23):1144-57.
421) Nixon AE, Sexton DJ, Ladner RC, editors. Drugs Derived from Phage Display: From Candidate Identification to Clinical Practice. MAbs; 2014: Taylor & Francis.
422) Molineux G, Newland A. Development of Romiplostim for the Treatment of Patients with Chronic Immune Thrombocytopenia: From Bench to Bedside. British Journal of Haematology. 2010;150(1):9-20.
423) Stolz LE, Horn PT. Ecallantide: A Plasma Kallikrein Inhibitor for the Treatment of Acute Attacks of Hereditary Angioedema. DRUGS OF TODAY. 2010;46(8):547-55.
424) Rogers JM, Passioura T, Suga H. Nonproteinogenic Deep Mutational Scanning of Linear and Cyclic Peptides. Proceedings of the National Academy of Sciences. 2018;115(43):10959-64.
425) Luster AD. Chemokines—Chemotactic Cytokines That Mediate Inflammation. New England Journal of Medicine. 1998;338(7):436-45.
426) Guo R-F, Ward PA. Role of C5a in Inflammatory Responses. Annual Review of Immunology. 2005;23(Volume 23, 2005):821-52.
427) Huang F, Nau WM. A Conformational Flexibility Scale for Amino Acids in Peptides. Angewandte Chemie International Edition. 2003;42(20):2269-72.
428) Wipf P, Skoda EM, Mann A. Conformational Restriction and Steric Hindrance in Medicinal Chemistry. The Practice of Medicinal Chemistry: Elsevier; 2015. p. 279-99.

429) Kilgore HR, Raines RT. N→ Π* Interactions Modulate the Properties of Cysteine Residues and Disulfide Bonds in Proteins. Journal of the American Chemical Society. 2018;140(50):17606-11.
430) Wedemeyer MJ, Mueller BK, Bender BJ, Meiler J, Volkman BF. Comparative Modeling and Docking of Chemokine-Receptor Interactions with Rosetta. Biochemical and Biophysical Research Communications. 2020;528(2):389-97.
431) Ding T, Guseinov A-A, Milligan G, Plouffe B, Tikhonova IG. Exploring an Intracellular Allosteric Site of Cc-Chemokine Receptor 4 from 3d Models, Probe Simulations, and Mutagenesis. ACS Pharmacology & Translational Science. 2024;7(8):2516-26.
432) McDonald EF, Jones T, Plate L, Meiler J, Gulsevin A. Benchmarking Alphafold2 on Peptide Structure Prediction. Structure. 2023;31(1):111-19. e2.
433) Abramson J, Adler J, Dunger J, Evans R, Green T, Pritzel A, Ronneberger O, Willmore L, Ballard AJ, et al. Accurate Structure Prediction of Biomolecular Interactions with Alphafold 3. Nature. 2024;630(8016):493-500.
434) Guengerich FP, MacDonald JS. Applying Mechanisms of Chemical Toxicity to Predict Drug Safety. Chemical research in toxicology. 2007;20(3):344-69.
435) Lau JL, Dunn MK. Therapeutic Peptides: Historical Perspectives, Current Development Trends, and Future Directions. Bioorganic & medicinal chemistry. 2018;26(10):2700-07.
436) Baldwin RL. Energetics of Protein Folding. Journal of Molecular Biology. 2007;371(2):283-301.
437) Schirò A, Carlon A, Parigi G, Murshudov G, Calderone V, Ravera E, Luchinat C. On the Complementarity of X-Ray and Nmr Data. Journal of Structural Biology: X. 2020;4:100019.
438) Henninot A, Collins JC, Nuss JM. The Current State of Peptide Drug Discovery: Back to the Future? Journal of medicinal chemistry. 2018;61(4):1382-414.
439) Bumbaca B, Li Z, Shah DK. Pharmacokinetics of Protein and Peptide Conjugates. Drug Metabolism and Pharmacokinetics. 2019;34(1):42-54.
440) Diao L, Meibohm B. Pharmacokinetics and Pharmacokinetic–Pharmacodynamic Correlations of Therapeutic Peptides. Clinical pharmacokinetics. 2013;52:855-68.
441) Rink R, Arkema-Meter A, Baudoin I, Post E, Kuipers A, Nelemans SA, Akanbi MHJ, Moll GN. To Protect Peptide Pharmaceuticals against Peptidases. Journal of Pharmacological and Toxicological Methods. 2010;61(2):210-18.
442) Varland S, Silva RD, Kjosås I, Faustino A, Bogaert A, Billmann M, Boukhatmi H, Kellen B, Costanzo M, et al. N-Terminal Acetylation Shields Proteins from Degradation and Promotes Age-Dependent Motility and Longevity. Nature Communications. 2023;14(1):6774.
443) Tapeinou A, Matsoukas M-T, Simal C, Tselios T. Review Cyclic Peptides on a Merry-Go-Round; Towards Drug Design. Peptide Science. 2015;104(5):453-61.
444) Brayden DJ, Hill T, Fairlie D, Maher S, Mrsny R. Systemic Delivery of Peptides by the Oral Route: Formulation and Medicinal Chemistry Approaches. Advanced drug delivery reviews. 2020;157:2-36.
445) Wiśniewski K, Alagarsamy S, Galyean R, Tariga H, Thompson D, Ly B, Wiśniewska H, Qi S, Croston G, et al. New, Potent, and Selective Peptidic Oxytocin Receptor Agonists. Journal of medicinal chemistry. 2014;57(12):5306-17.
446) Jansson-Löfmark R, Hjorth S, Gabrielsson J. Does in Vitro Potency Predict Clinically Efficacious Concentrations? Clinical Pharmacology & Therapeutics. 2020;108(2):298-305.
447) Yeung YA, Leabman MK, Marvin JS, Qiu J, Adams CW, Lien S, Starovasnik MA, Lowman HB. Engineering Human Igg1 Affinity to Human Neonatal Fc Receptor: Impact of Affinity Improvement on Pharmacokinetics in Primates. The Journal of Immunology. 2009;182(12):7663-71.

448) Li A, Qu G, Sun Z, Reetz MT. Statistical Analysis of the Benefits of Focused Saturation Mutagenesis in Directed Evolution Based on Reduced Amino Acid Alphabets. ACS Catalysis. 2019;9(9):7769-78.
449) Tang L, Hui G, Xuechen Z, Xiong W, Ming Z, and Jiang R. Construction of "Small-Intelligent" Focused Mutagenesis Libraries Using Well-Designed Combinatorial Degenerate Primers. BioTechniques. 2012;52(3):149-58.
450) Mena MA, Daugherty PS. Automated Design of Degenerate Codon Libraries. Protein Engineering Design and Selection. 2005;18(12):559-61.
451) Calinsky R, Levy Y. Aromatic Residues in Proteins: Re-Evaluating the Geometry and Energetics of Π–Π, Cation−Π, and Ch−Π Interactions. The Journal of Physical Chemistry B. 2024;128(36):8687-700.
452) Zhou R-B, Lu H-M, Liu J, Shi J-Y, Zhu J, Lu Q-Q, Yin D-C. A Systematic Analysis of the Structures of Heterologously Expressed Proteins and Those from Their Native Hosts in the Rcsb Pdb Archive. PLOS ONE. 2016;11(8):e0161254.
453) Katsarou A, Gudbjörnsdottir S, Rawshani A, Dabelea D, Bonifacio E, Anderson BJ, Jacobsen LM, Schatz DA, Lernmark Å. Type 1 Diabetes Mellitus. Nature Reviews Disease Primers. 2017;3(1):17016.
454) Pinkse GGM, Tysma OHM, Bergen CAM, Kester MGD, Ossendorp F, van Veelen PA, Keymeulen B, Pipeleers D, Drijfhout JW, et al. Autoreactive Cd8 T Cells Associated with B Cell Destruction in Type 1 Diabetes. Proceedings of the National Academy of Sciences. 2005;102(51):18425-30.
455) Pearson JA, Wong FS, Wen L. The Importance of the Non Obese Diabetic (Nod) Mouse Model in Autoimmune Diabetes. Journal of Autoimmunity. 2016;66:76-88.
456) Cabrera SM, Chen YG, Hagopian WA, Hessner MJ. Blood-Based Signatures in Type 1 Diabetes. Diabetologia. 2016;59(3):414-25.
457) Fasolino M, Schwartz GW, Patil AR, Mongia A, Golson ML, Wang YJ, Morgan A, Liu C, Schug J, et al. Single-Cell Multi-Omics Analysis of Human Pancreatic Islets Reveals Novel Cellular States in Type 1 Diabetes. Nature Metabolism. 2022;4(2):284-99.
458) Colli ML, Ramos-Rodríguez M, Nakayasu ES, Alvelos MI, Lopes M, Hill JLE, Turatsinze J-V, Coomans de Brachène A, Russell MA, et al. An Integrated Multi-Omics Approach Identifies the Landscape of Interferon-A-Mediated Responses of Human Pancreatic Beta Cells. Nature Communications. 2020;11(1):2584.
459) Eizirik DL, Sammeth M, Bouckenooghe T, Bottu G, Sisino G, Igoillo-Esteve M, Ortis F, Santin I, Colli ML, et al. The Human Pancreatic Islet Transcriptome: Expression of Candidate Genes for Type 1 Diabetes and the Impact of Pro-Inflammatory Cytokines. PLOS Genetics. 2012;8(3):e1002552.
460) Coomans de Brachène A, Alvelos MI, Szymczak F, Zimath PL, Castela A, Marmontel de Souza B, Roca Rivada A, Marín-Cañas S, Yi X, et al. Interferons Are Key Cytokines Acting on Pancreatic Islets in Type 1 Diabetes. Diabetologia. 2024;67(5):908-27.
461) Maxwell KG, Millman JR. Applications of Ipsc-Derived Beta Cells from Patients with Diabetes. Cell Reports Medicine. 2021;2(4).
462) Ziegenhain C, Vieth B, Parekh S, Reinius B, Guillaumet-Adkins A, Smets M, Leonhardt H, Heyn H, Hellmann I, et al. Comparative Analysis of Single-Cell Rna Sequencing Methods. Mol Cell. 2017;65(4):631-43.e4.
463) Wu L, Candille SI, Choi Y, Xie D, Jiang L, Li-Pook-Than J, Tang H, Snyder M. Variation and Genetic Control of Protein Abundance in Humans. Nature. 2013;499(7456):79-82.
464) Ponomarenko EA, Krasnov GS, Kiseleva OI, Kryukova PA, Arzumanian VA, Dolgalev GV, Ilgisonis EV, Lisitsa AV, Poverennaya EV. Workability of Mrna Sequencing for Predicting Protein Abundance. Genes (Basel). 2023;14(11).
465) Jones JA, Chang DT, Meyerson H, Colton E, Kwon IK, Matsuda T, Anderson JM. Proteomic Analysis and Quantification of Cytokines and Chemokines from Biomaterial Surface-

Adherent Macrophages and Foreign Body Giant Cells. Journal of Biomedical Materials Research Part A. 2007;83A(3):585-96.

466) Sims EK, Kulkarni A, Hull A, Woerner SE, Cabrera S, Mastrandrea LD, Hammoud B, Sarkar S, Nakayasu ES, et al. Inhibition of Polyamine Biosynthesis Preserves B Cell Function in Type 1 Diabetes. Cell Rep Med. 2023;4(11):101261.

467) Gregor CE, Foeng J, Comerford I, McColl SR. Chemokine-Driven Cd4+ T Cell Homing: New Concepts and Recent Advances. Advances in immunology. 2017;135:119-81.

468) Gonzalez-Duque S, Azoury ME, Colli ML, Afonso G, Turatsinze JV, Nigi L, Lalanne AI, Sebastiani G, Carré A, et al. Conventional and Neo-Antigenic Peptides Presented by B Cells Are Targeted by Circulating Naïve Cd8+ T Cells in Type 1 Diabetic and Healthy Donors. Cell Metab. 2018;28(6):946-60.e6.

469) Ramos-Rodríguez M, Raurell-Vila H, Colli ML, Alvelos MI, Subirana-Granés M, Juan-Mateu J, Norris R, Turatsinze JV, Nakayasu ES, et al. The Impact of Proinflammatory Cytokines on the B-Cell Regulatory Landscape Provides Insights into the Genetics of Type 1 Diabetes. Nat Genet. 2019;51(11):1588-95.

470) Russell MA, Redick SD, Blodgett DM, Richardson SJ, Leete P, Krogvold L, Dahl-Jørgensen K, Bottino R, Brissova M, et al. Hla Class Ii Antigen Processing and Presentation Pathway Components Demonstrated by Transcriptome and Protein Analyses of Islet B-Cells from Donors with Type 1 Diabetes. Diabetes. 2019;68(5):988-1001.

471) Sarkar SA, Wong R, Hackl SI, Moua O, Gill RG, Wiseman A, Davidson HW, Hutton JC. Induction of Indoleamine 2,3-Dioxygenase by Interferon-Γ in Human Islets. Diabetes. 2007;56(1):72-79.

472) Srivastava N, Hu H, Peterson OJ, Vomund AN, Stremska M, Zaman M, Giri S, Li T, Lichti CF, et al. Cxcl16-Dependent Scavenging of Oxidized Lipids by Islet Macrophages Promotes Differentiation of Pathogenic Cd8⁺ T Cells in Diabetic Autoimmunity. Immunity. 2024;57(7):1629-47.e8.

473) Martin AP, Rankin S, Pitchford S, Charo IF, Furtado GC, Lira SA. Increased Expression of Ccl2 in Insulin-Producing Cells of Transgenic Mice Promotes Mobilization of Myeloid Cells from the Bone Marrow, Marked Insulitis, and Diabetes. Diabetes. 2008;57(11):3025-33.

474) De Freitas RF, Schapira M. A Systematic Analysis of Atomic Protein–Ligand Interactions in the Pdb. MedChemComm. 2017;8(10):1970-81.

475) Uno S, Imagawa A, Okita K, Sayama K, Moriwaki M, Iwahashi H, Yamagata K, Tamura S, Matsuzawa Y, et al. Macrophages and Dendritic Cells Infiltrating Islets with or without Beta Cells Produce Tumour Necrosis Factor-A in Patients with Recent-Onset Type 1 Diabetes. Diabetologia. 2007;50:596-601.

476) Xiao X, Gaffar I, Guo P, Wiersch J, Fischbach S, Peirish L, Song Z, El-Gohary Y, Prasadan K, et al. M2 Macrophages Promote Beta-Cell Proliferation by up-Regulation of Smad7. Proceedings of the National Academy of Sciences. 2014;111(13):E1211-E20.

477) Brissova M, Aamodt K, Brahmachary P, Prasad N, Hong J-Y, Dai C, Mellati M, Shostak A, Poffenberger G, et al. Islet Microenvironment, Modulated by Vascular Endothelial Growth Factor-a Signaling, Promotes B Cell Regeneration. Cell metabolism. 2014;19(3):498-511.

478) Brissova M, Shostak A, Shiota M, Wiebe PO, Poffenberger G, Kantz J, Chen Z, Carr C, Jerome WG, et al. Pancreatic Islet Production of Vascular Endothelial Growth Factor-a Is Essential for Islet Vascularization, Revascularization, and Function. Diabetes. 2006;55(11):2974-85.

479) Weitz JR, Makhmutova M, Almaça J, Stertmann J, Aamodt K, Brissova M, Speier S, Rodriguez-Diaz R, Caicedo A. Mouse Pancreatic Islet Macrophages Use Locally Released Atp to Monitor Beta Cell Activity. Diabetologia. 2018;61(1):182-92.

480) Kelm N, Kespohl M, Smagurauskaite G, Vales S, Karuppanan K, Mburu P, Thiele A, Pinkert S, Bukur T, et al. Assessing Customized Multivalent Chemokine-Binding Peptide

Treatment in a Murine Model of Coxsackievirus B3 Myocarditis. Basic Res Cardiol. 2025;120(2):393-422.

481) Caesar CE, Esbjörner EK, Lincoln P, Nordén B. Membrane Interactions of Cell-Penetrating Peptides Probed by Tryptophan Fluorescence and Dichroism Techniques: Correlations of Structure to Cellular Uptake. Biochemistry. 2006;45(24):7682-92.

482) de Araujo AD, Hoang HN, Lim J, Mak JYW, Fairlie DP. Tuning Electrostatic and Hydrophobic Surfaces of Aromatic Rings to Enhance Membrane Association and Cell Uptake of Peptides. Angewandte Chemie International Edition. 2022;61(29):e202203995.

483) Datta A, Bhattacharyya D, Singh S, Ghosh A, Schmidtchen A, Malmsten M, Bhunia A. Role of Aromatic Amino Acids in Lipopolysaccharide and Membrane Interactions of Antimicrobial Peptides for Use in Plant Disease Control. J Biol Chem. 2016;291(25):13301-17.

484) Norman MU, Hickey MJ. Mechanisms of Lymphocyte Migration in Autoimmune Disease. Tissue Antigens. 2005;66(3):163-72.

485) Rotondi M, Chiovato L, Romagnani S, Serio M, Romagnani P. Role of Chemokines in Endocrine Autoimmune Diseases. Endocrine Reviews. 2007;28(5):492-520.

486) Montecucco F, da Silva R, Fraga-Silva RA, Capettini L, Quintao S, Lenglet S, Pelli G, Galan K, Braunersreuther V, et al. O043 Treatment with Chemokine-Binding Protein Evasin-3 Reduces Atherosclerotic Vulnerability for Ischemic Stroke in Mice. Cytokine. 2012;59(3):517-18.

487) So J. Improving Patient Compliance with Biopharmaceuticals by Reducing Injection-Associated Pain. Journal of mucopolysaccharidosis and rare diseases. 2015;1(1):15-18.

488) Gupta S, Jain A, Chakraborty M, Sahni JK, Ali J, Dang S. Oral Delivery of Therapeutic Proteins and Peptides: A Review on Recent Developments. Drug delivery. 2013;20(6):237-46.

489) Wang J, Hogenkamp DJ, Tran M, Li WY, Yoshimura RF, Johnstone TB, Shen WC, Gee KW. Reversible Lipidization for the Oral Delivery of Leu-Enkephalin. J Drug Target. 2006;14(3):127-36.

490) Gomez-Soler M, Olson EJ, Rubio de la Torre E, Zhao C, Lamberto I, Flood DT, Danho W, Lechtenberg BC, Riedl SJ, et al. Lipidation and Pegylation Strategies to Prolong the in Vivo Half-Life of a Nanomolar Epha4 Receptor Antagonist. European Journal of Medicinal Chemistry. 2023;262:115876.

491) Wong JY, Ekanayake AI, Kharchenko S, Kirberger SE, Qiu R, Kelich P, Sarkar S, Li J, Fernandez KX, et al. Genetically Encoded Discovery of Perfluoroaryl Macrocycles That Bind to Albumin and Exhibit Extended Circulation in Vivo. Nature Communications. 2023;14(1):5654.

492) Latvala S, Jacobsen B, Otteneder MB, Herrmann A, Kronenberg S. Distribution of Fcrn across Species and Tissues. Journal of Histochemistry & Cytochemistry. 2017;65(6):321-33.

493) Andersen JT, Dalhus B, Cameron J, Daba MB, Plumridge A, Evans L, Brennan SO, Gunnarsen KS, Bjørås M, et al. Structure-Based Mutagenesis Reveals the Albumin-Binding Site of the Neonatal Fc Receptor. Nature Communications. 2012;3(1):610.

494) Jackson SH, Martin TS, Jones JD, Seal D, Emanuel F. Liraglutide (Victoza): The First Once-Daily Incretin Mimetic Injection for Type-2 Diabetes. P t. 2010;35(9):498-529.

495) Wijesinghe A, Kumari S, Booth V. Conjugates for Use in Peptide Therapeutics: A Systematic Review and Meta-Analysis. PLOS ONE. 2022;17(3):e0255753.

496) Véniant MM, Lu S-C, Atangan L, Komorowski R, Stanislaus S, Cheng Y, Wu B, Falsey JR, Hager T, et al. A Gipr Antagonist Conjugated to Glp-1 Analogues Promotes Weight Loss with Improved Metabolic Parameters in Preclinical and Phase 1 Settings. Nature Metabolism. 2024;6(2):290-303.

497) Hogarth PM, Pietersz GA. Fc Receptor-Targeted Therapies for the Treatment of Inflammation, Cancer and Beyond. Nature Reviews Drug Discovery. 2012;11(4):311-31.

498) Abraham M, Wald H, Vaizel-Ohayon D, Grabovsky V, Oren Z, Karni A, Weiss L, Galun E, Peled A, et al. Development of Novel Promiscuous Anti-Chemokine Peptibodies for Treating Autoimmunity and Inflammation. Front Immunol. 2017;8:1432.

499) Liu J, Yu M, Ning X, Zhou C, Yang S, Zheng J. Pegylation and Zwitterionization: Pros and Cons in the Renal Clearance and Tumor Targeting of near-Ir-Emitting Gold Nanoparticles. Angew Chem Int Ed Engl. 2013;52(48):12572-6.

500) Bailon P, Palleroni A, Schaffer CA, Spence CL, Fung W-J, Porter JE, Ehrlich GK, Pan W, Xu Z-X, et al. Rational Design of a Potent, Long-Lasting Form of Interferon: A 40 Kda Branched Polyethylene Glycol-Conjugated Interferon A-2a for the Treatment of Hepatitis C. Bioconjugate chemistry. 2001;12(2):195-202.

501) Brunton SA, Mosenzon O, Wright Jr EE. Integrating Oral Semaglutide into Clinical Practice in Primary Care: For Whom, When, and How? Postgraduate Medicine. 2020;132(sup2):48-60.

502) Hart Jr BW. Adcetris: A Regulatory Case Study of a New-Generation Antibody-Drug Conjugate. Antibody-Drug Conjugates: The 21st Century Magic Bullets for Cancer: Springer; 2025. p. 227-39.

503) Meglio M. Fda Approves Compliment C5 Inhibitor Zilucoplan as Treatment for Myasthenia Gravis. Neurology Live. 2023:NA-NA.

504) Johns DG, Campeau L-C, Banka P, Bautmans A, Bueters T, Bianchi E, Branca D, Bulger PG, Crevecoeur I, et al. Orally Bioavailable Macrocyclic Peptide That Inhibits Binding of Pcsk9 to the Low Density Lipoprotein Receptor. Circulation. 2023;148(2):144-58.

505) Deacon C, Knudsen L, Madsen K, Wiberg F, Jacobsen O, Holst J. Dipeptidyl Peptidase Iv Resistant Analogues of Glucagon-Like Peptide-1 Which Have Extended Metabolic Stability and Improved Biological Activity. Diabetologia. 1998;41:271-78.

506) Wang K, Qi J, Weng T, Tian Z, Lu Y, Hu K, Yin Z, Wu W. Enhancement of Oral Bioavailability of Cyclosporine A: Comparison of Various Nanoscale Drug-Delivery Systems. International journal of nanomedicine. 2014:4991-99.

507) Castro TG, Melle-Franco M, Sousa CEA, Cavaco-Paulo A, Marcos JC. Non-Canonical Amino Acids as Building Blocks for Peptidomimetics: Structure, Function, and Applications. Biomolecules. 2023;13(6).

508) Franck C, Foster SR, Johansen-Leete J, Chowdhury S, Cielesh M, Bhusal RP, Mackay JP, Larance M, Stone MJ, et al. Semisynthesis of an Evasin from Tick Saliva Reveals a Critical Role of Tyrosine Sulfation for Chemokine Binding and Inhibition. Proceedings of the National Academy of Sciences. 2020;117(23):12657-64.

509) Ludeman JP, Stone MJ. The Structural Role of Receptor Tyrosine Sulfation in Chemokine Recognition. British journal of pharmacology. 2014;171(5):1167-79.

510) Wang X, Sanchez J, Stone MJ, Payne RJ. Sulfation of the Human Cytomegalovirus Protein Ul22a Enhances Binding to the Chemokine Rantes. Angew Chem Int Ed Engl. 2017;56(29):8490-94.

511) Johansen-Leete J, Passioura T, Foster SR, Bhusal RP, Ford DJ, Liu M, Jongkees SAK, Suga H, Stone MJ, et al. Discovery of Potent Cyclic Sulfopeptide Chemokine Inhibitors Via Reprogrammed Genetic Code Mrna Display. Journal of the American Chemical Society. 2020;142(20):9141-46.

512) Stone MJ, Payne RJ. Homogeneous Sulfopeptides and Sulfoproteins: Synthetic Approaches and Applications to Characterize the Effects of Tyrosine Sulfation on Biochemical Function. Accounts of Chemical Research. 2015;48(8):2251-61.

513) Dilly JJ, Morgan AL, Bedding MJ, Low JK, Mackay JP, Conibear AC, Bhusal RP, Stone MJ, Franck C, et al. Tyrosine Sulfation Modulates the Binding Affinity of Chemokine-Targeting Nanobodies. ACS Chemical Biology. 2024;19(7):1426-32.

514) Shandell MA, Tan Z, Cornish VW. Genetic Code Expansion: A Brief History and Perspective. Biochemistry. 2021;60(46):3455-69.

515) Dien VT, Morris SE, Karadeema RJ, Romesberg FE. Expansion of the Genetic Code Via Expansion of the Genetic Alphabet. Curr Opin Chem Biol. 2018;46:196-202.
516) Raguine L, Ali M, Bender V, Diefenbach E, Doddareddy MR, Hibbs D, Manolios N. Alanine Scan of an Immunosuppressive Peptide (Cp): Analysis of Structure–Function Relationships. Chemical Biology & Drug Design. 2013;81(2):167-74.
517) Weiss GA, Watanabe CK, Zhong A, Goddard A, Sidhu SS. Rapid Mapping of Protein Functional Epitopes by Combinatorial Alanine Scanning. Proceedings of the National Academy of Sciences. 2000;97(16):8950-54.
518) Nandagopal S, Wu D, Lin F. Combinatorial Guidance by Ccr7 Ligands for T Lymphocytes Migration in Co-Existing Chemokine Fields. PLOS ONE. 2011;6(3):e18183.
519) Schumann K, Lämmermann T, Bruckner M, Legler DF, Polleux J, Spatz JP, Schuler G, Förster R, Lutz MB, et al. Immobilized Chemokine Fields and Soluble Chemokine Gradients Cooperatively Shape Migration Patterns of Dendritic Cells. Immunity. 2010;32(5):703-13.
520) Pickens SR, Chamberlain ND, Volin MV, Pope RM, Mandelin Ii AM, Shahrara S. Characterization of Ccl19 and Ccl21 in Rheumatoid Arthritis. Arthritis & Rheumatism. 2011;63(4):914-22.
521) Forman S, editor Safety and Efficacy of Ly3041658, a Novel Septa-Specific Monoclonal Antibody to Cxcr1 and Cxcr2 Ligands, in a Phase 2 Study in Hidradenitis Suppurativa. Annual Meeting of the American Academy of Dermatology; 2023; New Orleans, Louisiana: Dermatology Times.
522) Ruoslahti E. Molecular Zip Codes in Targeted Drug Delivery. Proceedings of the National Academy of Sciences. 2022;119(28):e2200183119.
523) Blanchetot C, Verzijl D, Mujić-Delić A, Bosch L, Rem L, Leurs R, Verrips CT, Saunders M, de Haard H, et al. Neutralizing Nanobodies Targeting Diverse Chemokines Effectively Inhibit Chemokine Function *. Journal of Biological Chemistry. 2013;288(35):25173-82.
524) Tanaka Y. Ozoralizumab: First Nanobody® Therapeutic for Rheumatoid Arthritis. Expert Opinion on Biological Therapy. 2023;23(7):579-87.
525) Kwon S, Duarte JN, Li Z, Ling JJ, Cheneval O, Durek T, Schroeder CI, Craik DJ, Ploegh HL. Targeted Delivery of Cyclotides Via Conjugation to a Nanobody. ACS Chemical Biology. 2018;13(10):2973-80.
526) Balhuizen A, Massa S, Mathijs I, Turatsinze J-V, De Vos J, Demine S, Xavier C, Villate O, Millard I, et al. A Nanobody-Based Tracer Targeting Dpp6 for Non-Invasive Imaging of Human Pancreatic Endocrine Cells. Scientific Reports. 2017;7(1):15130.
527) Demine S, Garcia Ribeiro R, Thevenet J, Marselli L, Marchetti P, Pattou F, Kerr-Conte J, Devoogdt N, Eizirik DL. A Nanobody-Based Nuclear Imaging Tracer Targeting Dipeptidyl Peptidase 6 to Determine the Mass of Human Beta Cell Grafts in Mice. Diabetologia. 2020;63(4):825-36.
528) Drucker DJ, Nauck MA. The Incretin System: Glucagon-Like Peptide-1 Receptor Agonists and Dipeptidyl Peptidase-4 Inhibitors in Type 2 Diabetes. The Lancet. 2006;368(9548):1696-705.
529) Denroche HC, Verchere CB. Iapp and Type 1 Diabetes: Implications for Immunity, Metabolism and Islet Transplants. Journal of molecular endocrinology. 2018;60(2):R57-R75.
530) Nielsen LL, Young AA, Parkes DG. Pharmacology of Exenatide (Synthetic Exendin-4): A Potential Therapeutic for Improved Glycemic Control of Type 2 Diabetes. Regulatory peptides. 2004;117(2):77-88.
531) Duarte DB, Vasko MR, Fehrenbacher JC. Models of Inflammation: Carrageenan Air Pouch. Current Protocols in Pharmacology. 2012;56(1):5.6.1-5.6.8.
532) Patil KR, Mahajan UB, Unger BS, Goyal SN, Belemkar S, Surana SJ, Ojha S, Patil CR. Animal Models of Inflammation for Screening of Anti-Inflammatory Drugs: Implications for the Discovery and Development of Phytopharmaceuticals. Int J Mol Sci. 2019;20(18).

533) Xu H, Lin S, Zhou Z, Li D, Zhang X, Yu M, Zhao R, Wang Y, Qian J, et al. New Genetic and Epigenetic Insights into the Chemokine System: The Latest Discoveries Aiding Progression toward Precision Medicine. Cellular & Molecular Immunology. 2023;20(7):739-76.
534) Mccoy KD, Léger E, Dietrich M. Host Specialization in Ticks and Transmission of Tick-Borne Diseases: A Review. Frontiers in Cellular and Infection Microbiology. 2013;Volume 3 - 2013.
535) Walker DK. The Use of Pharmacokinetic and Pharmacodynamic Data in the Assessment of Drug Safety in Early Drug Development. British Journal of Clinical Pharmacology. 2004;58(6):601-08.
536) Fielden MR, and Kolaja KL. The Role of Early in Vivo Toxicity Testing in Drug Discovery Toxicology. Expert Opinion on Drug Safety. 2008;7(2):107-10.
537) Tucker GT. Measurement of the Renal Clearance of Drugs. Br J Clin Pharmacol. 1981;12(6):761-70.
538) Dorato MA, Buckley LA. Toxicology in the Drug Discovery and Development Process. Current Protocols in Pharmacology. 2006;32(1):10.3.1-10.3.35.
539) Reed JC, Herold KC. Thinking Bedside at the Bench: The Nod Mouse Model of T1dm. Nature Reviews Endocrinology. 2015;11(5):308-14.
540) Elding Larsson H, Vehik K, Gesualdo P, Akolkar B, Hagopian W, Krischer J, Lernmark Å, Rewers M, Simell O, et al. Children Followed in the Teddy Study Are Diagnosed with Type 1 Diabetes at an Early Stage of Disease. Pediatric diabetes. 2014;15(2):118-26.
541) Tatovic D, Narendran P, Dayan CM. A Perspective on Treating Type 1 Diabetes Mellitus before Insulin Is Needed. Nature Reviews Endocrinology. 2023;19(6):361-70.
542) Ziegler AG, Rewers M, Simell O, Simell T, Lempainen J, Steck A, Winkler C, Ilonen J, Veijola R, et al. Seroconversion to Multiple Islet Autoantibodies and Risk of Progression to Diabetes in Children. Jama. 2013;309(23):2473-79.
543) Khine A, Quandt Z. From Prediction to Prevention: The Intricacies of Islet Autoantibodies in Type 1 Diabetes. Curr Diab Rep. 2025;25(1):38.
544) Weyand CM, Goronzy JJ. The Immunology of Rheumatoid Arthritis. Nature Immunology. 2021;22(1):10-18.
545) Lucchinetti CF, Popescu BF, Bunyan RF, Moll NM, Roemer SF, Lassmann H, Brück W, Parisi JE, Scheithauer BW, et al. Inflammatory Cortical Demyelination in Early Multiple Sclerosis. New England Journal of Medicine. 2011;365(23):2188-97.
546) Zhang GX, Ma CG, Xiao BG, Bakhiet M, Link H, Olsson T. Depletion of Cd8+ T Cells Suppresses the Development of Experimental Autoimmune Myasthenia Gravis in Lewis Rats. European journal of immunology. 1995;25(5):1191-98.
547) McKinney EF, Lyons PA, Carr EJ, Hollis JL, Jayne DR, Willcocks LC, Koukoulaki M, Brazma A, Jovanovic V, et al. A Cd8+ T Cell Transcription Signature Predicts Prognosis in Autoimmune Disease. Nature medicine. 2010;16(5):586-91.
548) Fujihara T, Fujita H, Tsubota K, Saito K, Tsuzaka K, Abe T, Takeuchi T. Preferential Localization of Cd8+ Aeβ7+ T Cells around Acinar Epithelial Cells with Apoptosis in Patients with Sjogren's Syndrome. The Journal of Immunology. 1999;163(4):2226-35.
549) Fox CK, Furtwaengler A, Nepomuceno RR, Martinez OM, Krams SM. Apoptotic Pathways in Primary Biliary Cirrhosis and Autoimmune Hepatitis. Liver. 2001;21(4):272-79.
550) Rottembourg D, Deal C, Lambert M, Mallone R, Carel J-C, Lacroix A, Caillat-Zucman S, le Deist F. 21-Hydroxylase Epitopes Are Targeted by Cd8 T Cells in Autoimmune Addison's Disease. Journal of Autoimmunity. 2010;35(4):309-15.
551) Gravano DM, Hoyer KK. Promotion and Prevention of Autoimmune Disease by Cd8+ T Cells. Journal of Autoimmunity. 2013;45:68-79.

552) Jubb HC, Higueruelo AP, Ochoa-Montaño B, Pitt WR, Ascher DB, Blundell TL. Arpeggio: A Web Server for Calculating and Visualising Interatomic Interactions in Protein Structures. Journal of Molecular Biology. 2017;429(3):365-71.

553) Dunnett CW. A Multiple Comparison Procedure for Comparing Several Treatments with a Control. Journal of the American Statistical Association. 1955;50(272):1096-121.